ASSESSMENT OF GAS TRANSFER – ANSTO MODEL AT HEATH STEELE MINES

MEND Project 1.22.1b

This work was done on behalf of MEND and sponsored by
Noranda Technology Centre
the Province of New Brunswick and
the Canada Centre for Mineral and Energy Technology (CANMET)
through the CANADA/ New Brunswick Mineral Development Agreement

July 1997

FINAL REPORT ON

ASSESSMENT OF GAS TRANSFER - ANSTO MODEL AT HEATH STEELE MINES

File No. 28-1264-046.1

Submitted to:

CANMET
Mineral Sciences Laboratories
555 Booth Street
Ottawa, Ontario
K1A 0G1

DSS File Number: O2SQ.23440-1-9210
DSS Contract Number: 23440-1-9210
CANMET Scientific Authority:
Marcia C. Blanchette

by:

ADI Nolan Davis Inc.
403 Regent Street, Suite 6
Fredericton, N.B.
E3B 3X6

in association with:

Australian Nuclear Science and Technology Organisation (ANSTO)
Private Mailbag 1, Menai, NSW
Australia, 2234

Project Manager: M.D. Riley
Reviewed by: A.I.M. Ritchie
Date: 94/06/30

File # O2SQ.23440-1-9210

TITLE: ASSESSMENT OF GAS TRANSFER - ANSTO MODEL AT HEATH STEELE MINES.

CANADA/NEW BRUNSWICK MINERAL DEVELOPMENT AGREEMENT (MDA) COST SHARED 36%/64%

FINAL REPORT

by:

ADI Nolan Davis Inc.
403 Regent Street, Suite 6
Fredericton, N.B., E3B 3X6
Canada

in association with:

Australian Nuclear Science & Technology Organisation
Private Mailbag 1, Menai, NSW
Australia, 2234

Work on this project was conducted under the auspices of the Department of Energy, Mines and Resources.

DSS File Number: O2SQ.23440-1-9210
DSS Contract Number: 23440-1-9210
CANMET Scientific Authority: Marcia Blanchette

Executive Summary

Acid Mine Drainage (AMD) research under the Mine Environment Neutral Drainage (MEND) program has been ongoing since 1988 at the Heath Steele Mines site outside Newcastle, New Brunswick. This research consists of two distinct projects. The initial study, noted as "Heath Steele Waste Rock Study" (MEND Project 2.31.1), has been ongoing since 1988 and has as its objective the evaluation of the nature of several waste rock piles and the examination of the performance of a composite soil cover on top of pile 7/12 with respect to its effectiveness in limiting the AMD. In 1990, this study recommended that further investigative work be carried out at the site to determine the air permeability of the Heath Steele waste rock piles and to assess the gas transfer mechanisms present in the piles, this initiated the "Assessment of Gas Transfer - ANSTO Model at Heath Steele" project. The objectives of the project were to develop an understanding of the processes governing the pyrite oxidation rates in acid waste rock piles at Heath Steele using both the field data and the numerical model FIDHELM developed by the Australian Nuclear Science & Technology Organisation (ANSTO), to quantify those processes and to evaluate the effectiveness of the composite soil cover for acid waste rock management.

The project had two major components: field measurements and modeling using FIDHELM. The field work that included the installation of monitoring probes permitted in situ measurements of various parameters required by FIDHELM, namely the oxygen diffusion coefficient, air permeability and thermal conductivity. The modeling consisted of running FIDHELM utilizing the Heath Steele data collected in the field program. The gas transport mechanisms dominating the oxidation rates in the Heath Steele waste rock piles were identified using observed temperature and oxygen profiles in conjunction with FIDHELM simulations. A user's manual for FIDHELM was also presented with the report.

The air permeability, oxygen diffusion coefficient and thermal conductivity were measured successfully and the values were found to be within the range measured in four other piles of waste rock at three different mine sites and in climates ranging from tropical to arctic.

FIDHELM was shown to be a useful tool to assess the various gas transfer mechanisms in pyritic waste rock piles. Numerical simulations using FIDHELM with the average measured values of oxygen diffusion coefficient, thermal conductivity and gas permeability indicate that gas transport was dominated by diffusion. FIDHELM results also indicate that particular details in the oxygen profile measured at the Heath Steele waste rock piles can be explained by the heterogeneity of the pile with respect to both gas permeability and IOR. The modeling of the pile with the soil cover (pile 7/12) and the field data indicate that the composite soil cover is an effective way to reduce the ingress of oxygen to acid generating waste rock. The data collected to date from covered pile 7/12 is consistent with the simulations.

While the piles at Heath Steele are small compared to waste rock piles at many mine sites around the world, and while the balance of gas transport mechanisms in these larger piles may be different from those at work in the piles at Heath Steele, it is also clear that the cover system has been effective in reducing oxygen ingress and, with this, in reducing the oxidation rate.

Since it is possible that advection driven by wind effects is a mechanism in some of the piles, it is recommended that a program of work be set up to quantify this effect and to compare measured values with the results of modeling with a version of FIDHELM modified to accept space/time varying surface pressure. Continuous monitoring of temperature and pore gas oxygen concentration profiles throughout the entire year is also recommended and may provide better understanding of the chemical processes and gas transfer mechanisms present in waste rock piles. This may allow any temperature dependence of the IOR to be estimated. Monitoring and simulations using FIDHELM should be used to assess the importance of pile inhomogeneity on the overall pollutant load from a pile. Finally, the IOR and the sulphur content of the waste rock from Heath Steele should be estimated using laboratory testing.

Sommaire

L'étude du drainage minier acide (DMA) sous le Programme de neutralisation des eaux de drainage dans l'environnement minier (NEDEM) se poursuit depuis 1988 aux mines Heath Steele, près de Newcastle au Nouveau-Brunswick. Cette étude comporte deux projets distincts. La première étude, intitulée "Heath Steele Waste Rock Study" (Projet NEDEM 2.31.1) se poursuit depuis 1988 et a comme objectifs l'évaluation des propriétés de plusieurs haldes de stériles et l'examen de la performance de la couverture de sol composite au-dessus de la pile 7/12 par rapport à son éfficacité à limiter le DMA. En 1990, cette étude recommenda que d'autres travaux soient effectués afin de déterminer la perméabilité à l'air des haldes de stériles aux mines Heath Steele et d'évaluer les mécanismes de transfert des gaz présents dans les haldes, d'où la création du projet "Assessment of Gas-Transfer - ANSTO Model at Heath Steele". Les objectifs de ce projet étaient de mieux comprendre les procédés gouvernant le taux d'oxydation de la pyrite dans les haldes de stériles acides aux mines Heath Steele en utilisant à la fois les données in situ et le modèle numérique FIDHELM développé par l'Australian Nuclear Science & Technology Organisation (ANSTO), ainsi que de quantifier ces procédés et d'évaluer l'efficacité de la couverture de sol composite pour la gestion des stériles acides.

Le projet comporta deux composantes majeures: soient les prises de données sur le terrain et la modélisation numérique utilisant FIDHELM. Les travaux sur le terrain, qui incluèrent l'installation des sondes d'échantillonnage, ont permis la mesure in situ de divers paramètres requis par FIDHELM, c'est-à-dire le coefficient de diffusion de l'oxygène, la perméabilité à l'air et la conductivité thermique. La modélisation consista à utiliser FIDHELM avec les données récoltées lors du programme de collecte de données sur le terrain. Les mécanismes de transport des gaz dominant le taux d'oxydation des haldes de stériles aux mines Heath Steele furent identifiés en utilisant les profils de température et d'oxygène observés sur le terrain, et les simulations effectuées avec FIDHELM. Un manuel d'usager pour FIDHELM est inclu avec le rapport.

La perméabilité à l'air, le coefficient de diffusion de l'oxygène et la conductivité thermique furent mesurés avec succès et les valeurs obtenues se situent à l'intérieur de la plage de valeurs mesurées à quatre autres haldes de stériles provenant de trois sites différents et sous des climats variant de tropical à arctique.

FIDHELM s'est avéré un outil très utile pour évaluer les divers mécanismes de transfert des gaz à l'intérieur des haldes de stériles pyritiques. Les simulations numériques de FIDHELM, en utilisant la moyenne des valeurs mesurées du coefficient de diffusion d'oxygène et de la conductivité thermique, indiquent que le transport des gaz est dominé par la diffusion. Les résultats de FIDHELM indiquent aussi certaines particularités dans les mesures de profils d'oxygène dans les haldes des mines Heath Steele qui peuvent être attribuées à l'hétérogéinité des haldes par rapport à leur perméabilité à l'air et de leur taux d'oxydation intrinsèque (TOI). Les données in situ et la modélisation de la halde avec la couverture de sol composite (pile 7/12) indiquent que la couverture de sol composite est un moyen efficace pour réduire l'entrée d'oxygène vers les stériles producteurs d'acide. Les données récoltées à date provenant de la halde 7/12 qui est couverte, sont consistantes avec les simulations numériques.

Etant donné que les haldes de stériles des mines Heath Steele sont petites par rapport à la plupart des haldes à travers le monde, et étant donné que l'équilibre des mécanismes de transports des gaz dans ces plus grosses haldes peut être différent de celui présent aux haldes des mines Heath Steele, il est clair que la couverture de sol composite fut un moyen efficace pour réduire l'entrée d'oxygène ainsi que le taux d'oxydation.

Etant donné que l'advection due à l'effet du vent soit l'un des mécanismes possible dans certaines des haldes, l'étude recommende qu'un programme soit mis en place afin de quantifier cet effet et de comparer les valeurs mesurées avec les résultats de modélisation en utilisant une version modifiée de FIDHELM afin d'accepter une variation spacio-temporelle de la pression à la surface de la halde. Un suivi continu de la température et de la teneur en oxygène gazeux interstitiel durant toute l'année est aussi recommandé et permettra une meilleure compréhension des procédés chimiques et des mécanismes de transfert des gaz présents dans les haldes de stériles. Ceci permettra peut-être l'estimation de toute dépendance du TOI en fonction de la température. Le suivi et les simulations numériques utilisant FIDHELM devraient être utilisés pour évaluer l'importance de l'inhomogéinité d'une halde sur la charge polluante globale d'une halde. Finalement, le TOI et la teneur en soufre des stériles des mines Heath Steele devraient être estimés en effectuant des essais en laboratoire.

Table of Contents

Table of Contents (Continued)

List of Figures

List of Figures (Continued)

List of Tables

1. INTRODUCTION

Acid Rock Drainage (ARD) is the most important environmental problem facing the Canadian mining industry today. ARD is caused by exposure of ore and waste rock containing sulphide minerals. When sulphide minerals, in particular pyrite and pyrrhotite, are exposed to an environment containing oxygen and water, sulphide is converted to sulphate. The contact of these oxidizing minerals with water generates acidic drainage with elevated levels of heavy metals and dissolved salts. As the oxidation reactions continue, temperature and acidity increase, in turn accelerating the reactions. As rainfall and snow melt infiltrate waste rock piles, acidic drainage is released to surface and groundwater, contaminating the environment.

The oxidation of pyritic waste rock and the subsequent generation of ARD is controlled usually by the availability of oxygen. The movement of oxygen through a reactive waste rock pile is very important since it controls the extent of the zone of active oxidation. If the rate of oxygen transport is rapid compared to the consumption of oxygen by pyritic oxidation, the zone of oxidation is extended. Therefore, any understanding of the generation of ARD requires a thorough understanding of the gas transfer mechanism within the waste rock and the effect of various other physical factors such as temperature and oxygen content.

A recent study on acid waste rock management at Canadian base-metal mines (Nolan Davis, 1987) identified the need for field performance data on waste rock pile covers and other management systems. To address this need, research is being carried out at the Heath Steele Mines site, located 50 km north of Newcastle in New Brunswick (N.B.).

Presently, there are two distinct research projects ongoing at Heath Steele Mines, both of which are being conducted under the Mine Environment Neutral Drainage (MEND) program. The initial study, noted as "Heath Steele Waste Rock Study" (Waste Rock Study) (MEND Project 2.31.1) has been ongoing since 1988. The overall objective of the Waste Rock Study is to evaluate the nature of several waste rock piles and to examine the performance of a composite soil cover with respect to its effectiveness in limiting the generation of acid mine drainage. In 1990, this study recommended that further investigative work be carried out at the site to determine the air permeability of the Heath Steele waste rock piles. Furthermore, it was recommended that an attempt be made to develop a computer model of the gas transfer mechanisms as a tool for understanding the factors influencing gas transfer and the interaction between diffusion, convection and advection within the waste rock piles (Nolan Davis, 1990).

As a result of this recommendation, a proposal was submitted to MEND by Nolan, Davis and Associates (N.B.) Limited (Nolan, Davis) in association with the Australian Nuclear Science and Technology Organisation (ANSTO) for an assessment, through modeling, of the gas transfer relationships at the Heath Steele waste rock piles. The overall approach involved in situ measurements of bulk physical parameters important in the gas transfer process and then utilizing the measured parameters in the FIDHELM model developed by ANSTO to gain a better understanding of the gas transfer mechanisms within waste rock piles at Heath Steele. On May 6, 1992, a contract was issued by Supply and Services Canada to proceed with the "Assessment of

Gas Transfer" (Gas Transfer) (MEND Project 1.22.1) at Heath Steele Mines. The funding for the project was provided by the Canada/New Brunswick Mineral Development Agreement (MDA), ANSTO and Noranda Inc. under the auspices of the Department of Energy, Mines and Resources. The Gas Transfer project is a separate project from the Waste Rock Study but is being carried out concurrently using data from the ongoing monitoring for the Waste Rock Study.

The following report summarizes the results of the Gas Transfer project. More specifically, it provides a summary of the bulk physical parameter measurements carried out at the Heath Steele site as well as the results of FIDHELM applications using the measured bulk physical parameters. Also provided are some recommendations for acid waste pile management alternatives.

1.1 Project Objectives and Scope of Work

The overall objective of the study is to develop an understanding and quantify the process which governs the pyrite oxidation rate in acid waste rock piles and, based on this understanding, evaluate the effectiveness of the composite soil cover for acid waste rock management. The project was carried out in four phases, as described below:

Phase 1: Project Scoping
The initial phase of the project consisted of collecting available information on acid mine drainage and gas transfer topics, and carrying out preliminary modeling using FIDHELM to assess sensitive parameters before the field work was to be carried out. The field monitoring and testing program was also prepared during this initial phase.

Phase 2: Field Investigations
The field work was carried out during Phase 2. This included the installation of monitoring probes and in situ testing which permitted the measurements of various parameters required by FIDHELM. These measured in situ parameters also provided important information for the assessment of gas transfer mechanisms present in waste rock piles at Heath Steele.

Phase 3: FIDHELM Model Application
This phase consisted of rerunning FIDHELM utilizing the Heath Steele data collected in Phases 1 and 2. The observed temperature and oxygen profiles in conjunction with FIDHLEM simulations were used to identify the gas transport mechanisms dominating the oxidation rates in the Heath Steele waste rock piles.

Phase 4: Waste Rock Pile 7/12
In the final phase, FIDHELM was used to quantify the oxidation mechanisms of the waste rock pile 7/12, both prior to and after the application of the composite soil cover placed in August-September, 1991. A manual for the running of FIDHELM was also prepared during this final phase.

2. HEATH STEELE MINES HISTORICAL SETTING

2.1 Background

The Heath Steele Mines site is located 50 km north of Newcastle in N.B. (see location plan in Figure 2-1) and was initiated in 1953 with the discovery of a massive sulphide deposits. Mine development and plant construction started in 1955, and ore benefication commenced in 1957. The operation closed in May 1958 as a result of low metal prices and metallurgical problems with oxidized portions of the ore zones. Production was resumed in 1960 and the capacity of the mill was steadily increased through the 1960s reaching 3000 tonnes per day (tpd) in 1969. In 1977, it was further increased to 4000 tpd.

In May 1983, the sulphide ore operation was again shut down due to low metal prices. However, the mill was modified and operated until October 1984 to treat the gold-silver gossan ore that had been stockpiled on site for over 20 years, since the development of the B-Zone open pit. The collection and treatment of both surface water and mine drainage were maintained, and continue to operate in essentially the same manner today. The system involves the operation of a comprehensive site drainage collection scheme that allows contaminated drainage to be pumped to the tailings pond for treatment. Lime slurry is mixed with the drainage to neutralize acid and precipitate heavy metals from solution. In 1989, production commenced at the new Stratmat mine and was reinstated at the existing B-Zone underground mine. The Stratmat site is located approximately 4.5 km northwest of the mill complex.

In total, at least 756,000 tonnes of pyritic waste rock and reject ore have been stockpiled in more than 20 piles at the Heath Steele site. The widely dispersed nature of this acid-generating material poses a particular challenge to currently available reclamation technology. Under the initial Waste Rock Study, three of the Heath Steele piles, numbered Pile 17, 18A and 18B were selected, using a matrix evaluation, as most amenable to monitoring and evaluation of remedial measures (see Tables 2-1 and 2-2). A fourth pile, noted as Pile 7/12, was constructed in 1989 by moving waste rock from Piles 7 and 12, which were to be moved as part of the ongoing reclamation plan, to a prepared site. The waste rock was placed on a prepared sand base with an underlying impermeable membrane made of fabrene fabric strips glued together. Installation of the pad and relocation of Pile 7/12 was completed in June 1989.

Instrumentation was installed in piles 18A, 18B and 17 in November and December 1988 and in waste rock Pile 7/12 in June 1989. The instrumentation which consisted of clusters of thermocouples and oxygen probes has been monitored on a regular basis since installation and provides an extensive data base.

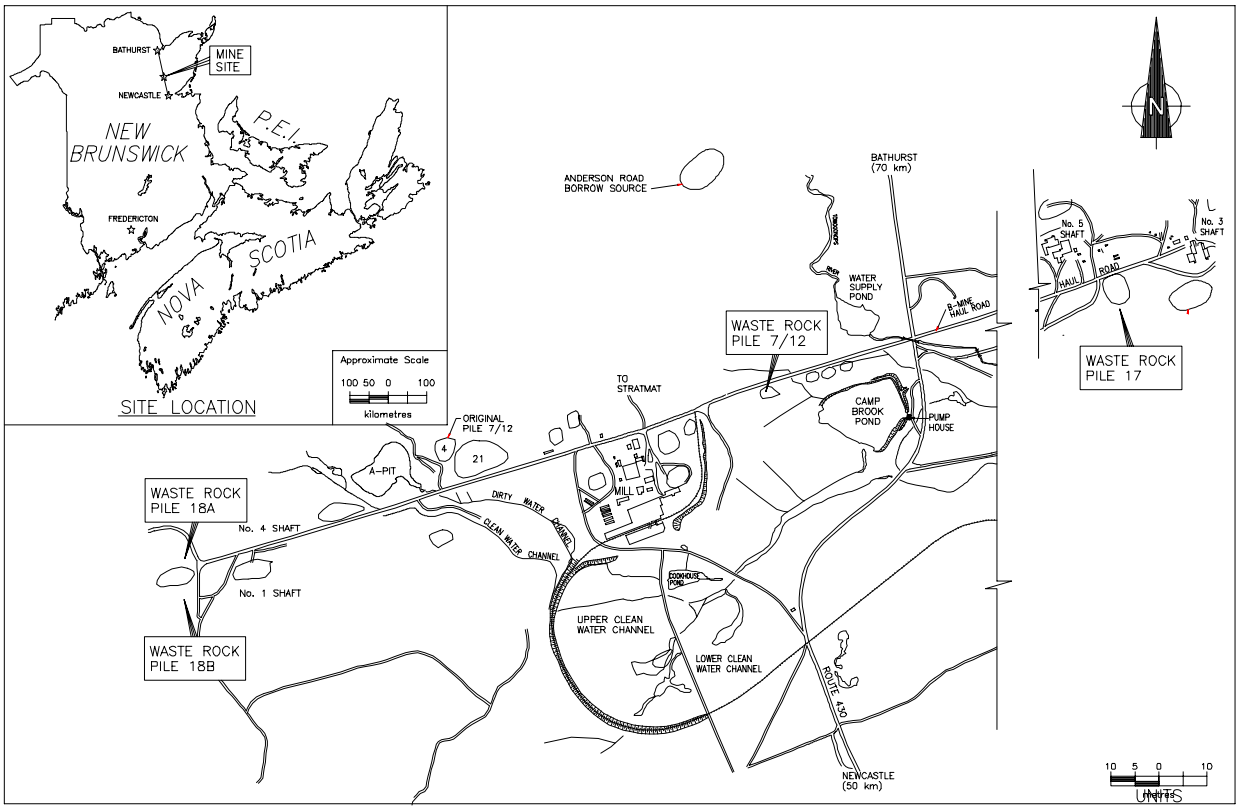

Figure 2-1: Site Location, Heath Steele Mines

2.2 Waste Rock Pile Characteristics

The pile characteristics, size, shape and tonnage of the waste rock, are important to the interpretation of the monitoring data. The pile sizes, in order of increasing volume, are 18A, 7/12, 18B and 17, with volumes of 1900, 6200, 8300, and 100,300 m^3, respectively. The mineralogy and acid producing / acid consuming potential of each waste rock pile are summarized in Tables 2-1 and 2-2, respectively. The particle size distribution within the waste rock piles varies considerably from silt and clay sizes to cobbles and boulders. A void ratio of 31 percent estimated for Pile 7/12 is considered to be within the lower range typical for piles of blasted rock. The bulk specific gravity of the broken waste rock is estimated to range from 1.8 - 2.3. Additional details on waste rock pile characteristics determined as part of the Waste Rock Study are contained in the Heath Steele Waste Rock Study - Phase II Report (Nolan Davis, 1990).

2.3 Climatology

The climate at the Heath Steele site can be described as Maritime continental, with hot, relatively dry summers and cold, snowy winters. Mean annual precipitation at the Little River Mine Atmospheric Environment Service (AES) Station is 1134 mm, of which 762 mm is rainfall. The station records an average of 93 days per year with rain and 47 with snowfall. The coldest months are January and February with mean daily temperatures of -12.5 °C. July is the warmest

month with a daily mean of 17.9 °C. Winds are predominantly from the Northwest. Historical climate data are presented in Table 2-3. Additional details are contained in the previously noted Phase II Report (Nolan Davis, 1990).

Table 2-1: Acid Consuming Potential

Sample	Sulphur (%) [a]	Acid Production (kg/tonne) [b]	Acid Consumed (kg/tonne) [b]	AP-AC (kg/tonne) [c]	Theoretical Acid Producer
Pile 18A					
BH 1 9'6"-10' Waste Rock	2.60	79.6	1.47	78.1	Yes
BH 1 10'-12' Bedrock	0.22	6.8	1.47	5.3	Yes
Pile 18B					
BH 2 5' - 7' Waste Rock	3.94	120.7	<0.5	120.4	Yes
BH 2 15'-17' Waste Rock	6.40	196.0	0.74	195.3	Yes
Beside Pile 18B ("PAD")					
BH 3 0-1' Outwash	0.15	4.6	0.5	4.1	Yes
Pile 7/12					
BH 4 4' - 5' Waste Rock	6.69	204.9	<0.3	204.6	Yes
BH 4 14'6"-15'9" Waste Rock	7.07	216.5	0.49	216.0	Yes
Beside Pile 7/12					
Bedrock Sample 0-1'	4.98	152.5	1.72	150.8	Yes
Pile 17					
BH 5 15'-17' Waste Rock	1.28	39.2	1.23	38.0	Yes
BH 6 5' - 7' Waste Rock	1.05	32.2	<0.3	31.9	Yes

[a] Sulphur (%) = total pyritic sulphur
[b] kg[H_2SO_4]/tonne
[c] AP = all sulphur oxidizable by iron oxidizing bacteria
AC = acid consumption as determined by titration with sulphuric acid
Analyses by Research and Productivity Council, Fredericton, N.B.

Table 2-2: Mineralogy and Acid Production

Pile	Surface Area (m^2)	Average Depth (m)	Maximum Depth (m)	Estimated Volume (m^3)	Foundation Condition [a]	Mineralogy (b) AP (kg/tonne)	AC (kg/tonne)	Sulphides Present	Percent
18A	1,210	1.6	3.4	1,900	Thin OB [c] over rock	79.6	1.5	Pyrite Galens Sphalerite	5-7 <1 <1
18B	3,570	2.3	6.7	8,300	Thin OB over rock	158.4	0.5	Pyrite Fe-S Sphalerite Galena Chalcopyrite	7-10 7-10 <1 <1 <1
17	25,640	3.9	10.5	100,300	Thin OB over rock	35.7	0.8	Sphalerite Pyrite Arsenopyrite Chalcopyrite	7-10 <1 <1 <1
7/12[c]	2,100	2.9	5	6,200	Impermeable Membrane Base	210.7	0.4	Pyrite Fe-S Galena Chalcopyrite Arsenopyrite Sphalerite Pyrrhotite	7-10 5-7 <1 <1 <1 <1 <1

[a] Based on geophysical, borehole and field observations
[b] AP & AC: Theoretical Acid Production & Acid-Consumed (refer to Table 2-1)
[c] OB: Overburden

Table 2-3: Historical Climate Data

LITTLE RIVER MINE 47° 17'N 66° 4'W	JAN	FEB	MAR	APR	MAY	JUN	JUL	AUG	SEP	OCT	NOV	DEC
Daily Maximum Temperature (°C)	-7.4	-5.9	-0.1	5.6	13.5	20.7	23.3	22.2	16.8	10.2	2.8	-4.2
Daily Minimum Temperature (°C)	-17.5	-17.0	-10.5	-4.3	2.0	9.0	12.5	10.9	6.0	0.7	-5.1	-13.2
Mean Daily Temperature (°C)	-12.5	-11.5	-5.3	0.7	7.8	14.9	17.9	16.6	11.4	5.5	-1.2	-8.7
Standard Deviation, Daily Temperature	2.2	1.8	2.0	1.1	1.8	1.2	1.6	1.2	1.4	1.4	1.9	2.6
Maximum Temperature (°C)	12.2	10.0	20.0	21.7	31.7	33.3	33.3	35.0	30.0	24.5	19.4	13.3
Years of Record	20	21	21	22	22	21	20	21	20	20	20	20
Minimum Temperature (°C)	-37.2	-35.0	-29.4	-19.4	-15.0	-5.0	1.1	-1.1	-6.7	-10.6	-20.0	-29
Years of Record	21	21	22	22	23	21	20	21	20	21	21	21
Mean Rainfall (mm)	16.4	9.9	23.9	43.5	90.4	85.6	100.7	83.9	95.5	104.7	74.0	33.8
Mean Snowfall (mm)	76.0	58.1	72.3	43.5	5.7	0.0	0.0	0.0	0.0	4.2	35.6	81
Mean Total Precipitation (mm)	91.1	68.0	96.1	86.8	96.4	85.6	100.7	83.9	95.5	108.8	105.8	115.6
Standard Deviation, Total Precipitation	45.9	26.7	36.3	51.0	49.3	47.4	48.5	41.7	43.0	47.3	45.9	42.7
Maximum Rainfall in 24 hours (mm)	49.3	42.9	44.5	76.2	68.6	50.5	55.4	99.6	99.3	86.6	52.8	58.4
Years of Record	19	22	20	23	21	22	22	22	21	22	18	22
Maximum Snowfall in 24 hours (mm)	43.2	34.8	35.6	50.8	20.3	T	0.0	0.0	T	17.8	35.6	48.3
Years of Record	22	20	21	21	23	22	23	22	22	22	22	22
Maximum Precipitation in 24 hours (mm)	49.3	42.9	44.5	76.2	68.6	50.5	55.4	99.6	99.3	86.6	52.8	58.4
Years of Record	22	21	21	22	21	22	22	22	21	22	21	23
Days with Rain	2	1	4	6	12	12	13	11	11	11	7	3
Days with Snow	9	8	9	5	1	0	0	0	0	1	5	9
Days with Precipitation	10	9	12	11	13	12	13	11	11	11	11	11

Note: Climatic data from 1968 to 1991.

3. LITERATURE REVIEW

One of the tasks associated with this project is the assembly and review of available information related to gas transfer and acid mine drainage. A library search was carried out utilizing electronic linkages to access selected university and government data sources. A partial listing of bibliographical references is provided in Appendix I at the end of this report.

While there is extensive information in the literature related to Acid Rock Drainage, there are only limited references to gas transfer mechanisms in pyritic waste rock piles. The following summarizes the literature review on these two topics.

A number of mathematical models have been developed over the last twenty years or so to describe the leaching process, the emphasis being on commercial production of copper from heap leach piles but with some work on the extraction of other metals such as nickel and uranium. The first of these models was from Harris (1969) who developed a model to describe leaching of copper from the piles of sulphide and oxide ore at the Rum Jungle mine site in Australia.

In the mid 1970s, a number of models describing the extraction of minerals by heap and in-situ leaching were published. Three main types of model were proposed, each describing the leaching behavior of the entire ore mass by focusing on the leaching behavior of individual particles within the ore. The three types, which can be characterized by the models of Barlett (1973), Braun et al. (1974) and Roman et al. (1974), differ primarily in the assumptions made about the rate of chemical reaction compared to the rate of reactant transport to the reaction site within the particles. All three models assume that the particles are spherical and describe the kinetics in terms of the inward radial diffusion of reactant driven by the chemical reaction within the particles.

Models describing heap leaching behavior have also been proposed several authors (Roach et al. 1975, 1977, 1978; Cathles et al. 1975, 1977; Cathles 1979; Averill 1976). Cathles (1979) extended the earlier model to include the effects of bacterial catalysis and, after calibration of the model on test dumps, its predictions were compared with results from large scale leaching experiments. The large scale tests confirmed the general validity of the model, however, detailed predictions were quite inaccurate in some circumstances. Subsequently, a two-dimensional model was proposed by Cathles and Schlitt (1980) in an attempt to account for lateral transport of heat and oxidant within leaching dumps. During the same period, there have been a number of studies on oxidant transport and oxidation of pyritic material within the particles (Brierley 1978; Box and Prosser 1986; Lin et Sohn 1987; Whittemore 1981). Jaynes et al. (1984) put forward a model describing the long-term oxidation of pyrite and removal of reaction products from reclaimed coal strip mines. The oxygen supply into the reclaimed profile was assumed to be by one dimensional diffusion. The oxidation rate of the pyrite was based on first-order, solid-liquid kinetics and the rate of simple diffusion of oxidant into reactive, coarse stone fragments. In more recent years, Guo and Parizek (1992) developed a model that incorporates coupled heat and gas flow, dispersion-advection of oxygen in the gas-phase, steady-state soil water flow and acid reactions which produce acid mine drainage. Scharer et al. (1993) presented a model which included one

dimensional oxygen diffusion into the heap coupled with a shrinking radius (fine particles) and the shrinking reactive front (massive sulphides) concepts.

The models mentioned above largely attempt to predict oxidation of entire heaps based on the reaction kinetics within individual particles with little or no consideration of the macroscopic transport mechanisms, with the consequent assumption that the oxidant concentration surrounding each particle of the dump is considered constant. In some cases, a bulk advective transport mechanism is included in the model.

The assumption of constant oxidant concentration throughout the heap may be valid in commercial leaching operations where liquor is circulated through the heaps but is less likely to be true for natural weathering processes in pyritic mine wastes. A model of natural oxidation in a pyritic waste rock dump was first developed by Ritchie (1977) in which the dump was assumed to be a homogeneous slab, that all the nutritional requirements for bacterial growth were freely available, that the oxidation reaction proceeded as fast as reactants were fed to the oxidation sites and that all the reactants for the oxidation of pyrites were also freely available except for oxygen. The oxygen supply rate was assumed to be limited by the rate that oxygen could diffuse through the pore space of the dump. Davis and Ritchie (1986) incorporated the effect of transport of oxygen into the particles comprising the dump with transport through the pore space of the dump. In a companion paper, Davis et al. (1986) presented the results of a numerical solution to the model for the oxidation of pyritic mine wastes with the oxidation proceeding at a moving front within the particles comprising the wastes. Davis and Ritchie (1987) extended the model to take proper account of the range of particle sizes in the waste rock piles. Pantelis and Ritchie (1991) based their study on the same model by coupling the macroscopic transport and the microscopic particle reaction kinetics which incorporate oxygen and heat transport based on the two major mechanisms of convection and diffusion. This proposed model omitted the water phase passing through the dump and was for cylindrical-shaped dumps. An important practical conclusion drawn from these simulations was that an increase in the oxidation rate at the particle (microscopic) level by a factor of 6-7 translates to only about a 1-5% increase in the global oxidation rate in the dump. Another was the importance of gas permeability on dump performance. Because convection is a more effective gas transport process than diffusion, convection has to be established if high oxidation rates are to be maintained through the life of the dump. Pantelis and Ritchie (1992) continued their research by adding the water phase and truncated cone geometries to their model. Water movement transports heat and an increased water flow increases the water content of the pore space and decreases the air-filled porosity, leading to decreases in diffusion coefficient and gas permeability, which in turn lead to decreased gas transport. Their results confirmed previous findings that convection is not an important air transport mechanism in the heaps with air permeability exceeding 10^{-10} m^2 or less but becomes so at permeabilities exceeding 10^{-10} m^2, and that a substantial increase in the oxidation rate at the microscopic level translated to an increase of only a few percent in the rate of oxidation of the entire heap. Also, a truncated cone showed less oxidation than a cylindrical shaped pile. This model presented by Pantelis and Ritchie (1992) represents the basis of FIDHELM that was used for this study.

In regards to field work about gas transfer in waste rock piles, ANSTO personnel have published several papers on the subject, especially the research work carried at the Rum Jungle in Australia. The hydrology of the waste rock dumps at this site and the temperature and gas compositions in them have been studied to provide information on the pyritic oxidation process and the release of pollutants. These studies indicated that at many locations in the dumps, the supply of oxygen was the rate-limiting mechanism for the oxidation of pyrite. The data was recovered from this project was used for numerical model verifications (see above) and also, the temperature profiles were used to estimate the pyritic oxidation rate in the waste rock dump. Waste rock material was covered with clay and clay with soil, all supporting a vegetation cover to protect the clay. Field measurements showed that placement of the cover reduced the infiltration of water to less than 5% of the rainfall, reduced the oxygen levels, the temperature and the oxidation rates. The performance of the soil cover at the Rum Jungle project is similar to what is reported by Yanful et al. (1991, 1993).

4. FIELD MEASUREMENTS

The objective of the field investigations was to make in situ determinations of the bulk physical parameters known to be important in describing gas transport mechanisms that govern oxidation rates in waste rock piles. Specifically, measurements made in Pile 18B included:

- gas permeabilities;
- thermal conductivities; and
- gas diffusion coefficients.

Being of similar dimensions and containing the same type of rock, 18B is considered to be a control pile for Pile 7/12 which is being intensively studied to assess the effectiveness of its engineered cover system in reducing acid rock drainage (Waste Rock Study). Pile 18B was also constructed using similar construction methods as for Pile 7/12. Pile 18B was chosen for the bulk physical parameter measurements because it had no cover and therefore could be drilled and instrumented without the risk of altering the dynamic behavior of the system. Figures 4-1 and 4-2 show the location of the monitoring ports at piles 18B and 7/12, and Figures 4-3 and 4-4 show cross-sections of the two piles.

The following sections provide brief description of the measurement techniques and a summary of the results of field investigations. A summary of the ongoing in situ monitoring, which is part of the Waste Rock Study, is also presented. Details on the methodology and techniques used to measure the bulk physical parameters are contained in the Nolan Davis "Field Techniques Manual" (Nolan Davis, 1993), also developed under this project.

The data collected from the ongoing monitoring program at Heath Steele that was used for this study is presented in Appendix II. The data consists of gaseous oxygen concentrations, temperatures and carbon dioxide concentrations. The results of the in situ testing carried out by ANSTO for the bulk physical parameters (thermal conductivity, air permeability and oxygen diffusion coefficient) are also included in Appendix II.

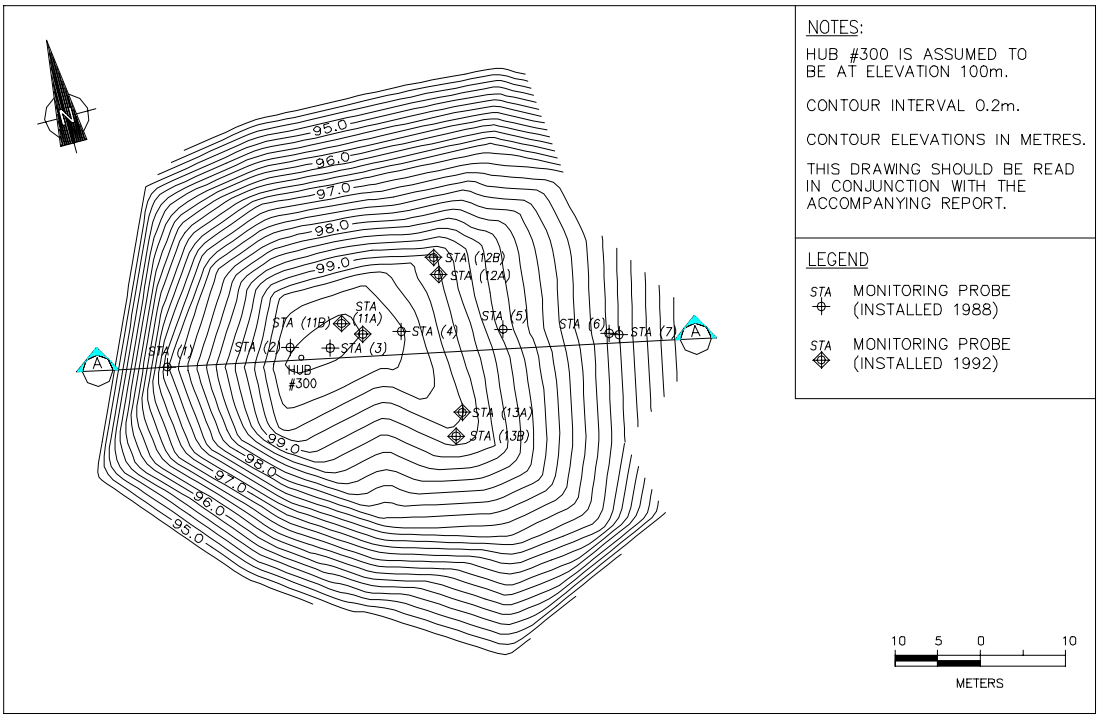

Figure 4-1: Site Plan, Waste Rock Pile 18B

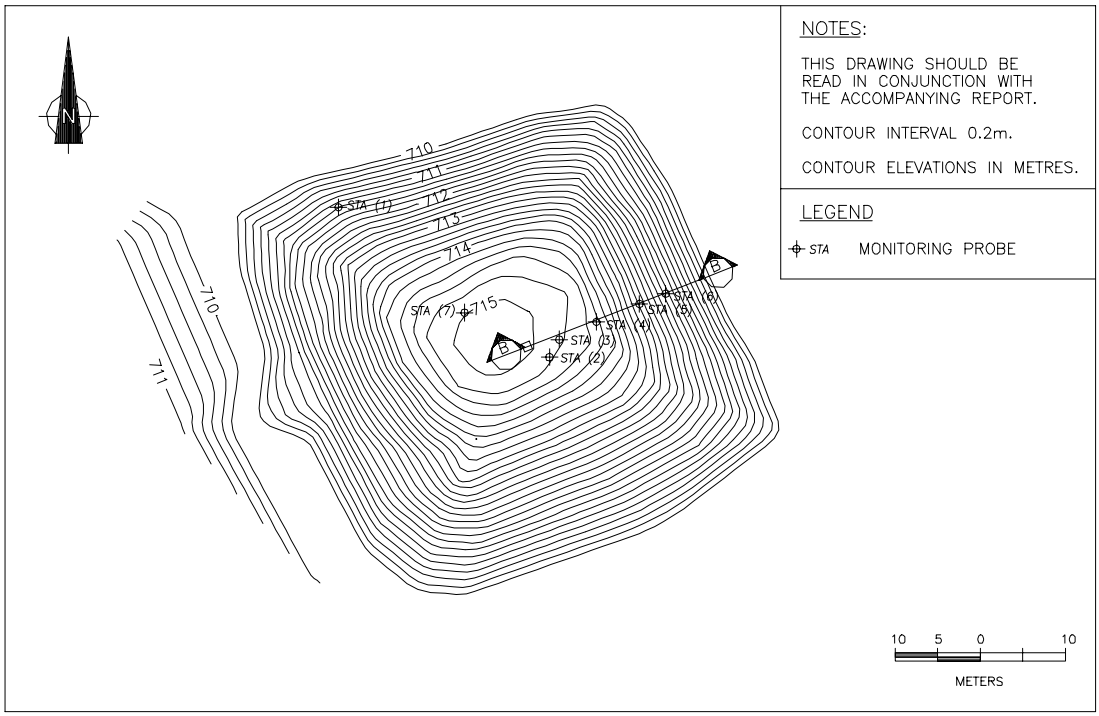

Figure 4-2: Site Plan, Waste Rock Pile 7/12

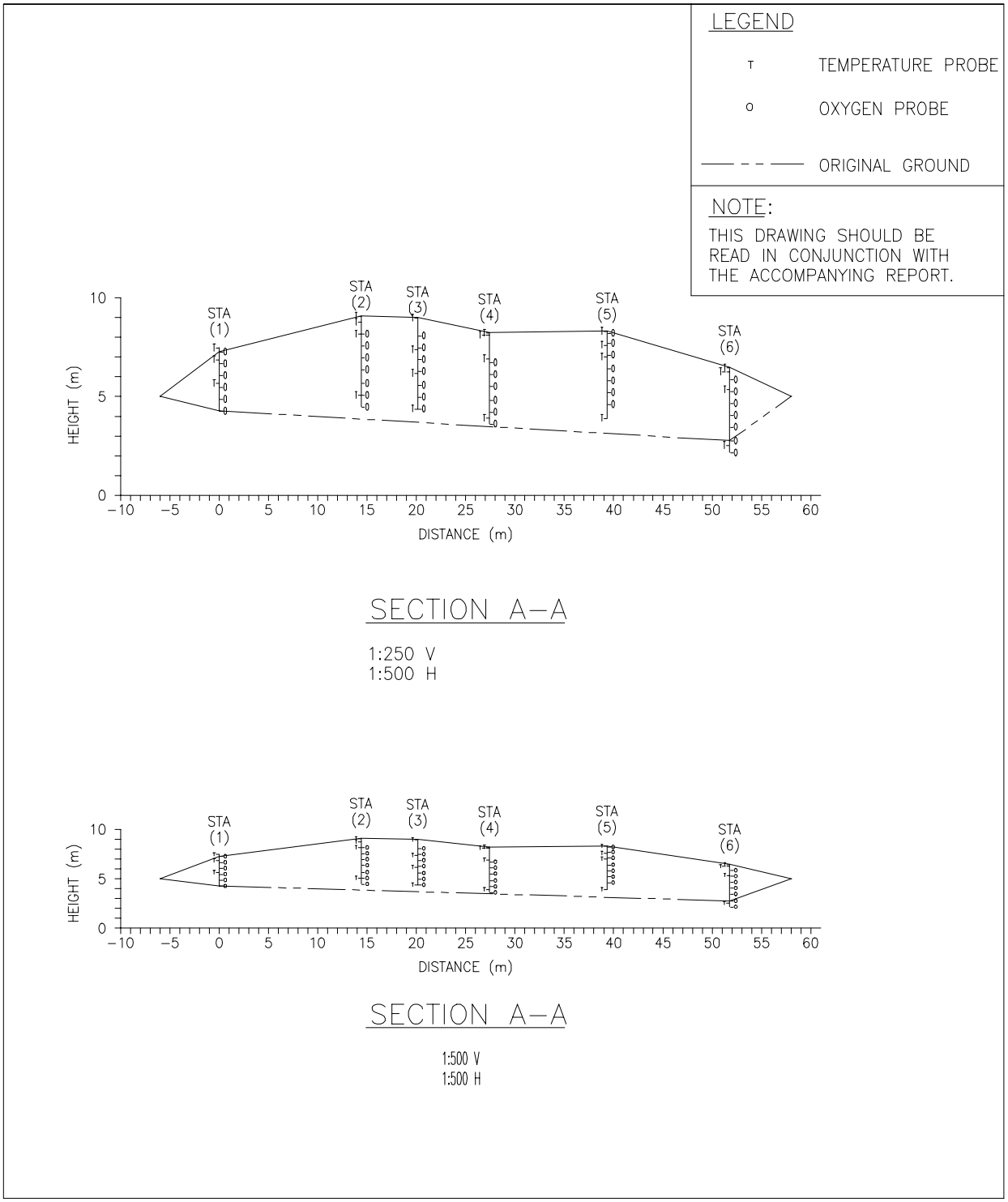

Figure 4-3: Cross-Section, Waste Rock Pile 18B

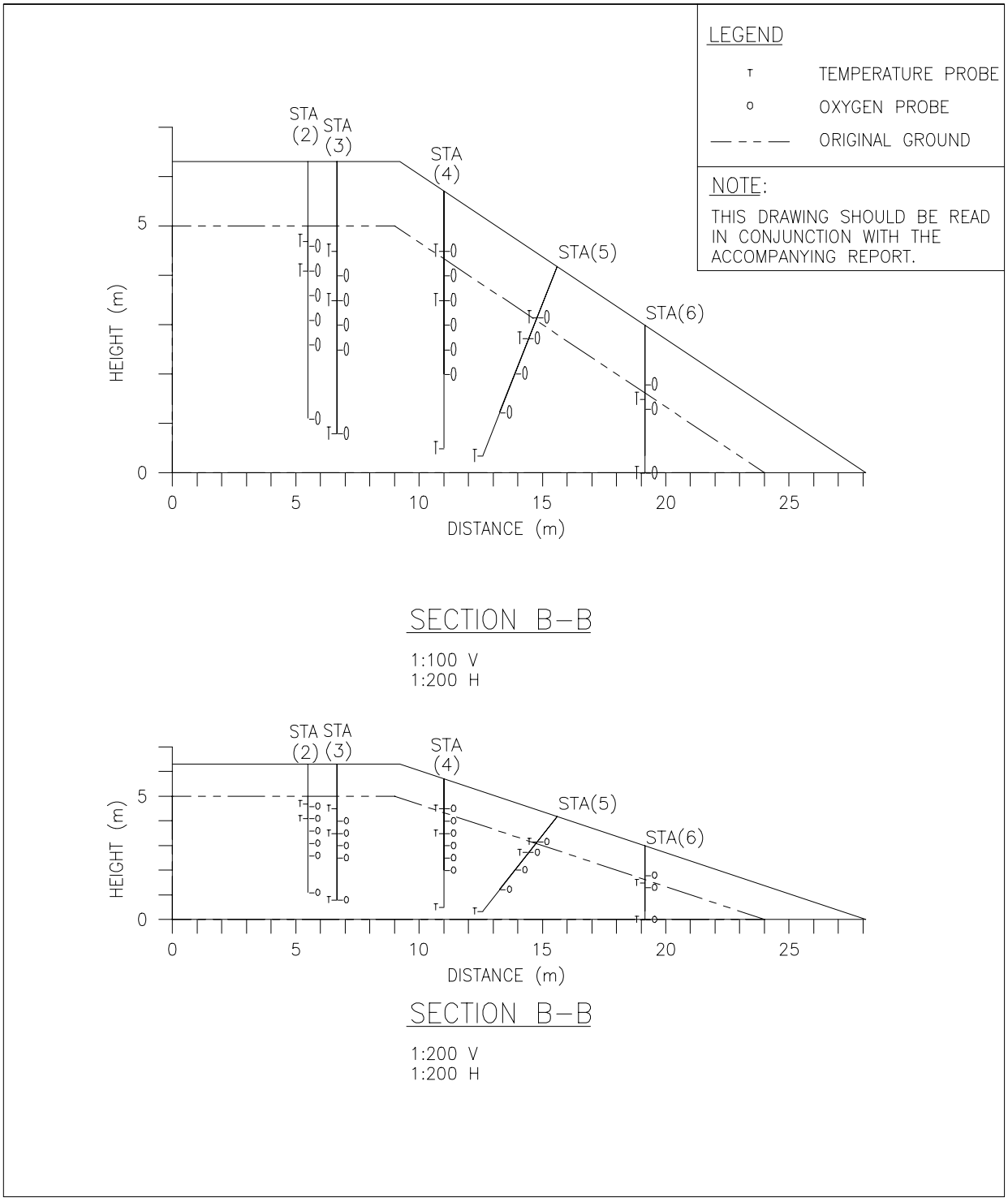

Figure 4-4: Cross-Section, Waste Rock Pile 7/12

4.1 Installation of Monitoring Probes

The installation of monitoring probes at pile 18B was carried out during the period of May 18-22, 1992, during which time, three pairs monitoring probes were installed to the technical specifications of ANSTO. Two monitoring probes (A and B) were spaced about 1.5 m apart at each of the three locations, numbered as 11, 12 and 13. The location of each monitoring probe cluster was selected in the field by Nolan Davis personnel to provide representative coverage of the piles. The location of the monitoring probes at pile 18B is shown in Figures 4-1.

An air rotary percussion hammer was used to drill through the full depth of the waste rock pile. The diameter of the drilled holes was 150 mm which allowed a sufficient annulus for the installation of backfill material without bridging. In each drilled hole, a prepared PVC liner was installed, with a number of 3 mm inside diameter nylon tubes attached to the perimeter for gas measurements. The PVC liner, which extended for the entire depth of each hole, was then backfilled with alternating layers of clean 500 mm thick gravel rock around the open port of each gas sampling tube. A sand pack and bentonite seal were provided between each port.

During backfilling operations, a detailed record was maintained of the levels of backfill placed within the probe hole and the overall volumes of backfill material placed. This data was then used to determine the effective radius of the outer boundary of the backfilled chambers, which is required for the analysis of air permeability measurements. Each probe hole was sealed with 300 to 400 mm of bentonite at the surface to prevent surface water infiltration and reduce the inflow of air.

A stainless steel plate was provided to mount the sampling valve assembly at the top of the PVC liner. In order to secure the Schraeder valves, the valves were tightened to the straight connector through the plate. Each of the nylon gas sampling tubes attached to the exterior of the PVC liner was terminated with a Schraeder valve.

Additional details on the field installations and equipment are contained in the previously noted "Field Techniques Manual".

4.2 Methodology

The FIDHELM model calls for a number of bulk physical parameters that require in situ measurements in the completed probe holes. These measurements are then used to compute the bulk physical parameters and subsequent gas transfer potential of the waste rock material. A brief summary of each of the measurements is provided below. The details on the procedures and equipment used to carry out these measurements are contained in the previously noted “Field Procedures Manual.” While the Manual is sufficiently detailed so that qualified technical personnel can perform the measurements in the field, most of the equipment required for the measurements has been specially fabricated by ANSTO personnel and may not be commercially available.

4.2.1 Thermal Conductivity

The thermal conductivity (λ) of a solid is a function of the thermal diffusivity (κ), the bulk density (ρ_s) and the specific heat (C_s):

$$\kappa = \frac{\lambda}{\rho_s C_s}$$

The heat conduction equation can be readily solved for a line source of heat to give the temperature distribution as a function of time.

Thermal conductivity was measured in the probe holes to determine the value and variability of this parameter within the waste rock pile. The measurement involves placing a linear heat source at some depth inside one of the monitoring probe holes and recording the temperature in the liner over a period of about 10 hours with the heat source switched on, and then, for a further 10 hours after it is switched off. The two data sets obtained in this way were fitted with a theoretical curve to obtain estimates of the thermal conductivity.

4.2.2 Air Permeability

The gas permeability, K (m^2), of a porous medium such as a waste rock pile is a coefficient which relates the gas convective velocity to an applied pressure gradient. For the air permeability measurements, dry compressed air was injected at predetermined depths into the waste rock pile through the pressure tubing on one side of the probe hole liner. The second pressure tubing, fixed on the opposite side of the liner, was used to monitor the consequent pressure rise in the gravel-filled chamber. The air flow was measured using a mass flow meter and pressure transducers monitored the pressure rise. The instruments were interfaced directly with a laptop computer. The air permeability was found by applying a theoretical relationship between air flow, pressure rise and chamber geometry.

4.2.3 Oxygen Diffusion Coefficient

The oxygen diffusion coefficient is a term of proportionality relating oxygen flux to oxygen concentration gradient. The oxygen diffusion coefficient of the waste rock material was determined with the injection and subsequent monitoring of the movement of a tracer gas SF_6 (sulphur hexafluoride). SF_6 is a heavy, inert, non-native gas, which is insoluble in water and is not consumed within the environment of the waste rock pile. SF_6 was injected into a selected gas sampling tube at a predetermined level within the waste rock pile with detection equipment set up at a second monitoring probe within 3 to 5 m of the injection point. Depending on the diffusion coefficient of the waste rock pile, the detection of SF_6 over this distance can require several hours. At the Heath Steele Mine site, this test procedure was carried out for approximately 24 hours. These measurements produced a value for the diffusion coefficient of SF_6 in the waste rock pile, which can then be readily converted to provide a value for the oxygen diffusion coefficient on the basis that both gases diffuse through a background gas which can be approximated as air.

4.3 Bulk Parameters

4.3.1 Oxygen Diffusion Coefficient

Oxygen diffusion coefficients measured in Pile 18B at the three new probe holes ranged from 2.1 x 10^{-6} to 3.6 x 10^{-6} m^2/s, with an average value of (3.0 ± 0.5) x 10^{-6} m^2/s. Measured values of diffusion coefficients in waste rock piles are not available in the published literature but a valid comparison can be made with the value of 3.6 x 10^{-6} m^2/s, which was estimated by Ritchie (1977) as being the diffusion coefficient at the Rum Jungle mine site in Australia.

4.3.2 Air Permeability

The measured air permeability with Pile 18B ranged from a minimum of (1.6 ± 0.1) x 10^{-10} m^2 to a maximum of (1.7 ± 0.7) x 10^{-8} m^2, with a mean value of 2.9 x 10^{-9} m^2, averaged over 24 measurements. These values are similar to the ones measured in a number of waste rock piles at other sites (Ritchie, 1977; Pantelis and Ritchie, 1991). The air permeabilities measured in pile 18B are high enough for advective processes to play a significant role in oxygen transport in the system.

4.3.3 Thermal Conductivity

Thermal conductivities measured at three locations in waste rock pile 18B had an average value of 1.17 ± 0.11 W/m·K, corresponding to an estimated average thermal diffusivity of (5.2 ± 0.5) x 10^{-7} m^2/s. This latter value falls within the range from 5 to 7 x 10^{-7} m^2/s used in earlier FIDHELM modeling studies (Pantelis and Ritchie, 1991).

4.4 In Situ Monitoring

Monthly measurements of temperature and gaseous oxygen content, available for piles 18B and 7/12, were used to assess the effectiveness of the composite soil cover of pile 7/12, and also, to validate the modeling results generated by FIDHELM.

The performance of the composite soil cover itself was also monitored on a regular basis after placement, including measurements of soil suction, soil temperature, water content, and oxygen concentration at a number of points throughout the pile. Heat-dissipation sensors and electrical-resistance sensors were used to measure soil suction, and time-domain reflectometry (TDR) was used to measure water content. In addition, two large-size lysimeters located directly below the cover have been used to evaluate the flux of water through the cover by collecting water that percolated through the cover. Because the cover pile is an enclosed system, the total volume of leachate generated by the encapsulated waste rock was captured with the drains installed beneath the pile and along the perimeter of the pile.

The following sections summarize the data collected to date from piles 18B and 7/12 for temperature, gaseous oxygen content and leachate quantities.

4.4.1 Gaseous Oxygen Content

As mentioned previously, the measurement of oxygen concentrations throughout piles 18B and 7/12 has been ongoing since 1988. Typical curves of gaseous oxygen content versus time for one station at piles 18B and 7/12 are presented in Figures 4-5 and 4-6. These two figures show the minimum and maximum values over time that was collected in all the ports at a given station. Average values over time were also calculated at each port using the entire set of data that was collected between the months of June and September inclusive. These calculated average values over time for summer conditions will be used for comparison with FIDHELM results because the form of FIDHELM used in the simulations does not allow for seasonal climatic variation. The calculated average summer values are to obtain representative values without the seasonal cyclic effects. The calculated averages for pile 7/12 were divided in 2 groups: *before* and *after* the placement of the cover. The average gaseous oxygen content profiles for pile 18B and 7/12 are presented in Figures 4-7 and 4-8 respectively. Figures 4-9 and 4-10 show a cross section of pile 7/12 with iso-values of gaseous oxygen content before and after the cover was placed, Figure 4-11 shows a cross section of pile 18B with the same type of iso-values.

The results of oxygen measurement from pile 7/12 indicate the following:

- Prior to placement of the cover at pile 7/12, oxygen concentrations at station 3, which is a typical station, ranged from 7.3 percent to 20.8 percent. The overall range of concentration in the other monitoring stations was 3.2 percent to 20.8 percent.
- About a year after pile 7/12 was reconstructed, the oxygen levels, particularly near the surface of the pile, are influenced by the weather, with gaseous oxygen content increasing in the winter. In summer, as temperatures in the pile increase, some thermal convection of oxygen into the pile causes oxygen levels to increase.
- After cover placement in September 1991, there was a dramatic decrease in oxygen concentrations throughout the pile.
- High temperature and relatively low oxygen concentrations observed at the reconstruction of the pile and during mid-1989 indicate that reconstruction had disturbed the steady state of oxygen / gas transport expected in such piles. This makes generalizations about the trends in temperature and oxygen concentrations in pile 7/12 prior to cover emplacement of doubtful value for comparison with pile 18B and with FIDHELM results.

The gaseous oxygen content profiles at pile 18B (Figures 4-7 and 4-8) indicate that the gaseous oxygen content increases with depth at some of the monitoring station, in particular Stations 3 and 4. This is an indication that some additional gas transport mechanisms are present with the diffusion process.

The magnitude of the change in oxygen concentration in Pile 7/12 is more clearly illustrated in Figure 4-12, where the oxygen profiles are plotted for May 1990 and 1991 (prior to cover placement) and May 1992 and 1993 (after cover placement). It is apparent from Figure 4-9 that the most significant decrease in oxygen occurred within several months after cover placement. However, monitoring results indicate oxygen within the system is still being depleted. The oxygen concentration in pile 7/12 dropped from about 20 percent in May 1991 to about one percent in May 1992 and to 0.2 percent or less in May 1993.

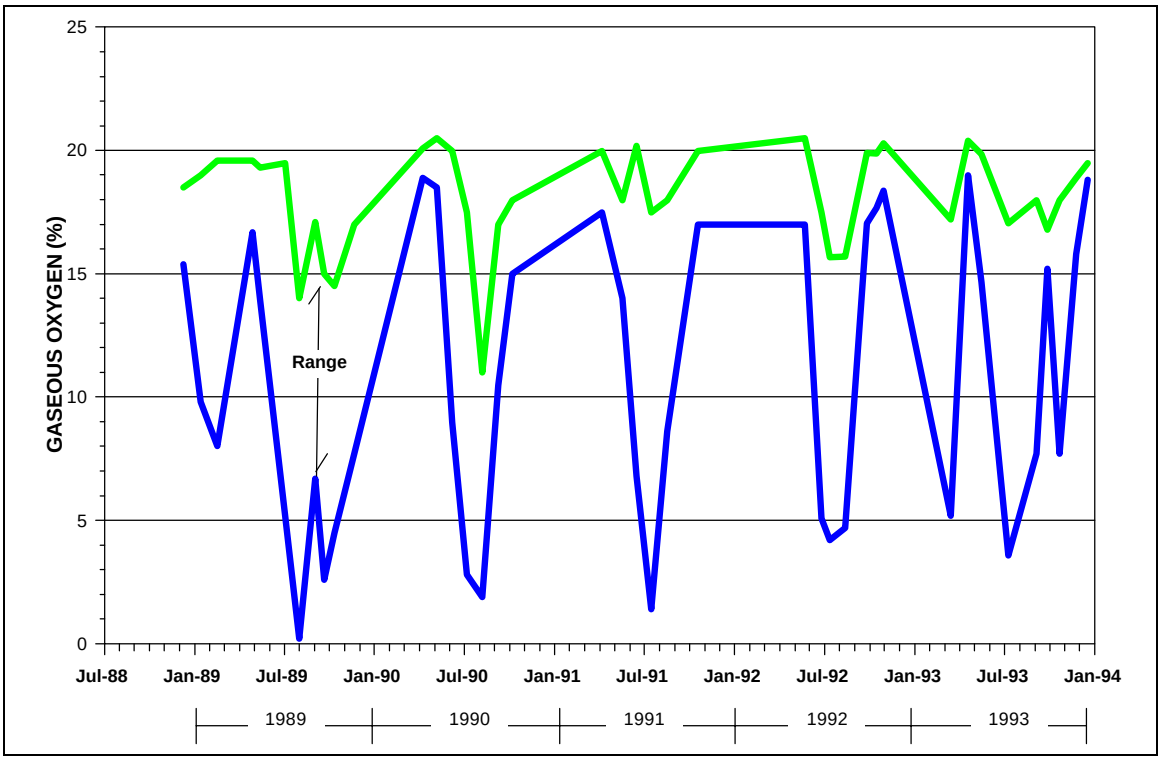

Figure 4-5: Minimum and Maximum of Measured Gaseous Oxygen Content vs Time, Station 3, Pile 18B.

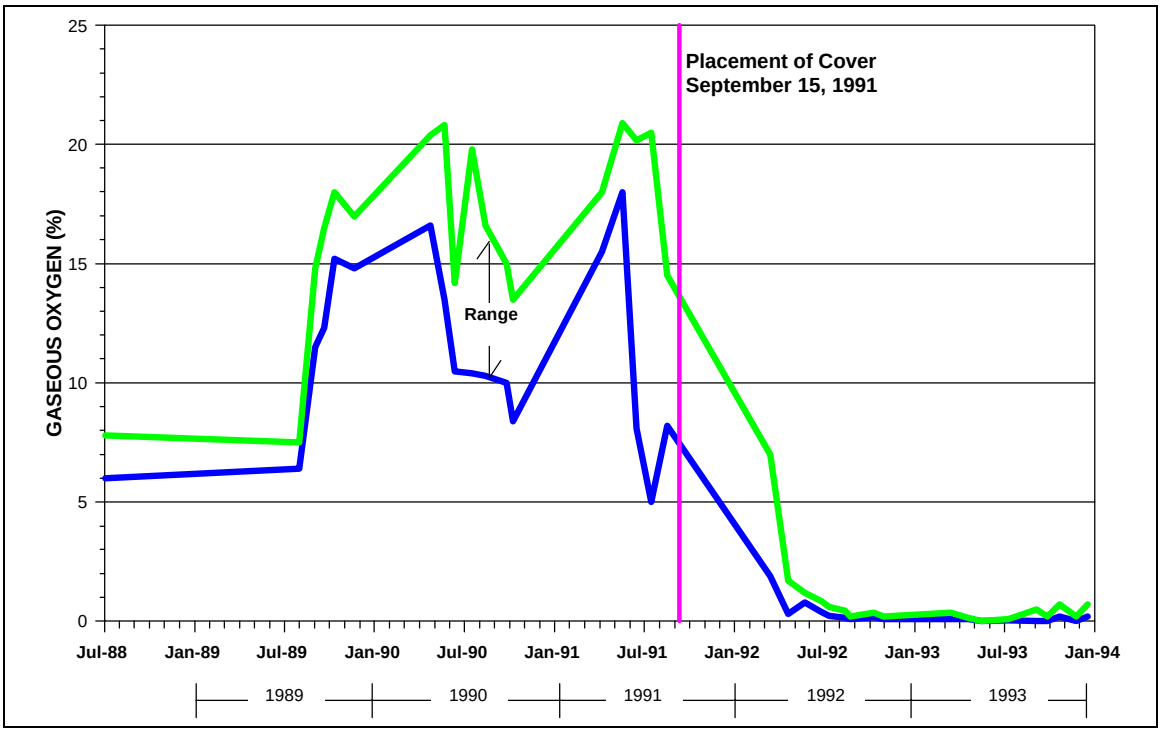

Figure 4-6: Minimum and Maximum of Measured Gaseous Oxygen Content vs Time, Station 3, Pile 7/12

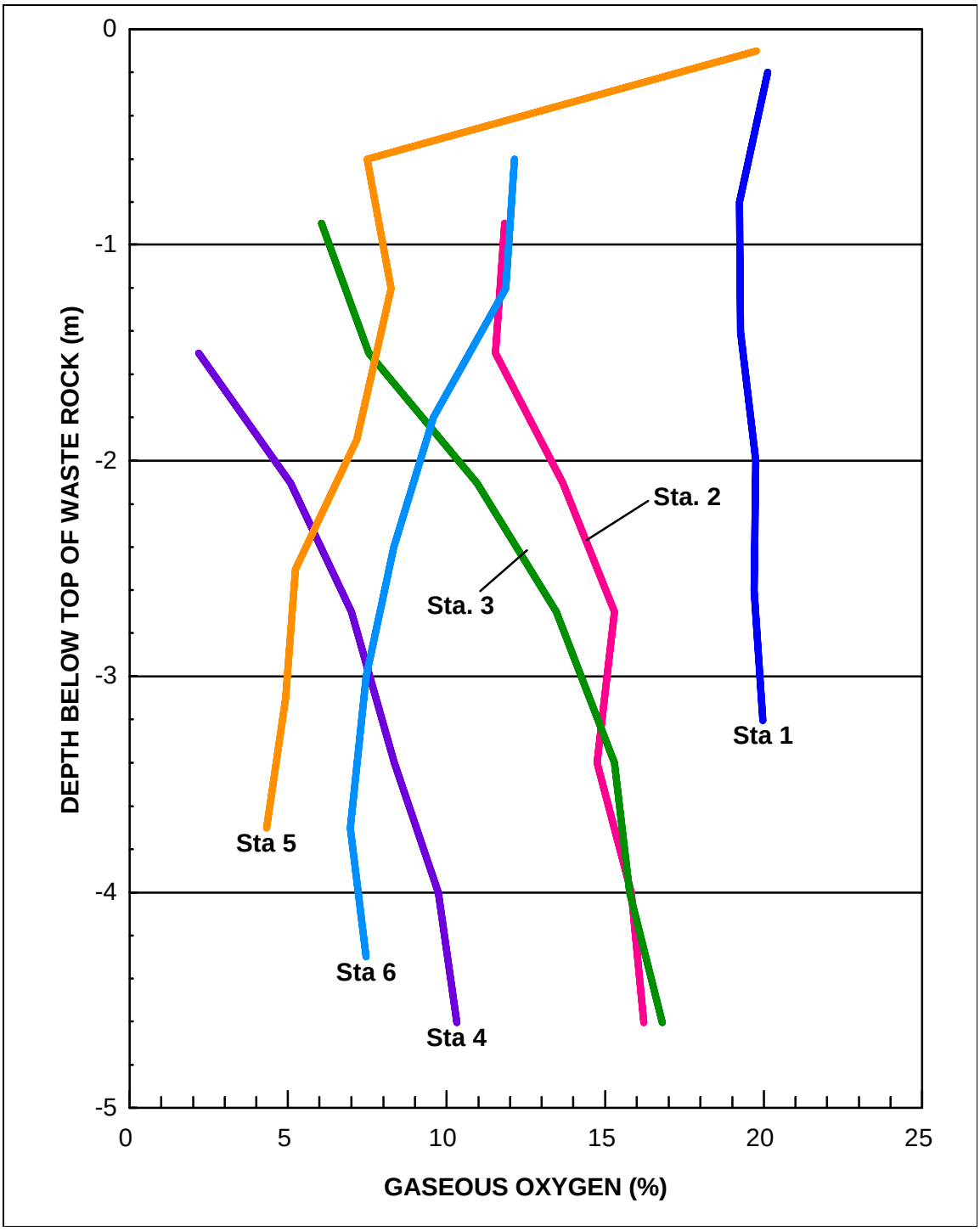

Figure 4-7: Measured Gaseous Oxygen Content vs Depth, Average of Summer Values, Pile 18B

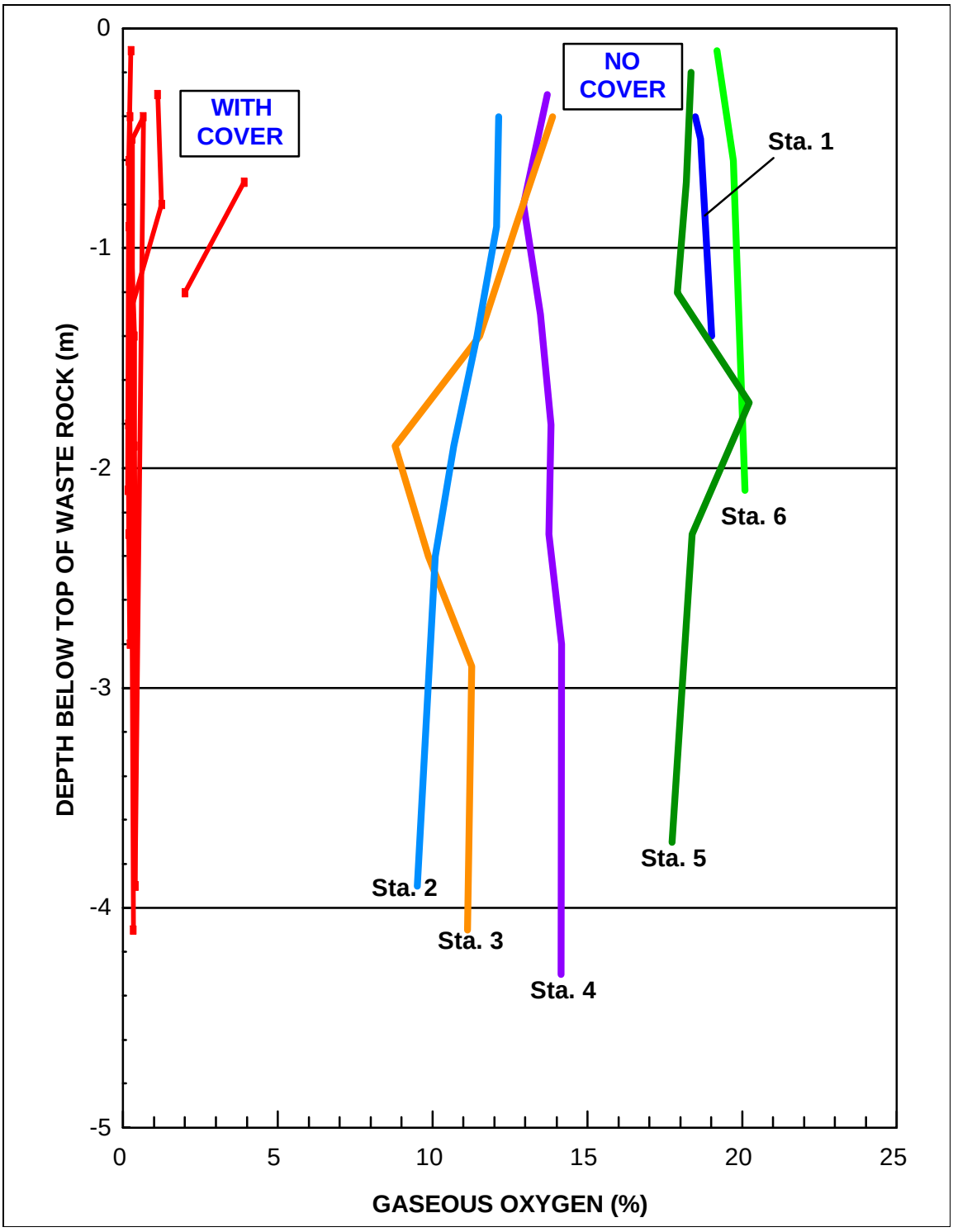

Figure 4-8: Measured Gaseous Oxygen Content vs Depth, Average of Summer Values, Pile 7/12

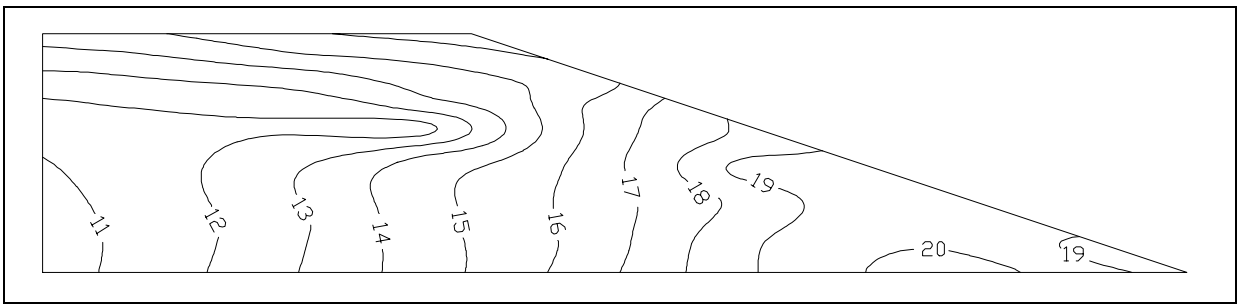

Figure 4-9: Iso-Values, Measured Gaseous Oxygen Content, Average of Summer Values, Before Placement of Cover, Pile 7/12

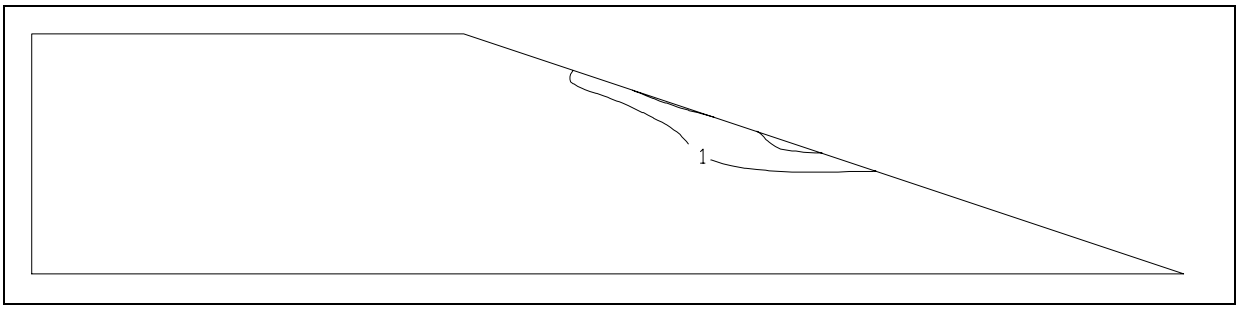

Figure 4-10: Iso-Values, Measured Gaseous Oxygen Content, Average of Summer Values, After Placement of Cover, Pile 7/12

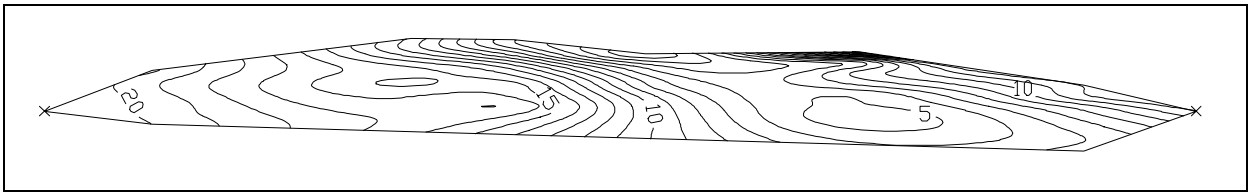

Figure 4-11: Iso-Values, Measured Gaseous Oxygen Content, Average of Summer Values, Pile 18B

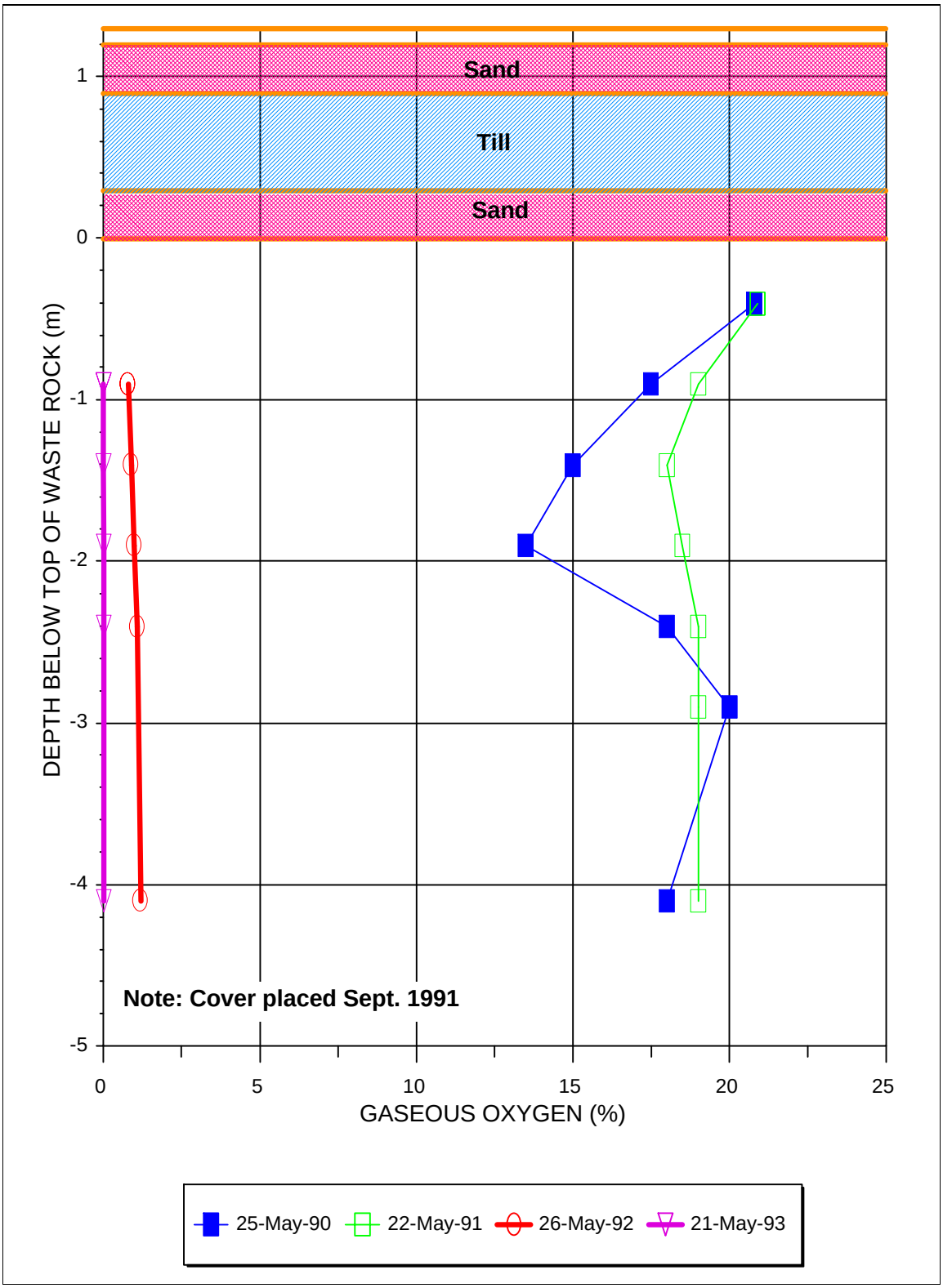

Figure 4-12: Measured Gaseous Oxygen Content Profile, Station 3, Pile 7/12

4.4.2 Temperature

Similar figures as the ones presented in the previous section for the gaseous oxygen content were also prepared for the in situ temperature data for piles 18B and 7/12. Figures 4-13 and 4-14 show the minimum and maximum temperature variation over time, Figures 4-15 and 4-16 show the temperature profiles using calculated average summer values. Figure 4-17 and 4-18 show a cross section of pile 7/12 with iso-values of temperature before and after the cover was placed while Figure 4-19 shows a cross section of pile 18B with the average summer temperature iso-values. As indicated in the previous section, the average summer values were used to validate FIDHELM results.

The presented temperature monitoring results for pile 7/12 indicate the following:

- In 1989 very high temperatures (50°C) were noted at the centre of the pile, which are indicative of the very rapid establishment of the exothermic oxidation process, and indicating that the waste rock has been disturbed by the aeration from its manipulation.
- By 1990, temperatures decreased to under 40°C, indicating a stabilization of the reaction process.
- There was not a direct correlation between temperatures and weather conditions until about January 1990.
- At station 3 for example, the temperatures immediately prior to placement of the cover ranged from 17.1°C to 24.0°C. One month after cover placement, temperatures dropped to a range of 14.1°C to 18.3°C.

The magnitude of the temperature change prior to and after cover placement is more clearly illustrated in Figure 4-20, which shows temperature profiles measured at a typical station in May 1990 and 1991 before cover placement and in May 1992 and 1993 after cover placement.

As with oxygen concentration, the most significant decrease occurred within several months after cover placement. However, temperatures are still decreasing throughout the pile but at a much reduced rate. For all temperature probes installed in pile 7/12, there has been a significant temperature decrease on a year to year basis since placement of the cover.

The temperature profiles at pile 18B indicate that the temperature generally increases with depth. This is an indication that some additional gas transport mechanisms are present with the diffusion process.

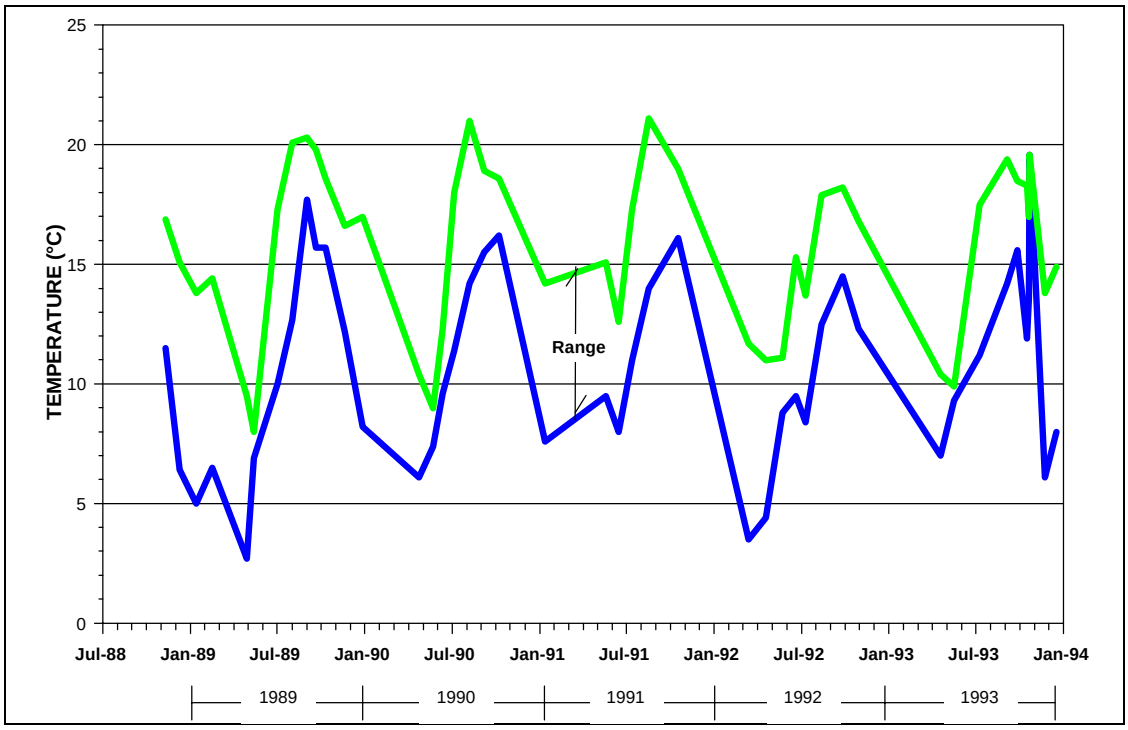

Figure 4-13: Minimum and Maximum of Measured Temperature vs Time, Station 3, Pile 18B.

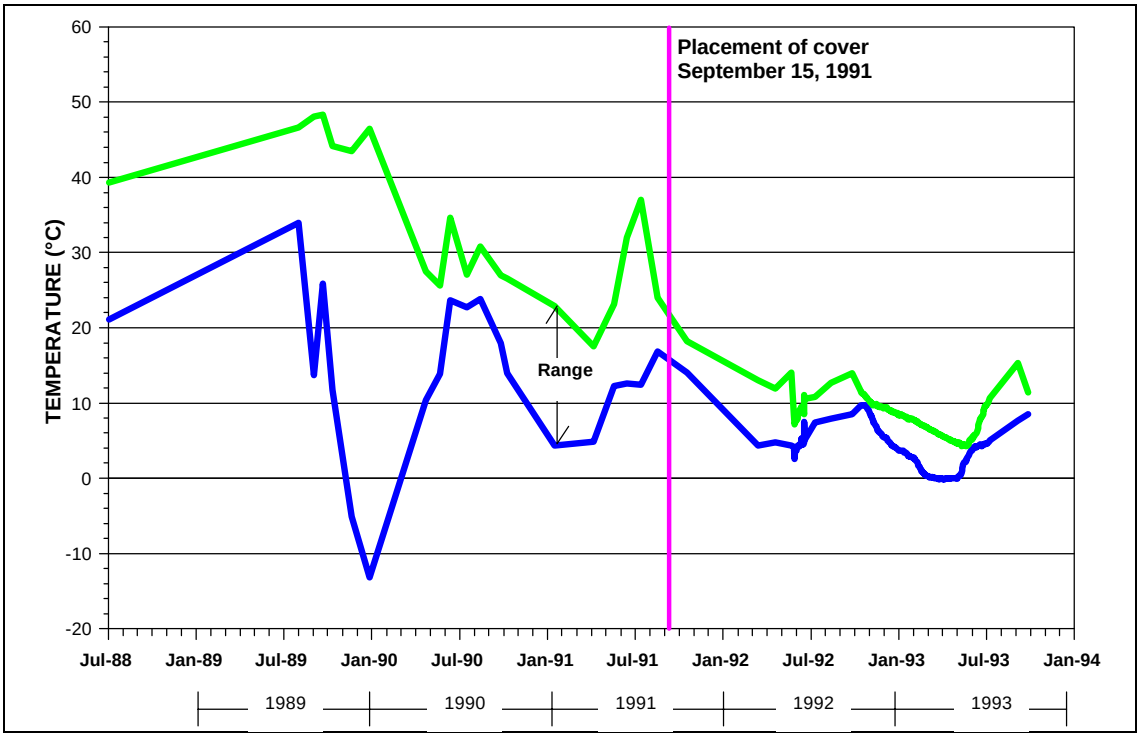

Figure 4-14: Minimum and Maximum of Measured Temperature vs Time, Station 3, Pile 7/12.

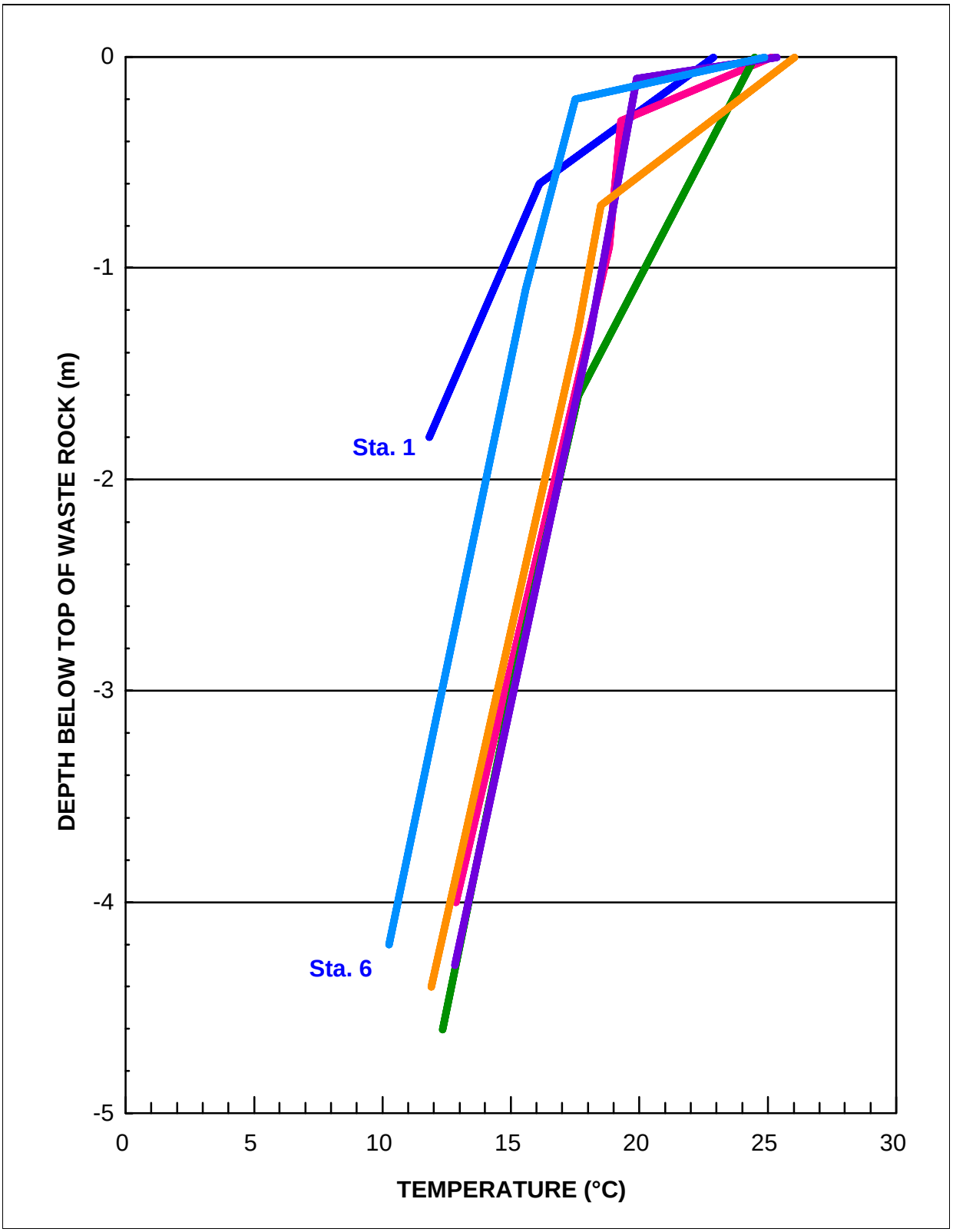

Figure 4-15: Measured Temperature vs Depth, Average of Summer Values, Pile 18B

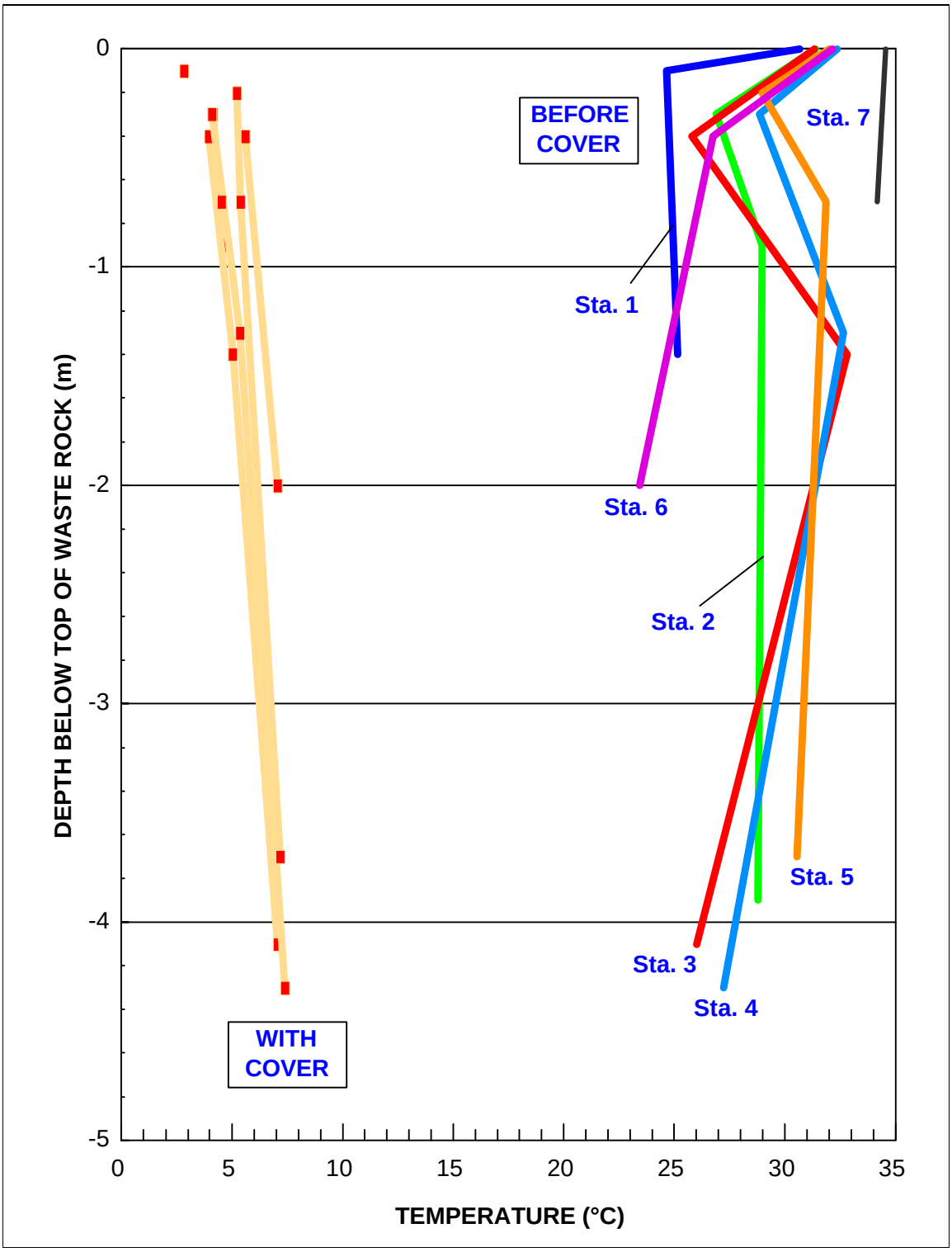

Figure 4-16: Measured Temperature vs Depth, Average of Summer Values, Pile 7/12

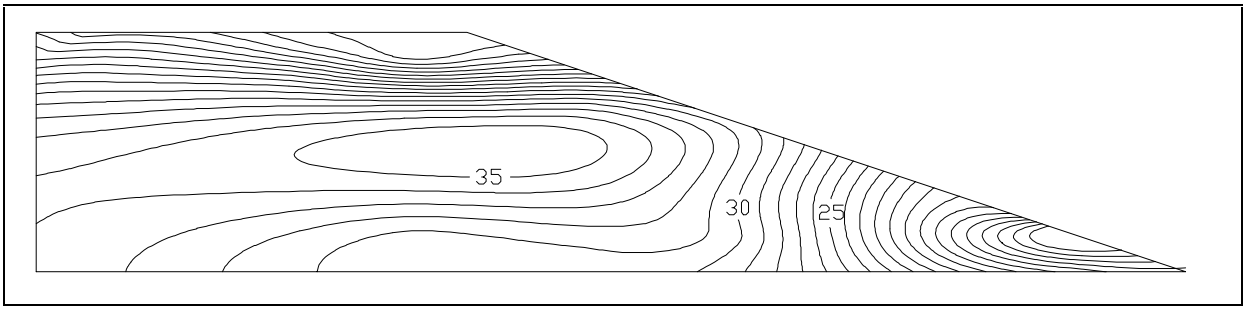

Figure 4-17: Iso-Values, Measured Temperature, Average of Summer Values, Before Placement of Cover, Pile 7/12

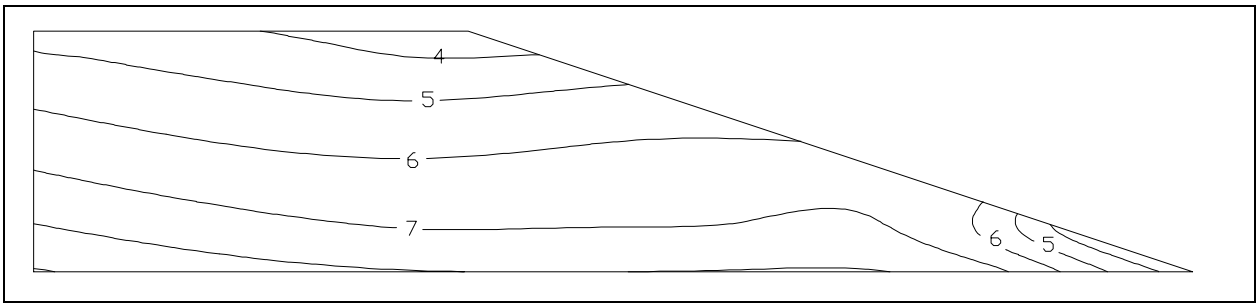

Figure 4-18: Iso-Values, Measured Temperature, Average of Summer Values, After Placement of Cover, Pile 7/12

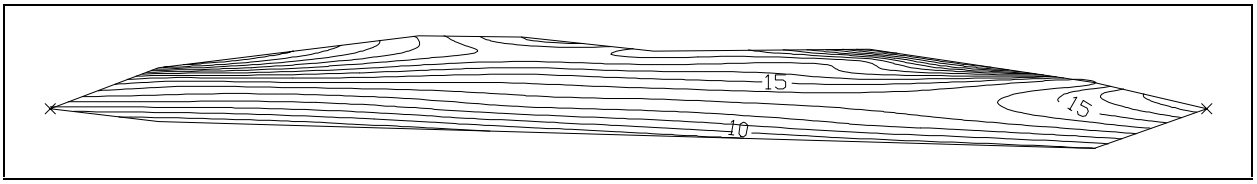

Figure 4-19: Iso-Values, Measured Temperature, Average of Summer Values, Pile 18B

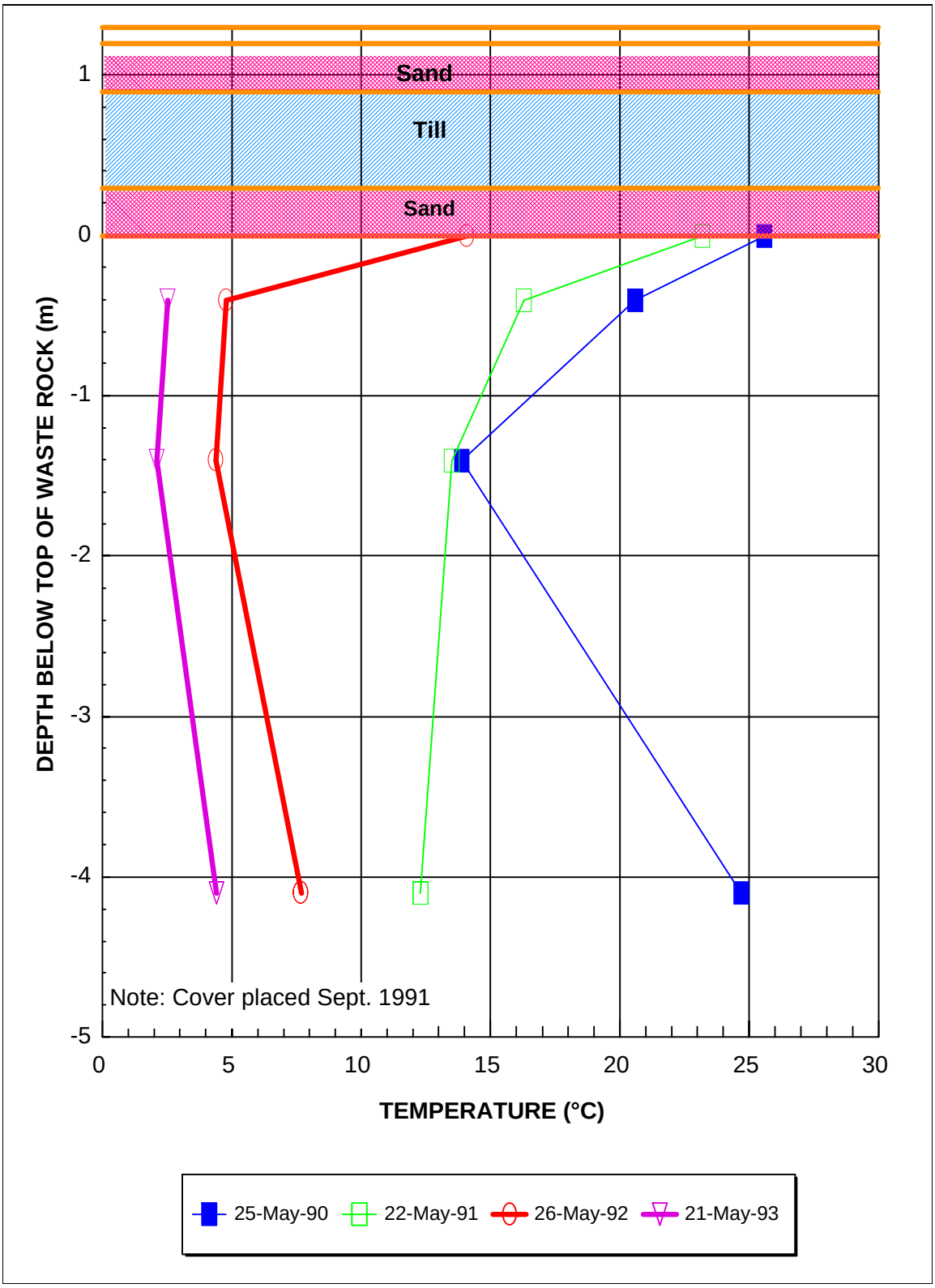

Figure 4-20: Measured Temperature Profiles, Station 3, Pile 7/12

4.4.3 Seepage Through Cover

During the relocation of pile 7/12 and the construction of the soil cover, drains were installed to collect the leachate at the base of the pile (Center Drain) and at the interface between the waste rock and the soil cover (Perimeter Drain). Two lysimeters were installed immediately below the soil cover but above the waste rock to collect water infiltration through the cover. The results of analytical testing of leachate monitoring to date for pile 7/12 are presented in Table 4-1. Since the pile is a closed system, the leachate collected after placement of the cover represents the total volume of leachate that has moved through the pile. In the 2 years since cover placement, a total of about 1,000 litres has been recovered. The lysimeter discharge data shown in Table 4-2 indicate that only a small portion of the rainfall percolates through the cover (about 1 to 2%).

Table 4-1: Water Quality Summary, Leachate, Pile 7/12

	July 1989 - Oct 1990	1992	1993
pH	2.1 - 2.8	2.3 - 2.9	3.0 - 3.2
Acidity($CaCO_3$), mg/L	15,800 -73,250	15,800 - 54,450	NA
Sulphate, mg/L	12,700 - 43,440	5,140 - 71,042	9,970 - 73,854
Dissolved iron, mg/L	3,510 - 13,767	15,800 - 54,000	5,000 - 30,844

NA: Not available.

Table 4-2: Lysimeter Measurements

	Rainfall		Lysimeters	
Date	Depth, mm	Volume, litre	Volume, litre	Ratio, %
June 24 - August 18, 1992	198	2455.2	50.3	2.0%
May 21 - July 13, 1993	188	2331.2	20.0	0.9%

Note : Total areal surface of lysimeters = 12.4 m^2

A simple seepage analysis using a transient saturated/unsatured finite element model indicated that with a water cover up to the upper boundary of the erosion protection layer, the steady state infiltration rate through the cover is about 1.5 mm per day. The results also indicated near steady state conditions to be achieved about 8 hours after the modeled cover was subject to a constant water cover. The numerical simulation had saturated conditions for initial conditions. Figure 4-21 summarizes the geometry, the soil parameters and the boundary conditions used in the numerical seepage model.

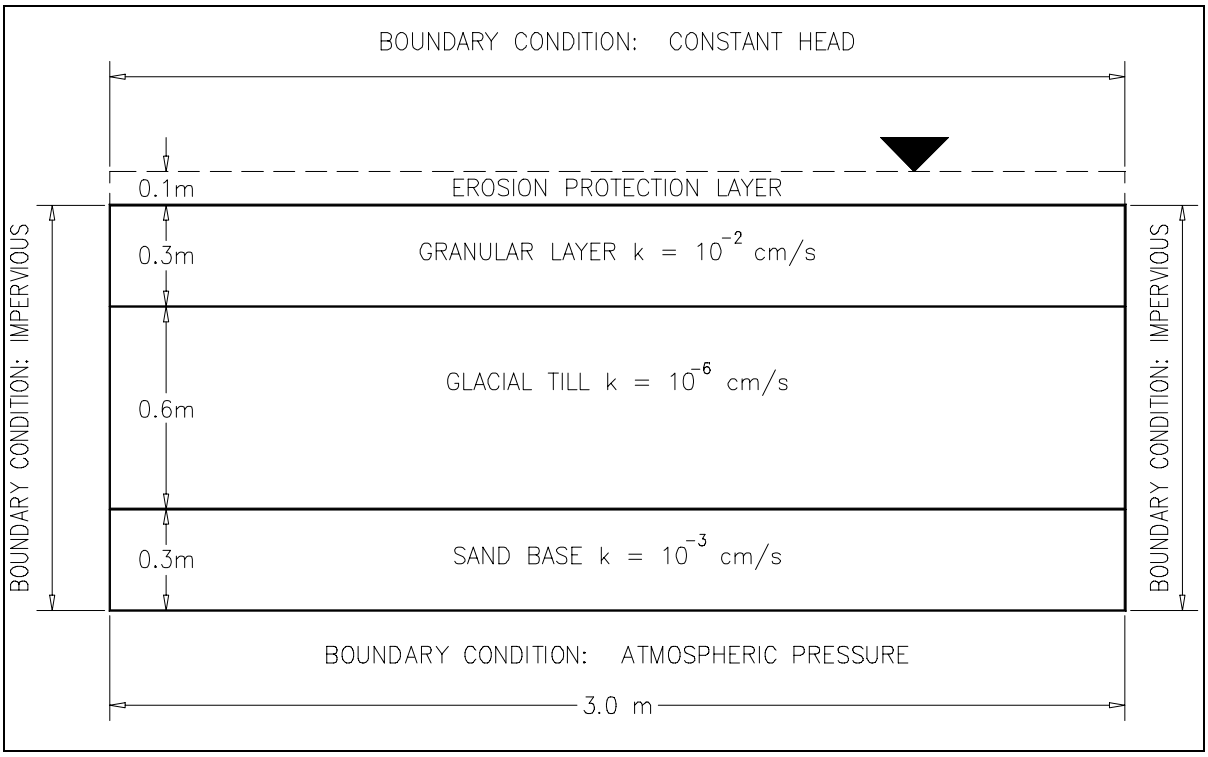

Figure 4-21: Seepage Analysis Conditions Summary, Composite Cover, Pile 7/12

These simulations corresponds to conditions where the upper boundary of the cover is covered with water. In reality, the upper zone of the soil cover will become unsaturated between precipitation events. If the upper zone of the soil cover does not maintain its complete saturation, the seepage quantities and velocities will be reduced because the system will have to saturate before steady flow conditions are achieved again.

Performance monitoring of instrumentation to measure soil suction and moisture content in the composite soil cover has shown that the cover is performing as designed, with moisture content in the till showing little change from measurements taken immediately after cover placement (Yanful et al 1993).

5. FIDHELM MODELING

5.1 Model Description

The computer model FIDHELM, developed by ANSTO, was used to gain an understanding of the gas transfer mechanisms that dominate the oxidation of the Heath Steele waste rock piles. FIDHELM models waste rock piles as a three phase system consisting of a rigid solid porous phase through which flows a gas and water phase. It models oxygen transport and depletion, heat transport, production and reactant depletion in the solid phase. Included is the transport of a single conservative chemical in the aqueous phase. The chemical is a product of the oxidation of the solid reactant. FIDHELM is a finite difference model which is solved using a Eulerian-Lagrangian approach that can consider a two-dimensional vertical slice or a truncated cone (cylindrical coordinates) shaped waste rock pile.

Oxygen supply is seen in the model as a two stage process; namely transport of oxygen in the air through the pore space of the pile followed by its transport from the pore space to reaction sites within the particles which comprise the pile.

Gas transport through the pore space is, initially at least, by diffusion and is driven by oxygen concentration gradients caused by the consumption of oxygen in the pyritic oxidation process. Transport can also be by advection driven by pressure gradients. These can arise from density gradients which in turn are caused by temperature gradients resulting from heat released in the oxidation of pyrite. This type of advection (convection) has been observed experimentally. Pressure gradients can also arise in other ways such as from wind passing over the pile but the version of FIDHELM used for this project does not incorporate pressure fields on the outside which deviate from static atmospheric equilibrium.

Davis and Ritchie (1986, 1987) considered the case where gas transport through the pore space was by diffusion. Their model is applicable to columns, tailings dams and heaps with low ratio of height to width, and low heaps where convection is negligible. Cathles (1980) considered the case where convection through the pile was the only macroscopic transport process. FIDHELM attempts to combine air convection and diffusion since it is likely that the initial period (i.e. starting up period) preceding the onset of convection is sufficiently long to warrant the inclusion of the two macroscopic transport mechanisms. The mathematical and numerical development is fully described in the FIDHELM user's guide which is included in Appendix III of this report. Additional mathematical background to the model and some results are also presented by Pantelis and Ritchie (1991, 1992).

A basic parameter required for the manual is the rate of oxygen consumption by the material at any point in the pile under the conditions which apply at that point. This parameter is called the intrinsic oxidation rate (IOR), generally expressed in units of $kg[O_2]/m^3/s$. The IOR may depend on many parameters, such as:

- physical conditions: - temperature
  - particle size distribution
  - form of pyrite
- chemical conditions: - oxygen concentration
  - sulphur density
  - pH
  - Fe^{3+}/Fe^{2+} ratio
- microbiology: - bacterial type
  - bacterial density

In practice, limited data is available for only three of the above parameters:

- oxygen concentration: - falloff at low oxygen concentrations (linear or monod)
- sulphur density: - falloff at low sulphur concentrations (linear or monod)
- temperature: - falloff at high temperatures (monotonic decrease above a defined limit). Based on limited information from elsewhere, the IOR is not significantly dependent on temperature down to freezing.

The parameters that are calculated by FIDHELM consist of the gaseous oxygen content, the reactant (sulphur) density, the temperature, gas pressure, the sulphur oxidizing rate as a function of space and time, the aqueous phase mass fraction, the air flow velocity, the sulphate load, the global oxidation and the global oxidation rate. The sulphate load is the time dependent flux of sulphate in drainage water at the base of the pile integrated over the base of the pile. The global oxidation is the total amount of oxidisable material (sulphur) oxidised up to a given time.

Although FIDHELM is a very sophisticated numerical model, some of the basic processes simulated by FIDHELM were approximated or simplified by making some assumptions in the version of FIDHELM used in the present study. Most of these approximations or simplifications are reasonable. The following presents some of these approximations:

- The gas phase equations in the present version of FIDHELM use an approximated relationship instead of the ideal gas law but a modified version of FIDHELM (not available yet) which incorporated the ideal gas law in the model confirmed the validity of the approximation used in the current version of FIDHELM.

- Changes in temperature in the near surface of a pile due to changes in ambient temperature at the pile surface decrease in amplitude with increasing distance from the pile surface. Typically, the decrease is by about a factor of ten some 5 m from the surface for changes on the timescale of a year and some 1 m from the surface for changes on the timescale of a month. Hence, unless the piles are very small, or oxidation rates are high enough to generate

high temperatures within the pile, or oxidation is confined to the top meter or so of the pile, neglect of the temperature dependence of the IOR does not impact greatly on simulated physico-chemical conditions within a pile. Moreover, there are few data available on the temperature dependence of the IOR of bulk pile material and it is ANSTO's experience, from measurements in a pile in a similar climatic regime to those at Heath Steele, that the temperature dependence of the IOR is significantly less than that expected on the basis of laboratory experiments quoted in the literature.

- The IOR of the material is assumed to be constant in time even though oxidation may lead to processes such as exfoliation. The simplification is warranted partly because of lack of data on very long term (tens to hundreds of years) changes in the IOR and partly the desire to assess the impact of gas transport processes rather than predict the pollution load from a particular pile at a particular time.

- The capillary fringe present in unsaturated conditions is considered typically small relative to the height of the pile and is approximated considering the water volume fraction along the entire pile vertical profile being uniform. Again, results from the "improved" version of FIDHELM compare very well with the ones generated by the actual version.

- In calculating the sulphate loads, the following assumptions are made:
  - the oxidisable sulphur is all in the form of pyrite;
  - the sulphate is produced in proportion to the oxygen consumption in the pile, the proportionality being given by the stoichiometric ratio of the governing chemical equation (Section 6.1);
  - the sulphate is in the mobile pore water as soon as it is produced;
  - the transport of water is based on Darcy's law;
  - there is no loss of sulphate, as for example through precipitation;
  - solute dispersion and diffusion are ignored.

As indicated above, the updated version of FIDHELM will contain fewer simplifying assumptions than the version used for the simulations presented in this report. It is not expected that the removal of these simplifications will change the results of the simulations in a significant way. The new version will include:

- external wind pressure effects along the pile boundary;
- ambient temperature variability;
- complete transient unsaturated aqueous transport, including the entire suction curves (full capillary fringe);
- ideal gas law equation and the removal of the Boussinesq approximation for the gas mass balance equation;
- heterogeneous material properties (without abrupt discontinuities).

5.2 Applications: Heath Steele Piles

The piles 7/12, 18A, 18B and 17 were modeled as truncated cones with height height y_o and radius x_o. Table 5-1 gives the values used for these parameters for each of the piles together with values of a few other parameters specific to each pile. Table 5-2 defines the symbols for the parameters used in FIDHELM together with the values used for these parameters in the simulations of pile behavior. The choice of the values for some of the more important parameters is discussed below.

The values for bulk physical parameters used in FIDHELM to model the four piles 7/12, 18A, 18B and 17 are based on data obtained in the Waste Rock Study and on measurements of some bulk physical properties in pile 18B carried out in June 1992. These bulk physical properties were the gas permeability, the gas diffusion coefficient and the thermal diffusivity (see Section 4). In all of the simulations, the average value found for the thermal diffusivity κ=5 x 10^{-7} m^2/s was used; in most of the simulations, the average measured value of the gas permeability K=2.9 x10^{-9} m^2 was used.

In the present study, a constant ambient temperature, T_{amb}, is assumed on the outer face of the pile. Similarly, the infiltration rate used in the model, Q_w, is assumed to be constant and taken as the annual average of the *Total Precipitation* over the entire year.

Three measurements of the oxygen diffusion coefficient D were carried out by ANSTO in the pile 18B. The definition of D can be stated as:

$$D = \Lambda(\varepsilon_g) D_b$$

where Λ is the tortuosity, a function of the gas volume fraction ε_g, which can be assumed as:

$$\Lambda = \Lambda_o \varepsilon_g$$

where Λ_o is the tortuosity factor of the porous medium. For a constant infiltration rate Q_w, the water volume fraction ε_w is given by:

$$\varepsilon_w = (1-\varepsilon_S)\left(\frac{Q_w \mu_w}{K \rho^w g}\right)^{1/3}$$

The gas volume fraction is given by:

$$\varepsilon_g = 1 - \varepsilon_s - \varepsilon_w$$

Given these definitions, with the values in the Table 5-1 and Table 5-2, and the average measured value of D as (3.0±0.5) x 10^{-6} m^2/s, Λ_o can be calculated as:

$$\Lambda_o = 0.59 \pm 0.10$$

For simplicity, FIDHELM includes a temperature ceiling $T_{kill} > 0$ at which the microorganisms cease to be effective as catalysts for the oxidation of pyrite. In reality, the temperature dependence is more complicated and that there are a range of microorganisms which come into play at different temperatures (Lawrence et al. 1986; Norris et al. 1987). An additional parameter T_{sick} is introduced to define a temperature above which the microorganism catalytic activity diminishes.
The average IOR used for these simulations was taken as 10^{-8} kg[O_2]/m^3/s which is considered typical for the type of waste rock encountered at Heath Steele as indicated by the work carried out by Harries et al. (1981) in Australia.

To further study the gas transfer mechanisms at Heath Steele, piles 7/12 and 18B were modeled using two additional IOR values (10^{-7} and 10^{-9} kg[O_2]/m^3/s) and the maximum air permeability value measured in the field (10^{-8} m^2). These additional values were used to assess the possible effects of the inhomogeneity of the piles in regards to gas transfer.

Table 5-1: Physical Parameters, Piles 18A, 18B, 17 and 7/12

Parameter	Unit	18A	18B	17	7/12
Radius of Pile, x_0	m	20	34	80	24
Height, y_0	m	3.4	6.7	10.5	5
σ_1 (for IOR=10^{-8} kg[O_2]/m^3/s)	m^3/kg/s	2.709×10^{-9}	1.354×10^{-9}	5.708×10^{-9}	8.146×10^{-10}
Solid Volume Fraction, ε_s		0.763	0.763	0.763	0.690
Density of Reactant, ρ_{rs}	kg/m^3	59	118	28	150
Side Slope, Angle of Pile, θ	radians	0.291	0.245	0.245	0.321

Table 5-2: FIDHELM Parameters

Quantity	Definition	Values	Type[a]
T_{amb}	ambient temperature (°C)	3	M
ρ_o^a	intrinsic air density (kg/m^3)	1.2	C
g	acceleration due to gravity (m/s^2)	9.8	C
K	Air permeability (m^2)	2.9x10^{-9} 10^{-8}	M
μ_a	viscosity of air (kg/(m·s))	1.9x10^{-5}	C
β	thermal coefficient of volume expansion (K^{-1})	3.47x10^{-3}	C
D_b	oxygen diffusion coefficient of oxygen in air (m^2/s)	2.26x10^{-5}	C
σ_1	parameter in particle oxidation model (m^3/(kg·s))	Table 5-1	E
ρ_s	bulk density of solid (kg/m^3)	2200	M
c_s	specific heat of solid (m^2/(s^2·K))	866	E
c_a	specific heat of air (m^2/(s^2·K))	1.06x10^3	C
κ	thermal diffusivity (m^2/s)	5.0x10^{-7}	M
δ	heat of oxidation reaction per mass of reactant oxidized (J/kg)	2.2x10^7	C
ω_o^a	mass fraction of oxygen in air	0.22	C
ε	mass of oxygen used per mass of reactant in oxidation reaction	1.746	C
S	IOR (kg[O_2]/m^3/s)	10^{-8} 10^{-7} 10^{-9}	E
Q_w	infiltration rate (m/y)	1.134	M
μ_w	viscosity of water (kg/m·s)	0.001	C
ρ^w	intrinsic water density (kg/m^3)	1000	C
c_w	specific heat of water (m^2/(s^2·K))	4.184x10^3	C
T_{kill}	temperature at which microorganisms cease to be effective as catalysts (°C)	50	E
T_{sick}	temperature above which the microorganism catalytic activity diminishes, $T_{amb} \le T_{sick} \le T_{kill}$ (°C)	40	E
Λ_o	a tortuosity factor	0.59±0.10	M
θ	side slope angle of heap (radians)	Table 5-1	M

[a]: E: Estimated
C: Constant
M: Measured

5.3 Modeling Results

The FIDHELM results are summarized in the following sections. The results for piles 7/12 and 18B are also included in Appendix IV of this report.

5.3.1 Pile 7/12

The results of modeling for pile 7/12 for 1, 10 and 100 years are shown in Figures IV-1 to IV-12 of Appendix IV. The results indicate that the rate of oxidation occurring in the pile is limited by the supply of oxygen to reaction sites by diffusion from the pile/atmosphere interface into the pile. As indicated in Figure 5-1, the pattern of the air flow velocities within the pile show some characteristics of convection occurring but the magnitudes of the velocities, which are in the order of 10^{-6} to 10^{-5} m/s, which represents an oxygen flux comparable to diffusion but which applies only to the edges of the pile; the overall contribution to the global oxidation rate is small. Maximum temperatures of 8 °C (the ambient temperature is 3 °C) are approached in the first ten years. As indicated by the low air flow velocities, these temperatures are not high enough to induce a significant convective flow of the gas.

When the air permeability is increased to 10^{-8} m^2 from 2.9 x 10^{-9} m^2, the FIDHELM results show that convection does influence the oxygen concentrations within the pile, especially at the base, as Figure 5-2 shows. Unless the IOR is high (10^{-7} kg[O_2]/m^3/s), however, the effect of the higher permeability on the overall oxidation rate is marginal, as can be seen from Figures 5-3 and 5-6. Figures IV-13 to IV-21 of Appendix IV summarize the results for K=10^{-8} m^2.

The fraction of the initial sulphur inventory remaining versus time is shown in Figure 5-3 for three values of IOR and two values of gas permeability. Figures IV-22 to IV-24 of Appendix IV show the total amount of pyritic sulphur oxidized (kg and normalized) and the load (sulphate).

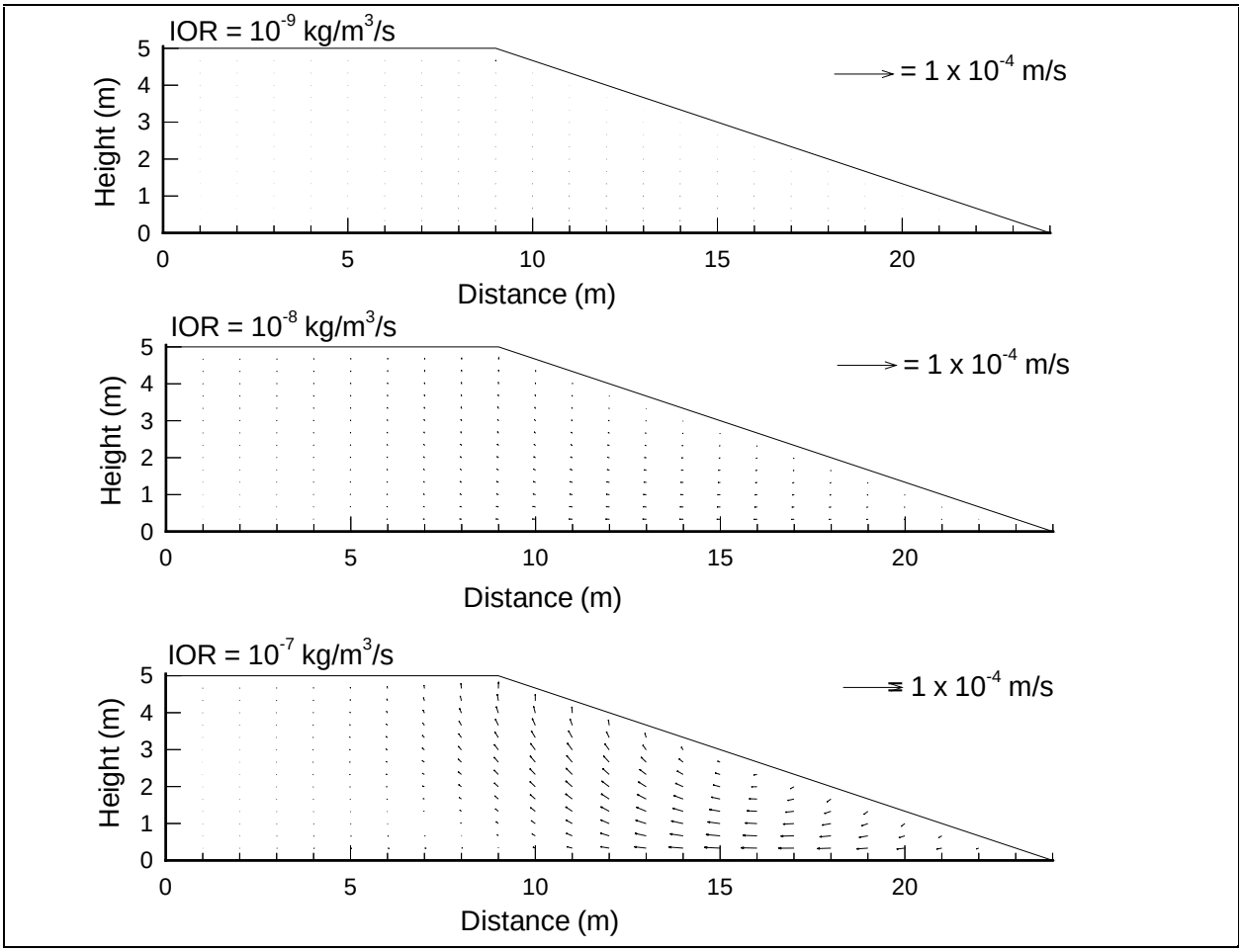

Figure 5-1: FIDHELM Results - Pile 7/12: Air Flow Velocities, K=2.9x10^{-9}m^2, Time=10 years

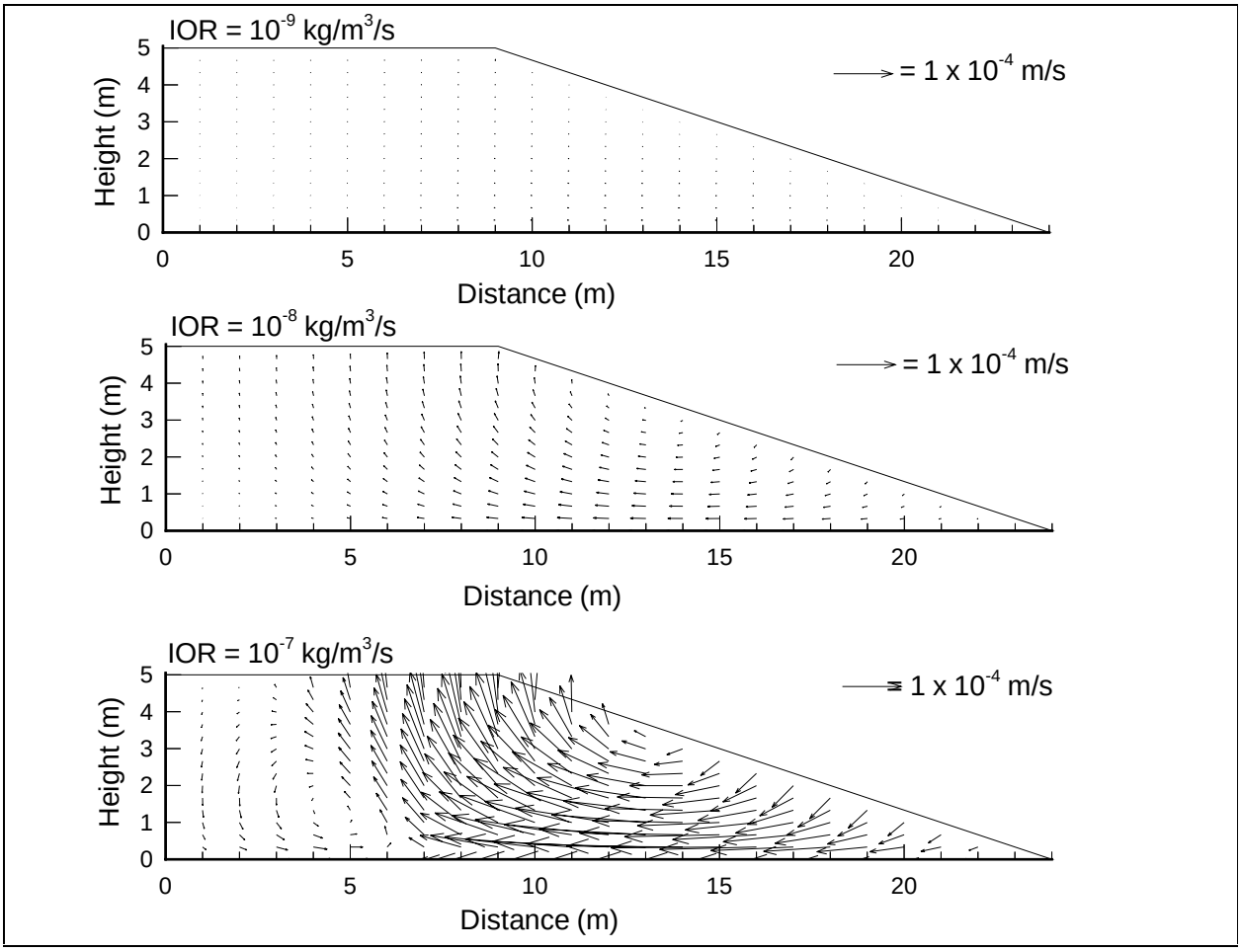

Figure 5-2: FIDHELM Results - Pile 7/12: Air Flow Velocities, K=1x10^{-8}m^2, Time=10 years.

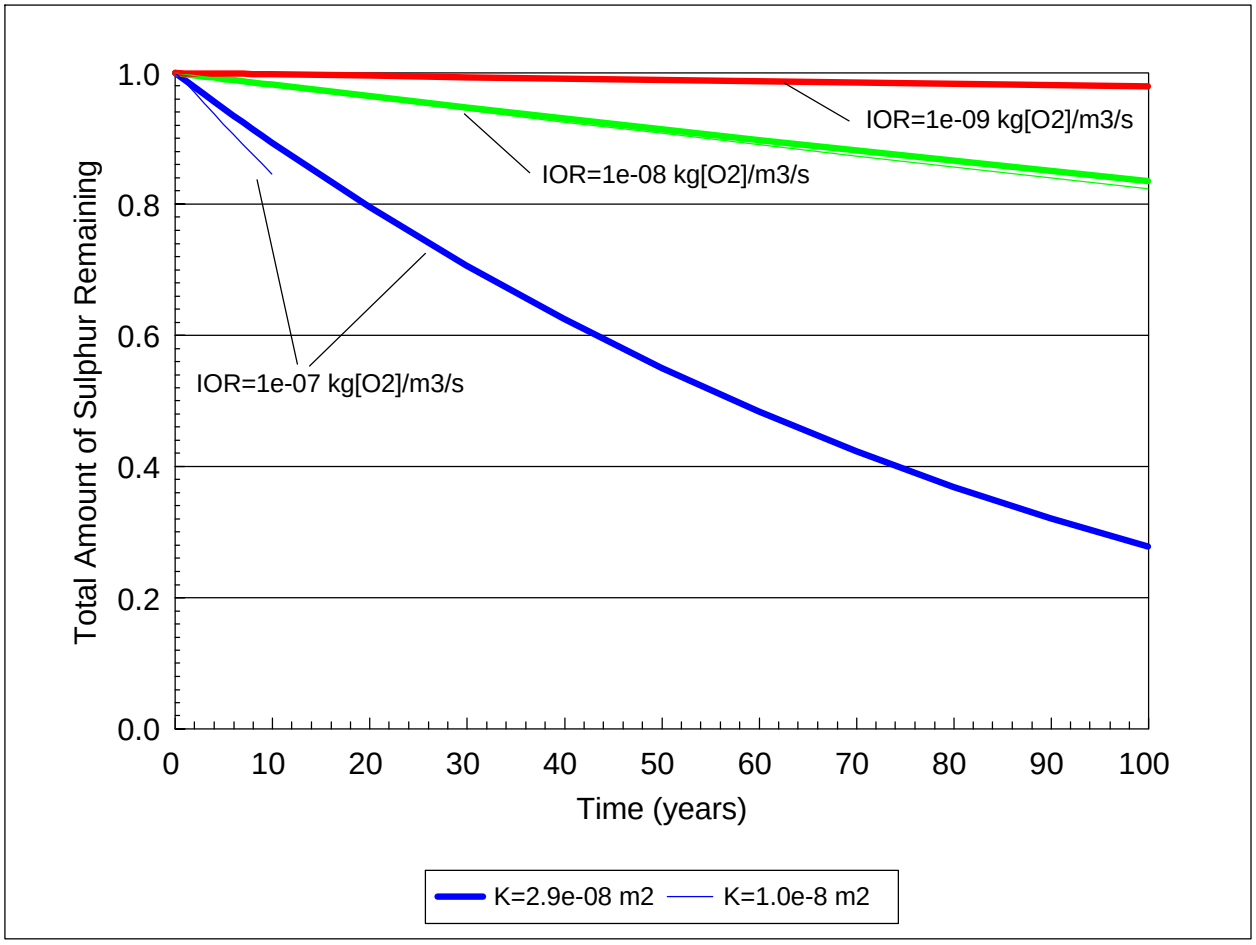

Figure 5-3: FIDHELM Results - Pile 7/12: Normalized Total Amount of Sulphur Remaining from Solid Phase versus Time

5.3.2 Pile 18B

The results of modeling for Pile 18B for 1, 10 and 100 years are shown in Figures IV-25 to IV-36 of Appendix IV. As for pile 7/12, the rate of oxidation occurring in the pile is mainly by the diffusion process from the pile/atmosphere interface when the average parameters were used. As shown in Figure 5-4, the air flow velocities are similar to pile 7/12. Maximum temperatures of 6 °C (the ambient temperature being 3 °C) are approached in the first ten years. These temperatures are not high enough to induce a significant gas convective flow.

As for pile 7/12, convection becomes an important contributor in the gas transfer when a higher air permeability value of 10^{-8} m^2 is used in the simulation. Figure 5-5 shows a typical air flow velocity vectors for this simulation after 10 years. Figures IV-37 to IV-45 of Appendix IV summarize the FIDHELM results for $K=10^{-8}$ m^2.

The fraction of the initial sulphur inventory remaining versus time is shown in Figure 5-6 for three values of IOR and two values of gas permeability. Figures IV-46 to IV-48 of Appendix IV show the total amount of pyritic sulphur oxidized (kg and normalized) and the load (sulphate).

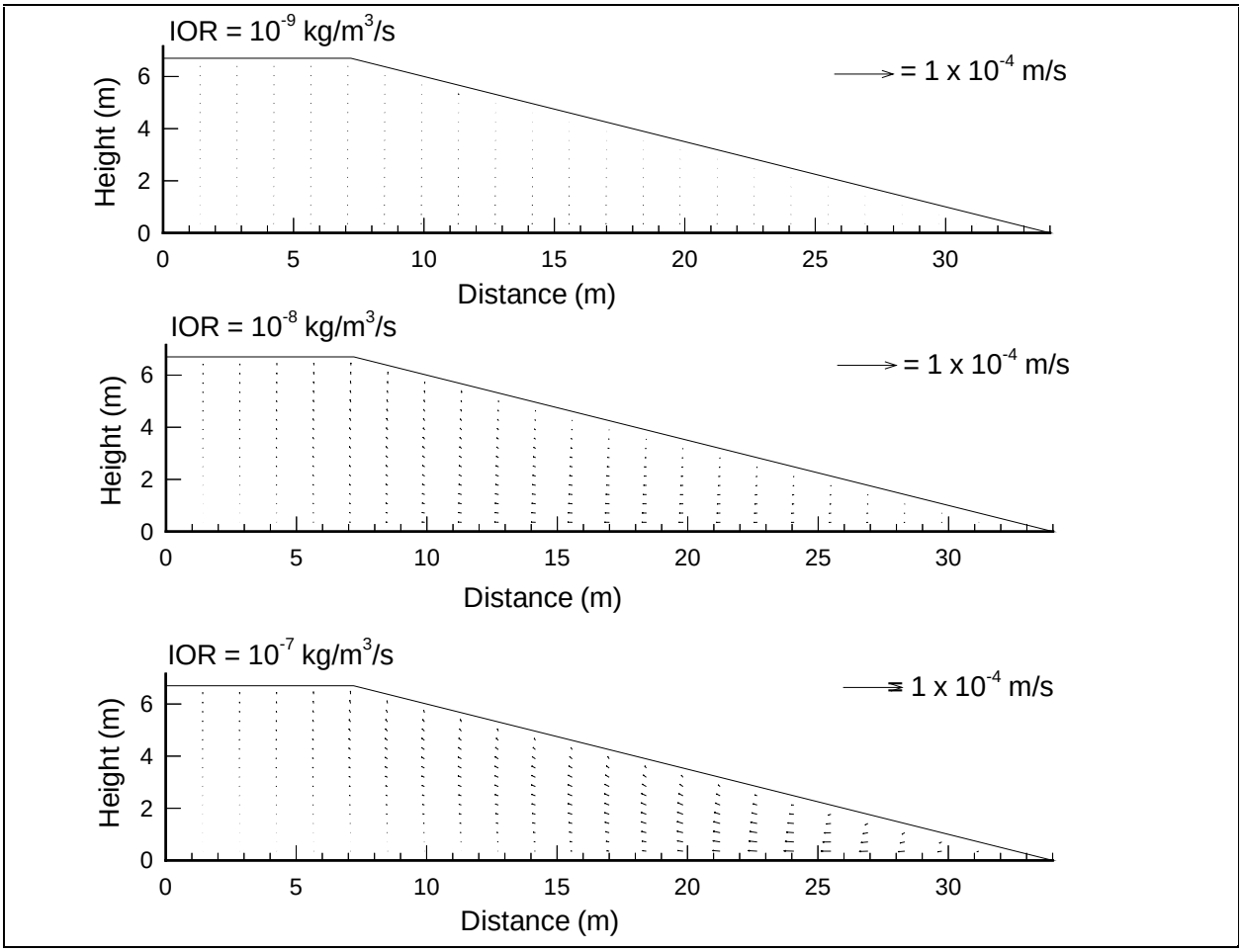

Figure 5-4: FIDHELM Results - Pile 18B: Air Flow Velocities, K=2.9x10^{-9}m^2, Time=10 years.

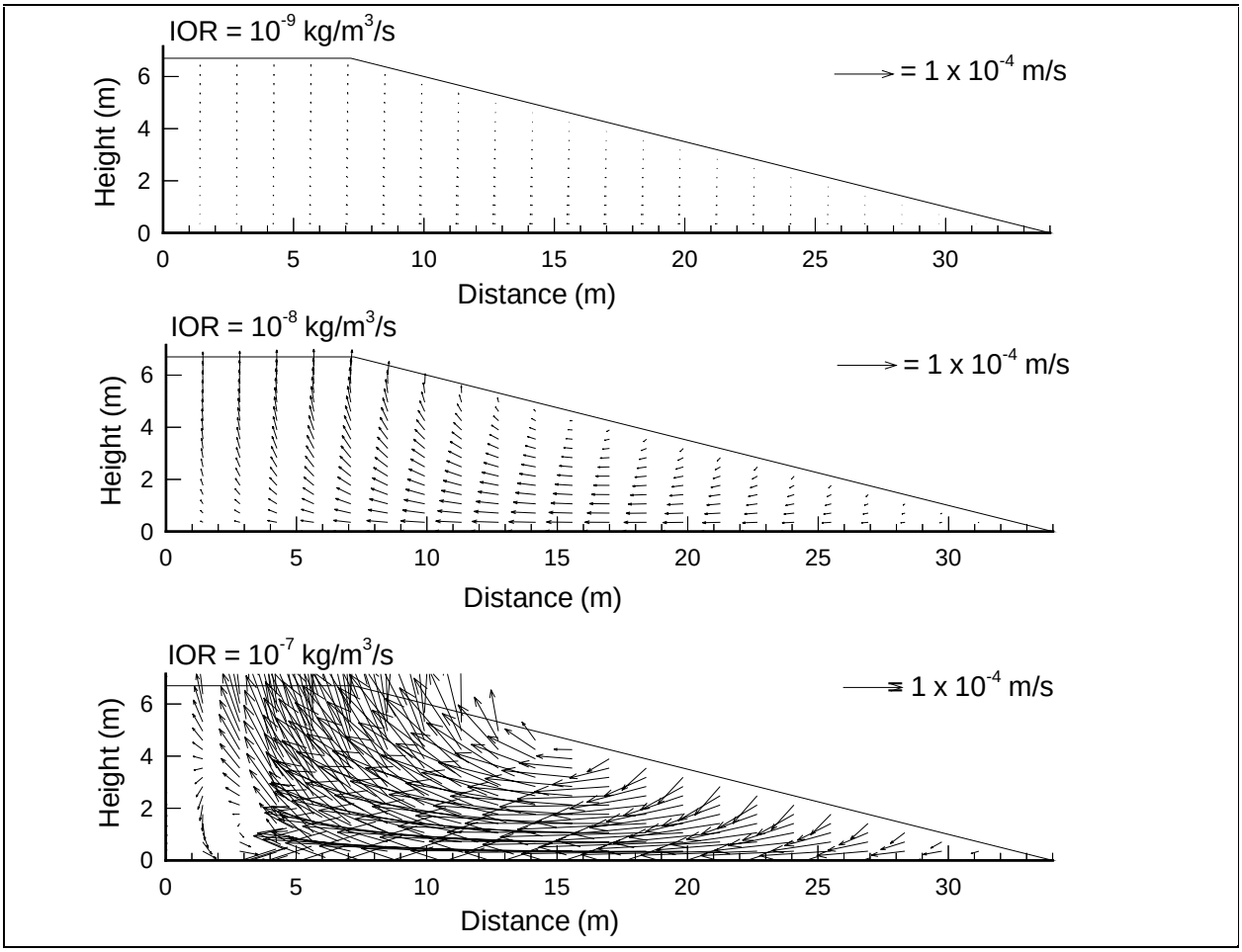

Figure 5-5: FIDHELM Results - Pile 18B: Air Flow Velocities, K=1x10^{-8}m^2, Time=10 years

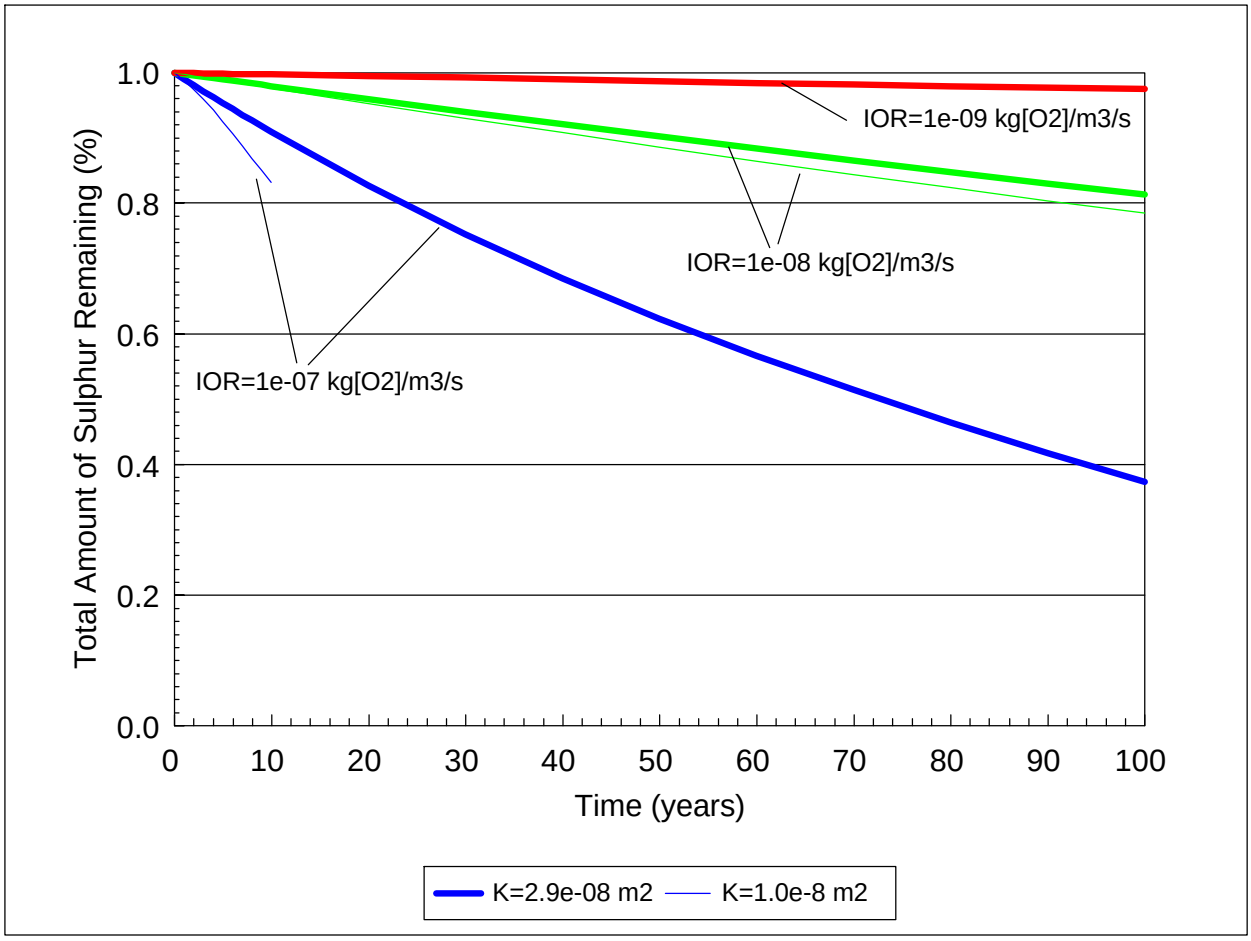

Figure 5-6: FIDHELM Results - Pile 18B: Normalized Total Amount of Sulphur Remaining from Solid Phase versus Time

5.3.3 Pile 17

The results of the simulations for Pile 17 are shown in Figures IV-49 to IV-54 of Appendix IV. As in the previous simulations for piles 7/12 and 18B, oxidation of the pile material is confined to the pile/atmosphere interface and maximum air flow velocities are considered too small for convection to be a significant process in the oxidation of the pile (see Figure 5-7 below). Temperatures in the first 10 years are similar to those observed in the simulations for piles 7/12 and 18B with maximum temperatures close to 3 °C above ambient being reached.

For Pile 17, less than 1 percent of the total pyritic sulphur in the pile has oxidized at 1 year, climbing to about 6 percent after 10 years and reaching 47% after 100 years. The normalized total amount of sulphur oxidized versus time is shown in Figure 5-8.

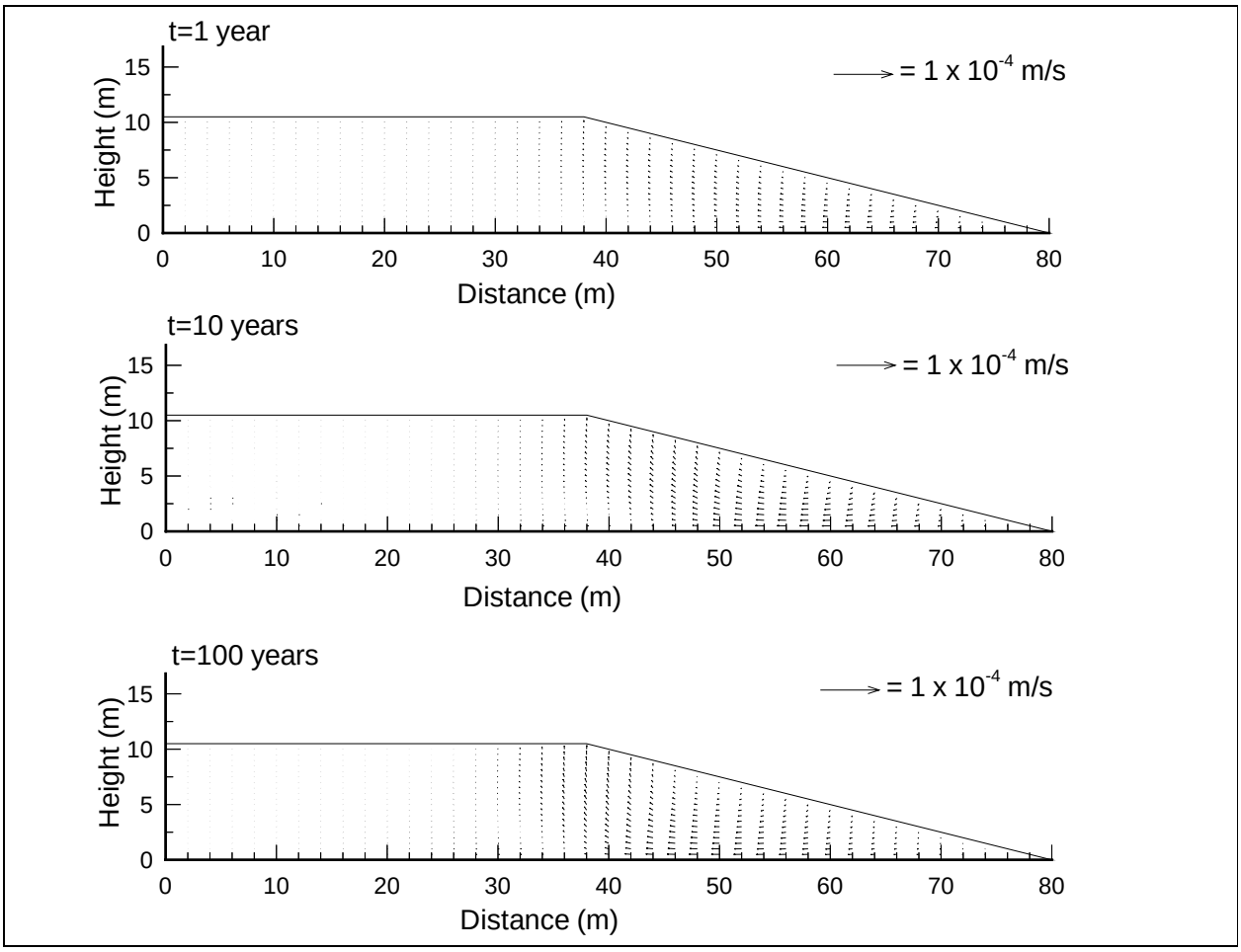

Figure 5-7: FIDHELM Results - Pile 17: Air Flow Velocities, $K=2.9x10^{-9}m^2$, $IOR=10^{-8}$ kg$[O_2]/m^3/s$.

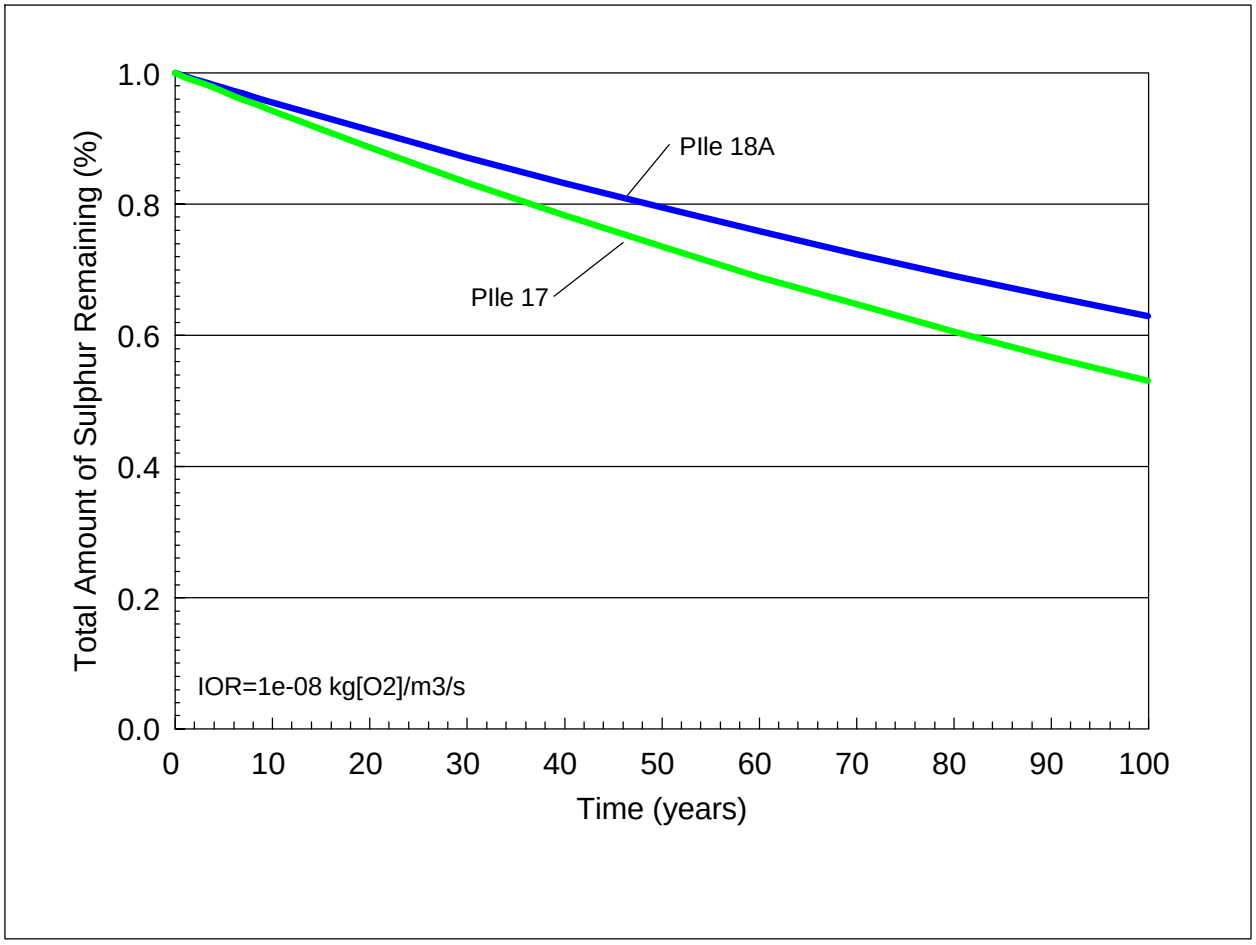

Figure 5-8: FIDHELM Results - Pile 18A and Pile 17: Normalized Total Amount of Sulphur Remaining from Solid Phase versus Time

5.3.4 Pile 18A

The simulations for pile 18A for 1, 10 and 100 years are shown in Figure IV-55 to IV-60 of Appendix IV. As in the other simulations, diffusion appears to be the dominant process of oxygen into the pile. Convection plays a negligible role in transporting oxygen into the heap with maximum gas velocities in the range of 10^{-6} to 10^{-5} m/s. Maximum temperatures are only about 2°C above ambient. Figure 5-9 shows the gas velocities obtained from these simulations.

For pile 18A, less than 1 percent of the total pyritic sulphur in the pile has oxidized at 1 year, climbing to about 4.5 percent at 10 years and to 37 percent at 100 years. The normalized total amount of sulphur oxidized versus time is shown in Figure 5-8.

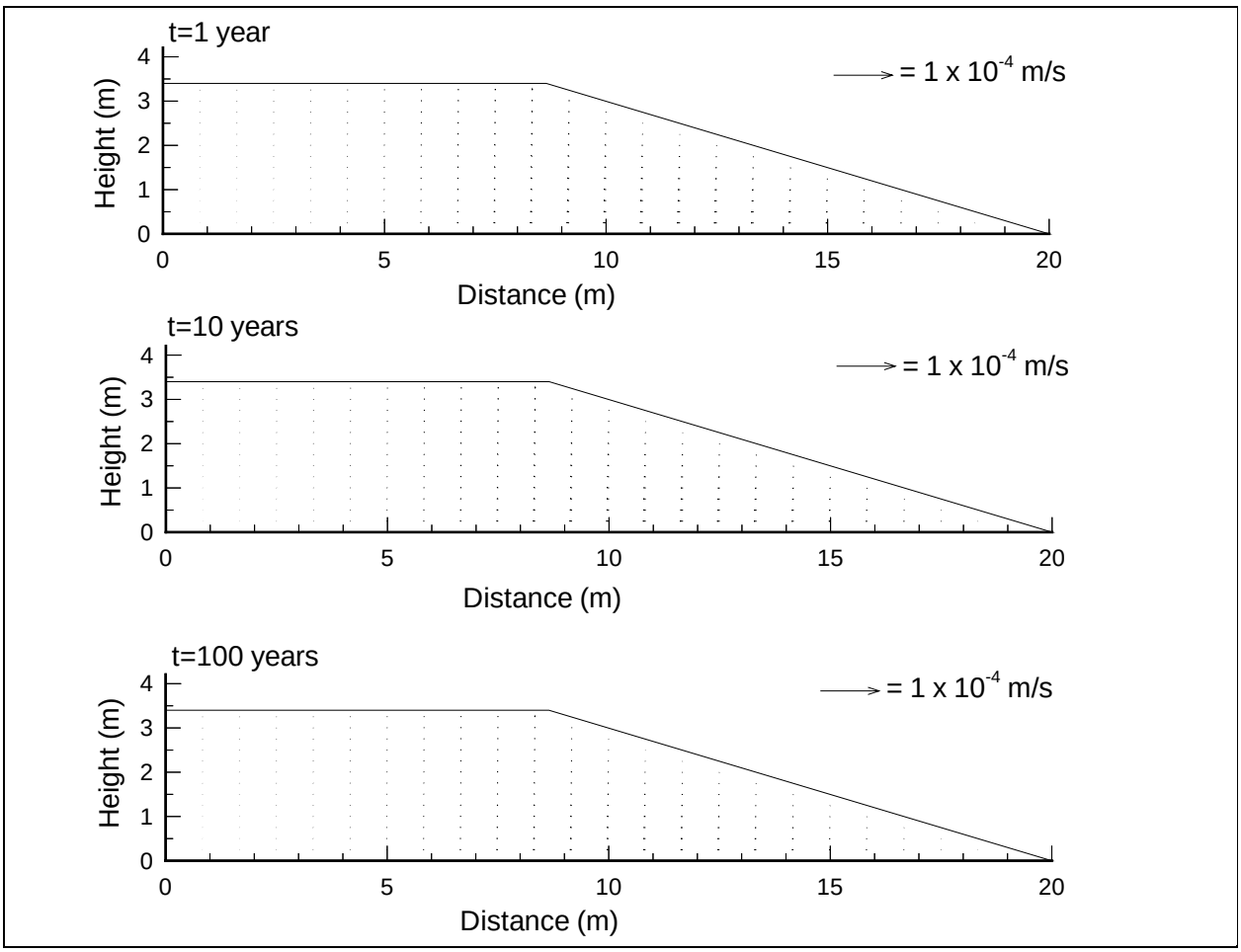

Figure 5-9: FIDHELM Results - Pile 18B: Air Flow Velocities, K=2.9x10^{-9}m^2, IOR=10^{-8} kg[O_2]/m^3/s.

5.4 Discussion

5.4.1 General

The FIDHELM simulations of the Heath Steele piles 7/12, 18A, 18B and 17 using *average* parameter values have been performed for a period up to 100 years. Under the assumptions of the model, the dominant mechanism of transport of oxygen into the piles is molecular diffusion. There is no evidence of gas convection which would significantly increase the oxygen supply into the heap, and in turn, increase the oxidation rates of the heap. Temperatures in the interiors of each pile do not exceed about 5 °C above ambient temperature in the first 10 years. The results of the modeling studies from *average* parameters indicate that convection will not be an important process in the oxidation of the Piles 7/12, 18/A, 18/B and 17 on the intrinsic properties of the heap under the idealized environmental conditions just stated.

The additional simulations carried out for piles 7/12 and 18B to study the effect of the variability of the air permeability indicated that pronounced convection will likely occur in the piles in the zones of higher air permeability. The interpretation of the FIDHELM results for piles 7/12 and 18B is presented in the following section.

5.4.2 Pile 7/12 and 18B

For piles 7/12 and 18B, a more rigorous analysis was carried out on the results of the FIDHELM modeling. Following is a summary of the results and conclusions.

The temperature distribution within the piles indicates some internal heating. The size of the waste rock pile is such that the annual temperature wave penetrates right into the base of the pile, so making it harder to separate that portion of the temperature rise due to internal heating from that due to insulation.

The oxygen profiles show that oxygen is being absorbed within the waste rock pile. The high oxygen concentrations at depth in the northern toe of the pile are consistent with advective transport of gas. The measured air permeability of the pile is large enough to make convective transport a possibility.

A number of additional simulations have been run for pile 18B using a diffusion coefficient and a gas permeability taken from field measurements judged appropriate for this pile. The simulation times range from one to 100 years.

The temperature and oxygen profiles in these simulations revealed the following:

- A hot spot 1-2 m in size, close to the base of the pile and 5-13 m from the toe of the pile.
- A maximum temperature in this hot spot of 15 ºC for a 3 year old pile and a 42 ºC for a 10 year pile.
- 5 m or so away from this spot, towards the central regions of the pile, temperatures were no more than 6 ºC at 3 years and 11 ºC at 10 years.
- An oxygen gradient dominated by diffusive transport.

- Very low oxygen concentrations at distances more than about 0.5 m from the surface in the very bulk of the pile. The exception was a region at the base of the pile near the toe where convective transport increased the distance from 0.5 m to about 8 m.
- Symmetry about the centre line of the pile.

The observed temperature and oxygen profiles are not consistent with these characteristics. In particular:

- The lack of a hot spot but the existence of an area of elevated temperatures at the base of the pile towards the north end of the pile. The temperatures in this 'hot' zone are about 14 °C.
- The centre of the zone is 25 m from the edge rather than 5 - 13 m.
- There is no steep oxygen gradient within the first meter or so of the surface.
- The lack of symmetry indicates different mechanisms occurring in the north from those occurring in the south end of the pile.

The conclusion is that gas transport for this pile is not adequately described by diffusion and convection with the assumed oxygen-consumption properties of the waste rock material.

A preliminary conclusion is that the temperature distribution and the relatively high aeration throughout pile 18B (particularly in the northern toe) is consistent with advection driven by pressure gradients over the pile arising from prevailing north-westerly winds. This conclusion was reached previously by Nolan, Davis and Associates (December 1990). FIDHLEM can be modified to simulate such advective processes provided the pressure distribution over the surface of the pile arising from wind-driven effects is known.

It is also possible that the IOR in this set of FIDHELM simulations is much higher than that which applies to the material in these piles. A lower IOR would allow greater penetration of oxygen into the pile for the same diffusion coefficient. The oxygen concentration profile in the southern part of the pile 18B is consistent with a low IOR. The effect of the lower IOR can be investigated using FIDHELM provided there is some indication as to its likely value for the material comprising pile 18B.

The seasonal variation in the oxygen concentrations indicates that the IOR may be temperature dependent. In its present form, FIDHELM simulates the long-term physical properties in waste rock piles. There are plans to modify the program to incorporate short-term (about monthly) temperature dependencies.

Consideration should be given to extracting an IOR from the data. Since the thermal conductivity of the waste rock material is now known and a long-time series is available for the temperature profiles, it should be possible to extract an IOR from the temperature data (Harries and Ritchie, 1981). For successful extraction of the IOR, good quality temperature data is required at roughly monthly intervals throughout the year, particularly through the colder parts of the year. Such data analysis should include the temperature-dependence of the IOR if temperature dependence is going to be included in FIDHELM simulations. The amount of temperature data collected to date

for pile 18B does not allow for an accurate evaluation of its IOR using the method presented by Harries et al. (1981).

6. GAS TRANSPORT/ACID GENERATION REDUCTION

6.1 Background

Access of air and water to pyritic rock as a result of mining allows oxidation to occur and the generation of acid mine drainage. The basic chemistry of the oxidation process is described by the following equation:

$$FeS_2 + H_2O + \frac{7}{2}O_2 \rightarrow FeSO_4 + H_2SO_4 + 1440kJ/mol$$

At pH levels above about 4, the reaction is purely chemical and proceeds quite slowly. However, over time, the generation of acid causes the pH to fall and the concentration of ferrous ions also builds up. These conditions permit the oxidation to proceed as a two stage process, which yields the same net chemical conversion as above but can proceed at a much faster rate. The first stage is the oxidation of ferrous ions to ferric; this rate of chemical reaction falls quickly with decreasing pH, but bacterial action at the lower pH can counteract this effect and cause the reaction to proceed quickly, as follows:

$$Fe^{2+} + \frac{1}{4}O_2 + H^+ \rightarrow Fe^{3+} + \frac{1}{2}H_2O$$

At pH below about 2.5, ferric ions remain in solution, and will be available to oxidize pyrite in the second stage. This chemical reaction proceeds rapidly.

$$FeS_2 + 14Fe^{3+} + 8H_2O \rightarrow 15Fe^{2+} + 2SO_4^{2-} + 6H^+$$

It appears that the ferric oxidation mechanism is required to explain the high pyrite oxidation rates observed in laboratory experiments. With respect to oxidation rates within a pile, a distinction must be made between the intrinsic rate (the rate of consumption of oxygen by the material of the pile under conditions which apply to that material) and the pile oxidation rate, which is mostly limited by oxygen supply. The present discussion refers to intrinsic rates. For reasons as yet not fully understood, the intrinsic rates observed in actual waste rock piles are in general about 100 times lower than the laboratory rates. In fact, the ferric oxidation mechanism need not be invoked to account for the pile rates. It is clear that a number of factors will control the intrinsic rate of oxidation of pyrite in a pile. Almost certainly, details of the physical state of the pyrite and its rock matrix has an influence. An oxidation rate per tonne of rock of $6.7x10^{-9}$ kg[O_2]/tonne per second is typical for a pile (with typical bulk density of 1500 kg/m^3 and sulphur content of 2 percent), in comparison with laboratory measured oxidation rates of $1.3x10^{-5}$ kg[O_2]/tonne per second (with bacteria) and 2.1xl0^{-6} /tonne per second(chemical) have been measured (Ritchie 1992).

To examine further the apparently very low pile IOR of $6.7x10^{-9}$ kg[O_2]/tonne per second means in practice, consider a tonne of waste rock containing 2 percent sulphur (see Table 2-1 for the

values measured at Heath Steele). The stoichiometric ratio of oxygen to sulphur is 1.75, so the pile rate expressed in terms of sulphur oxidation is approximately $4x10^{-9}$ kg[S]/tonne per second. The time required for oxidation of the 20 kg sulphur in the cubic metre of pile is $5x10^{9}$ seconds or 160 years. Assume a 10 m high pile with an infiltration rate of 500 mm per year. The sulphate concentration in the water leaving the bottom of the pile over this period can be calculated to be 5700 mg/l, more than ten times greater than the maximum recommended sulphate concentration in drinking water of 400 mg/l.

For the above reasoning to be valid, it must be known that the whole pile is reasonably well oxygenated. A simple 1-D formula gives the oxygen penetration depth, assuming diffusion is the only transport mechanism, as follows:

$$d = \sqrt{\frac{2DC_0}{S}}$$

Putting the diffusion coefficient $D=3x10^{-6}$ m^2/s, the concentration of oxygen in the atmosphere $C_o=0.265$ kg/m^3 and an IOR $S=1x\ 10^{-8}$ $kg[O_2]/m^3/s$ (equivalent to $5.6\ x\ 10^{-9}$ $kg[O_2]$/tonne of waste rock per second at a bulk density of 1.8 $tonne/m^3$) yields d=12.6 m. Thus, it is safe to assume that the small Heath Steele piles are well oxygenated.

6.2 Oxidation Mechanisms

The oxidation rate of pyrite in waste rock piles may be controlled by the intrinsic rate or by the supply of the necessary reactants, oxygen and water. Therefore, in principle, there are two broad avenues for inhibiting oxidation. The possibilities for reducing the intrinsic rate are as follows:

1. ***Removal of catalyzing bacteria***
   Removal of the catalyst for the oxidation reaction is often put forward as a control strategy. However, there are two criticisms of this technique:
   First, as already mentioned, the uncatalysed chemical reaction rate can be sufficiently high to cause environmental problems. Second, although surfactants have been used to inhibit bacterial activity with some success, they are effective for only for a limited time. On these grounds, this technique is not appropriate as a long term measure, in addition to its probable rejection on the grounds of the first point.

2. ***Maintenance of high pH***
   Another technique that is discussed is the incorporation of quantities of acid consuming material such as lime during the construction of a pile. The idea here is to maintain a high pH, supposedly inhibiting bacterial activity and reducing ferric ion concentrations through the precipitation of ferric salts. Again, this method is based on the assumption that the uncatalysed oxidation rate is slow enough to be environmentally acceptable and that the product reactions are permanently immobilized by the alkali.

6.3 Techniques to Increase Oxidation Rate

The collection and treatment of leachate is feasible during the course of mining. Therefore, if the oxidation rate could be increased enough during this time for the waste rock pile to be in an environmentally acceptable state at mine closure, or shortly after, a viable management option would exist. There are two states that could be considered as acceptable:

1) Enough of the sulphide would be oxidized that the rock heap could be considered inactive

2) A layer of oxidized material would be established, thick enough to reduce the diffusive oxygen flux to a level that throttles acid production by the required amount.

In a well oxygenated pile, the pile oxidation rate is controlled by the IOR, and the time to oxidize the whole pile is the same as that taken to completely oxidize the sulphur in one cubic metre of pile, and is given by:

$$t = \frac{\varepsilon \rho_{rs}}{S}$$

where: t = time
ε = Mass of O_2 consumed per unit mass
ρ_{rs} = Bulk density of pile material
S = IOR

With ε = 1.75, ρ_{rs} varying between 30 and 150 kg/m^3, and S=10^{-8} kg[O_2]/m^3/s, the above equation gives an oxidation time of about 160 to 830 years. If a IOR value of 10^{-7} kg[O_2]/m^3/s is used instead, the calculated times range from about 20 to 85 years, which can be considered to be limited to localized areas within the pile. These periods would be considered far too long for engineered water treatment. The option of increasing the pile oxidation is therefore not realistic.

6.4 Techniques for Inhibition of Waste Rock Oxidation Rates

Inhibition of the oxidation rate through attempting to reduce the intrinsic rate to environmentally acceptable levels is impractical because there is no practical way to reduce the chemical oxidation rate, other than to attack the catalyst to the reaction. Inhibition is therefore best addressed by the options for restricting the reagents needed for oxidation, namely water and oxygen.

1. ***Restriction of water supply***
   The chemical reaction requires 6.2 times more oxygen than water. The reaction rate in terms of water usage is therefore ~10^{-9} kg[H_2O]/tonne per second assuming an IOR value of 10^{-8} kg[O_2]/m^3/s. The water required per square metre of a 20 m high pile, with bulk density 1.5 tonne/m^3, would therefore be 20x1.5x10^{-9} kg[H_2O] per second, or one kg per year, equivalent to an infiltration rate of one mm per year. No practical cover could reduce the infiltration to this level, so limitation of water is not a feasible way to inhibit oxidation.

2. ***Restriction of oxygen supply***
   In the previous example, a cubic metre of rock contains 30 kg sulphur and requires 53 kg oxygen for its oxidation. The rock will contain about 0.3 kg oxygen. Assuming a porosity of 0.3, this is only 0.5 percent of the required amount. Oxygen must therefore be transported into the heap from the atmosphere, generally by diffusion. This is a practical opportunity for reducing the oxidation rate. Convection, which requires high permeabilities to be significant, is much easier to control and the means taken to limit diffusion will ensure that convection will not play any significant part in supplying oxygen.

There is only one practical method for reducing oxygen diffusion into waste rock piles, that is to cover the reactive rock with some material which will reduce the rate of diffusion of oxygen. Three techniques are commonly used to achieve this, namely:

- Isolation: placement of the pyritic material so that it is surrounded by non acid-producing material.
- Compaction: construction of a low porosity layer on top of the pile by compaction
- Capping: covering the pile with one or more layers of material, at least one of which has low diffusivity.

To calculate the effects of a cover, it is necessary to know the rainfall infiltration rate and the values of the parameters: thickness, hydraulic conductivity, porosity, permeability for the cover layers and the pile material. The calculations are the same for the three techniques defined above. What sort of cover is in place is specified by the parameters. The following comments are offered on the sort of result that might be achieved by the three techniques, before proceeding to more quantitative analysis.

1. ***Isolation:***
   The cover in this option is formed from material which is substantially the same as the pile material in all respects except that it is not acid-producing. Piles all tend towards this case as oxidation depletes the sulphur from the outer layers of the pile material. The trouble with this option is that the diffusion coefficient that applies to the pile material is generally high enough to permit an unacceptably high rate of oxidation to proceed even though the layer of inert waste may be quite thick.

2. ***Compaction*:**
   The deficiency of isolation can be overcome to a varying extent by compacting the surface material to form a denser layer, less permeable to oxygen, and to water. The porosity of the layer can be greatly reduced by compaction. This reduces the diffusion coefficient immediately, but also has a very important multiplier effect in that the compaction also reduces the hydraulic conductivity which leads to the layer having a higher moisture content for the same infiltration rate. As the gas diffusivity depends on the gas filled porosity, it is reduced when the pores are filled with water. The ideal is to have a layer at least part of which maintains a state of saturation at all times. The very low diffusion coefficient for oxygen in water then ensures a very low diffusion rate into the pile. Layers of 300 mm to 1000mm can be compacted at reasonable cost.

3. ***Capping:***
   Clay or other fine grained soil with a high water retention can provide an effective cover material if available. Multi-layered covers can be designed to maximize the water retention of the clay. For instance, covering the clay with soil or rock will reduce water loss through evapo-transpiration. A coarse layer beneath the clay can also assist by reducing the capillary suction which tends to draw moisture from the clay. In its limit the coarse layer is called a capillary break layer and water can only leave the clay when its base is saturated (Collin and Rasmuson 1988; Yanful and St-Arnaud 1991, Yanful et al. 1993).

6.5 Composite Soil Cover Effectiveness

In this section, a quantitative evaluation of cover systems is made. A multi-layer system is considered with the bottom two layers containing oxidizable material and the top two layers having properties designed to reduce the oxygen flux into the oxidizable material The calculations assume that gas transport is one dimensional. Calculations using a two dimensional model have shown that a one dimensional model will describe gas transport adequately, except close to the edges of those piles where the air permeability is high enough for advective gas transport to occur.

Various layers can be specified with different sulphur contents, different hydraulic properties and densities. The diffusive properties of each layer depends on the dry void porosity of the material and the degree of water saturation. The diffusion coefficient D is expressed as $D = A(E_a)D_b$ where D_b is the coefficient of diffusion of oxygen in the air and E_a is the volume fraction of air in the wetted soil. It is assumed that the function $A(E_a) = A_o E_a$ where A_o is known as the tortuosity of the material. This approach allows the oxygen diffusion rate to be calculated from the degree of compaction of the layers and infiltration rate.

In the calculations, the infiltration has been taken as uniform in time. The validity of this will depend on the uniformity of the annual rainfall, and the time constants of the drainage. In the present simulations, the behavior of the waste rock piles over tens to hundreds of years is not performed in detail for seasonal variation. The validity of assuming a constant rate of infiltration would have to be examined for each specific case, because it is not justifiable in some cases. The unsaturated hydraulic conductivity is specified by the capillary factor α in the expression:

$$K = K_s e^{\alpha\psi}$$

where K_s is the saturated hydraulic conductivity and ψ is the matric potential in the soil.

The magnitude of the diffusive oxygen flux through the cover layer depends on the interaction between a number of factors. Since the diffusion coefficient varies with the air filled porosity of the cover material, any factor that reduces the air filled porosity will reduce the diffusion coefficient. Such factors will include an increase in the water infiltration rate, a decrease in the saturated hydraulic conductivity or change in the hydraulic properties which increase the degree of saturation for a given infiltration rate. The factors may be non-linear. For example, compaction of a layer will decrease the porosity and tend to decrease the hydraulic conductivity;

an increase in the thickness of a layer of low hydraulic conductivity will lead to a higher amount of water in that layer, leading to a decrease in oxygen flux both from the increased thickness and from the decreased diffusion coefficient.

The total oxidation rate in the pile has been calculated assuming various properties of the cover and sulphur containing layers. The sulphate generated in the oxidation process and transported to the bottom of the pile by water infiltrating the pile is also calculated. It is assumed in this calculation that dissolved sulphate is conserved.

Table 6-1 specifies the thicknesses of the cover layers and the layers of pyritic material and other relevant properties of the layers. Table 6-2 specifies the parameters which were varied in each of the cases in order to evaluate the effect of various layer properties. Table 6-2 also contains a brief description of the differences between each case and the base case.

It is possible to specify parameter values for the "compacted" layer that lead to the layer becoming saturated. As the coefficient of diffusion of oxygen in water is about four orders of magnitude lower in water than in air, a layer of saturated cover material only a few millimeters thick is equivalent to an unsaturated layer many meters thick. Reducing the diffusive flux of oxygen to the oxidation region by designing for near-saturation covers has been investigated by Collin and Rasmuson (1988) and by Yanful and St-Arnaud (1991). The approach in the present work is different in that the effect of the cover is combined with a calculation of the time dependence of the oxidation of the material within a pile. Also, the water transport is calculated on the basis of Darcy flow. Hydraulic continuity between the layers is assumed, and the cover layer does not become saturated, even in cases where the infiltration rate is equal to the saturated hydraulic conductivity of the material in the cover layer. The concept of capillary break layers is not invoked in our calculations. Our treatment of the variation of diffusivity with water content is also somewhat different than Collin and Rasmuson. Yanful and St-Arnaud used a measured relationship between diffusivity and water content instead of our assumed proportionality between the diffusivity and the air filled porosity of the material, as described above. The oxygen diffusion coefficient of the Heath Steele till material used for the cover has been measured and reported by Yanful (1993). The measured values of diffusivity fall very rapidly as the water content approaches saturation.

The total oxidation rates for the various cases are shown in Figure 6-1 and the sulphate load is shown in Figure 6-2. The assumptions used in calculating these loads are specified in Section 5.1. In Figure 6-2, the behavior of the sulphate load at the base close to t=0 needs some explanation: in all cases the load is initially zero, rises to a peak and then falls off. The different appearance of the various cases depends on the time-scale for this process compared with the time-step of the calculation, 2.5 years. Likewise, in Figure 6-1, the first points plotted are at the end of the first time step.

It has been shown that reduction of pollution loads from waste rock piles by reduction of the IOR or by restriction of the water infiltration rate cannot be achieved practically, taking cost and the long timescale involved into account. On the other hand, it is practical to reduce the oxygen flux to oxidation sites within the waste rock by constructing suitable covers, and by so doing, to

reduce the overall oxidation rate in the waste rock piles to levels where acceptable rates of pollution generation occur. Compaction of a layer reduces its diffusion coefficient both by the reduction in porosity and by the reduction in air-filled porosity due to the increased water content for a given infiltration rate. A reduction by about a factor of 50 in the long term sulphate concentration can be achieved with practical cover thickness. The reduction during the first 5 to 10 years after pile construction is more than two orders of magnitude.

An analysis of the effectiveness of the cover at pile 7/12 was carried out using a one-dimensional numerical model with oxidation processes similar to FIDHELM. The geometry used in the model is similar to the one used for the seepage analysis (see Section 4.4.3). The results are shown in Figure 6-3 for time= 10 years. The Figure shows that the cover has a high degree of saturation; the overall oxidation rate can be estimated from the Figure and corresponds to a reduction by about 10^6 compared with the no cover case. Thus, the results indicate that the cover is effective in reducing the gas transport to the waste rock pile.

Table 6-1: Specification of Layered System

Layer	Material	Depth of layer (m)	Sat. hydr. conductivity K_s (m/d)	α (m-1)	Bulk density ρ_s (kg/m^3)	Volume fraction of solid ε_s	Sulphur density ρ_{rs} (kg/m^3)
1	Soil	0.3	1.0	2.0	1500	0.7	0
2	Compacted material	0.0-0.3-1.0	0.001-0.01	1.0-2.0	2000	0.7-0.9	0
3	Low sulphur material	5	1.0	2.0	1500	0.6	10
4	High sulphur material	15	1.0	2.0	1500-2000	0.6	70

Table 6-2: Specification of Cases and Comments on Results

Case	Description	Layer 2 parameters				Infiltr.	Comment
		Depth (m)	K_s (m/day)	α (m-1)	ε_s	(m/day)	
1	Base Case	0.3	0.001	1.0	0.9	0.001	
2	No compacted layer	0	-	-	-	0.001	The oxygen flux through the cover layer is enhanced compared with Case 1. The oxidation rate and SO_4 load are about 5x larger than in Case 1.
3	Thick compacted layer	1	0.001	1.0	0.9	0.001	Considerable quantities of water are held in the compacted layer, thereby reducing the O_2 flux. Oxidation rates are reduced by - 10x conpared with Case 1.
4	Low infiltration rate	0.3	0.001	1.0	0.9	0.0005	The oxidation rate and SO_4 load are almost double that in Case 1, as the air-filled porosity of the compacted layer is almost doubled.
5	Lightly compacted layer	0.3	0.01	1.0	0.9	0.001	The 10x increase in K_s compared with Case 1 leads to lower water content. The Oxidation rate is increased by about 2x.

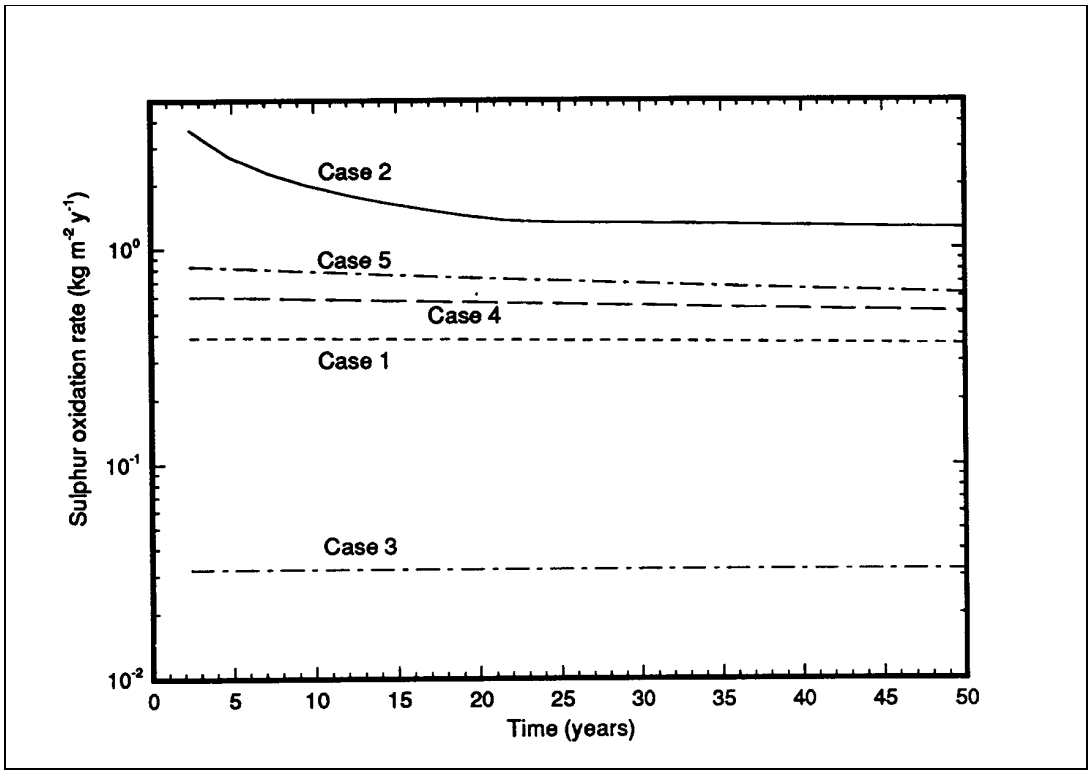

Figure 6-1: Sulphur Oxidation Rate for 5 Cover Options

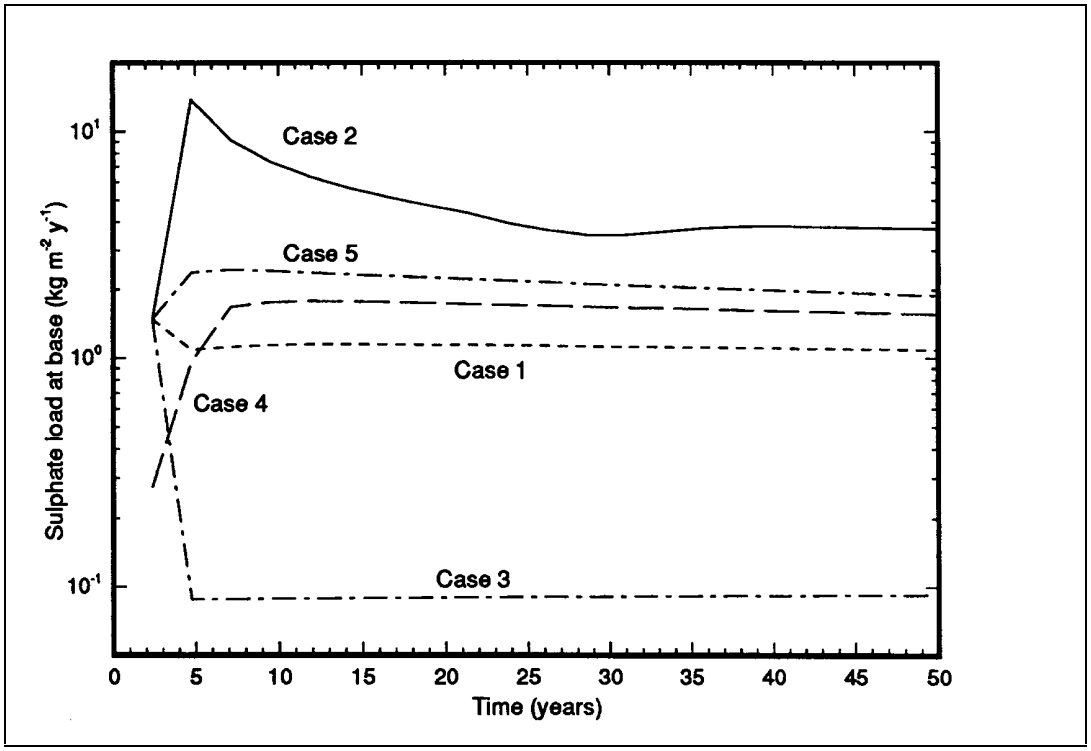

Figure 6-2: Sulphate Load Leaving the Base of the Pile Carried by Water

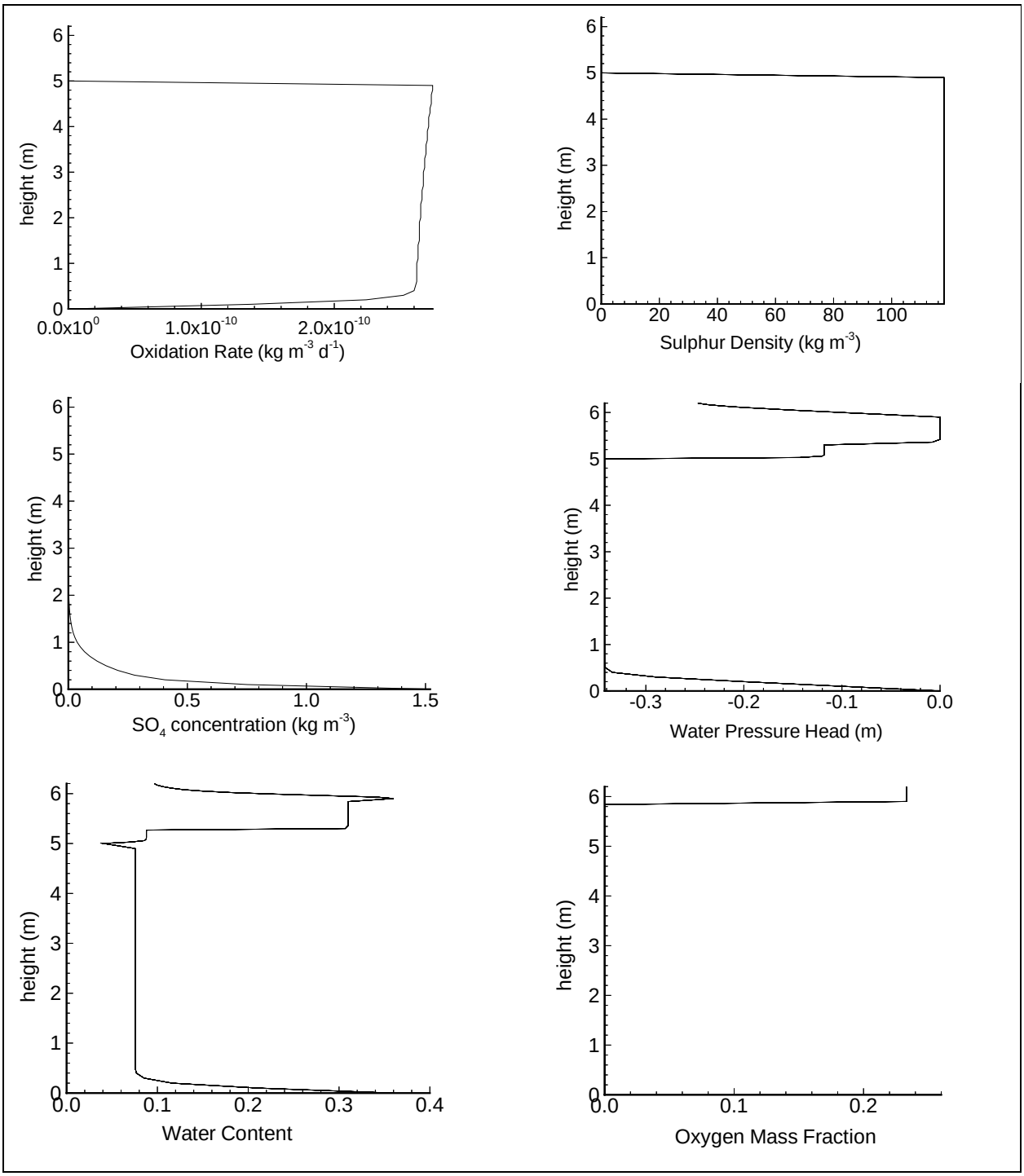

Figure 6-3: HEAPCOV Results, Pile 7/12 with Cover, Time=10 years

7. CONCLUSIONS & RECOMMENDATIONS

The objectives of the project were to develop an understanding, using both the numerical model FIDHELM and field data, of the processes governing the pyrite oxidation rates in acid waste rock piles at Heath Steele and, to quantify those processes and evaluate the effectiveness of the composite soil cover for acid waste rock management. FIDHELM was shown to be a useful tool to assess the various gas transport mechanisms in pyritic waste rock piles.

The following conclusions can be reached from the project:

1. Measurements of the bulk physical parameters for air permeability, oxygen diffusion coefficient and thermal conductivity were carried out successfully in pile 18B. Measured oxygen diffusion coefficients ranged from 2.1×10^{-6} to 3.6×10^{-6} m^2/s with an average of $(3.0 \pm 0.5) \times 10^{-6}$ m^2/s; measured gas permeability ranged from 1.6×10^{-10} to 1.7×10^{-8} m^2 with a mean value of 2.9×10^{-9} m^2 and measured thermal conductivity ranged from 1.04 to 1.25 W/m/K with a average value of 1.2 W/m/K.

2. The measured values of the bulk physical parameters were found to be within the range measured in four other piles of waste rock at three different mine sites and in climates ranging from tropical to arctic.

3. Numerical simulations using FIDHELM and the average measured values of oxygen diffusion coefficient and gas permeability indicated that gas transport was dominated by diffusion. While convective transport was apparent, specific gas discharge rates were low and did not contribute significantly to the oxidation rate within the pile.

   A feature of these simulations were oxygen concentration profiles which decreased steadily from the surface of the pile into the pile. This is consistent with profiles measured in the southern part of pile 18B.

4. Using the highest value of the measured gas permeability and an IOR varying from 10^{-8} to 10^{-7} $kg[O_2]/m^3/s$, FIDHELM results showed pronounced convection. In these cases, for both piles 7/12 and 18B, oxygen profiles at points up to almost the complete width of the pile increased towards the bottom of the pile. FIDHELM results indicate that details in the oxygen profile can be explained by the heterogeneity of the pile with respect to both gas permeability and IOR.

5. The modeling of pile 7/12 with the soil cover and the field data indicate that the composite soil cover placed on pile 7/12 is an effective way to reduce the ingress of oxygen to acid generating waste rock. The temperatures measured in the field and the results obtained from the model show a decrease following cover installation, indicating a low level of the exothermic reaction of the oxidation process. The data collected to date from covered pile 7/12 is consistent with the simulations.

6. It is clear that oxidation occurred in both piles 7/12 (prior to cover emplacement on the pile) and 18B, and that the oxidation rates were maintained by both diffusion and advection of oxygen into the piles from their external surfaces. While piles 18B and 7/12 are small compared to waste rock piles at many mine sites around the world, and while the balance of gas transport mechanisms in these larger piles may be different from those at work in the two piles at Heath Steele, it is also clear that the cover system has been effective in reducing oxygen ingress and, with this, in reducing the oxidation rate.

The following recommendations are made as a results of the work:

1. Since it is possible that advection driven by wind effects is a mechanism occurring in 18B and in other piles, a program of work should be set up to quantify this effect and to compare measured values with a FIDHELM modified to accept space/time varying surface pressure.

2. Monitoring of temperatures, oxygen concentrations, drainage flow rates and drainage water quality should be continued for an extended period to quantify the long term effect of a cover system on oxidation levels and pore water chemistry. It is important in this respect that the chemical analysis includes major ions as well as trace metals to ensure a sound understanding of the chemical processes. It is also important that monitoring of temperatures and oxygen concentration be done at least monthly for an extended period (2-3 years) to ensure enough data for a quantitative analysis of these variables. This will provide better understanding of mechanisms and may allow any temperature dependence of the IOR to be estimated.

3. Monitoring on 18B and simulations using FIDHELM should be used to assess the importance of pile inhomogeneity on the overall pollutant load from a pile.

4. The IOR and the sulphur content of the waste rock from Heath Steele should be estimated using laboratory testing.

APPENDIX I

References

BIBLIOGRAPHY: ACID MINE DRAINAGE

Ackman, T.E. and Kleinmann, R.L.P. 1984. In-line aeration of acid mine drainage. U.S. Department of Interior, Bureau of Mines. Pittsburgh, PA.

Allen, C.G. and Verhoeven, T.J. (Eds.) 1986. The Rum Jungle Rehabilitation Project, Final Project Report. Northern Territory Department of Mines and Energy. Australia.

Akindunni, F.F., Gillham, R.W. and Nicholson, R.V. 1991. Numerical simulations to investigate moisture-retention characteristics in the design of oxygen-limiting covers for reactive mine tailings. Can.Geotech. Journal, V.28:446-451.

Applegate, R.J. and Kraatz, M. 1991. Rehabilitation of Rum Jungle Uranium Mine. Proceedings, Second International Conference on the Abatement of Acidic Drainage, Tome 3. September 16-18, 1991. Montréal.

Arkesteyn, G.J.M.W. 1980. Pyrite oxidation in acid sulphate soils: the role of microorganisms. Plant and Soil, V. 54, pp. 119-134.

Arnesan, R.T., Iversen, E.R. Källqvist, S.T., Laake, M., Lien, T. and Christensen, B. 1991. Monitoring Water Quality During Filling of the Løkken Mine: A Possible Role of Sulfate-Reducing Bacteria in Metals Removal. Proceedings, Second International Conference on the Abatement of Acidic Drainage, Tome 3. September 16-18, 1991. Montréal.

Averill, W.A., 1976. The chemistry and modelling aspects of copper dump leaching. Ph.D. Thesis, University of Utah.

Barlett, R.W. 1973. Int. symp. on hydrometallurgy, A.I.M.E., New York, pp. 331-374.

Barton-Bridges, J.P. and Robertson, A.M. 1989. Geotechnical considerations in the control af acid mine drainage. Proceedings, Geotechnical Aspects of Tailings Disposal and Acid Mine Drainage, Canadian Geotechnical Society, Vancouver.

Beaudoin, P. and McMullen, J. 1990. L'approche Environnementale pour le Contrôle des Effluents Miniers Acides à La Mine Doyon.

Béchard, G., Rajan, S., Salley, J. and McCready, R.G.L. 1990. An anaerobic microbial ecosystem for the treatment of acid mine drainage. CANMET, Energy Mines and Resources Canada. Divison Report MSL 90-44 (OP) Ottawa.

Béchard, G., Goudey, P., Rajan, S., and McCready, R.G.L. 1991. Microbiological Process for the Treatment of Acidic Drainage at the Halifax International Airport. Proceedings, Second International Conference on the Abatement of Acidic Drainage, Tome 3. September 16-18, 1991. Montréal.

Bell, A.V. 1988. Acid Waste Rock Management at Canadian Base Metal Mines. Proceedings, InternationalConference on Control of Environmental Problems from Base Metal Mines. June 1988. Roros, Norway.

Bell, A.V., Surges, L. and Groskopf, G.R. 1991. An Update on the Acid Waste Rock Field Trials at Heath Steele Mines, New Brunswick. Proceedings, Second International Conference on the Abatement of Acidic Drainage, Tome 3. September 16-18, 1991. Montréal.

Bennett, J.W., Gibson, D.K., Harries, J.R., Pantelis, G., Ritchie, A.I.M., Verhoeven, T.J., Alcock, J., Henkel, H. and Apllegate, R.J. 1989. Rehabilitation of the Rum Jungle Site. Canadian Land Reclamation Association/American Society for Surface Mining and Reclamation Meeting. August 27-31, 1989. Calgary.

Bennet, J.W., Harries, J.R., and Ritchie, A.I.M. 1992. Chemical activity and water balance of the overburden heaps. Rum Jungle Rehabilitation Project: Monitoring Report 1986-88. Kratz, M. and Applegate, R.J. (Eds.) Technical Report 51, Northern Territory Conservation Commission. Ch. 7, pp. 103-119.

Bennet, J.W., Harries, J.R., Pantelis, G. and Ritchie, A.I.M. 1989. Limitations on Pyrite Oxidation Rates set by Air transport Mechanisms. Proceedings, Biohyrometallurgy International Symposium, August 13-18, 1989. Jackson Hole, Australia.

Bennett, J. W., Harries, J.R. and Ritchie, A.I.M. 1988. Rehabilitation of Waste Rock Dumps at the Rum Jungle Site. Proceedings, Mine Drainage and Surface Mine Reclamation Conference. April 17-22, 1988. Pittsburgh, PA.

Bennett, J.W. and Pantelis, G. 1991. Construction of a Waste Rock Dump to Minimise Acid Mine Drainage - A Case Study. Proceedings, Second International Conference on the Abatement of Acidic Drainage, Tome 3. September 16-18, 1991. Montréal.

Bennett, J.W. and Ritchie, A.I.M. 1991. Measurements of the Transport of Oxygen Into Two Rehabilitated Waste Rock Dumps. Proceedings, Second International Conference on the Abatement of Acidic Drainage, Tome 3 September 16-18, 1991. Montréal.

Boorman, R.S. and Watson, D.M. 1976. Chemical processes in abandoned sulphide tailings dumps and environmental implications for northeastern New Brunswick. Can. Inst. Mining Metall. Bull. Vol. 50, pp. 231-257.

Braun, R.L., Lewis, A.E. and Wadsworth, M.E. 1974. Solution Mining Symposium, A.I.M.E. New York, pp. 292-323.

Brierly, C.L. 1978. Bacterial leaching. CRC Critical Rev. Microbiol., Vol. 6, pp. 207-262.

Box, J.C. and Prosser, A.P. 1986. A general model for the reaction of several minerals and several reagants in heap and dump leaching. Hydrometallurgy, Vol. 16, pp. 77-92.

Calkley, M.E. (Ed.) 1989. Tailings and effluent management. Proceedings, The International Symposium on Tailings and Effluent Managment. August 20-24, 1989. Halifax.

Caruccio, F.T. and Geigel, G. 1978. Geochemical factors affecting coal mine drainage quality. Reclamation of Drastically Disturbed Lands. Scaller, F.W. and Sutton, P. (Eds.) American Society of Agronomy. Madison, Wisconsin. pp. 437-443.

Caruccio, F.T., Geigel, G. and Pelletier, A. 1980. The assessment of a stratum's capability to produce acid drainage. Proceedings, 1980 Symposium Surface Mining Hydrology, Sedimentology, and Reclamation. University of Kentucky, Lexington, KY.

Casagrande, D.J., Finkelman, R.B. and Caruccio, F.T. 1989. The non-participation of organic sulphur in acid mine drainage generation. Environmental Geochemistry and Health. Vol.11, No. 3/4, pp. 187-192.

Cathles, L.M. 1979. J. Int. Assn for Mathematical Geol., Vol. II(2), pp. 175-191

Cathles, L.M. and Apps, J.A. 1975. Met. Trans., Vol. 6B, pp. 617-624.

Cathles, L.M., Reese, D.A. and Murr, L.E. 1977. Amer. Nucl. Soc., Topical meeting on energy and mineral ressource recovers. CONF-770440, pp. 584-595.

Cathles, L.M. and Schlitt, W.J. 1980. A model of the dump leaching process that incorporates oxygen balance, heat balance, and two dimensional air convection. Proceedings, Las Vegas Symposium on Leaching and Recovering Copper from: As-Mined Materials. February 26, 1980. pp. 9-27.

Coastech Research Inc. 1989. Investigation of prediction techniques for acid mine drainage. CANMET, Energy, Mines and Resources Canada.

Collin, M. 1987. Mathematical Modelling of Water and Oxygen Transport in Layered Soil Covers for Deposits of Pyritic Mine Tailings. Licentiate Treatise, Royal Institute of Technology. Stockholm, Sweden.

Collin, M. and Rasmuson, A. 1988. A Comparison of Gas Diffusivity Models for Unsaturated Porous Media. Soil Sci. Soc. Am. J.52;1559-1565.

Davis, G.B. and Ritchie, A.I.M. 1986. A model of oxidation in pyritic mine wastes -I. Equations and approximate solutions. Appl. Math. Model, Vol.10, pp. 314-322.

Davis, G.B., Doherty, G. and Ritchie, A.I.M. 1986. A model of oxidation in pyritic mine wastes - II. Comparisons of numerical and approximate solutions. Appl. Math. Model, Vol. 10, pp. 323-330.

Davis, G.B. and Ritchie, A.I.M. 1987. A model of oxidationin pyritic mine wastes-III. Import of perticle size distribution. Appl. Math. Model, Vol. 11, pp. 417-422.

Ferguson, K.D. and Erickson, P.M. 1988. Approaching the AMD Problem - from Prediction and Early Detection. Proceedings, International Conference on Control of Environmental Problems form Metal Mines. June 20-24, 1988. Roros, Norway.

Ferguson, K.D. and Morin, K.A. 1991. The Prediction of Acid Rock Drainage - Lessons from the Database. Proceedings, Second International Conference on the Abatement of Acidic Drainage, Tome 4. September 16-18, 1991. Montréal.

Ferguson, K.D., 1985. Static and Kinetic Methods to Predict Acid Mine Drainage. Environmental Protection Manuscript Report, Conservation and Protection. Environment Canada, Pacific and Yukon Region.

Ferguson, K.D. and Erickson, P.M. 1988. Pre-mine prediction of acid mine drainage. Environmental Management of Solid Waste - Dredged Material and Mine Tailings. Salomons, W. and Forstner, U. (Eds.) Springer - Verlag Berlin Heidelberg. pp. 24-43.

Ferguson, K.D. and Erickson, P.M. 1988. Will It Generate AMD? An Overview of Methods to Predict Acid Mine Drainage.

Fillion, M.P., Sirois, L.L. and Ferguson, K. 1990. Acid Mine Drainage in Canada. CIM Bulletin, December 1990.

Fillion, M.P. and Ferguson, K. 1990. Acid drainage research in Canada. In: Proceedings, 92nd Annual General Meeting of CIM. Paper No. 131.

Finkelman, R.B. and Griffin, D.E. 1986. Hydrogen peroxide oxidation: an improved method for rapidly assessing acid-generating potential of sediments and sedimentary rocks. Recreation and Revegetation Research. Vol.5, pp. 521-534.

Firlotte, F.W., Gelinas, P., Knapp.,R. and McMullen, J. 1991. Acid Drainage Treatment at the Mine Doyon: Evolution and Future Direction. Proceedings, Second International Conference on the Abatement of Acidic Drainage, Tome 4. September 16-18, 1991. Montréal.

Geigel, G. 1980. Alkaline and acid production potentials of overburden material: the rate of release. Reclamation Review, Vol.2, pp. 101-107.

Gerencher, E.H., Wong, J.Y., van Dyk, R. and Konasewich, D.E. 1991. The Use of Mine Tailings in Concrete Surface Covers to Control Acid Mine Drainage in Waste Rock Dumps. Proceedings, Second International Conference on the Abatement of Acidic Drainage, Tome 4. September 16-18, 1991. Montréal.

Gibson, D.K. and Ritchie, A.I.M. 1992. Options to Control Acid Generation in Existing Pyritic Mine Waste Dumps. Environmental Science Program, Australian Nuclear Science and Technology Organization. Menai, Australia.

Gleason, V.E . and Russel, H.H. 1976. Mine Drainage Bibliography, 1910-1976. United States Environmental Protection Agency and Pennsylvania Department of Environmental Resources.

Gleason, V. E. 1980. Mine drainage bibliography, 1929-1980. Industrial Environmental Research Laboratory, Office of Research and Development, U.S. Environmental Protection Agency ; Springfield, VA.

Goodman, A.E., Babij, T. and Ritchie, A.I.M. 1983. Leaching of a sulphide ore by Thiobacillus Ferrooxidans under anaerobic conditions. International Symposium on Biohydrometallurgy. May 1-4, 1983. Cagliari.

Guertin, D.F., Emerick, J.C., and Howard, E.A. 1985. Passive mine drainage treatment systems; a theoretical assessment and experimental evaluation. Colorado Mined Land Reclamation Division. Colorado School of Mines, Dept. of Environmental Sciences and Engineering Ecology, Golden, CO.

Guo, W. and Parizek, R.R. 1992. Research on thermal anomalies indicating acid reactions in mine spoil and temperature prediction by numerical model. Proceedings - Environmental Geochemistry of Sulfide Oxidation, ACS Symposium Series 550 (Eds. C.N. Alpers and D.W. Blowes), Washington DC, August 23-28, 1992.

Haile, J.P. and East, D.R. 1986. Recent developments in the design of drained tailings impoundments. Geotechnical and Geohydrological Aspects of Waste Management. pp. 301-306.

Hallam, R.L., Haile, J.P., and Brouwer, K.J. 1991. Waste Disposal Practices for Control of Acidic Drainage. Proceedings, Second International Conference on the Abatement of Acidic Drainage, Tome 4. September 16-18, 1991. Montréal.

Hammack, R.W. and Watzlaf, G.R. 1990. The effect of oxygen on pyrite oxidation. In Proceedings of the Mining and Reclamation Conference (Charleston, WV, April 23-26, 1990).

Harries, J.A. 1969. Proc. Australasian Inst. Min. Met. Vol. 230, pp. 81-92.

Harries, J.R. and Ritchie, A.I.M. 1981. The use of temperature profiles to estimate the pyritic oxidation rate in a waste rock dump from an opencut mine. Pollution, Vol. 15, pp. 405-423.

Harries, J.R. and Ritchie, A.I.M. 1982. Pyritic Oxidation in Mine Wastes: its incidence, its impact on water quality and its control. Proceedings, Prediction on Water Quality, Nov. 30 - Dec. 2, 1982. Canberra, Australia

Harries, J.R. and Ritchie, A.I.M. 1984. The effects of rehabilitation on the oxygen concentrations in waste rock dumps containing pyritic material. Proceedings, 1984 Symposium on Surface Mining, Hydrology, Sedimentology and Reclamation, December 2-7, 1984. Lexington, KY.

Harries, J.R. and Ritchie, A.I.M. 1985. Pore gas composition in waste rock dumps undergoning pyritic oxidation. Soil Science, Vol. 140, pp. 143-152.

Harries, J.R. and Ritchie, A.I.M. 1987. Measurement and Control of Oxidation Rates in Pyritic Mine Wastes. International Seminar on Heap and Underground Bacterial Leaching Metals. June 1-5, 1987. Leningrad, USSR.

Harries, J.R. and Ritchie, A.I.M. 1987. The effect of rehabilitation on the rate of oxidation of pyrite in a mine waste dump. Environmnetal Geochemistry and Health, Vol. 9, No. 2, pp. 27-36.

Harries, J.R. and Ritchie, A.I.M. 1988. Rehabilitation of waste rock dumps at the Rum Jungle Mine Site. Proceedings, International Conference on Control of Environmental Problems from Metal Mines, June 1988. Roros, Norway.

Harries, J.R. and Ritchie, A.I.M. 1990. Australian Experience in Controlling Acid Generation in Mine Waste Rock Dumos. Proceedings, GAC-MAC Conference, May 16-18, 1990. Vancouver.

Hill, R. D. and Bates, E.R. 1978. Acid mine drainage and subsidence : effects of increased coal utilization. Environmental Protection Agency, Office of Research and Development, Industrial Environmental Research Laboratory ; Springfield, VA.

Hood, W.C. and Oertel, A.O. 1984. A leaching column method for predicting effluent quality from surface mines. Proceedings, 1984 Symposium Surface Mining Hydrology, Sedimentolgy, and Reclamation. University of Kentucky, Lexington, KY.

Hustwit, C. C., Ackman, T.E., and Erickson, P.M. 1992. Role of oxygen transfer in acid mine drainage treatment. U.S. Department of Interior, Bureau of Mines, Washington, D.C.

Jambor, J.L. and Blowes, D.W. 1989. Minerological Examination of Tailings from the Heath Steele Mill, Newcastle Area, New Brunswick. CANMET, Energy, Mines and Resources Canada, No. MSL 91-26(IR).

Jaynes, D.B., Rogowski, A.S. and Pionke, H.B. 1984. Acid mine drainage from reclaimed strip mines. 1. Model description. Water Resources Research, Vol. 20, pp. 233-242.

Jongejan, A. 1983. Progress report on the use of wood waste for acid mine water pollution abatement. CANMET, Energy, Mines and Resources and Resources Canada. No. MRP/MSL 83-116 (IR). Ottawa.

Kim, A.G. 1982. Acid Mine Drainage: control and abatement research. U.S. Department of Interior, Bureau of Mines. Pittsburgh, PA.

Kleinmann, R.L.P., Hedin, R.S. and Edenborn, H.M. 1991. Biological Treatment of Mine Water: An Overview. Proceedings, Second International Conference on the Abatement of Acidic Drainage, Tome 4. September 16-18, 1991. Montréal.

Kleinnmann, R.L.P. and Erickson, P.M. 1983. Control of acid drainage from refuse using anionic surfactants. U.S. Department of Interior, Bureau of Mines. Pittsburgh, PA.

Konasewich, D., Jones, C., Morin, K. and Gerencher, E., 1990. Hydrogeological Assessment and Development of AMD Control Technical Report for Myra Falls Waste Rock. British Columbia Acid Mine Drainage Task Force.

Lapakko, K. 1987. Prediction of AMD from Duluth Complex Mining Waste in North Eastern Minnesota. Proceedings, Acid Mine Drainage Workshop. DSS cat. No. En. 40-11-7 11987E, pp. 187-221.

Lin, H.K and Sohn, Y. 1987 Mixed-control kinetics of oxygen leaching of chalcopyrite and pyrite from primary ore fragments, Metallurg. Trans. B. Vol. 18B, pp. 497-503.

Lindhal, L-A. 1990. Acid Mine Drainage - Research and Remedial Actions in Sweden. Proceedings, Acid Mine Drainage Designing for Closure - GAC/MAC Joint Annual Meeting, May 16-18, 1990. Vancouver.

Liseth, P. 1991. Abatement Measures for the Acid Mine Drainage at Skorovas Mine, Norway. Proceedings, Second International Conference on the Abatement of Acidic Drainage, Tome 4. September 16-18, 1991. Montréal.

Lowson, R. T. 1982. Aqueous oxidation of pyrite by molecular oxygen. Chemical Reviews, Vol. 82, pp. 461-497.

Lowson, R.T. 1991. An O_2 Tracer Study of Pyrite Oxidation. Proceedings, Second International Conference on the Abatement of Acidic Drainage, Tome 4. September 16-18, 1991. Montréal.

Lundgren, T. and Lindhal, L.-Å. 1991. The Efficiency of Covering the Sulphidic Waste Rock in Bersbo, Sweden. Proceedings, Second International Conference on the Abatement of Acidic Drainage, Tome 3. September 16-18, 1991. Montréal.

Lundgren, T. and Lindhal, L.-Å. 1991. Remedial Action Programs for Sulphidic Wastes From Ancient Mining in Central Sweden. Proceedings, Second International Conference on the Abatement of Acidic Drainage, Tome 3. September 16-18, 1991. Montréal.

Macalady, D. L., Smith, K.S. and Ranville, J.F. 1990. Acid Mine Drainage: streamed adsorption of copper, cadmium and zinc. Colorado Water Resources Research Institute, Colorado State University, Fort Collins, CO.

MacDonald, D.G. and Grandt, A.F. 1981. Limestone-lime treatment of acid drainage -full scale. U.S. Environmental Portection Agency, Office of Research and Development, Industrial Environmental Research Laboratory. Cincinnati, OH.

Malhotra, V.H., Carette, G.G. and Bilodeau, A. 1990. Fibre-reinforced high-volume fly ash shotcrete for controlling aggressive leachates from exposed rock surfaces and mine tailings. CANMET International Workshop on Fly Ash in Concrete. Calgary, Canada.

McIntire, P.E., and Edenborn, H.M. 1990. The Use of Bacterial Sulfate Reduction in the Treatment of Drainage from Coal Mines. Proceedings, 1990 Mining and Reclamation Conference and Exhibition Volume II. April 23-26, 1990. Charleston, WV.

Meek, A., 1991. Assessment of Acid Preventative Techniques Employed at Island Creek Mining Company Ten Mile Site. Proceedings, West Virginia Surface Mine Drainage Task Force Symposium, Morgantown, WV.

Miller, S.D., Jeffery, J.J. and Wong, J.W.C. 1991 In-pit identification and management of acid-forming waste rock. Second International Conference on the Abatement of Acidic Drainage, Tome 3, September 16-18, 1991. Montréal.

Miller, S.D., Jeffery, J.J. and Wong, J.W.C. 1991. Use and Misuse of the Acid-Base Account for 'AMD' Prediction. Proceedings, Second International Conference on the Abatement of Acidic Drainage. Tome 3. September 16-18, 1991. Montréal.

Mills, A.L., Bell, P.E., and Herlihy, A.T. 1989. Microbes, sediments and acidified water: the importance of biological buffering. Acid Stress and Aquatic Microbial Interactions. CRC Press. pp. 1-19.

Morin, K.A. 1990. Problems and proposed solutions in predicting acid drainage with acid-base accounting. Proceedings, Acid Mine Drainage - Designing for Closure - GAC/MAC Joint Annual Meeting, May 16-18, 1990. Vancouver.

Morrison, B. and Pfeiffer, J.B. 1989. Application of Terta's Crysta Bond Service for Treatment of Gold Mine Acid Waste Waters. Sacramento. pp 165-169.

Nicholson, R.V. 1984. Pyrite oxidation in carbonate-buffered systems: experimental kinetics and control by oxygen diffusion in porous media. Ph.D. thesis, University of Waterloo, Waterloo, Ont.

Nicholson, R.V., Gillham, R.W., Cherry, J.A., Reardon, E.J. 1989. Reduction of acid generation in mine tailings through the use of moisture-retaining cover layers as oxygen barriers. Candian Geotechnical Journal, Vol. 26, No. 1, pp.1-8.

Nicholson, R.V., Akundunni, F.F., Sydor, R.C. and Gillham, R.W. 1991. Saturated tailings covers above the water table; the physics and criteria for design. Proceedings of the 2nd Int. Conf. on Abatement of Acidic Drainage. Montreal, Que.

Nolan, Davis & Associates Ltd. 1987. Study of Acid Waste Rock Management at Canadian Base Metal Mines. CANMET, Energy, Mines and Resources Canada, Ottawa.

Nolan, Davis and Associates (N.S.) Limited. 1990. Heath Steele Waste Rock Study Phase II Report. Brunswick Mining & Smelting Corporation Limited.

Nordstrom, D.K. 1982. Aqueous Pyrite Oxidation and the Consequent Formation of Secondary Minerlas. Acid Sulphate Weathering, Soil Scinece of America, pp. 37-56.

Northwest Geochem. 1990. Hydrogeological assessment and Development of AMD Control Technology for Myra Falls Waste Rock. Westmin Resources and the British Columbia Acid Mine Drainage Task Force.

Pantelis, G. and Ritchie, A.I.M. 1991. Macroscopic transport mechanisms as a rate-limiting factor in dump leaching of pyritic ores. Appl. Math. Modelling. Volume 15, pp. 136-143.

Pantelis, G. and Ritchie, A.I.M. 1992. Rate-limiting factors in dump leaching of pyritic ores. Appl. Math. Modelling. Volume 16, pp. 553-559.

Perrier, R. and MacLatchy, J.E. 1991. The Federal Regulatory Perspective in Canada on Acid Mine Drainage. Proceedings, Second International Conference on the Abatement of Acidic Drainage, Tome 4. Annexe I September 16-18, 1991. Montréal.

Peters, T.H. 1984. Rehabilitation of mine tailings: A case of complete ecosystem reconstruction and revegetation of industrially stressed lands in the Sudbury area, Ontario, Canada. Effects of Pollutants at the Ecosystem Level. John Wiley and Sons, New York. pp. 403-421.

Rasmuson, A. and Eriksson, J.-C. 1986. Capillary barriers in covers for mine tailings. National Swedish Environmental Protection Board, Report 3307.

Renton, J., Rymer, T. and Stiller, A. 1988. A Laboratory Procedure to Evaluate the Acid Producing Potential of Coal Associated Rocks. Mining Science and Technology, Vol. 1988, No. 7.

Rescan Environmental Services Ltd. 1990. A Preliminary Assessment of Subaqueous Tailings Disposal in Anderson Lake, Manitoba. British Columbia Ministry of Energy, Mines and Petroleum Resounses, CANMET, Environment Canada, Hudson Bay Mining and Smelting Co. Ltd.

Ritchie, A.I.M. 1977. Heap Leaching: A Gas Diffusion Rate-Limited Model. Australian Atomic Energy Commission Report E429.

Ritchie, A.I.M. 1992. Rates of mechanisms which govern pollutant generation from pyritic wastes. Paper presented at Environmental Geochemistry of Sulphide Oxidation, Washington.

Ritchie, A.I.M. 1992. Rates of mechanisms which govern pollutant generation from pyritic wastes. Proceedings, Acid Mine Drainage Workshop, Tasmania Chamber of mines, July 1992. ACN 009 554 616. Strahan, Tasmania.

Robertson, A. M. and Barton-Bridges J.P. 1990. Cost Effective Methods of Long Term Acid Mine Drainage from Waste Rock Piles. Proceedings of Acid Mine Drainage Designing for Closure - GAC/MAC Joint Annual Meeting, May 16-18, 1990. Vancouver.

Robertson, A.M., 1986. Mine Waste Disposal: an update on geotechnical and geohydrological aspects. Geotechnical and Geohydrological Aspects of Waste Management, pp. 31-50.

Robertson, J.D. 1991. Subaqueous Disposal of Reactive Mine Waste: An overview of the practice with case studies. Proceedings, Second International Conference on the Abatement of Acidic Drainage, Tome 3. September 16-18, 1991. Montréal.

Roach, G.I.D. and Prosser, A.P. 1975. Hydrometallurgy, V.1, pp. 79-91.

Roach, G.I.D. and Prosser, A.P. 1977. Hydrometallurgy, V.1, pp. 211-218.

Roach, G.I.D. and Prosser, A.P. 1978. Trans. Instn Min. Metall. (Sect. C), Vol. 87, pp. C129-C138.

Roman, R.J. Benner, B.R. and Becker, G.W. 1974. Tans., S.M.E., A.I.M.E., V.256, pp. 247-252.

Rymer, T., Renton, J.J., and Ziemkiewicz, P.F. 1991. Isolation of Critical Predictive Acid Producing Parameters from Variable Field Data Using Advanced Computer Technology. Proceedings, Second International Conference on the Abatement of Acidic Drainage, Tome 4. September 16-18, 1991. Montréal.

Scharer, J.M., Bryerley, J.J., Kwong, E. and Nicholson, R.V. 1993. Role of Biologically assisted pyrrhotite oxidation in acid mine drainage. Proccedings - International Biohydro-metallurgy Symposium (Eds. A.E. Torma, M.L. Apel and C.L. Brierley), Jackson Hole, Wyoming, USA, August 22-25, 1993.

Senes and Beak. 1986. Estimation of the limits of acid generation by bacterially assisted oxidation in uranium mill tailings. Report by Senes Consultants and Beak Consultants for the National Uranium Tailings Program, Energy, Mines and Resources Canada, Ottawa, Ont.

Shilbey, P.W.M. and Dymov, I.K. 1991. Flocculated Precipitants Reaction Technique Yields Coarse Precipitates. Proceedings, Second International Conference on the Abatement of Acidic Drainage, Tome 3. September 16-18, 1991. Montréal.

Singer, P.C. and Stumm, W. 1970. Acid mine drainage: the rate determining step. Science, Washinton, D.C., Vol. 167.

Skousen, J.G. 1991. Cooperative Efforts in Solving AMD Problems: The Surface Mine Drainage Task Force and the AMD Technical Advisory Committee. Proceedings, Second International Conference on the Abatement of Acidic Drainage, Tome 4. September 16-18, 1991. Montréal.

Smith, A. and Barton-Bridges, J.B. 1991. Some Considerations in the Prediction and Control of Acid Mine Drainage Impact on Groundwater from Mining in North America. Proceedings of the EPPIC Water Symposium, May 16-17, 1991. Johannesburg.

Smith, K.S. and Macalady, D.L. 1991. Water/Sediment Partitioning of Trace Elements in a Stream Receiving Acid-Mine Drainage. Proceedings, Second International Conference on the Abatement of Acidic Drainage, Tome 3. September 16-18, 1991. Montréal.

Sobek, A.A., Hossner, L.R., Sorenson, D.L., Sullivan, P.J., and Fransway, D.F. 1987. Acid-base potential and sulphur forms. Reclaiming Mine Soils and Overburden in the Western United States Analytic Parameters and Porcedures. Williams, R.D. and Schuman, G.E.(Eds.) Soil Conservation Society of America. Iowa. pp. 233-258.

Sodermark, B., Lundgren, T. 1988. The Bersbo project - The first full scale attempt to control acid mine drainage in Sweden. Proc. Intl. Conf. on Control of Environmental Problems from Metal Mines. Roros, Norway. June 1988.

State of Colorado, Department of Natural Resources, Division of Minerals and Geology. 1992. Prediction, prevention and control of acid mine drainage in the west. Breckenridge, CO.

Steffen, Robertson and Kirsten (B.C.) Inc. 1991. A Conceptual Rock Classification System For Waste Management and a Laboratory Method For ARD Prediction from Rock Piles. Proceedings, Second International Conference on the Abatement of Acidic Drainage, Tome 3. September 16-18, 1991. Montréal.

Steffen, Robertson and Kirsten (B.C.) Inc. 1991. Modelling of Leachate Quality From Acid Generating Waste Rock Dumps. Proceedings, Second International Conference on the Abatement of Acidic Drainage, Tome 3. September 16-18, 1991. Montréal.

Steffen, Robertson and Kirsten (B.C.) Inc. 1989. Draft Acid Rock Drainage Technical Guide (Vol I). British Columbia Acid Mine Drainage Task Force Report.

Steffen, Robertson and Kirsten (B.C.) Inc. 1992 Mine rock guidelines; design and control of drainage water quality. Saskatchewan Environment and Public Safety, Mines Pollution Control Branch.

Stuart D. Miller & Associates Pty Ltd. 1991. In-Pit Identification and Management of Acid Forming Waste Rock at the Golden Cross Gold Mine, New Zealand. Proceedings, Second International Conference on the Abatement of Acidic Drainage, Tome 3. September 16-18, 1991. Montréal.

Stuart D. Miller & Associates Pty. Ltd. 1987. Geochemistry of waste rock and tailings, Golden Cross Project. Cyprus Minerals (New Zealand) Ltd.

Sturey, C.S., Freeman, J.R., Keeney, T.A., and Sturm, J.W. 1982. Overburden analyses by acid-base accounting and simulated weathering studies as a means of determining the probable hydrologic consequences of mining and reclamation. Proceedings, 1982 Symposium Surface Mining Hydrology, Sedimentology, and Reclamation. University of Kentucky, Lexington, KY.

Veillette, G. and Desrochers, C.J. 1991. Reclamation of the Sobec Mine Site by Flooding Waste Rock in Open Pit. Proceedings, Second International Conference on the Abatement of Acidic Drainage, Tome 3. September 16-18, 1991. Montréal.

Whittemore, R.G. 1981. The modelling of vat, heap, dump and in-situ leaching systems. Pub. LR 381 (ME), Warren Spring Laboratory.

Williams, B.C., Lambeth, R.H., and Stewart, B.M. 1989. Determining Heavy Metal Leaching and Transport from Abandoned Mine Wastes. Proceedings, Society of Mining Engineers Annual Meeting, Las Vegas, NV.

Williams, E.G., Rose, A.W., and Parizekb, R.R. 1982. Factors controlling the operation of acid mine drainage. Final Report. U.S. Department of Interior, Bureau of Mines. Washington, D.C.

Wilson, G.W., Barbour, S.L. and Fredlund, D.G. 1991. The Evaluation of Evaporative Fluxes from Soil Surfaces for the Design of Dry Covers and the Abatement of Acid Drainage. Proceedings, 44th Annual Candian Geotechnical Conference, Ocober, 1991. Calgary.

Wood, I.B. 1991. Acid Mine Drainage: A Tasmanian Case Study in the Context of Australian Environmental Legislation. Proceedings, Second International Conference on the Abatement of Acidic Drainage, Tome 3. September 16-18, 1991. Montréal.

Yanful, E.K. 1991. Engineered Soil covers for Reactive Tailings Management. Theoretical Concepts and Laboratory Development. Proceedings, Second International Conference on the Abatement of Acidic Drainage, Tome 1. September 16-18, 1991. Montréal.

Yanful, E.K. 1993. Oxygen diffusion through soil covers on sulphidic mill tailings. ASCE Journal of Geotechnical Engineering, Vol. 119, No. 8.

Yanful, E.K. and St-Arnaud, L.C. 1991. Design, instrumentation and construction of engineered soil covers for reactive tailings management. Proceedings of the Second International Conference on Abatement of Acidic Drainage, Montreal, September 1991.

Yanful, E.K., Bell, A.V. and Woyshner, M.R. 1993. Construction and monitoring of a composite soil cover on an experimental waste rock pile near Newcastle, New Brunswick, Canada. Canadian Geotech. Journal, V.30;588-599.

Yanful, E.K., Riley, M.D., Woyshner, M.R. and Duncan, J. 1993. Construction and monitoring of a composite soil cover on an experimental waste rock pile near Newcastle, New Brunswick, Canada. Canadian Geotech. Journal, V.30;588-599.

APPENDIX II

Field Data

Station	Port	Depth (m)	28 91/01/18	91/04/11	91/05/22	91/06/19	91/07/19	91/08/21	92/03/17	92/04/22	92/05/26	92/06/29	92/07/14	92/08/17
1	1	1.40	20.50	20.00	21.00	19.00	15.50	20.50	6.80	0.60	0.60	0.50	0.46	0.80
	2	0.50	20.50	20.00	21.00	18.50	15.00	20.00	6.70	0.30	0.50	0.30	0.40	0.90
	3	0.40	20.50	20.80	21.00	18.20	15.00	19.50	11.50	1.60	0.60	2.50	0.32	1.20
2	1	3.90	20.50	19.50	19.50	11.00	9.00	11.50	NA	NA	1.90	0.50	0.29	0.22
	2	2.40	NA	15.50	18.50	13.50	10.00	9.40	NA	NA	1.60	1.10	0.39	0.60
	3	1.90	NA	14.50	17.00	17.50	14.00	9.60	NA	0.80	1.40	0.80	0.31	0.60
	4	1.40	17.50	15.50	18.50	20.30	12.00	13.50	NA	0.80	1.50	0.85	0.27	1.50
	5	0.90	NA	16.50	20.50	20.80	18.50	13.50	NA	1.10	1.30	0.72	0.29	0.20
	6	0.40	18.00	18.00	20.50	20.80	20.00	12.00	NA	0.80	1.20	0.50	0.21	0.45
3	1	4.10	NA	18.00	19.00	11.80	9.50	13.00	3.10	0.30	1.20	0.60	0.60	0.45
	2	2.90	NA	NA	19.00	10.00	13.20	NA	NA	NA	NA	NA	NA	NA
	3	2.40	NA	18.00	19.00	8.10	6.70	11.50	7.00	0.60	1.10	0.80	0.47	NA
	4	1.90	NA	15.50	18.50	11.00	5.00	8.20	4.20	0.60	1.00	0.85	0.42	0.32
	5	1.40	NA	16.50	18.00	16.50	13.00	9.50	2.10	1.00	0.90	0.50	0.27	0.20
	6	0.90	NA	18.00	19.00	19.20	15.00	12.50	1.90	1.70	0.80	0.40	0.25	0.14
	7	0.40	NA	18.00	20.90	20.20	20.50	14.50	NA	NA	NA	NA	NA	NA
4	1	4.30	NA	NA	20.50	20.20	NA	NA	NA	NA	NA	NA	NA	NA
	2	2.80	NA	19.00	19.00	14.00	11.50	15.00	2.00	0.60	0.90	0.20	0.35	0.15
	3	2.30	NA	19.00	17.50	13.00	10.50	14.50	NA	0.20	0.80	0.30	0.10	0.24
	4	1.80	NA	19.00	19.00	13.50	10.50	14.50	1.90	4.40	0.70	0.05	0.09	0.15
	5	1.30	NA	19.00	18.00	13.50	10.50	13.50	2.20	4.80	0.70	0.10	0.29	0.13
	6	0.80	NA	18.50	18.00	13.00	10.00	12.50	NA	4.80	0.80	2.50	0.36	0.21
	7	0.30	NA	19.00	20.00	15.50	NA	12.50	NA	3.30	0.80	2.35	0.21	0.13
5	1	3.70	NA	20.00	18.50	16.00	12.00	16.00	NA	NA	NA	NA	NA	NA
	2	2.30	NA	20.50	18.50	17.00	12.50	18.00	NA	1.00	0.90	0.50	0.29	0.07
	3	1.70	NA	20.50	20.00	19.50	NA	NA	NA	NA	NA	NA	NA	NA
	4	1.20	NA	19.00	17.50	18.50	10.50	15.50	NA	NA	NA	6.80	5.21	0.58
	5	0.70	NA	19.00	19.50	19.00	11.00	16.00	NA	9.00	0.80	4.10	1.20	2.94
	6	0.20	NA	18.50	20.50	19.00	12.50	17.50	NA	8.10	1.40	13.00	1.61	13.25
6	1	2.10	20.80	NA	18.50	18.00	19.00	20.50	NA	NA	0.70	0.05	0.12	0.15
	2	0.60	20.80	NA	18.00	17.50	18.00	20.50	NA	NA	0.70	0.05	0.41	0.21
	3	0.10	20.80	NA	18.00	17.50	16.00	19.00	NA	5.40	0.50	0.05	0.13	0.18

Station	Port	Depth (m)	92/08/26	92/10/14	92/11/03	93/03/19	93/04/24	93/05/21	93/07/13	93/09/10	93/10/01	93/10/26	93/11/29	93/12/22
1	1	1.40	0.17	0.15	0.19	NA	0.35	0.41	0.13	0.10	0.10	0.40	0.20	0.10
	2	0.50	0.07	0.15	0.11	NA	0.28	0.28	0.13	0.10	0.10	0.80	0.40	0.20
	3	0.40	0.12	0.12	0.11	NA	NA	NA	NA	NA	NA	NA	NA	0.30
2	1	3.90	0.28	0.35	0.33	0.40	0.23	0.13	0.11	0.00	0.20	0.40	1.00	0.20
	2	2.40	0.26	0.30	0.26	0.20	0.25	0.08	0.08	0.00	0.10	0.40	0.60	0.20
	3	1.90	0.20	0.27	0.21	0.10	0.14	0.07	0.11	0.00	0.80	0.60	0.20	0.20
	4	1.40	0.16	0.23	0.18	0.15	0.18	0.06	0.10	0.00	0.10	0.30	0.20	0.30
	5	0.90	0.13	0.20	0.18	0.10	0.17	0.06	0.10	0.00	0.10	0.30	0.30	0.20
	6	0.40	0.11	0.16	0.14	0.07	0.14	0.07	0.09	0.00	0.00	0.30	0.20	0.20
3	1	4.10	0.20	0.18	0.11	0.20	0.14	0.02	0.10	0.50	0.20	0.50	0.20	0.20
	2	2.90	NA	NA	NA	NA	NA	NA	NA	NA	NA	NA	NA	NA
	3	2.40	0.14	0.29	0.11	0.35	0.11	0.02	0.06	0.00	0.10	0.70	0.20	0.20
	4	1.90	0.13	0.32	0.20	0.20	0.09	0.02	0.06	0.00	0.00	0.60	0.30	0.30
	5	1.40	0.12	0.35	0.15	0.10	0.08	0.01	0.06	0.00	0.10	0.40	0.20	0.20
	6	0.90	0.11	0.28	0.11	0.08	0.08	0.01	0.04	0.00	0.10	0.20	0.20	0.30
	7	0.40	NA	NA	NA	NA	NA	NA	NA	NA	NA	NA	NA	NA
4	1	4.30	NA	NA	NA	NA	NA	NA	NA	NA	NA	NA	NA	NA
	2	2.80	0.12	0.15	0.08	0.25	0.08	0.07	0.10	0.00	0.20	0.50	0.20	0.30
	3	2.30	0.10	0.12	0.08	0.10	0.08	0.04	0.06	0.00	0.20	0.40	0.20	0.20
	4	1.80	0.09	0.15	0.07	NA	0.07	0.02	0.06	0.00	0.20	0.50	0.20	0.20
	5	1.30	0.09	0.14	0.06	NA	0.07	0.02	0.21	NA	0.20	0.60	0.20	0.30
	6	0.80	1.70	0.09	0.06	NA	3.23	0.15	2.88	0.00	0.30	6.10	0.20	0.30
	7	0.30	1.34	0.11	0.04	NA	3.22	0.09	1.43	0.00	0.40	6.30	0.20	0.30
5	1	3.70	NA	NA	NA	NA	NA	NA	NA	NA	NA	NA	NA	NA
	2	2.30	0.06	0.10	0.07	NA	0.09	0.03	0.06	0.00	0.10	0.50	0.20	0.20
	3	1.70	NA	NA	NA	NA	NA	NA	NA	NA	NA	NA	NA	NA
	4	1.20	0.54	0.32	0.08	NA	0.19	0.18	2.34	0.00	0.70	1.60	7.20	2.30
	5	0.70	3.19	0.10	0.22	NA	3.59	1.36	6.99	0.00	4.10	7.60	14.00	8.60
	6	0.20	12.66	0.12	0.80	NA	8.65	4.81	17.76	0.00	11.70	12.90	19.70	18.20
6	1	2.10	0.12	0.10	0.06	NA	0.07	0.04	0.06	0.00	0.10	0.40	0.20	0.30
	2	0.60	0.13	0.12	0.04	NA	0.05	0.01	0.04	0.00	0.10	0.30	0.20	0.40
	3	0.10	0.19	0.12	0.04	NA	0.05	0.01	0.04	0.00	0.10	0.20	1.80	0.50

Station	Port	Depth (m)	93/02/18	94/03/30	94/05/03
1	1	1.40	0.20	0.50	0.60
	2	0.50	0.20	0.30	0.20
	3	0.40	NA	NA	NA
2	1	3.90	NA	NA	0.50
	2	2.40	0.20	NA	0.30
	3	1.90	NA	NA	0.40
	4	1.40	0.20	0.20	0.30
	5	0.90	0.20	NA	0.30
	6	0.40	0.20	NA	0.40
3	1	4.10	0.50	NA	0.80
	2	2.90	NA	NA	NA
	3	2.40	0.30	NA	0.60
	4	1.90	0.30	NA	0.80
	5	1.40	NA	NA	NA
	6	0.90	NA	NA	NA
	7	0.40	NA	NA	NA
4	1	4.30	NA	NA	NA
	2	2.80	0.30	NA	0.30
	3	2.30	0.20	0.20	0.30
	4	1.80	0.20	0.20	0.90
	5	1.30	0.20	NA	0.60
	6	0.80	0.20	0.20	0.50
	7	0.30	0.10	0.20	0.50
5	1	3.70	0.50	NA	NA
	2	2.30	0.30	0.20	0.50
	3	1.70	NA	NA	NA
	4	1.20	0.20	0.10	0.60
	5	0.70	1.20	0.10	0.40
	6	0.20	5.10	0.20	0.40
6	1	2.10	0.20	0.20	1.10
	2	0.60	0.20	0.30	0.80
	3	0.10	0.20	NA	0.60

Station	Port	depth (m)	31.00 91/04/11	91/05/22	91/06/19	91/07/19	91/08/21	91/10/22	92/03/17	92/04/22	92/05/26	92/06/29	92/07/15	92/08/17
1	1	3.20	NA	21.00	NA	20.80	NA	NA	21.00	NA	NA	NA	NA	NA
	2	2.60	20.00	19.50	20.00	NA	20.00	21.80	NA	NA	20.00	20.20	19.59	20.50
	3	2.00	20.00	19.50	20.20	20.00	20.00	21.80	17.50	NA	18.00	20.20	19.29	20.50
	4	1.40	20.00	19.50	11.00	20.00	20.00	21.80	NA	NA	19.20	20.30	19.22	20.20
	5	0.80	NA	20.00	11.00	20.00	20.00	21.80	NA	NA	19.00	20.50	19.28	20.20
	6	0.20	20.50	20.00	NA	20.50	20.00	21.80	16.50	NA	19.00	20.80	20.50	20.80
2	1	4.60	19.50	18.50	19.50	16.00	17.50	20.00	NA	NA	20.00	16.20	15.96	15.20
	2	4.00	19.50	18.50	19.00	14.50	17.00	10.00	NA	NA	20.00	16.00	15.26	16.10
	3	3.40	19.00	19.00	19.50	11.50	16.50	20.00	NA	NA	20.00	14.80	13.91	13.80
	4	2.70	19.00	19.00	19.50	10.50	17.00	20.00	NA	NA	20.00	14.00	15.54	14.40
	5	2.10	19.00	19.00	17.00	7.00	17.00	20.00	NA	NA	20.00	13.00	13.10	12.80
	6	1.50	19.00	18.50	13.50	4.70	17.00	20.00	NA	NA	20.00	12.00	12.48	11.40
	7	0.90	15.00	17.50	13.00	11.50	16.50	19.50	NA	NA	20.00	16.50	14.39	18.00
3	1	4.60	NA	17.50	20.20	17.50	18.00	20.00	NA	NA	NA	17.50	15.68	15.70
	2	4.00	20.00	17.50	20.00	16.00	16.50	20.00	NA	NA	20.50	17.10	14.14	14.70
	3	3.40	19.50	17.50	20.00	14.00	15.50	20.00	NA	NA	20.50	16.00	12.21	13.70
	4	2.70	19.00	18.00	15.50	10.50	14.00	19.50	NA	NA	20.50	15.50	11.34	12.90
	5	2.10	18.00	17.50	8.40	3.80	13.00	19.00	NA	NA	19.50	13.50	9.59	11.50
	6	1.50	18.50	16.50	6.80	1.40	10.50	18.50	NA	NA	18.50	8.60	6.96	6.80
	7	0.90	17.50	14.00	10.00	3.30	8.60	17.00	NA	NA	17.00	5.10	4.20	4.70
4	1	4.60	18.00	14.50	11.50	11.20	12.00	14.00	NA	20.00	18.50	11.60	9.09	9.90
	2	4.00	18.00	14.00	11.20	8.80	10.50	14.00	NA	20.00	18.00	10.40	7.29	7.90
	3	3.40	19.00	13.50	10.00	6.00	8.80	14.00	NA	19.50	17.50	8.10	5.91	9.60
	4	2.70	19.00	11.00	8.60	4.30	7.10	14.50	NA	20.00	15.50	6.00	5.17	4.60
	5	2.10	18.00	7.50	6.20	2.00	4.30	13.50	NA	19.50	14.50	3.90	2.78	4.50
	6	1.50	13.50	5.00	3.00	0.70	0.15	8.80	NA	19.00	11.50	0.50	0.93	3.00
	7	0.60	11.50	NA	3.00	1.40	0.10	6.50	17.50	18.00	8.10	0.08	0.20	5.20
5	1	3.70	15.00	8.50	2.80	3.80	NA	6.50	9.80	NA	6.00	2.90	1.24	1.50
	2	3.10	7.20	7.50	4.40	4.00	5.20	4.90	6.00	19.50	8.80	5.00	3.68	3.80
	3	2.50	7.80	9.00	5.50	4.50	5.80	6.10	8.20	19.50	10.50	4.60	4.12	7.20
	4	1.90	8.00	11.50	9.20	21.50	8.10	9.70	12.50	19.50	12.50	6.00	6.64	6.10
	5	1.20	11.50	14.00	14.50	7.00	9.80	12.50	8.50	19.50	14.50	6.90	6.59	7.20
	6	0.60	11.50	16.00	17.50	6.80	8.20	12.50	7.40	19.50	13.50	5.80	5.38	6.00
	7	0.10	20.00	NA	21.00	21.70	20.50	21.80	20.00	NA	20.80	20.80	NA	NA
6	1	4.30	NA	NA	18.00	20.00	9.60	NA	20.00	NA	NA	NA	3.51	4.70
	2	3.70	6.00	NA	12.50	9.30	9.60	5.20	18.50	21.80	12.50	5.10	7.41	6.50
	3	3.00	5.30	NA	13.50	7.10	4.70	1.50	NA	21.80	15.50	5.50	4.23	7.00
	4	2.40	13.50	NA	13.00	7.20	8.60	NA	19.00	21.80	13.50	5.00	4.78	9.50
	5	1.80	20.80	NA	14.00	7.00	NA	21.80	20.00	21.80	14.50	8.40	6.65	10.30
	6	1.20	NA	NA	16.00	10.50	11.50	21.80	19.00	21.80	16.00	13.70	11.64	11.30
	7	0.60	14.50	NA	14.50	7.30	12.00	17.50	15.00	21.80	NA	11.90	12.24	11.00

Station	Port	depth (m)	92/09/29	92/10/19	92/11/03	93/03/19	93/04/24	93/05/21	93/07/13	93/09/10	93/10/01	93/10/26	93/11/29	93/12/22
1	1	3.20	NA	NA	NA	NA	NA	NA	NA	NA	NA	NA	NA	NA
	2	2.60	20.48	20.35	20.33	17.50	20.50	19.20	19.49	19.50	20.80	20.50	21.40	20.30
	3	2.00	20.63	20.46	20.35	17.80	20.50	19.70	19.54	19.70	20.80	20.30	21.40	20.30
	4	1.40	20.75	20.46	20.45	17.80	20.55	19.60	19.54	19.70	20.80	20.60	21.30	20.40
	5	0.80	20.81	20.28	20.51	NA	20.60	19.80	19.56	19.60	20.80	20.60	21.40	20.50
	6	0.20	20.81	20.68	20.61	NA	20.80	20.60	20.80	20.80	21.50	20.70	21.60	NA
2	1	4.60	19.21	19.69	19.95	17.40	20.00	19.30	17.86	18.20	19.60	19.70	21.60	19.60
	2	4.00	19.06	19.55	19.86	17.50	20.40	19.41	16.97	17.90	19.70	19.60	20.70	19.60
	3	3.40	18.73	19.31	19.78	17.00	20.40	19.35	16.11	NA	20.10	19.90	20.90	19.70
	4	2.70	18.66	19.92	19.93	17.00	20.50	19.31	16.93	19.80	20.30	18.50	20.80	19.90
	5	2.10	18.39	20.09	19.91	15.90	20.65	19.12	15.58	17.70	20.10	18.60	20.60	19.90
	6	1.50	17.68	19.91	19.78	13.70	20.80	18.93	13.21	17.00	20.00	19.40	20.40	19.70
	7	0.90	18.88	19.27	19.61	10.00	20.80	18.12	10.45	15.90	19.30	19.60	20.10	19.00
3	1	4.60	19.91	19.88	20.29	16.90	20.40	19.87	16.65	18.00	16.80	18.00	18.30	19.10
	2	4.00	19.61	19.86	20.16	17.20	20.40	19.77	17.05	17.20	15.70	17.20	18.70	19.10
	3	3.40	19.53	19.79	20.18	17.20	20.40	19.65	16.75	15.40	16.00	15.40	18.90	19.30
	4	2.70	19.28	19.58	19.95	15.60	20.25	19.28	15.66	14.00	15.80	14.00	18.00	19.50
	5	2.10	19.23	19.23	19.55	10.60	19.95	18.09	12.32	13.30	15.20	13.30	18.40	19.20
	6	1.50	18.46	18.98	19.01	5.20	19.25	16.09	6.98	10.30	15.80	10.30	17.90	NA
	7	0.90	17.04	17.67	18.37	NA	19.00	14.65	3.58	7.70	16.30	7.70	15.80	18.80
4	1	4.60	17.97	16.07	16.33	11.40	18.70	16.86	10.16	9.80	12.90	9.80	17.40	18.30
	2	4.00	17.85	15.44	17.08	12.60	19.15	17.42	9.38	8.50	12.70	8.50	17.50	18.50
	3	3.40	17.71	14.74	17.68	13.60	19.70	16.76	7.63	6.90	12.40	6.90	17.40	18.90
	4	2.70	17.55	12.26	16.89	14.80	19.75	14.74	5.79	5.30	11.50	5.30	17.10	18.90
	5	2.10	16.75	10.21	15.22	NA	19.10	12.42	3.40	3.40	9.70	3.40	16.20	NA
	6	1.50	15.62	6.35	12.32	9.70	16.60	8.58	0.46	0.70	4.80	0.70	14.80	19.10
	7	0.60	15.28	3.74	11.18	5.40	15.35	5.22	0.04	0.50	1.20	0.50	13.40	NA
5	1	3.70	16.63	2.98	1.46	1.80	7.80	6.62	1.62	2.40	3.00	2.40	2.50	2.70
	2	3.10	17.38	4.89	4.23	NA	9.90	7.87	4.01	4.60	6.30	4.60	5.30	5.00
	3	2.50	17.51	7.92	6.62	6.70	10.30	8.77	4.80	5.30	7.90	5.30	9.00	7.80
	4	1.90	17.94	12.42	10.79	8.20	11.45	10.35	6.55	7.30	11.30	7.30	12.40	10.70
	5	1.20	18.29	14.59	13.61	7.60	12.70	11.30	7.16	8.10	14.20	8.10	13.80	11.50
	6	0.60	18.02	14.31	13.82	NA	12.75	10.98	4.62	7.10	14.10	7.10	13.10	10.80
	7	0.10	NA	NA	NA	NA	NA	NA	NA	NA	NA	NA	NA	NA
6	1	4.30	18.43	5.16	3.91	NA	9.60	9.73	4.91	1.70	4.50	1.70	4.40	2.80
	2	3.70	18.49	6.04	4.26	NA	9.75	9.85	5.35	1.80	5.00	1.80	8.00	3.10
	3	3.00	18.43	6.51	8.11	18.10	10.90	10.82	5.32	3.00	8.90	3.00	14.90	5.90
	4	2.40	19.13	10.78	16.03	16.90	11.50	11.77	5.07	6.30	12.80	6.30	17.50	15.10
	5	1.80	19.39	13.60	15.85	NA	15.80	NA	5.81	6.20	12.70	6.20	17.50	14.90
	6	1.20	19.66	15.75	16.67	NA	17.30	14.18	7.76	8.00	15.10	8.00	17.90	14.70
	7	0.60	20.05	16.70	18.17	NA	NA	14.23	7.08	9.10	17.80	9.10	18.20	14.60

Station	Port	depth (m)	93/10/01	93/11/29	93/12/22	94/02/18	94/03/30	94/05/03
1	1	3.20	NA	NA	NA	NA	NA	NA
	2	2.60	20.80	21.40	20.30	18.70	12.20	20.40
	3	2.00	20.80	21.40	20.30	18.70	12.10	20.20
	4	1.40	20.80	21.30	20.40	18.80	12.40	20.00
	5	0.80	20.80	21.40	20.50	18.90	12.00	19.80
	6	0.20	21.50	21.60	NA	NA	NA	19.70
2	1	4.60	19.60	20.60	19.60	18.10	NA	17.30
	2	4.00	19.70	20.70	19.60	18.50	NA	19.30
	3	3.40	20.10	20.90	19.70	19.00	NA	19.90
	4	2.70	20.30	20.80	19.90	18.80	NA	20.20
	5	2.10	20.10	20.60	19.90	NA	NA	20.00
	6	1.50	20.00	20.40	19.70	17.30	NA	19.70
	7	0.90	19.30	20.10	19.00	NA	NA	NA
3	1	4.60	16.80	18.30	19.10	15.40	NA	16.80
	2	4.00	15.70	18.70	19.10	15.70	NA	17.00
	3	3.40	16.00	18.90	19.30	NA	NA	17.30
	4	2.70	15.80	18.00	19.50	NA	NA	17.20
	5	2.10	15.20	18.40	19.20	NA	NA	16.90
	6	1.50	15.80	17.90	NA	NA	NA	16.70
	7	0.90	16.30	15.80	18.80	NA	2.30	17.30
4	1	4.60	12.90	17.40	18.30	15.30	11.30	16.70
	2	4.00	12.70	17.50	18.50	15.10	11.60	16.50
	3	3.40	12.40	17.40	18.90	14.80	12.10	16.40
	4	2.70	11.50	17.10	18.90	NA	NA	16.30
	5	2.10	9.70	16.20	NA	NA	11.00	15.90
	6	1.50	4.80	14.80	19.10	14.00	6.80	13.90
	7	0.60	1.20	13.40	NA	13.70	4.00	13.00
5	1	3.70	3.00	2.50	2.70	2.00	0.60	3.70
	2	3.10	6.30	5.30	5.00	5.60	1.40	6.10
	3	2.50	7.90	9.00	7.80	9.40	2.00	7.80
	4	1.90	11.30	12.40	10.70	11.90	2.60	10.90
	5	1.20	14.20	13.80	11.50	11.20	2.70	12.70
	6	0.60	14.10	13.10	10.80	NA	NA	14.10
	7	0.10	NA	NA	NA	NA	NA	NA
6	1	4.30	4.50	4.40	2.80	16.20	12.70	NA
	2	3.70	5.00	8.00	3.10	17.40	12.20	9.00
	3	3.00	8.90	14.90	5.90	18.80	13.30	9.60
	4	2.40	12.80	17.50	15.10	18.90	15.20	10.10
	5	1.80	12.70	17.50	14.90	18.90	15.20	13.10
	6	1.20	15.10	17.90	14.70	18.40	9.40	17.10
	7	0.60	17.80	18.20	14.60	17.40	5.30	19.20

Station	Port	DEPTH (m)	DEPTH (m)	21.0 91/01/18	91/04/11	91/05/22	91/06/19	91/07/17	91/08/21	91/10/22	92/03/17	92/04/22	92/05/26	92/07/14
1	Surface	0	0	NA	NA	24.3	30.2	40.7	17.3	NA	NA	5.0	12.2	NA
	Black	NA	NA	NA	NA	NA	NA	19.3	23.2	14.6	3.3	4.3	2.1	7.5
	Blue	0.1	0.1	-0.7	1.8	14.2	18.4	NA	17.7	11.9	-0.2	2.1	5.7	10.8
	Red	1.4	1.4	6.3	4.8	8.6	13.5	NA	NA	NA	NA	NA	NA	NA
2	Surface	0	0	NA	NA	33.1	32.0	39.4	15.7	NA	NA	5.5	14.1	NA
	Black	0.3	0.3	4.4	5.1	14.6	19.2	23.3	15.3	15.5	4.4	4.8	4.5	9.7
	Blue	0.9	0.9	13.8	9.1	13.5	17.5	9.3	22.8	17.3	6.4	6.5	4.2	8.9
	Red	3.9	3.9	22.9	16.9	12.9	13.7	16.2	21.3	19.0	11.9	11.5	6.8	NA
3	Surface	0	0	NA	NA	23.2	32.0	37.1	17.1	NA	NA	4.8	14.1	NA
	Black	0.4	0.4	4.4	4.9	16.3	21.8	24.3	16.9	14.1	4.4	4.8	4.8	10.8
	Blue	1.4	1.4	13.8	NA	13.5	17.1	12.5	24.0	17.4	8.0	7.5	4.4	NA
	Red	4.1	4.1	22.9	17.6	12.3	12.6	15.2	18.6	18.3	13.1	12.0	7.7	7.5
4	Surface	0	0	NA	NA	22.7	39.0	40.1	17.2	NA	NA	4.7	17.2	NA
	Black	0.3	0.3	3.0	4.9	17.5	24.4	26.7	17.5	14.2	3.5	3.6	6.5	NA
	Blue	1.3	1.3	17.6	12.9	14.2	17.6	22.7	25.5	18.3	7.1	6.7	5.3	NA
	Red	4.3	4.3	23.1	17.7	13.5	13.7	16.4	20.6	19.8	12.4	12.1	8.3	NA
5	Surface	0	0	6.5	NA	24.7	35.0	47.0	15.6	NA	NA	3.8	16.8	NA
	Black	0.2	0.2	3.3	5.0	16.6	23.8	27.7	17.7	14.1	4.5	NA	9.3	13.8
	Blue	0.7	0.7	9.0	8.5	15.7	20.9	27.2	24.4	16.2	5.9	5.5	7.7	13.1
	Red	3.7	3.7	23.5	17.6	15.6	16.8	20.7	26.1	21.2	12.3	10.0	7.6	8.6
6	Surface	0	0	NA	NA	21.8	36.0	44.7	17.7	NA	NA	3.5	14.4	NA
	Black	NA	NA	NA	NA	NA	NA	NA	NA	NA	NA	NA	NA	NA
	Blue	0.4	0.4	6.3	5.9	15.2	20.8	26.1	21.7	16.5	NA	6.2	6.5	11.4
	Red	2	2	11.1	10.3	13.5	17.6	22.1	24.8	18.1	NA	7.8	6.3	9.7
7	Surface	0	0	NA	NA	NA	42.0	45.5	17.2		NA	4.4	4.4	NA
	Black	0.7	0.7	17.3	12.1	NA	18.0	23.1	25.6	16.7	6.5	6.5	6.5	8.4

Station	Port	DEPTH (m)	92/08/17	92/09/29	92/11/03	93/03/19	93/04/24	93/05/21	93/07/13	93/09/10	93/10/01
1	Surface	0	26.7	13.8	NA	NA	NA	NA	NA	15.3	10.1
	Black	NA	9.2	11.4	NA	NA	NA	NA	7.8	12.3	9.4
	Blue	0.1	13.6	13.4	5.8	NA	NA	NA	13.9	15.3	NA
	Red	1.4	NA	NA	10.9	NA	NA	NA	NA	NA	NA
2	Surface	0	24.2	14.0	NA	NA	NA	NA	NA	15.3	10.1
	Black	0.3	12.1	13.3	6.1	NA	NA	NA	10.1	13.7	10.7
	Blue	0.9	11.1	12.8	8.9	NA	NA	NA	8.5	12.4	11.5
	Red	3.9	8.1	9.8	16.0	NA	NA	NA	4.2	8.1	7.5
3	Surface	0	NA	14.0	NA	NA	NA	NA	NA	15.3	10.1
	Black	0.4	12.7	12.8	12.3	NA	NA	NA	10.7	14.2	11.4
	Blue	1.4	NA	NA	16.8	NA	NA	NA	NA	NA	NA
	Red	4.1	8.0	8.6	16.0	NA	NA	NA	5.1	7.7	8.6
4	Surface	0	NA	14.0	NA	NA	NA	NA	NA	NA	NA
	Black	0.3	NA	NA	1.1	NA	NA	NA	NA	NA	NA
	Blue	1.3	NA	NA	9.5	NA	NA	NA	NA	NA	NA
	Red	4.3	NA	NA	14.9	NA	NA	NA	NA	NA	NA
5	Surface	0	NA	13.9	NA	NA	NA	NA	NA	15.3	10.1
	Black	0.2	15.5	14.9	5.1	NA	NA	NA	14.7	16.2	13.2
	Blue	0.7	14.8	14.9	8.9	NA	NA	NA	12.8	15.9	13.3
	Red	3.7	9.2	11.0	14.2	NA	NA	NA	6.5	9.9	9.8
6	Surface	0	NA	13.8	NA	NA	NA	NA	NA	15.3	10.1
	Black	NA	NA	NA	7.3	NA	NA	NA	NA	NA	NA
	Blue	0.4	12.8	13.4	10.9	NA	NA	NA	11.1	20.4	12.8
	Red	2	10.7	11.8	12.4	NA	NA	NA	8.1	12.0	10.7
7	Surface	0	NA	13.6	NA	NA	NA	NA	NA	15.3	NA
	Black	0.7	10.5	12.4	NA	NA	NA	NA	7.5	11.9	10.2

TABLE II-5

HEATH STEELE MINES

Station	Port	Depth (m)	93/11/29	93/12/22	93/02/18	94/03/30	94/05/03
1	1	1.40	9.98	9.32	10.80	8.49	8.32
	2	0.50	10.16	9.48	10.78	8.32	8.29
	3	0.40	9.42	8.96	NA	NA	NA
2	1	3.90	11.00	10.50	NA	NA	9.38
	2	2.40	9.69	9.36	12.19	NA	9.27
	3	1.90	8.49	8.18	NA	NA	8.77
	4	1.40	7.60	7.40	9.62	8.31	8.20
	5	0.90	7.41	7.14	9.53	NA	8.08
	6	0.40	6.86	6.76	9.05	NA	7.85
3	1	4.10	10.89	10.55	11.72	NA	9.45
	2	2.90	NA	NA	NA	NA	NA
	3	2.40	9.65	9.62	11.66	NA	9.33
	4	1.90	8.08	7.98	10.65	NA	8.55
	5	1.40	7.48	7.42	NA	NA	NA
	6	0.90	7.12	7.12	0.57	NA	8.14
	7	0.40	NA	NA	NA	NA	NA
4	1	4.30	NA	NA	NA	NA	NA
	2	2.80	9.70	9.84	11.05	NA	9.29
	3	2.30	9.12	9.34	10.93	9.00	9.27
	4	1.80	8.56	8.53	10.18	8.90	8.80
	5	1.30	8.28	8.13	9.85	NA	8.56
	6	0.80	6.64	6.61	8.69	7.98	8.06
	7	0.30	6.42	6.44	8.44	7.84	7.96
5	1	3.70	NA	10.38	10.81	NA	NA
	2	2.30	9.29	9.37	10.74	9.29	9.28
	3	1.70	NA	NA	NA	NA	NA
	4	1.20	6.33	7.91	9.78	8.97	8.91
	5	0.70	4.41	6.56	8.77	8.32	8.42
	6	0.20	0.92	3.41	7.72	8.09	8.04
6	1	2.10	10.40	10.05	10.45	9.26	9.24
	2	0.60	10.09	9.94	10.61	9.23	9.26
	3	0.10	8.79	9.14	10.24	NA	8.99

Station	Port	depth (m)	93/11/29	93/12/22	94/03/30	94/05/03
1	1	3.20	NA	NA	NA	NA
	2	2.60	0.33	0.30	0.94	0.17
	3	2.00	0.27	0.19	0.86	0.14
	4	1.40	0.27	0.14	0.85	0.13
	5	0.80	0.29	0.13	0.86	0.13
	6	0.20	0.18	NA	NA	-0.02
2	1	4.60	0.27	0.39	NA	0.68
	2	4.00	0.25	0.35	NA	0.64
	3	3.40	0.12	0.17	NA	0.16
	4	2.70	0.11	0.13	NA	0.12
	5	2.10	0.11	0.12	NA	0.14
	6	1.50	0.11	0.13	NA	0.16
	7	0.90	0.12	0.13	NA	NA
3	1	4.60	0.52	0.31	NA	0.39
	2	4.00	0.44	0.29	NA	0.37
	3	3.40	0.43	0.25	NA	0.31
	4	2.70	0.48	0.23	NA	0.30
	5	2.10	0.44	0.23	NA	0.32
	6	1.50	0.43	NA	NA	0.26
	7	0.90	0.43	0.22	0.71	0.19
4	1	4.60	0.64	0.43	0.62	0.37
	2	4.00	0.58	0.37	0.59	0.39
	3	3.40	0.57	0.33	0.56	0.42
	4	2.70	0.57	0.32	NA	0.43
	5	2.10	0.57	NA	0.84	0.44
	6	1.50	0.47	0.28	0.71	0.45
	7	0.60	0.44	NA	1.02	0.48
5	1	3.70	2.58	2.65	5.43	1.83
	2	3.10	2.37	2.30	3.73	1.54
	3	2.50	1.70	1.62	1.83	1.33
	4	1.90	1.20	1.04	1.22	1.11
	5	1.20	0.91	0.75	0.90	0.88
	6	0.60	0.80	0.70	NA	0.76
	7	0.10	NA	NA	NA	NA
6	1	4.30	4.90	4.80	3.41	NA
	2	3.70	4.22	4.67	3.14	2.85
	3	3.00	1.80	3.04	2.68	2.60
	4	2.40	1.32	1.23	1.39	2.39
	5	1.80	1.31	1.32	1.35	1.95
	6	1.20	1.01	1.30	1.17	0.89
	7	0.60	0.59	0.71	0.82	0.32

APPENDIX III

FIDHELM User Manual

ANSTO/M123

FIDHELM:
Description of Model and Users Guide

by
G. Pantelis

Prepared within the Environmental Science Program of the
Australian Nuclear Science an Technology Organisation
Program Director: W M Zuk

October 1993

ABSTRACT

FIDHELM is a finite difference heap leaching model involving 2 space dimensions. It models the air and water flow through a porous heap comprising of oxidizable material. It models oxygen transport and depletion, heat transport, production and reactant depletion in the solid phase. Included is the transport of a single conservative chemical in the aqueous phase. The chemical is a product of the oxidation of the solid reactant.

Table of Contents

Table of Figures

Table of Tables

1. INTRODUCTION

The leaching of metals such as copper, nickel, zinc and uranium from some ores depends on the conversion (oxidation) of largely insoluble metal sulphides to the much more soluble sulphates. The process is usually carried out in large heaps of sulphidic material through which water is passed. The water dissolves the metal sulphates and passes out through the base of the heap where it is processed to remove the metal of economic interest. The process is one of concentration and is generally applied to low grade ores where conventional hydrometallurgical and pyrometallurgical techniques are uneconomic. Crucial to the solubilisation process is bacterially catalyzed oxidation of iron pyrite or other iron containing pyrite [1,2].

There have been a number of studies on oxidant transport and oxidation of pyritic material within particles [3-6] and a number of models flowing from these studies. These models largely attempt to predict oxidation of entire heaps based on the reaction kinetics within individual particles with little or no consideration of the macroscopic transport mechanisms. In an industrial heap, which may measure tens to hundreds of meters in height, oxygen will initially enter the heap from the atmosphere/heap interface by the process of molecular diffusion. At this time, the oxidation reaction is confined to the surface layers of the heap. The heat released from the pyritic reaction will cause small changes in the air density within the heap. This in turn will induce a convective air current within the heap and in so doing increase the rate of atmospheric oxygen transport into the heap and permit oxidation throughout the heap.

Davis and Ritchie [7-9] considered the case where transport was a two stage process, diffusion through the pore space of the dump followed by diffusion into reaction sites within particles comprising the dump. This model is applicable to columns and thin heaps where convection is negligible. Cathles [10] considered a similar case but assumed convection through the dump to be the only macroscopic transport process. FIDHELM attempts to combine air convection and diffusion since it is likely that the initial period (or starting up period) preceding the onset of convection is sufficiently long to warrant the inclusion of the two macroscopic transport mechanisms.

FIDHELM models the heaps as a three phase system consisting of a rigid solid porous phase through which flows a gas and water phase. The following 2 sections describe the problem to be solved by FlDHELM and the numerical strategy used (see also references [15,16]).

2. MATHEMATICAL FORMULATION

Consider a heap comprised of pyritic ore lying on a relatively impermeable and insulating ground surface. This lower impermeable surface is denoted by Γ_1 and the sides and upper surface, which represent the heap/atmosphere interface, is denoted by Γ_2. We assume symmetry about the vertical boundary Γ_3 (see Figure 1). The mathematical description that follows is based on the macroscopic equations which describe multicomponent flows through porous media which are derived in Nguyen et al. [11]. The heap system involves the 3 phases, gas, water and solid. The mass balance of each of these phases is expressed as

$$\frac{\partial \rho_\alpha}{\partial t} + \nabla \bullet \left(\rho_\alpha \underline{v}^\alpha\right) = \sigma^\alpha \qquad \alpha = g,w,s \tag{2.1}$$

where the sub/superscript $\propto$=g,w,s denote gas, water and solid phase, respectively. For an N_2/O_2 gas phase with O_2 depletion and ignoring any other gas products resulting from reactions in other phases σ^g=-εS. The intrinsic density ρ^α is related to the bulk density , by the relationship

$$\rho_\alpha = \varepsilon_\alpha \rho^\alpha \qquad \propto=g,w,s \tag{2.2}$$

We assume the solid phase to be rigid, i.e. $\underline{v}^s = 0$, and the movement of the water and gas phases through this rigid porous structure to be described by Darcy's Law

$$\varepsilon_\alpha \underline{v}^\alpha = -\frac{K k_{r\alpha}}{\mu_\alpha}\left(\nabla p^\alpha + \rho^\alpha g \underline{e}_z\right) \qquad \propto=g,w \tag{2.3}$$

The gas pressure p^g, is taken relative to the atmospheric pressure at ground level (z=0). The temperature on the entire atmosphere/heap interface is assumed to be constant at the ambient atmospheric temperature. The gas density within the dump will remain close to its atmospheric ground level value but will deviate from it due to heat released from reactions. We assume that the temperature T is in local thermodynamic equilibrium with all phases and introduce the relationship

$$\rho^g = \rho_0^g\left[1-\beta\left(T-T_{amb}\right)+\gamma\left(\omega^g-\omega_0^g\right)\right] \qquad \gamma = \frac{\left(1-\frac{\rho_{00}^g}{\rho_0^g}\right)}{\omega_0^g} \tag{2.4}$$

We consider only the oxygen species in the gas phase and set ω^g as the mass fraction of the oxygen in the gas phase. We have

$$\frac{\partial}{\partial t}\left(\rho_g \omega^g\right) + \nabla \bullet \left(\rho_g \underline{v}^g \omega^g - \rho_g D \nabla \omega^g\right) = -\varepsilon S\left(\omega^g, \omega^s, T\right) \tag{2.5}$$

Figure 1: Two-dimentsional vertical crossection of a heap in planar or cylindrical coordinates as modeled by FIDHELM.

Here ω^s is the mass fraction of the reactant (sulphur) in the solid phase. The diffusion coefficient D can be expressed as

$$D = \Lambda\left(\varepsilon_g\right) D_b \tag{2.6}$$

where D_b is the diffusion coefficient of oxygen in air and $\Lambda\left(\varepsilon_g\right)$ is a tortuosity factor which is a function of the gas porosity ε_g. The simplest relationship that appears in the literature is given by (see page 271 of 17)

$$\Lambda = \Lambda_0 \varepsilon_g \tag{2.7}$$

where Λ_0 is some empirical constant.

The depletion of solid reactant is expressed as

$$\frac{d}{dt}\left(\rho_s \omega^s\right) = -S\left(\omega^g, \omega^s, T\right) \tag{2.8}$$

Since we are assuming that the temperature T is in local thermodynamic equilibrium with all phases the heat equation for all phases combined becomes

$$\left(\sum_\alpha \rho_\alpha c_\alpha\right)\frac{\partial T}{\partial t} + \sum_\alpha \rho_\alpha c_\alpha \underline{v}^\alpha \cdot \nabla T - \nabla \bullet \left(D_h \nabla T\right) = \delta S\left(\omega^g, \omega^s, T\right) \tag{2.9}$$

In the above we must have

$$\sum_\alpha \varepsilon_\alpha = 1 \tag{2.10}$$

The water and air intrinsic pressures within the porous medium are related by

$$p^c\left(\varepsilon_w\right) = p^g - p^w \tag{2.11}$$

where $p^c\left(\varepsilon_w\right)$ is the capillary pressure which is a function of the water volume fraction ε_w.

The following simplifications are made. It is assumed that the base of the heap is at water saturation and the heap is under unsaturated water conditions. The variation in air pressure is assumed negligible in equation (2.11), i.e. $p^w = -p^c\left(\varepsilon_w\right)$ and the following semi-empirical formulae are used (14)

$$\varepsilon_w = (1-\varepsilon_s)k_{rw}^{\frac{1}{3}} = (1-\varepsilon_s)\exp\left[\frac{-\tau p^c}{(3\rho^w g)}\right] \tag{2.12}$$

Under steady water infiltration at the upper heap surface of $Q_w ms^{-1}$ and immediate saturated water drainage at the base z=0 the water pressure profile is given by

$$\frac{p^w}{\rho^w g} = \frac{1}{\tau}\ln\left[Q_w\mu_w\frac{(1-e^{-\tau z})}{K\rho^w g} + e^{-\tau z}\right] \tag{2.13}$$

The parameter τ has the units of length^{-1} and its inverse gives a measure of the height of the capillary fringe above the water saturation interface. It is observed in the field that the capillary fringe is typically small relative to the height of the heap, i.e. $e^{-\tau z}$ decays rapidly with height. It is then reasonable to make the approximation that the water volume fraction along the entire vertical heap profile is effectively uniform and given by

$$\varepsilon_w = (1-\varepsilon_s)\left(\frac{Q_w\mu_w}{K\rho^w g}\right)^{\frac{1}{3}} \tag{2.14}$$

(obtained by taking τz large in (2.13)). Given now that the water and air volume fractions are constant in the heap, equations (2.1)-(2.4) can now be combined to obtain the gas pressure equation under the Boussinesq approximation

$$\nabla^2 \bar{p}^g = \rho_0^g g\left(\beta\frac{\partial T}{\partial z} - \Upsilon\frac{\partial \omega^g}{\partial z}\right) + \frac{\varepsilon\mu_g}{Kk_{rg}}S \tag{2.15}$$

where due to scaling consideration it is convenient to solve for the gas pressure perturbation $\bar{p}^g$ instead of p^g. They are related by

$$p^g(\underline{x},t) = p^g(\underline{x},t)\big|_{z=0} - \rho_0^g gz + \bar{p}^g(\underline{x},t) \tag{2.16}$$

Let n be the mass of a waterborne conservative chemical produced per mass of solid reactant oxidized. Then under the above simplifications for the water transport the mass balance of the chemical is given by

$$\rho_w\frac{\partial \omega^w}{\partial t} + \rho_w \underline{v}^w\frac{\partial \omega^w}{\partial z} = \eta S \qquad \varepsilon_w \underline{v}^w = -Q_w \tag{2.17}$$

where we have ignored diffusion and dispersion.

The boundary conditions are

$$\underline{n}_i \cdot \underline{v}^g = 0 \qquad \underline{n}_i \cdot \nabla \omega^g = 0 \qquad \underline{n}_i \cdot \nabla T = 0 \qquad \text{on} \qquad \Gamma_i \qquad \text{(i=1,3)}$$
$$\bar{p}^g = 0 \qquad \omega^g = \omega_0^g \qquad T = T_{amb} \qquad \omega^w = 0 \qquad \text{on} \qquad \Gamma_2 \tag{2.18}$$

where $\underline{n}_i$ is the unit normal vector on Γ_i. The first boundary condition in (2.18) is expressed in terms of $\bar{p}^g$ by using (2.3).

There are three quantities that are of special interest to the monitoring of the progress of the oxidation of the heap. The first quantity is the global oxidation (GO), i.e. the total amount of solid reactant remaining at a given time. Formally the GO is defined as

$$GO = \begin{cases} \int_0^{y_0}\int_0^{y_0} \rho_s \omega^s \, dxdy & (kgm^{-1}) \;\; planar \\ 2\pi \int_0^{y_0}\int_0^{y_0} \rho_s \omega^s \, dxdy & (kgm^{-1}) \;\; cylindrical \end{cases} \tag{2.19}$$

The global oxidation rate (GOR) is just the rate of global oxidation and is defined by

$$GOR = \frac{d}{dt} GO \tag{2.20}$$

The load is a measure of the amount of drainage of the aqueous phase chemical produced by the oxidation of the solid reactant being flushed out of the base at any given time. The load is defined here as

$$LOAD = \begin{cases} \int_0^{y_0} \underline{v}^w \rho_w \omega^w \, dxdy & (kgm^{-1}) \;\; planar \\ 2\pi \int_0^{y_0} \underline{v}^w \rho_w \omega^w \, xdx & (kgm^{-1}) \;\; cylindrical \end{cases} \tag{2.21}$$

3. PARTICLE OXIDATION MODEL

Earlier models employ the shrinking core model [7-10];

$$S(\omega,\omega,T)=\frac{\frac{3\gamma D_2\varepsilon_s}{\varepsilon a^2}\alpha(T)\rho^g\omega^g\left(\rho_s\omega^s\right)^{\frac{1}{3}}}{\left[\rho_r^{\frac{1}{3}}-\left(\rho_s\omega^s\right)^{\frac{1}{3}}\right]} \tag{3.1}$$

where

$$\alpha(T)=\begin{cases}1 & T_{amb}\le T\le T_{sick}\\ \alpha_0(T) & T_{sick}<T\le T_{kill}\end{cases} \tag{3.2}$$

Here α_0 (T) is some smooth function which decreases monotonically to zero for $T_{sick}<T\le T_{kill}$ and ensures that α (T) has sufficient smoothness for all T. Also; D_2 is the diffusion coefficient of oxygen into particles (m^2s^{-1}); γ is a proportionality constant encompassing both Henry's law and gas law (approx. 0.03) and a is the particle radius (approx. 0.001 - 0.05 m).

As has already been mentioned in the introduction, microorganisms play a crucial part in stepping up the oxidation rate of pyrite present in the particles. For simplicity we have included a temperature ceiling of $T_{kill}>0$ at which the microorganisms cease to be effective as catalysts for the oxidation of pyrite. We note that in reality the temperature dependence is more complicated and that there are a range of microorganisms which come into play at different temperatures [1,2]. Detailed data on temperature dependence is not available but it seems important to include the point that microbial activity will cease in heaps at temperatures approaching T_{kill}. An additional parameter T_{sick} is introduced to define a temperature above which the microorganism catalytic activity diminishes.

It is important to note that the source term S describing the mass rate of depletion of solid reactant makes sense only in some volume/mass average sense over a representative elementary volume (REV) over which all the other model variables are defined. The shrinjing core model (3.1), and other similar models, represent a description of the reaction kinetics at the pore particle level. Unfortunately, expressions representing microscopic reaction kinetics such as the shrinking core model do not translate linearly under the volume/mass average operation. Hence their inclusion into the macroscopic balance equations suffers from an inconsistency since one represents microscopic processes and the other macroscopic (REV) processes.

It appears more appropriate to seek a more empirically based formula for a description of the intrinsic oxidation rate. To this end we may make a slight generalization over the shrinking core model (3.1) by writing

$$S(\omega^g,\omega^s,T)=\rho^g\rho_s\alpha(T)R(\omega^g,\omega^s;\underline{\sigma}) \tag{3.3}$$

where α (T) is given by (3.2). Here $\underline{\sigma} = (\sigma_1, \sigma_2, ..., \sigma_n)$ are n parameters which may be determined empirically or may involve the other physical parameters given above. The variable S is reffered to as the intrinsic oxidation rate (IOR) of the material and in the form (3.3) defines the rate of solid reactant depletion in some average sense over some representative elementary volume (REV). Note that this REV should be the same as that over which all other variables are defined in the same averaged sense.

In the current version of FIDHELM there are 6 possible intrinsic oxidation models to choose from. The general form can be written:

$$R(\omega^g, \omega^s; \underline{\sigma}) = \sigma_1 U^{[1]}(\omega^g; \sigma_2) V^{[k]}(\omega^s; \sigma_3), 1 = 1,2; k = 1,2,3 \tag{3.4}$$

The functions $U^{[1]}$ and $V^{[k]}$ are given by

$$U^{[1]} = \begin{cases} \omega^g & 1 = 1 \\ \dfrac{\omega^g}{(\sigma_3 + \omega^g)} & 1 = 2 \end{cases} \tag{3.5}$$

$$V^{[k]} = \begin{cases} \omega^s & k = 1 \\ \dfrac{\omega^s}{(\sigma_2 + \omega^s)} & k = 2 \\ \exp[\sigma_3 \rho_s \omega^s] - 1 & k = 3 \end{cases} \tag{3.6}$$

For 1=k=1 we have

$$R(\omega^g, \omega^s; \underline{\sigma}) = \sigma_1 \omega^g \omega^s \tag{3.7}$$

which involves only one user supplied parameter σ_1. The parameter σ_1 may be estimated empirically.

One could use a value of σ_1 such that (3.7) best fits the shrinking core (3.1). The solutions ω^s of (2.6) with ω^g and T held constant at ω^g=0.22 and T=T_{amb} using (3.1) and (3.3)-(3.4) are very similar if we use the approximation formula

$$\sigma_1 = 9.0218 \frac{3\gamma D_2 \varepsilon_s}{\varepsilon a^2 \rho_r} \tag{3.8}$$

To obtain a solution to (2.6) under the shrinking core model (3.1) we use $\omega^s\big|_{t=0} = 0.9999(\rho_r / \rho_s)$ to avoid the singularity at t=0. The reasoning behind the approximation (3.7) - (3.8) is omitted here.

4. NONDIMENSIONAL FORMULATION

In the oxygen equation (2.5) we ignore the term $D\nabla\rho_g \cdot \nabla\omega^3$. The equations (2.5), (2.8), (2.9), (2.15) and (2.17) are first transformed into nondimensional form by introducing the nondimensional variables (barred quantities)

$$\bar{x}=\frac{x}{x_o} \qquad \bar{y}=\frac{y}{y_0} \qquad \bar{t}=\frac{t}{t_0} \quad \bar{\omega}^g=\frac{\omega^g}{\omega_0^g} \qquad \bar{\omega}^s=\frac{\omega^s}{\omega_0^s} \qquad \bar{\omega}^w=\frac{\omega^w}{\omega_0^w} \tag{4.1}$$

$$\bar{v}_x=\frac{\varepsilon_g\mu_g x_0}{Kk_{rg}\rho_0^g g y_0 a_1}v_x \qquad \bar{v}_y=\frac{\varepsilon_g\mu_g}{Kk_{rg}\rho_0^g g a_1}v_y \tag{4.2}$$

$$\bar{T}=\frac{T-T_{amb}}{T_{kill}-T_{amb}} \qquad \bar{p}=\frac{\bar{p}^g}{\rho_0^g g y_0 a_1} \qquad \bar{\rho}^g=\frac{\rho^g}{\rho_0^g} \tag{4.3}$$

where

$$S_0=\rho_0^g\rho_s\sigma_1 U_0^{[1]}V_0^{[k]} \qquad \omega_0^s=\frac{\rho_r}{\rho_s} \qquad \omega_0^w=\frac{\eta S_0 t_0}{\varepsilon_w\rho^w} \tag{4.4}$$

$$U_0^{[1]}=\begin{cases}\omega_0^g & 1=1\\ 1 & 1=2\end{cases} \tag{4.5}$$

$$V_0^{[k]}=\begin{cases}\omega_0^s & k=1\\ 1 & k=2,3\end{cases} \tag{4.6}$$

and the nondimensional constant a_1 is given below. Equations (2.5), (2.8), (2.9),(2.15) and (2.17) then become

$$a_2\frac{\partial^2\bar{p}}{\partial\bar{x}^2}+\frac{\partial^2\bar{p}}{\partial\bar{y}^2}-\frac{\partial\bar{T}}{\partial\bar{y}}+a_{13}\frac{\partial\bar{\omega}^g}{\partial\bar{y}}-a_{18}\bar{S}=0 \tag{4.7}$$

$$\frac{\partial\bar{\omega}^g}{\partial\bar{t}}+a_2a_3\bar{v}_x\frac{\partial\bar{\omega}^g}{\partial\bar{x}}+a_3\bar{v}_y\frac{\partial\bar{\omega}^g}{\partial\bar{y}}-a_2a_4\frac{\partial^2\bar{\omega}^g}{\partial\bar{x}^2}-a_4\frac{\partial^2\bar{\omega}^g}{\partial\bar{y}^2}=-a_5\bar{S}(\bar{\omega}^g,\bar{\omega}^s,T) \tag{4.8}$$

$$\frac{\partial\bar{T}}{\partial\bar{t}}+a_2a_6\bar{v}_x\frac{\partial\bar{T}}{\partial\bar{x}}+(a_6\bar{\rho}^g\bar{v}_y-a_{10})\frac{\partial\bar{T}}{\partial\bar{y}}-a_2a_7\frac{\partial^2\bar{T}}{\partial\bar{x}^2}-a_7\frac{\partial^2\bar{T}}{\partial\bar{y}^2}=a_8\bar{\rho}^g\bar{S}(\bar{\omega}^g,\bar{\omega}^s,T) \tag{4.9}$$

$$\frac{d\bar{\omega}^s}{d\bar{t}}=-a_9\bar{\rho}^g\bar{S}(\bar{\omega}^g,\bar{\omega}^s T) \tag{4.10}$$

$$\frac{\partial \overline{\omega}^{w}}{\partial \overline{t}} - a_{17}\frac{\partial \overline{\omega^{w}}}{\partial \overline{y}} = \overline{\rho}^{g}\overline{S}(\overline{\omega}^{g},\overline{\omega}^{s},T) \tag{4.11}$$

The nondimennsional intrinsic gas density $\overline{\rho}^{g}$ and the nondimensional horizontal and vertical gas specific discharges are given by

$$\overline{\rho}^{g} = 1 - a_{1}\overline{T} + a_{12}(\overline{\omega}^{g} - 1) \tag{4.12}$$

$$\overline{v}_{x} = -\frac{\partial \overline{p}}{\partial \overline{x}} \qquad \overline{v}_{y} = \left(-\frac{\partial \overline{p}}{\partial \overline{y}} - \overline{T} + a_{13}(\overline{\omega}^{g} - 1)\right) \tag{4.13}$$

The nondimensional source term $\overline{S}$ is given by

$$\overline{S}(\overline{\omega}^{g},\overline{\omega}^{s},\overline{T}) = \overline{\alpha}(\overline{T})\overline{U}^{[1]}(\overline{\omega}^{g},a_{14})\overline{V}^{[k]}(\overline{\omega}^{s},a_{15},a_{16}) \tag{4.14}$$

where

$$\overline{\alpha}\left(\overline{T}\right) = \begin{cases} 1 & 0 \le \overline{T} < a_{11} \\ \overline{\alpha_{0}}(\overline{T}) & a_{11} \le \overline{T} \le 1 \end{cases} \tag{4.15}$$

$$\overline{U}^{[1]}(\overline{\omega}^{g},a_{14}) = \begin{cases} \overline{\omega^{g}} & 1 = 1 \\ \dfrac{\overline{\omega}^{g}}{\left(a_{14} + \overline{\omega}^{g}\right)} & 1 = 2 \end{cases} \tag{4.16}$$

$$\overline{V}^{[k]}(\overline{\omega}^{s},a_{15},a_{16}) = \begin{cases} \overline{\omega^{s}} & k = 1 \\ \dfrac{\overline{\omega}^{s}}{\left(a_{15} + \overline{\omega}^{s}\right)} & k = 2 \\ \exp\left[a_{16}\overline{\omega}^{s}\right] - 1 & k = 3 \end{cases} \tag{4.17}$$

The nondimensional boundary conditions obtained from (2.16)-(2.17) are

$$\frac{\partial \overline{p}}{\partial \overline{x}} = 0 \qquad \frac{\partial \overline{\omega^{g}}}{\partial \overline{x}} = 0 \qquad \frac{\partial \overline{T}}{\partial \overline{x}} = 0 \qquad \text{on} \qquad \Gamma_{3} \tag{4.18}$$

$$\frac{\partial \bar{p}}{\partial \bar{y}} - \bar{T} + a_{13}(\bar{\omega}^{g} - 1) = 0 \qquad \frac{\partial \bar{\omega}^{g}}{\partial \bar{y}} = 0 \qquad \frac{\partial \bar{T}}{\partial \bar{y}} = 0 \qquad \text{on} \qquad \Gamma_1 \qquad (4.19)$$

$$\bar{p} = 0 \qquad \bar{\omega}^{g} = 1 \qquad \bar{T} = 0 \qquad \bar{\omega}^{w} = 0 \qquad \text{on} \qquad \Gamma_2 \qquad (4.20)$$

The nondimensional constants $a_1, a_2, \ldots, a_{17}$ are expressed in terms of the constant parameters through

$$a_1 = \beta\,(T_{kill} - T_{amb}) \qquad a_2 = \left(\frac{x_0}{y_0}\right)^2 \qquad a_3 = \frac{a_1 K k_{rg}\,\rho_0^{g}\,g t_0}{\mu_g y_0 \varepsilon_g} \qquad a_4 = \frac{\varepsilon_g \Lambda_0 D_b t_0}{y_0^2} \qquad (4.21)$$

$$a_5 = \frac{\varepsilon S_0 t_0}{\rho_0^{g} \varepsilon_g \omega_0^{g}} \qquad a_6 = \frac{a_1 K k_{rg} (\rho_0^{g})^2 g c_g t_0}{\rho_s c_s \mu_g y_0} \qquad a_7 = \frac{\kappa t_0}{y_0^2} \qquad a_8 = \frac{\delta S_0 t_0}{\rho_s c_s (T_{kill} - T_{amb})} \qquad (4.22)$$

$$a_9 = \frac{S_0 t_0}{\rho_r} \qquad a_{10} = \frac{Q_w \rho^{w} c_w t_0}{\rho_s c_s y_0} \qquad a_{11} = \frac{T_{sick} - T_{amb}}{T_{kill} - T_{amb}} \qquad a_{12} = 1 - \frac{\rho_{00}^{g}}{\rho_0^{g}} \qquad (4.23)$$

$$a_{13} = \frac{a_{12}}{a_1} \qquad a_{14} = \frac{\sigma_2}{\omega_0^{g}} \qquad a_{15} = \frac{\sigma_3 \rho_s}{\rho_r} \qquad a_{16} = \sigma_3 \rho_r \qquad (4.24)$$

$$a_{17} = \frac{Q_w t_0}{\varepsilon_w y_0} \qquad a_{18} = \frac{\varepsilon S_0 \mu_g y_0}{\rho_0^{g} K k_{rg} a_1 g} \qquad (4.25)$$

5. OUTLINE OF NUMERICAL SCHEME

The system of equations (4.7) - (4.11) are highly coupled and of a mixed type. The gas pressure equation (4.7) is of the elliptic type whereas the oxygen transport equation (4.8) and the heat equation (4.9) are parabolic but take on hyperbolic properties as convection becomes dominant. A decoupling finite difference scheme is used by first solving, at each time step, the oxygen transport equation (4.8), the heat equation (4.9) and the solid reactant depletion equation (4.10). The updated temperatures are then used in the finite difference approximation of (4.7) to obtain the gas pressures.

For the sake of the outline presented here the numerical solution of (4.7)-(4.l1) will be discussed in the context of a planar geometry x = (x,y) (y being the vertical coordinate) with a uniform grid system of intervals Δx and Δy (the bars indicating nondimensional quantities will be omitted in this section). The modification to cylindrical coordinates should then be straightforward. The incorporation of the boundary conditions into the finite difference systems presented will not be explicitly described since the details are cumbersome to write down but straight forward to implement.

Departing for the moment from the nomenclature of the previous sections the oxygen transport equation (4.8) and the heat equation (4.9) take the form of the convection-diffusion equation

$$\frac{\partial u}{\partial t} + \underline{v} \cdot \nabla u - D\nabla^2 u = S \qquad (5.1)$$

where u stands for ω^g or T. The convection coefficients $\underline{v}$ and the diffusion coefficient D are different for the oxygen transport and heat equations and we have linearised the diffusion term, although this is not an essential part of the scheme to be described.

The convection is decoupled from diffusion by rewriting (5.1) in its Lagrangian form [13]

$$\frac{du}{dt} = D\nabla^2 u = S \qquad (5.2)$$

where the substantial derivative d/dt indicates the time rate of change along the characteristic curves associated with pure advection. These advection flow paths are defined by

$$\frac{dx}{dt} = \underline{v} \qquad (5.3)$$

Let $\underline{x}_{ij} \equiv \left(x_i, x_j\right)$ denote the position of the space grid point on a prescribed fixed grid system of intervalsΔx and Δy. The origin of a fluid particle $\underline{\bar{x}}_{ij}^{n-1} \equiv (\bar{x}_{ij}^{n-1}, \bar{y}_{ij}^{n-1})$ at the previous time t^{n-1} reaching the grid point x_{ij} at time t^n is obtained from discretization of (5.3) through

$$\underline{\bar{x}}_{ij}^{n-1} = \underline{x}_{ij} - \underline{\bar{v}}_{ij}\Delta t \quad \underline{\bar{v}}_{ij}^{n} = 2\underline{v}_{ij}^{n-1} - \underline{v}_{ij}^{n-2} \tag{5.4}$$

where $\underline{\bar{v}}_{ij}^{n}$ are the velocities at the grid points $\underline{x}_{ij}$ at time t^n extrapolated from the velocities at the grid points $\underline{x}_{ij}$ from the previous two timesteps (the formula for $\underline{\bar{v}}_{ij}^{n}$ is modified in FIDHELM for variable timestep sizes). It is noticed that the origins of fluid particles $\underline{\bar{x}}_{ij}^{n-1}$ at time t^{n-1} are found by tracking particles backward in time from each grid point $\underline{x}_{ij}$ at time t^n . An implicit finite difference scheme for (3.2) can now be written in the form

$$u_{ij}^{n} = \bar{u}_{ij}^{n-1} + \Delta t\left\{\left[D\nabla^2 u\right]_{ij}^{n} + S_{ij}^{n}\right\} \tag{5.5}$$

where $\bar{u}_{ij}^{n-1} \equiv (\underline{\bar{x}}_{ij}^{n-1}, t^{n-1}), S_{ij}^{n} = S\left(\underline{x}_{ij}, t^n, u_{ij}^{n}\right)$ and $\left[D\nabla^2 u\right]_{ij}^{n}$ denotes some spatial discretion of the diffusion term centered at the point $\underline{x}_{ij}$ at time t^n. The finite difference equations resulting from (5.5) are solved by iteration to a given convergence criteria.

Since the points $\underline{\bar{x}}_{ij}^{n-1}$ will generally lie off the prescribed fixed grid points some interpolation scheme must be employed to obtain the values of $\bar{u}_{ij}^{n-1}$ from the known grid point values of u at the time t^{n-1}. One of the reasons for choosing the single step method (5.5) over other multistep schemes is that the computationally costly operation of interpolation is only performed once at each timestep.

The progressive stages of the computations in FIDHELM can be summarized as follows. Given the grid point values of $\omega^g, \omega^s, \underline{v}^g$ and T at time t^{n-1} the discretized convection-diffusion equations for ω^g and T given in the form (5.4)-(5.5) described above are iterated to convergence to obtain the grid point values of ω^g and T at the new timestep t^n. The solid reactant mass fraction ω^s is obtained by using, in the same iteration procedure, a backward in time difference approximation of equation (4.10) (here the integration occurs along the fixed paths $\underline{x} = \underline{x}_{ij}$ in (x,y,t) space). Within the same time step the new temperatures and oxygen mass fractions are then employed in the finite difference approximation of the air pressure equation (4.7) given by

$$a_2\frac{p_{i+1,j}^{n} + p_{i-1,j}^{n} - 2p_{i,j}^{n}}{\Delta x^2} + \frac{p_{i,j+1}^{n} + p_{i,j+1}^{n} - 2p_{i,j}^{n}}{\Delta y^2} = \frac{T_{i,j+1}^{n} - T_{i,j-1}^{n}}{2\Delta y} - a_{13}\frac{\left[\omega^g\right]_{i,j-1}^{n} - \left[\omega^g\right]_{i,j-1}^{n}}{2\Delta y} + a_{18}S_{ij}^{n} \tag{5.6}$$

where $p_{ij}^{n} = p_{ij}^{n}(x_{ij}, t^n)$, etc. Having obtained the air pressures at the new time t^n using (5.6), the new air velocities are obtained from a finite difference approximation of (4.13) and the entire procedure repeated.

6. REFERENCES

1. R.W. Lawrence, R.M.R. Branion and H.G. Ebner (eds.), Fundamental and Applied Biohydrometallurgy, Elsevier, 1986.

2. P.R. Norris and D.P Kelly, Biohydrometallurgy, Proceedings of the International Symposium, Warwick, 1987.

3. C.L. Brierley, Bacterial Leaching. CRC Critical Rev. Microbiol., (1978) 6:207-62.

5. H.K. Lin and Y Sohn, Mixed-control kinetics of oxygen leaching of chalcopyrite and pyrite from primary ore fragments, *Metallurgical Transactions B*, 8 (1987)497-503.

6. R.G. Whittemore, The Modelling of Vat, Heap, Dump and In-Situ Leaching Systems, Publication LR 381 (ME) of the Warren Spring Laboratory, 1981.

7. G.B. Davis and A.I.M. Ritchie, A model of oxidation in pyritic mine wastes: part 1 equations and approximate solution, *Appl. Math. Modelling, 10* (1986a) 314-322.

8. G.B. Davis, G. Doherty and A.I.M. Ritchie, A model of oxidation in pyritic mine wastes: part 2: Comparison of numerical and approximate solutions, *AppI. Math. Modelling, 10* (1986b) 323-330.

9. G.B. Davis and A.I.M. Ritchie, A model of oxidation in pyritic mine wastes: part 3: import of particle size distribution, *Appl. Math. Modelling*, 11(1987) 417-422.

10. L.M. Cathles and W.J. Schlitt, A model of the dump leaching process that incorporates oxygen balance, heat balance, and two dimensional air convection, In the proceedings of the Las Vegas Symposium on Leaching and Recovering Copper From As-Mined Materials (Ed. W.J. Schlitt), February 26 1980, pp. 9-27.

11. V.V. Nguyen, WO. Gray, J.F. Pinder, J.F. Botha and D.A. Crerar, A theoretical investigation on the transport of chemicals in reactive porous media, *Water Resources Research*, 18(1982)1149-1156.

12. C.A.J. Fletcher, *Computational Techniques for Fluid Dynamics*, Vol. 1, Springer-Verlag, 1988.

13. V. Casulli, Eulerian-Lagrangian for hyperbolic and convection dominated parabolic problems. Chapter 8, Computational Methods for Nonlinear Problems (Eds. C. Taylor, D.R.J. Owen and E. Hinton), Pineridge Press, Swansea, 1987.

14. J. Bear, *Hydraulics of Groundwater*, McGraw-Hill, New York, 1979.

15. G. Pantelis and A.I.M. Ritchie, Macroscopic transport mechanisms as a rate-limiting factor in dump leaching of pyritic ores, *Appl. Math. Modelling*, 15, pp. 136-143,1991.

16. G. Pantelis and A.I.M. Ritchie, Rate-limiting factors in dump leaching of pyritic ores, *Appl. Math. Modelling*, 16, pp. 553-559, 1992.

17. T.J. Marshall and J.W. Holmes, *Soil Physics*, Cambridge University Press, 1979.

7. DESCRIPTION OF COMPUTER PROGRAM

The program solves a 2 dimensional problem in either cylindrical or Cartesian coordinates. The geometry of the case problem is chosen by the input parameter IOEO (=1 planar; =2 cylindrical). In cylindrical coordinates the heap takes the shape of a truncated cone. In both cases the heap is symmetric, bounded on the left hand side by an axis of symmetry (see Figure 1). The right hand side of the heap is inclined at an angle of θ radians to the base of the heap (user supplied parameter).

7.1 Parameter Identification in Pogram

Upon output FIDHELM gives the numerical values of the constants a_1 (4.21) - (4.25). Also shown in the output are the parameter constants stored in an array b_1, i=1,... ,39. These are defined in the following table:

Table 1: Parameters stored in the array b_i

Index i of b_i	Parameter	Definition	Typical Values	
1	t_0	timescale (s)	2.629×10^6	user input
2	x_0	radius or half width of heap (m)	20 - 100	user input
3	y_0	height of heap (m)	1 - 25	user input
4	T_{amb}	average ambient temperature (^oC)	0- 30	user input
5	ρ^g	intrinsic air density (kg m^{-3})	1.2	user input
6	g	acceleration due to gravity (m s^{-2})	9.8	user input
7	K	intrinsic permeability (m^2)	10^{-11} - 10^{-7}	user input
8	μ_g	viscosity of gas phase (kg $m^{-1}s^{-1}$)	1.9×10^{-5}	user input
9	β	thermal coefficient of volume expansion of gas phase (K^{-1})	3.47×10^{-3}	user input
10	ε_s	solid volume fraction	0.6-0.8	user input
11	D_b	bulk oxygen diffusion coefficient in gas phase (m^2s^{-1})	2.26×10^{-5}	user input
12	σ_2	intrinsic oxidation model parameter (see definition (3.4))		user input
13	σ_1	intrinsic oxidation model parameter (see definition (3.4))		user input
14	σ_3	intrinsic oxidation model parameter (see definition (3.4))		user input
15	ρ_s	bulk density of solid phase (kg m^{-3})	1500	user input
16	c_s	specific heat of solid phase (m^2 s^{-1} K^{-1})	866	user input
17	c_g	specific heat of gas phase (m^2 s^{-1} K^{-1})	1060	user input
18	κ	thermal diffusivity (m^2 s^{-1})	5×10^{-7}	user input
19	δ	heat of oxidation per mass of reactant oxidised (J kg^{-1})	2.2×10^7	user input
20	ω_0^g	mass fraction of oxygen in air	0.22	user input
21	ε	mass of oxygen used per mass of reactant used in oxygen reaction	1.746	user input

Table 1 Parameters stored in the array b_i (continued)

Index i of b_i	Parameter	Definition	Typical Values	
22	ρ_r	bulk density of reactant (kg m^{-3})	15 - 100	user input
23	Q_w	water infiltration rate (m s^{-1})	$1.5x10^{-8}$	user input
24	μ_w	viscosity of water (kg m^{-1} s^{-1})	0.001	user input
25	ρ^w	intrinsic density of water (kg m^{-3})	1000	user input
26	c_w	specific heat of water (m^2 s^{-2} K^{-1})	$4.184x10^3$	user input
27	Λ_0	a tortuosity factor	1.67	user input
28	ρ_{00}^g	intrinsic density of oxygen depleted air (kg m^{-3})	1.16	user input
29	η	mass of aqueous phase chemical produced per mass of solid reactant used in oxidation reaction	3 (for SO_4)	user input
30	T_{kill}	temperature at which microorganisms cease to be effective as catalysts (°C)	40- 100	user input
31	T_{sick}	temperature at which catalytic activity of microorganisms begins to diminish (°C)	30 - 60	user input
32	ε_w	$\varepsilon_w = (1-\varepsilon_s)\left(\frac{Q_w \mu_w}{K \rho^w g}\right)^{\frac{1}{3}}$		evaluated in program
33	ε_g	$\varepsilon_g = 1-\varepsilon_s-\varepsilon_w$		evaluated in program
34	k_{rg}	$k_{rg} = \left[\varepsilon_g/(1-\varepsilon_s)\right]^3$		evaluated in program
35	ω_0^w	$\omega_0^w = \frac{\eta S_0 t_0}{\varepsilon_w \rho^w}$		evaluated in program
36	S_0	$S_0 = \rho_0^g \rho_s \sigma_1 U_0^{[1]} V_0^{[k]}$		evaluated in program
37	v_{y0}	$v_{y0} = \frac{\left(K k_{rg} \rho_0^g g a_1\right)}{\left(\varepsilon_g \mu_g\right)}$		evaluated in program
38	v_{x0}	$v_{x0} = \frac{v_{y0} y_0}{x_0}$		evaluated in program
39	p_0	$p_0 = \rho_0^g g y_0 a_1$		evaluated in program

7.2 Program Structure:

The computer program FIDHELM consists of a MAIN program and 14 subroutines.

SUBROUTINE TSTEP

This routine checks that the timestep size is such that any origin of a convective flow path reaching a grid point in a timestep does not deviate spatially too far from that grid point. If this occurs the timestep size is reduced.

SUBROUTINE SOLVE

This subroutine iterates till convergence the backward time difference equations for oxygen, heat and reactant depletion equations.

SUBROUTINE CONC

Computes the transport and production of the aqueous phase conservative chemical produce from the oxidation of the solid reactant.

SUBROUTINE SOURCE

Computes the intrinsic oxidation rate.

SUBROUTINE INTP

Interpolation routine to obtain temperatures and oxygen mass fractions at intersections of convective flow paths and the previous time slice.

SUBROUTINE MTXB

Having computed the new oxygen mass fractions and temperatures at the current time t^n the air pressures are computed iteratively. The subroutine MTXB computes the right hand side B of the linear system Ap=B, where p is the vector containing the nodal values of the air pressures.

SUBROUTINE MTXA

The subroutine MTXA computes the matrix A of the linear system Ap=B, where p is the vector containing the nodal values of the air pressures. Under the Bousinesq approximation the elements of A are independent of the air pressures and need only be computed once.

SUBROUTINE ITRTE

Given the elements of A and B computed in MTXA and MTXB the linear system Ap=B is solved using an SOR iterative procedure.

SUBROUTINE VEL

Given the updated air pressures the new air velocities are computed using a finite difference approximation of the first order spatial derivatives of the air pressures.

SUBROUTINE GOX

At each nondimensional time increment of $d\bar{t}_{out}^{(1)}$ (parameter input) the amount of unoxidised solid reactant remaining in the heap is evaluated.

SUBROUTINE GOR

At each nondimensional time increment of $d\bar{t}_{out}^{(1)}$ (parameter input) the reactant oxidation rate is evaluated.

SUBROUTINE LOAD

At each nondimensional time increment of $d\bar{t}_{out}^{(1)}$ (parameter input) the load is evaluated.

SUBROUTINE ERROR

This subroutine prints out an error code number and halts the computations if certain conditions are violated.

SUBROUTINE OUTP

This subroutine prints out the parameter data and the solution at the final timestep.

RELAX

This subroutine computes an optimum relaxation parameter for the SOR method used in subroutine ITRTE.

8. DATA INPUT GUIDE

A separate data file named "HEAPIN" must contain the following parameters in the given order and free format (real numbers except n_x, ITMXP, INIT, IGEO, ITMX, and IATD which are integers).

User supplied input data file "HEAPIN"

The input data file HEAPIN has the following form.

Table 2: Input data file HEAPIN in tabular form

t_0	x_0	y_0	T_{amb}	ρ_0^g
g	K	μ_g	β	ε_s
D_b	σ_2	σ_1	σ_3	ρ_s
c_s	c_g	κ	δ	ω_0^g
ε	ρ_r	Q_w	μ_w	ρ^w
c_w	Λ_0	ρ_{00}^g	η	T_{kill}
T_{sick}	--	--	--	--
t_{end}	θ	ε_0	ε_p	α_{dt}
$dt_{out}^{-(1)}$	$dt_{out}^{-(2)}$	--	--	--
INIT	*IGEO*	n_x	--	--
ITMX	*ITMXP*	*IATD*	*IOR1*	*IOR2*

The following table defines the quantities appearing in HEAPIN that are not defined in Table 1.

Table 3: Parameters appearing in HEAPIN

Input parameter	Definition	Typical values
t_{end}	Nondimensional simulation time required (s/t_0)	0.1 - 20
θ	side slope angle of heap (radians)	$0 < \theta < \pi/2$
ε_0	relative error teston backward time iteration	10^{-6} - 10^{-4}
ε_p	maximum allowable relative error in convergence test on gas pressures	10^{-6} - 10^{-4}
α_{dt}	see below	0.1 - 10
$d\bar{t}_{out}^{(1)}$	nondimensional time increment between evaluations of GO, GOR and Load	0.0- t_{end}
$d\bar{t}_{out}^{(2)}$	nondimensional time increment between outputs of variables (oxygen, temperature, etc.)	0.0- t_{end}
INIT	restart parameter	=1 first run =2 restart
IGEO	parameter defining geometry of heap	=1 planar =2 cylindrical
n_x	number of mesh points along radius	must be greater than 4
ITMX	maximum iterations on backward time iteration	100 - 5000
ITMXP	maximum number of iterations on gas pressures	100 - 5000
IATD	screen message	= 0 off = 1 on
IOR1	Intrinsic oxidation model	= 1 in (3.5a)
IOR2	Intrinsic oxidation model	= k in (3.5b)

8.1 Further Dtails of Iput Prameters:

The timescale t_0 is used by the program to find some suitable scaling factor with which to nondimensionalise the equations (typically of the order of 3.15536 x 10^7 s = 1 year). The parameter t_{end} is the nondimensional time required by the simulation (i.e. the dimensional simulation time is $t_0 t_{end}$). The user may set INIT=2 to restart where the previous run ended. Otherwise INIT=1 (initial run).

For a restart (INIT=2) all other data may remain as for the initial run except for t_{end} which is changed to the next time horizon. The irrigation rate Q_w is an important parameter in the model. Step changes in Q_w at restarts may be accompanied by adjustments of α_{dt}, ε_0, ε_p, ITMX, ITMXP. All other parameters must remain as for the initial run.

FIDHELM uses a backward time difference scheme to solve the reactant depletion equation coupled with the ordinary differential equations that result from the spatial discretization of the heat and oxygen convection-diffusion equations. To maintain second order accuracy in the finite difference scheme the nondimensional timestep size is set to $\Delta\bar{t} = \alpha_{dt} \max\left\{\Delta\bar{x}^2, \Delta\bar{y}^2\right\}$, where α_{dt} is a user input parameter (usually α_{dt}=1). In the course of a simulation the timestep size may be reduced if the convective flow paths traced back from each grid point deviates too far from that grid point.

The parameter n_x is the number of mesh points on the base radius of the heap. The program constructs automatically the number of vertical mesh points such that the right hand side boundary nodes lie on the sloping side boundary of the heap. The slope of the sides is fixed at an angle of θ radians to the base. In order to fix this geometry the program reevaluates the closest value of y_0 in order that this geometry condition is satisfied. If the value of the new y_0 is unacceptably different from that in the input data then the user needs to refine the mesh system by inserting a larger value of n_x.

The integer parameter ITMXP is the maximum allowable iterations in each timestep executed on the air pressure equation. The iterations are terminated when the maximum relative error ε_p between the solutions from any two consecutive iterations is attained. The air pressures are iterated separately from the other equations.

8.2 Error Messages

The program may halt at any time during the computations if certain conditions are violated. When this happens the output data will contain the message

ERROR TYPE = n

where n is an integer 1-6.

n=1: means that the height of the heap is too high for the given radius. Since a cone (or triangle in the planar case) is the limiting geometry the requirement is $y_0 \leq (x_0 - \Delta x) \tan\theta$, for sides at a slope of θ radians to the base. However, the program requires a horizontal upper boundary of at least 2 mesh points so that $y_0 \leq (x_0 - \Delta x) \tan\theta$. The shape of a cone (triangle), if required, can be approached by using a smaller Δx.

n=2: the infiltration rate Q_w exceeds the infiltration capacity of the porous matrix of the heap. The general rule is $Q_w < (Kp^w g)/\mu_w$..

n=3: The iteration for the air pressure equation has failed to converge after ITMXP iterations.

n=4: less than 2 mesh points in the vertical. Increase n_x.

n=5: The iterations in SOLVE have failed to converge after ITMX iterations.

n=6: $Q_w \leq 0$ (must have $Q_w > 0$)

9. OUTPUT FILES

During the execution FIDHELM creates 2 ASCII data files:

HEAPOUT

Outputs;

(1) final spatial grid point values of oxygen density in the air density in the air phase; reactant density; temperature; air pressure; horizontal and vertical air specific discharges

(2) time dependent GO; GOR; timestep size in computations; number of iterations used in backward time difference scheme to satisfy convergence test

(3) parameters related to the physical problem and parameters associated with the computations.

HEARPRST

This file contains numerical data used when the restart option is activated (INIT=2) and for use by graphics software. The details of the required read statements are:

OPEN(UNIT=12,FILE='HEARPRST')

.....

READ(12,100) n_x, n_y^0, n_a, n_b

READ(12,100) (n_y(1),1=1, n_x)

READ(12,200) (b_1, 1=1, n_b)

READ(12,200) (a_1 , 1=1, n_a)

READ(12,200) ($\bar{x}_1$, 1=1, n_x)

READ(12,200) $(\bar{y}_1, 1 = 1, n_y^0)$

55 READ(12,100)IREAD

if(IREAD.eq.1)then

READ(12,200) $\bar{t}, d\bar{t}$

READ(12,200) $(\bar{\omega}^{s}(\bar{x}_1, \bar{y}_k, \bar{t}), k = 1, n_y^0), 1 = 1, n_x)$

READ(12,200) $(\bar{T}(\bar{x}_1, \bar{y}_k, \bar{t}), k = 1, n_y^0), 1 = 1, n_x)$

READ(12,200) $(\bar{p}^{g}(\bar{x}_1, \bar{y}_k, \bar{t}) k = 1, n_y^0), 1 = 1, n_x)$

READ(12,200) $(\bar{\omega}^{g}(\bar{x}_1, \bar{y}_k, \bar{t}) k = 1, n_y^0), 1 = 1, n_x)$

READ(12,200) $(\bar{\omega}^{w}(\bar{x}_1, \bar{y}_k, \bar{t}) k = 1, n_y^0), 1 = 1, n_x)$

READ(12,200) $(\bar{v}_x(\bar{x}_1, \bar{y}_k, \bar{t}) k = 1, n_y^0), 1 = 1, n_x)$

READ(12,200) $(\bar{v}_x(\bar{x}_1, \bar{y}_k, \bar{t} - d\bar{t}) k = 1, n_y^0), 1 = 1, n_x)$

READ(12,200) $(\bar{v}_y(\bar{x}_1, \bar{y}_k, \bar{t}) k = 1, n_y^0), 1 = 1, n_x)$

READ(12,200) $(\bar{v}_y(\bar{x}_1, \bar{y}_k, \bar{t} - d\bar{t}) k = 1, n_y^0), 1 = 1, n_x)$

READ(12,200) $(\bar{S}(\bar{x}_1, \bar{y}_k, \bar{t}) k = 1, n_y^0), 1 = 1, n_x)$

go to 55

else

READ(12,100) n_t

READ(12,300) (t_1, GO (t_1), GOR (t_1), Load (t_1), RIT (t_1), $d\bar{t}$ (t_1), 1=1, n_t)

end if

.....

100 FORMAT(5I10)

200 FORMAT(5D16.8)

300 FORMAT(6D16.8)

These variables are defined by:

n_x = number of grids on the x-axes

$n_y^0 = n_y(1)$

n_t = number of timesteps at which t_1, GO (t_1), GOR (t_1), Load (t_1), RIT (t_1), d$\bar{t}$ (t_1) are output

n_a = dimensions of the array a_1

n_b= dimensions of the array b_1

$(\bar{x}_1, \bar{y}_k)$ grid point values of $(\bar{x}, \bar{y})$

$n_y(1)$= number of vertical grid points at $\bar{x}_1$

RIT(t_1)= number of iterations required to satisfy convergence test in the backward time difference scheme at time t_1

RITP(t_1)= number of iterations required to satisfy convergence test in the pressure difference equations at time t_1

$d\bar{t}$ = nondimensional timestep size at the nondimensional time $\bar{t}$

The output nondimensional times $\bar{t}$ are given in increments of $(d\bar{t}_{out}^{(2)}) / t_0$

APPENDIX IV

FIDHELM Results

List of Figures

Pile	Air Permeability (m^2)	Time (year)	IOR ($kg[O_2]/m^3/s$)	Page Number					
				Air Velocity	Temperature	Gaseous Oxygen Content	Total Amount of Sulphur Remaining	Normalized Total Amount of Sulphur Remaining	Sulphate Load from Aqueous Phase
7/12	2.9×10^{-9}	1, 10, 100	10^{-8}	1	2	3	-	-	-
		1	10^{-7}, 10^{-8}, 10^{-9}	4	5	6	-	-	-
		10	10^{-7}, 10^{-8}, 10^{-9}	7	8	9	-	-	-
		1, 10, 100	10^{-8}	13	14	15	-	-	-
		1	10^{-7}, 10^{-8}, 10^{-9}	16	17	18	-	-	-
		10	10^{-7}, 10^{-8}, 10^{-9}	19	20	21	-	-	-
	2.9×10^{-9} & 10^{-8}	1-100	10^{-7}, 10^{-8}, 10^{-9}	-	-	-	22	23	24
18B	2.9×10^{-9}	1, 10, 100	10^{-8}	25	26	27	-	-	-
		1	10^{-7}, 10^{-8}, 10^{-9}	28	29	30	-	-	-
		10	10^{-7}, 10^{-8}, 10^{-9}	31	32	33	-	-	-
		100	10^{-7}, 10^{-8}, 10^{-9}	34	35	36	-	-	-
	10^{-8}	1, 10, 100	10^{-8}	37	38	39	-	-	-
		1	10^{-7}, 10^{-8}, 10^{-9}	40	41	42	-	-	-
		10	10^{-7}, 10^{-8}, 10^{-9}	43	44	45	-	-	-
	2.9×10^{-9} & 10^{-8}	1-100	10^{-7}, 10^{-8}, 10^{-9}	-	-	-	46	47	48
18A	2.9×10^{-9}	1, 10, 100	10^{-8}	49	50	51	52	53	54
17	2.9×10^{-9}	1, 10, 100	10^{-8}	55	56	57	58	59	60

FIDHELM RESULTS

PILE 7/12

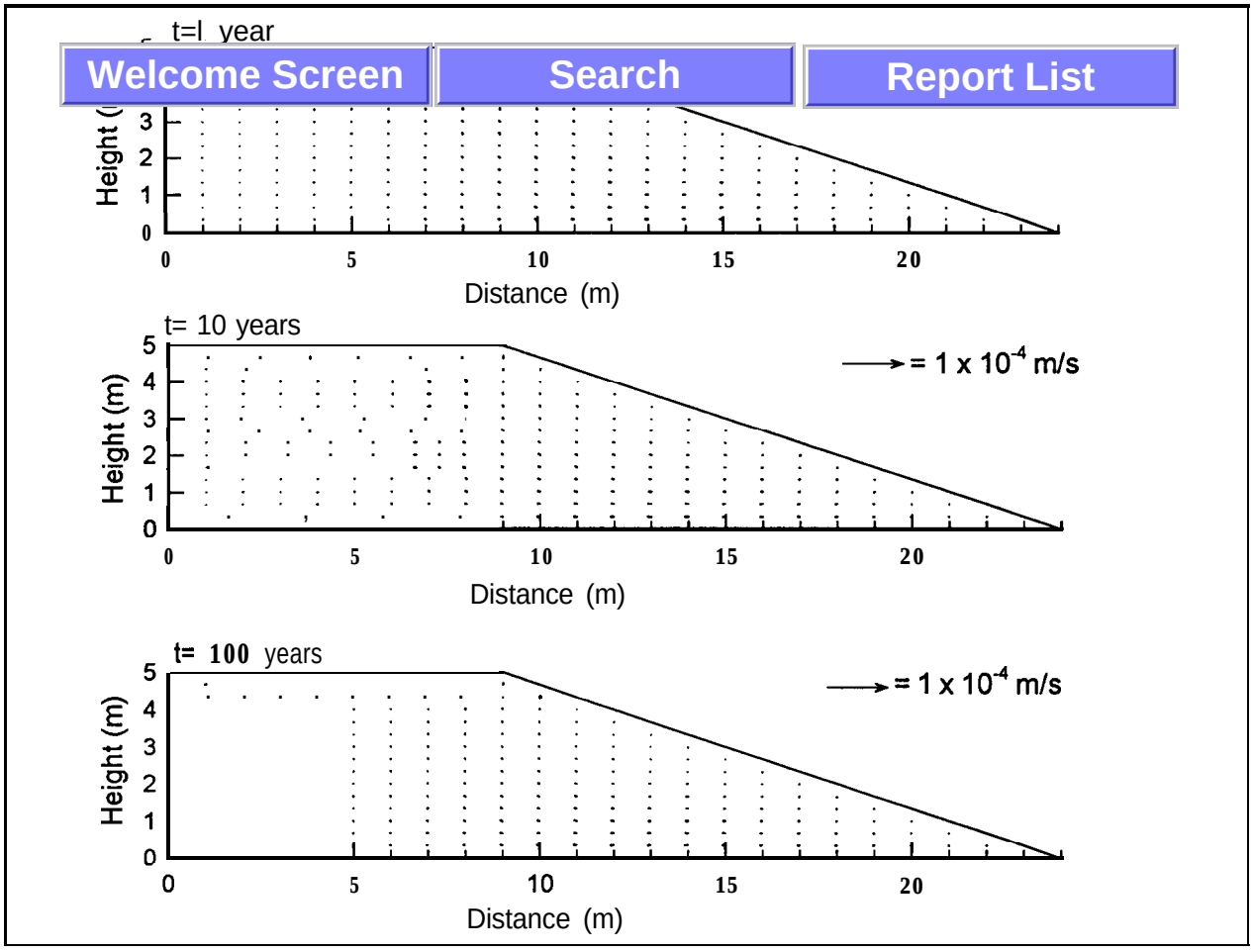

Figure IV - 1: **FIDHELM Results - Pile 7/12: Air flow velocity, K=2.9x10^{-9} m^2, IOR=10^{-8} kg[O_2]/m^3/s.**

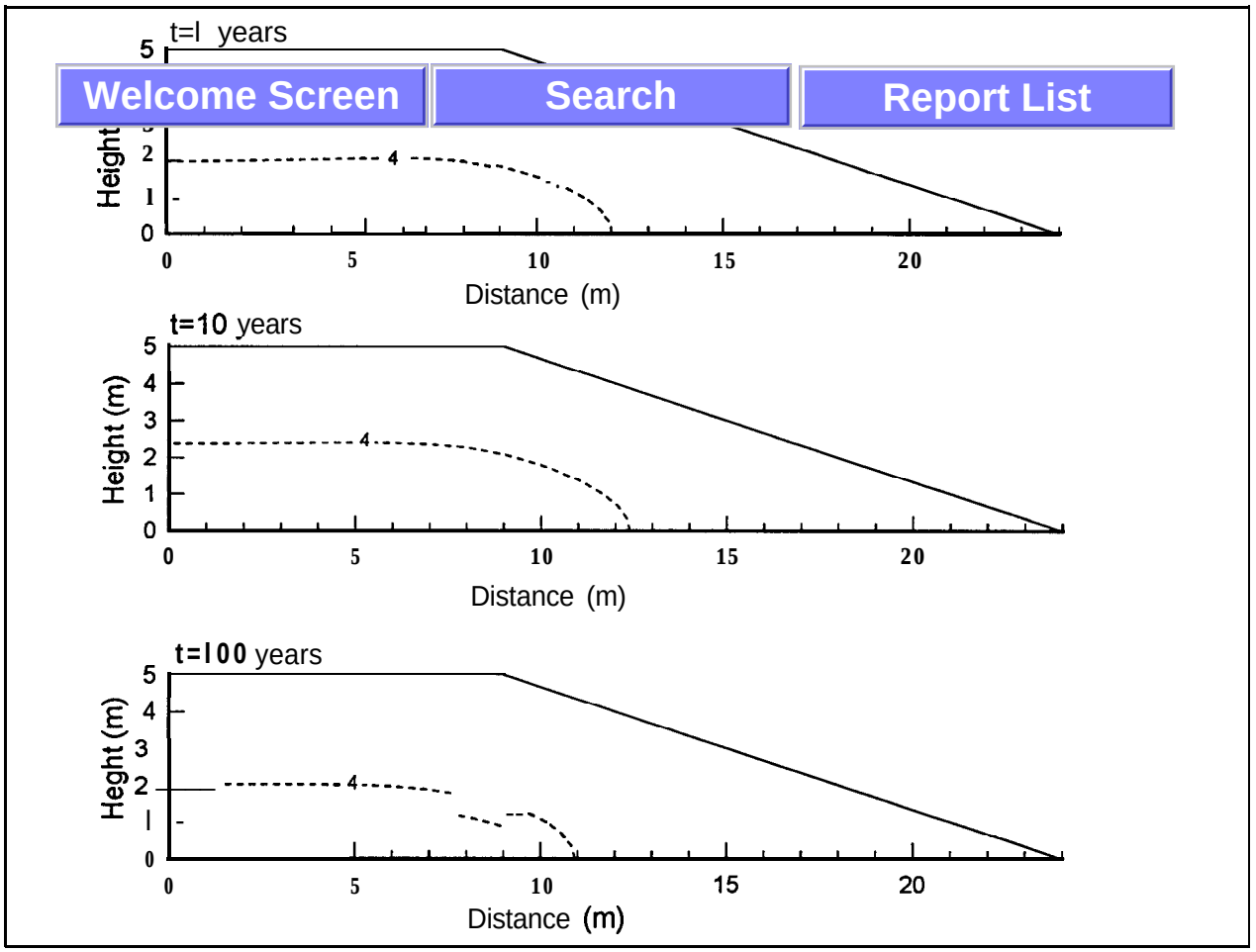

Figure IV - 2: **FIDHELM Results - Pile 7/12: Temperature iso - values (A =1°C), K=2.9x10^{-9} m^2, IOR =10^{-8} kg[O_2]/m^3/s.**

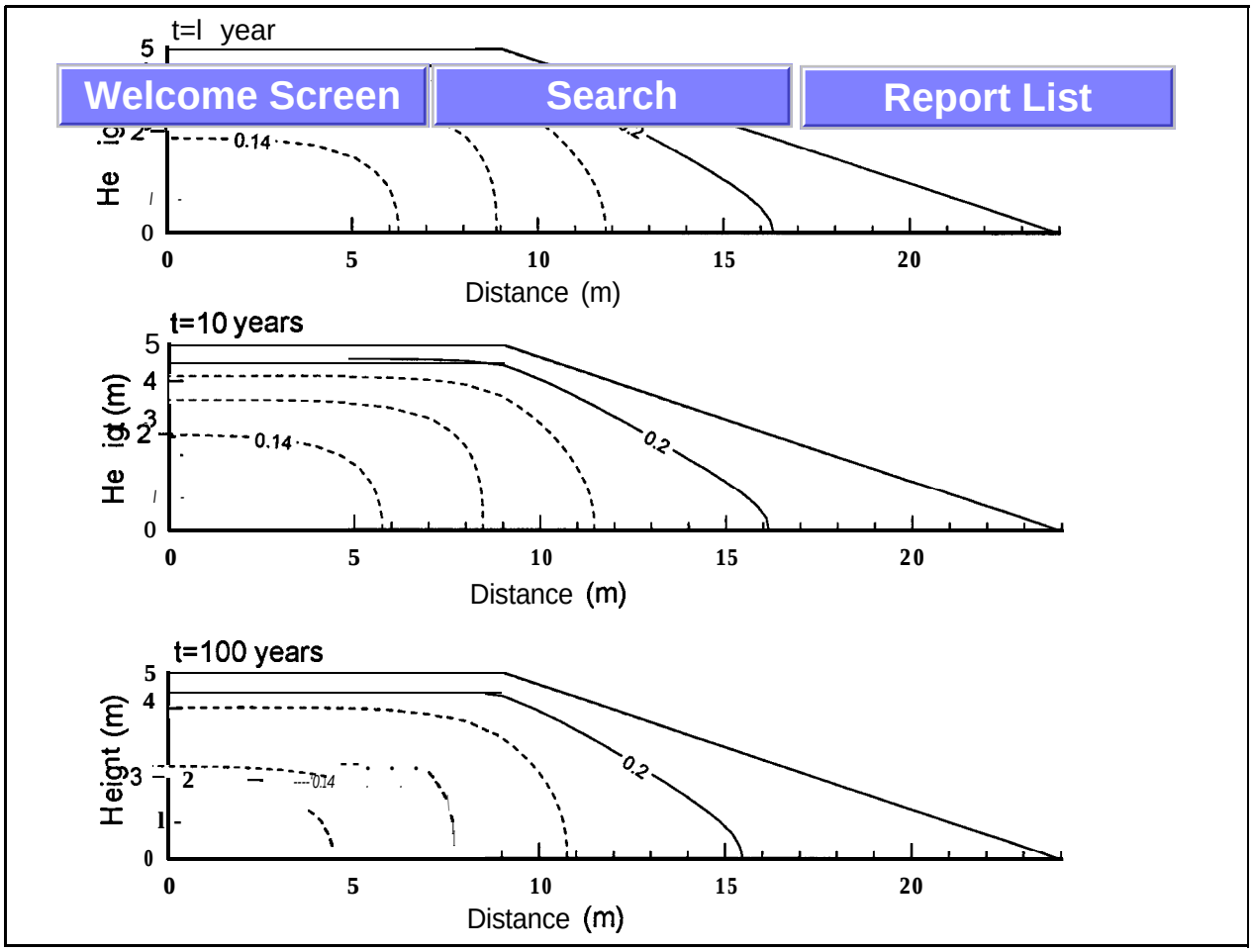

Figure IV - 3: **FIDHELM Results - Pile 7/12: Gaseous oxygen mass fraction iso-values (Δ=0.02), K=2.9x10^{-9} m^2, IOR =10^{-8} kg[O_2]/m^3/s.**

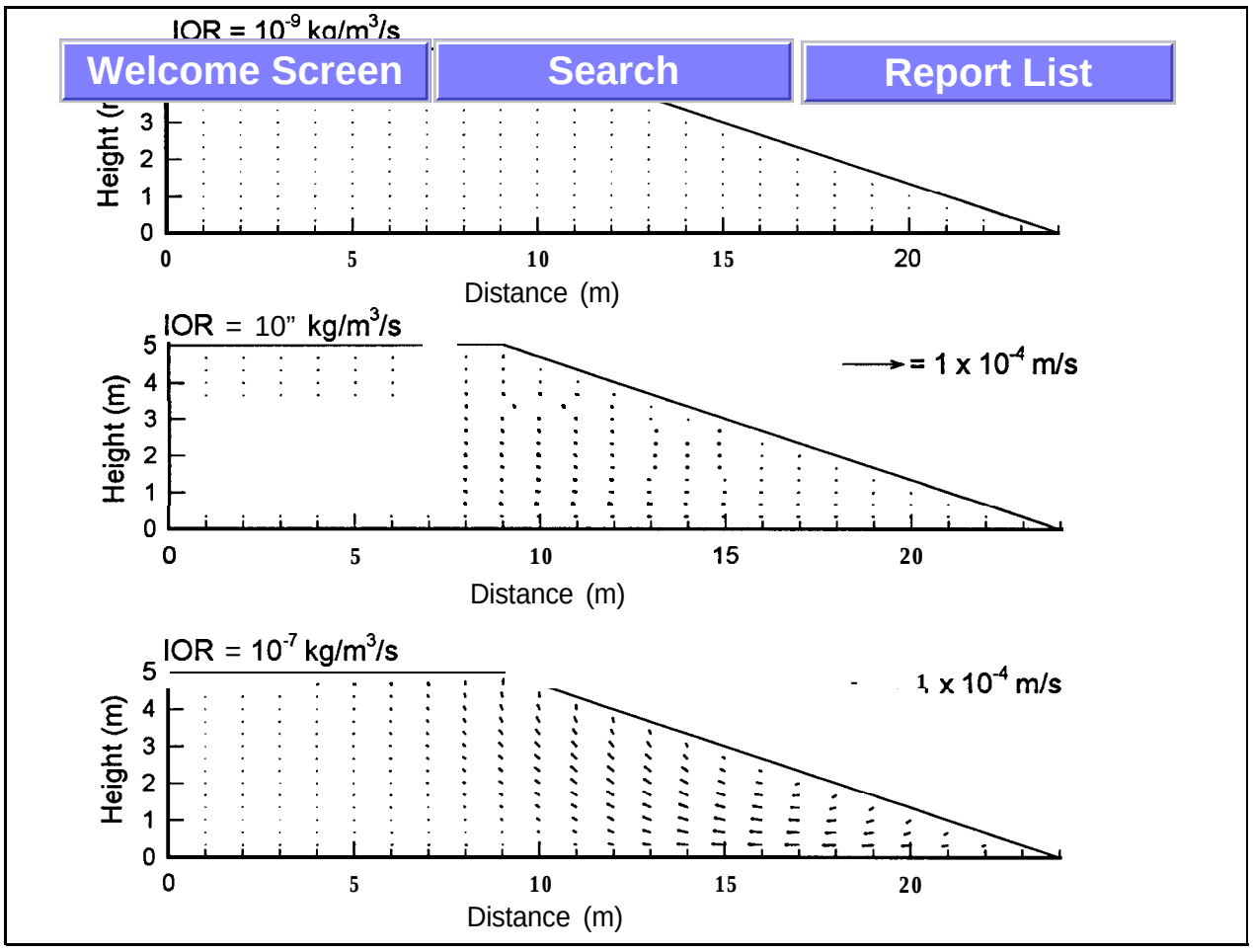

Figure IV - 4: **FIDHELM Results - Pile 7/12: Air flow velocity, K=2.9x10^{-9} m^2, Time = 1 year.**

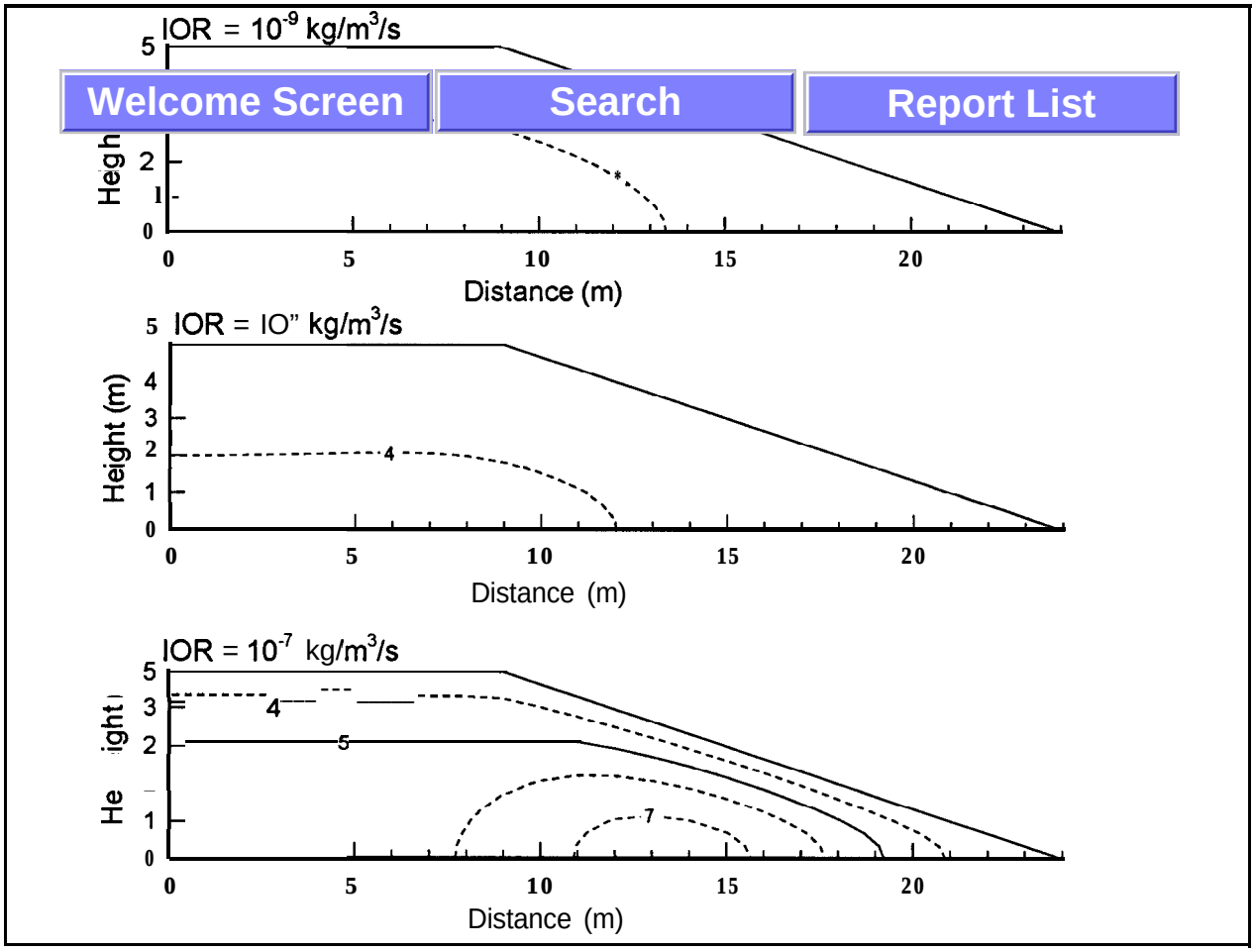

Figure IV - 5: FIDHELM Results - Pile 7/12: Temperature iso-values (A =1°C), K=2.9x10^{-9} m^2, Time = 1 year.

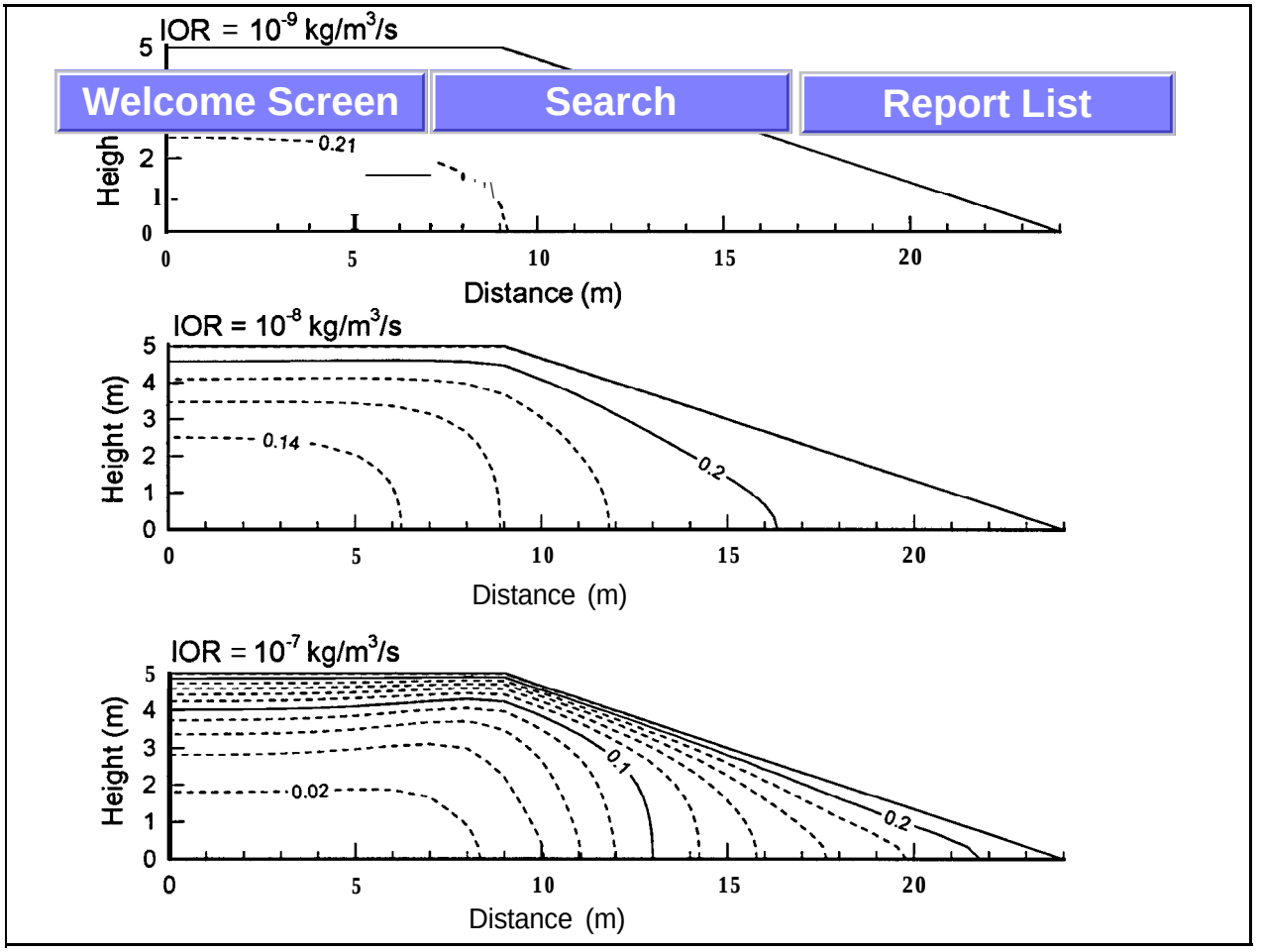

Figure IV - 6: **FIDHELM Results - Pile 7/12: Gaseous oxygen mass fraction iso-values (Δ=0.02), K=2.9x10^{-9}m^2, Time = 1 year.**

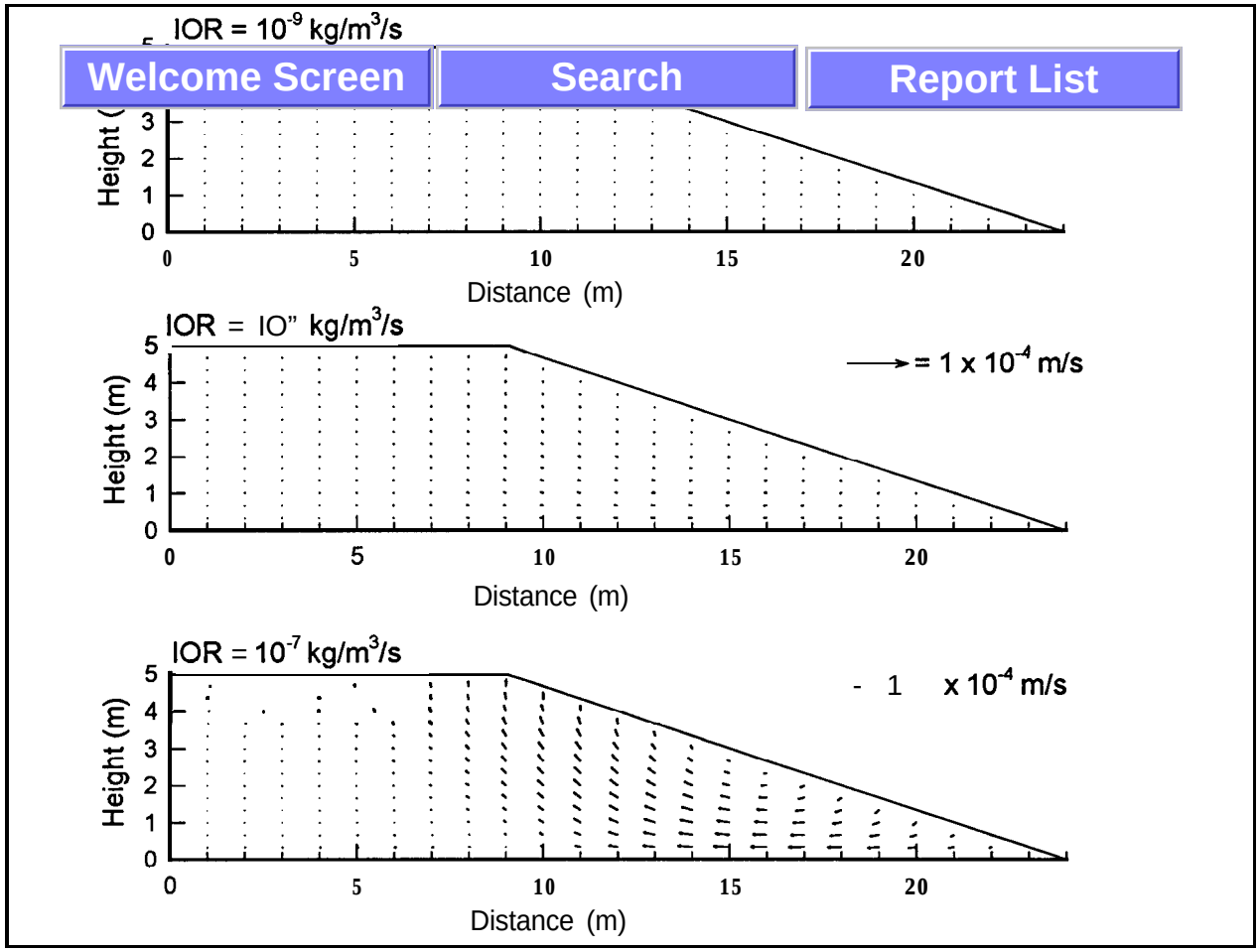

Figure IV - 7: **FIDHELM Results - Pile 7/12: Air flow velocity, K=2.9x10^{-9} m^2, Time = 10 years.**

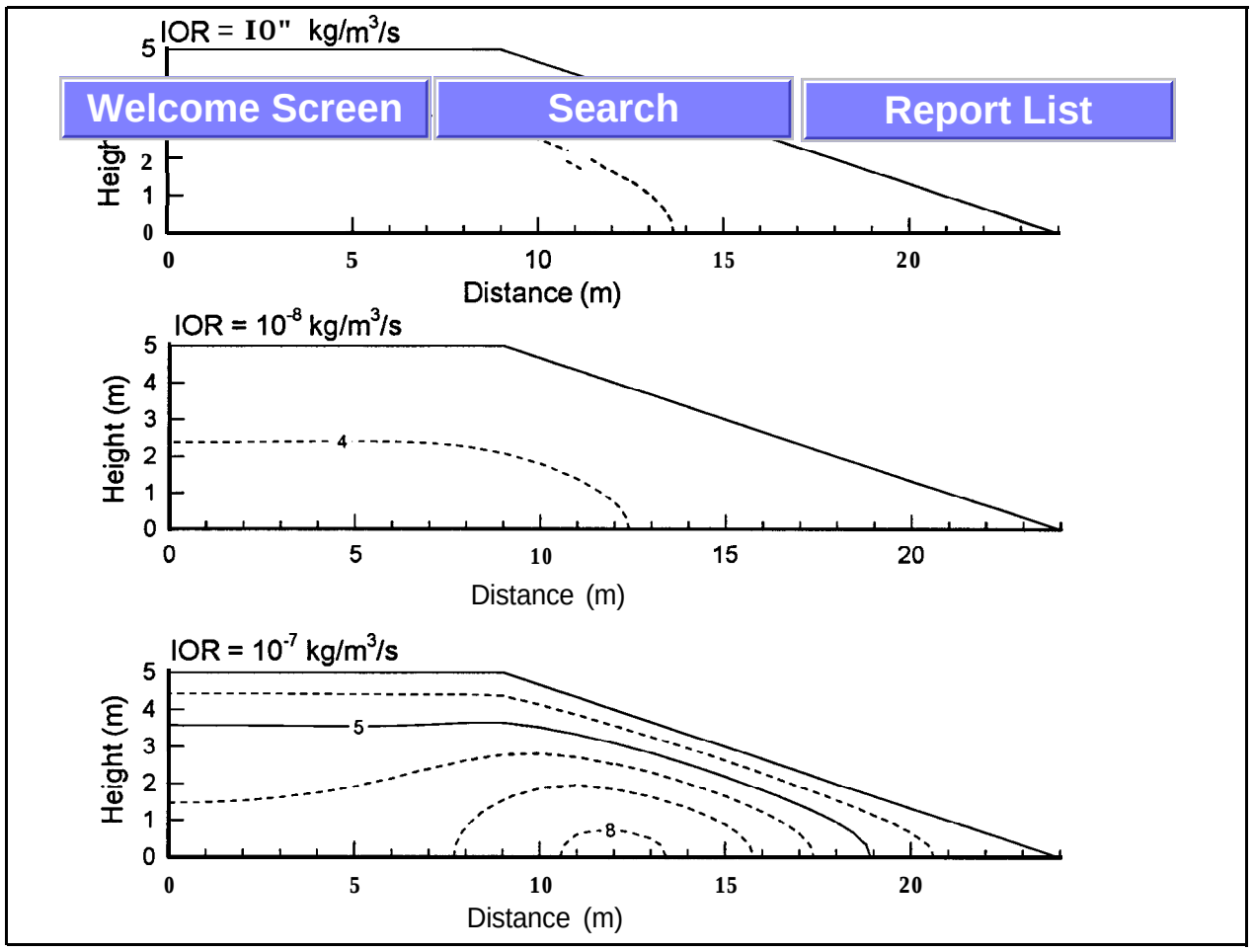

Figure IV - 8: **FIDHELM Results - Pile 7/12: Temperature iso - values (A =1°C), K=2.9x10^{-9} m^2, Time = 10 years.**

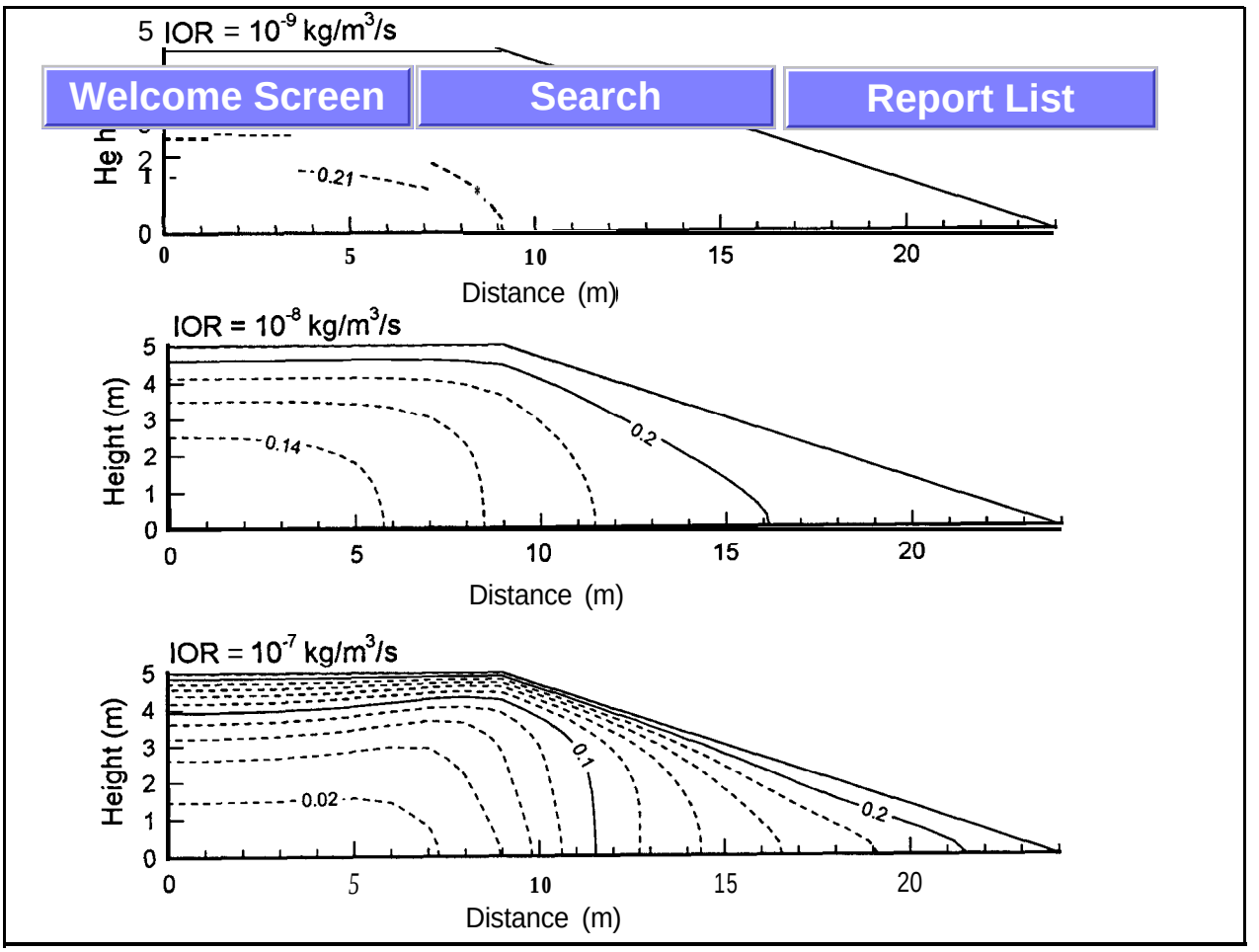

Figure IV - 9: **FTDHELM Results - Pile 7/12: Gaseous oxygen mass fraction iso-values (Δ=0.02), K=2.9x10^{-9}m^2, Time = 10 years.**

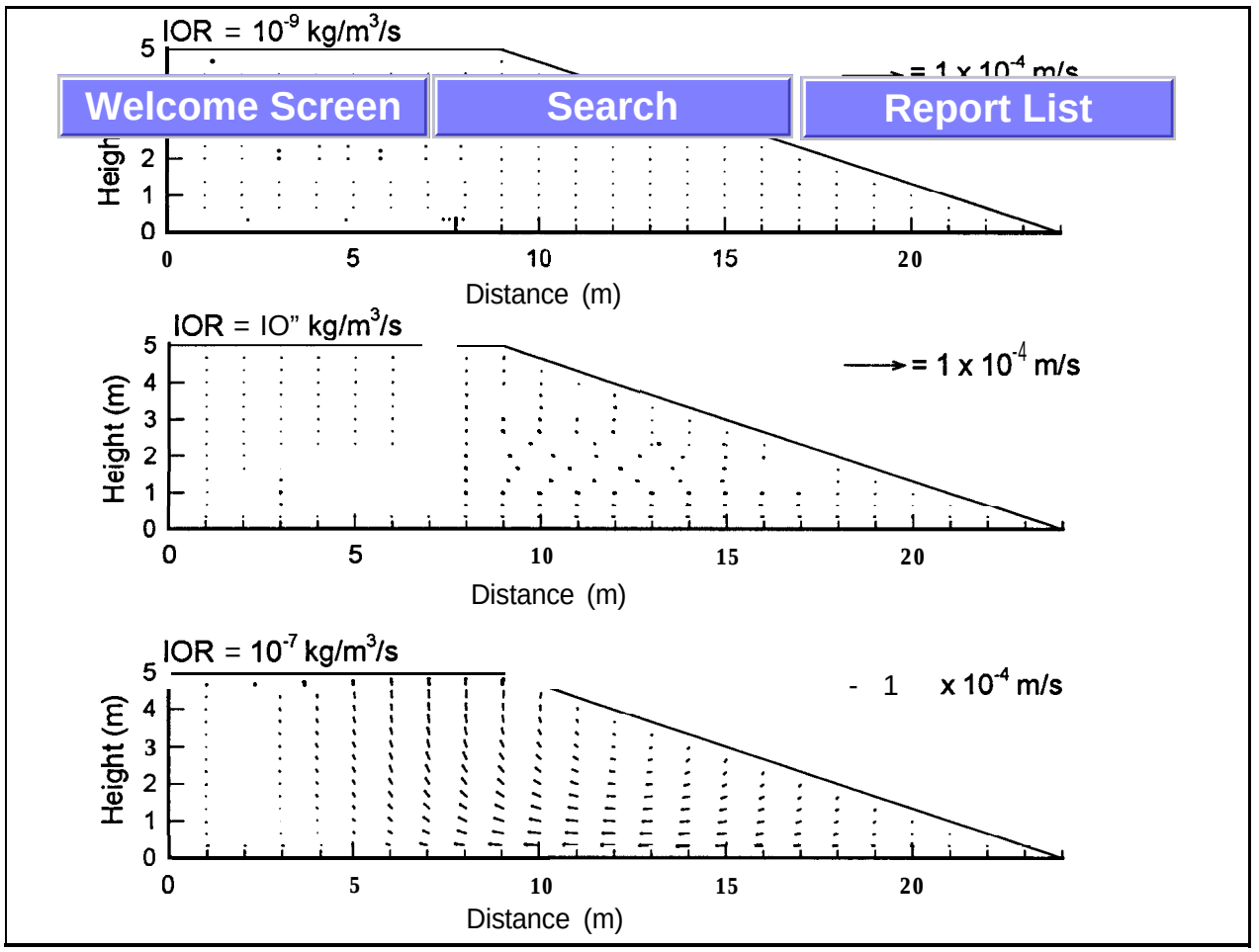

Figure IV - 10: **FIDHELM Results - Pile 7/12: Air flow velocity, K=2.9x10^{-9} m^2, Time = 100 years.**

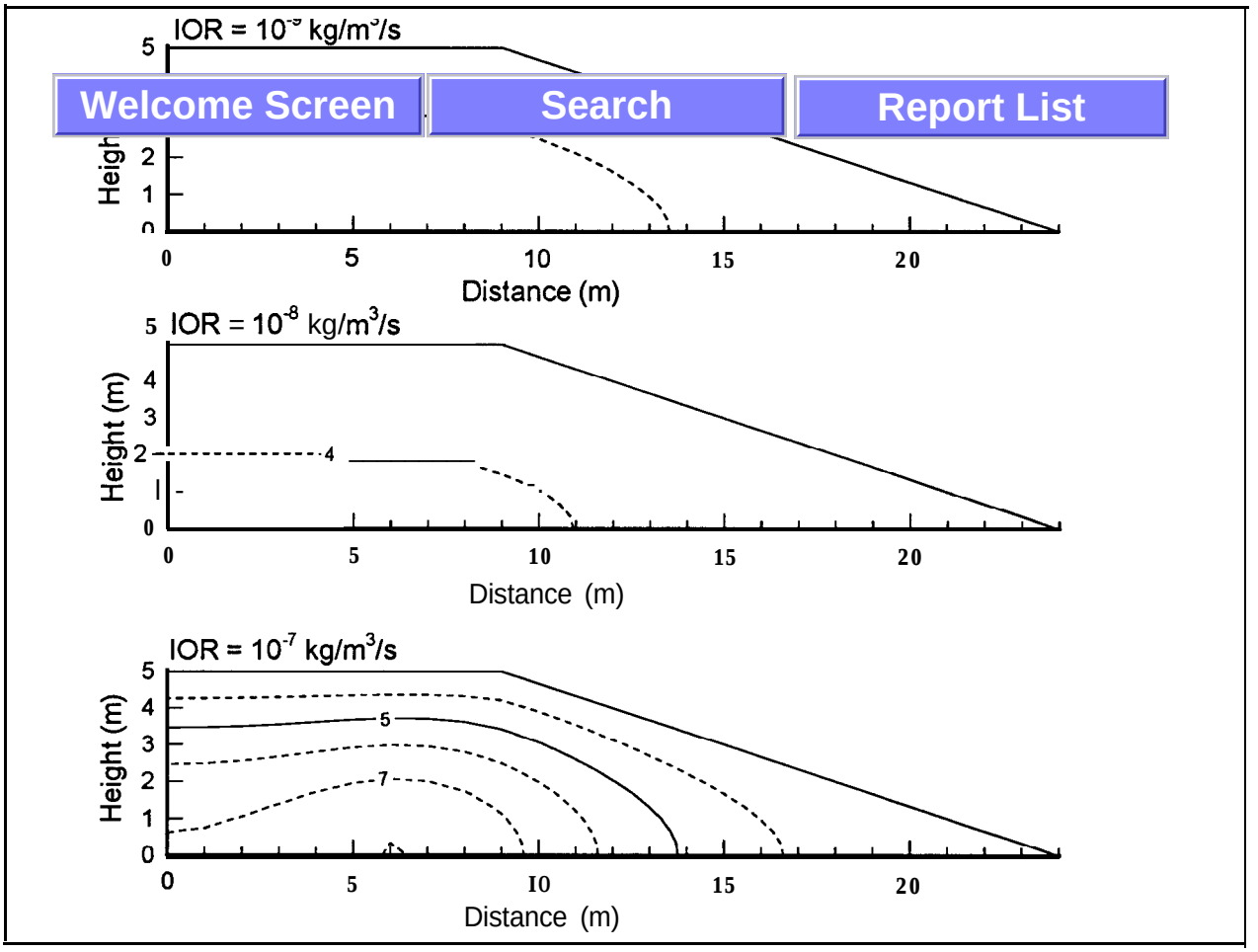

Figure IV - 11: **FIDHELM Results - Pile 7/12: Temperature iso - values (A =1°C), K=2.9x10^{-9} m^2, Time = 100 years.**

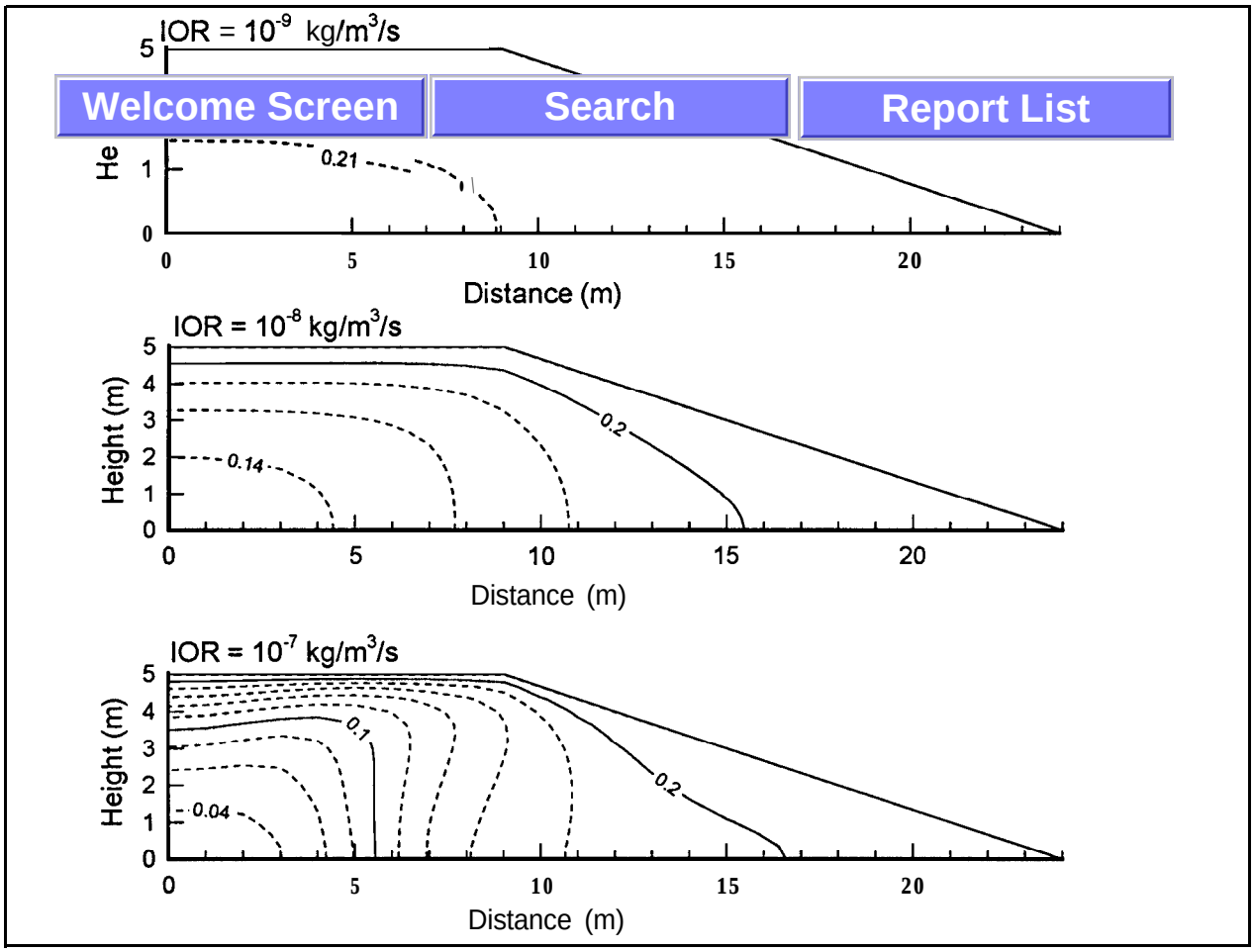

Figure IV - 12: **FIDHELM Results - Pile 7/12: Gaseous oxygen mass fraction iso-values (Δ=0.02), K=2.9x10^{-9}m^2, Time = 100 years.**

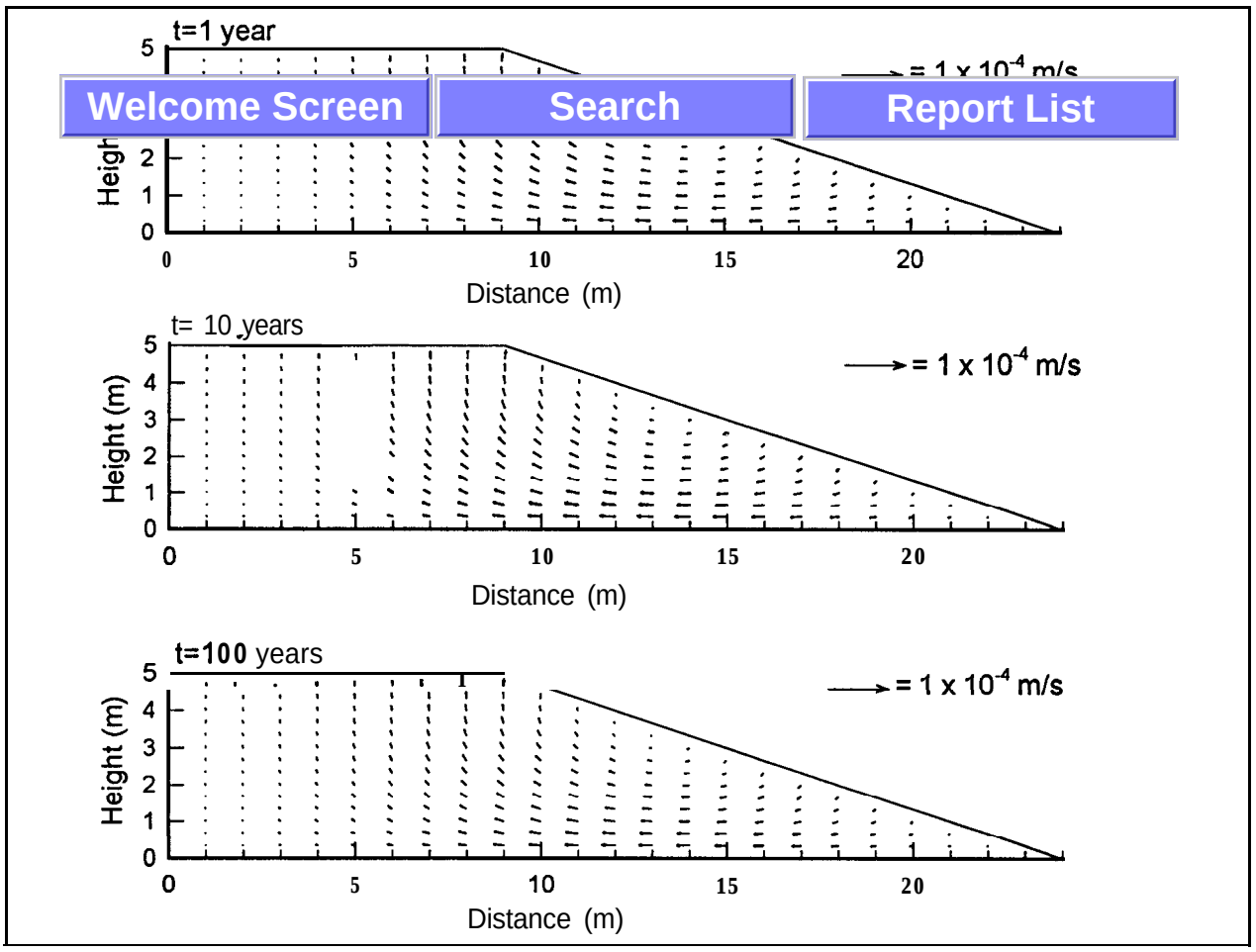

Figure IV - 13: **FIDHELM Results - Pile 7/12: Air flow velocity, $K=1.0x10^{-8}$ m^2, $IOR=10^{-8}$ $kg[O_2]/m^3/s$.**

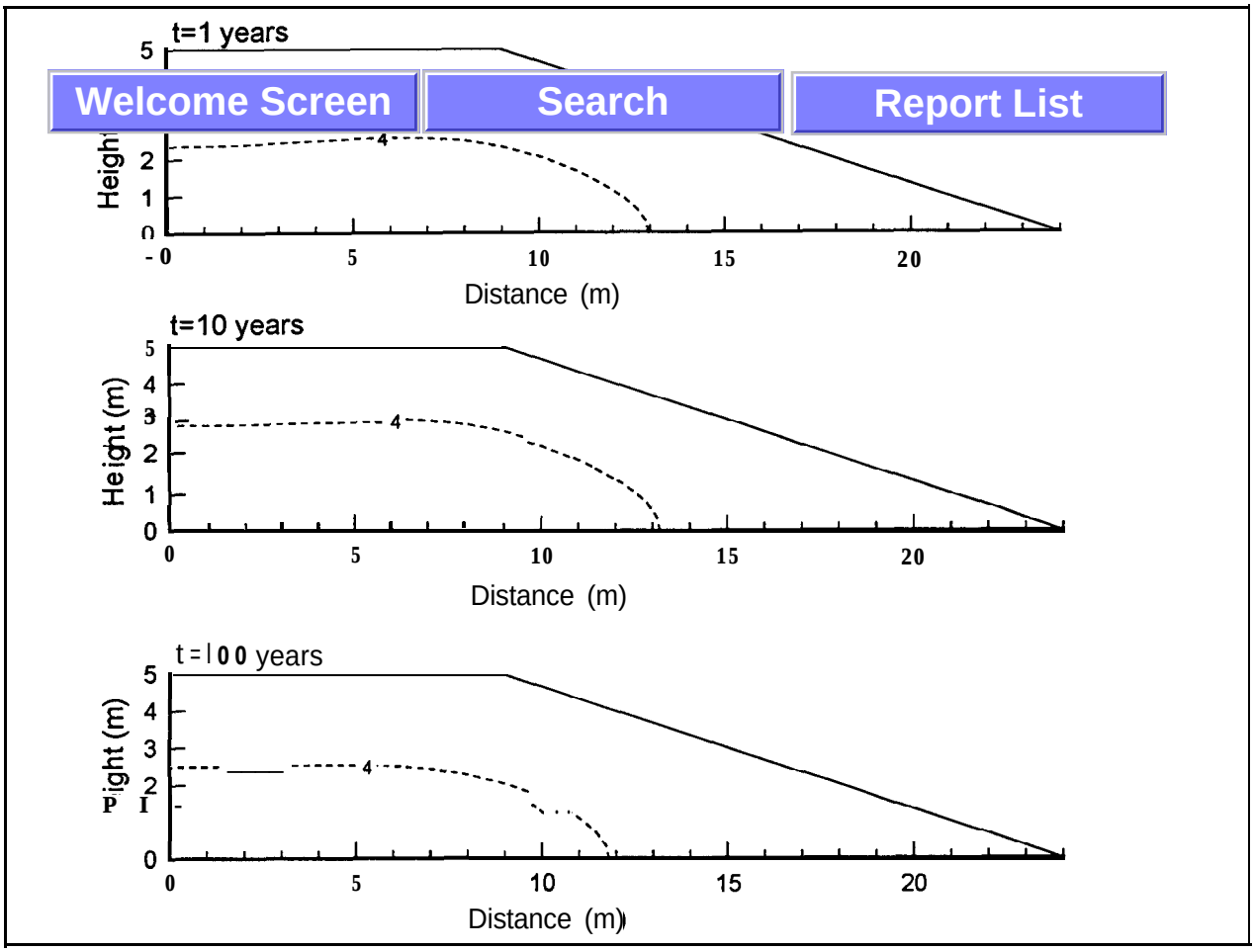

Figure IV - 14: **FIDHELM Results - Pile 7/12: Temperature iso - values (A =1°C), K=1.0x10^{-8} m^2, IOR =10^{-8} kg[O_2]/m^3/s.**

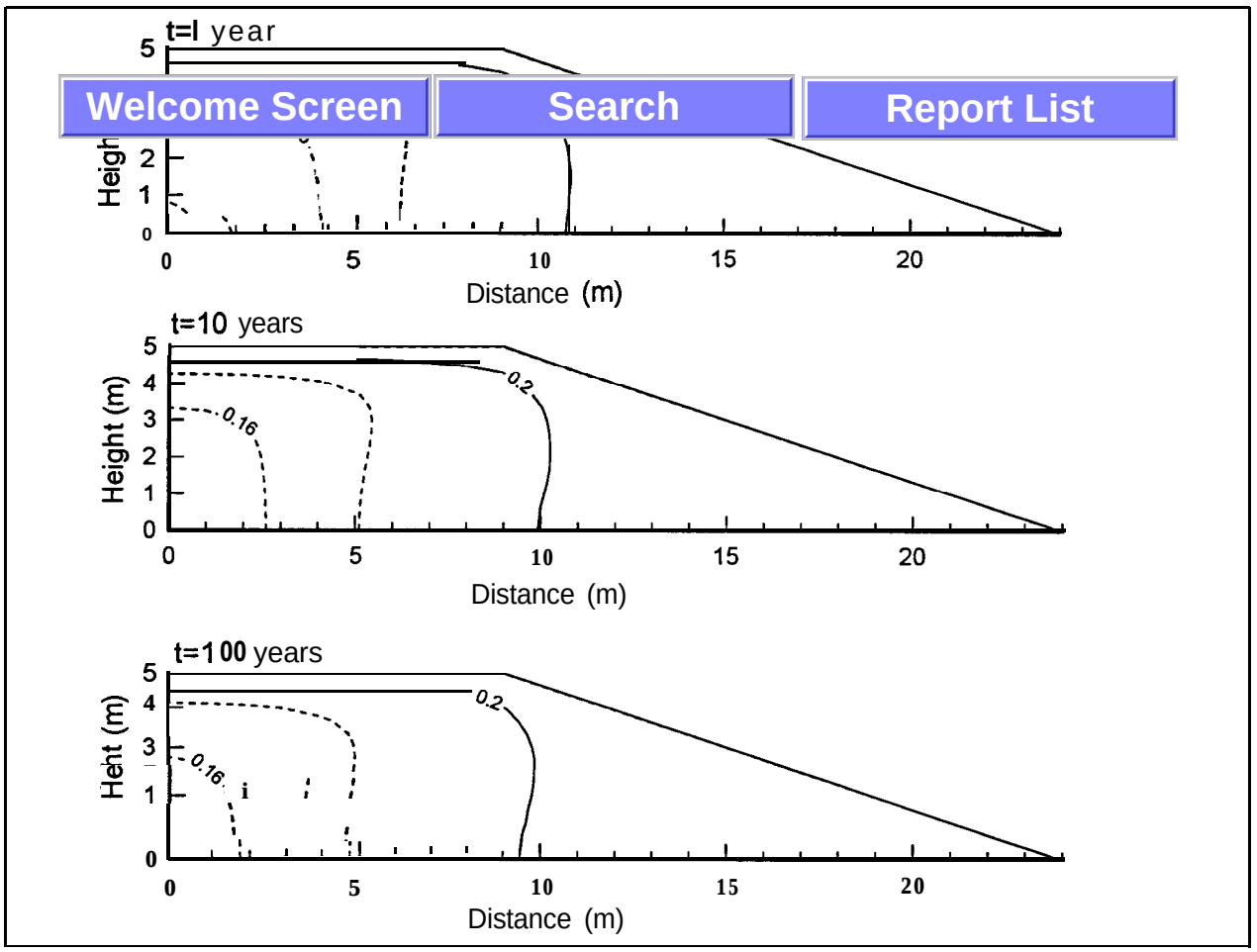

Figure IV - 15: **FIDHELM Results - Pile 7/12: Gaseous oxygen mass fraction iso-values (Δ=0.02), K=1.0x10^{-8} m^2, IOR =10^{-8} kg[O_2]/m^3/s.**

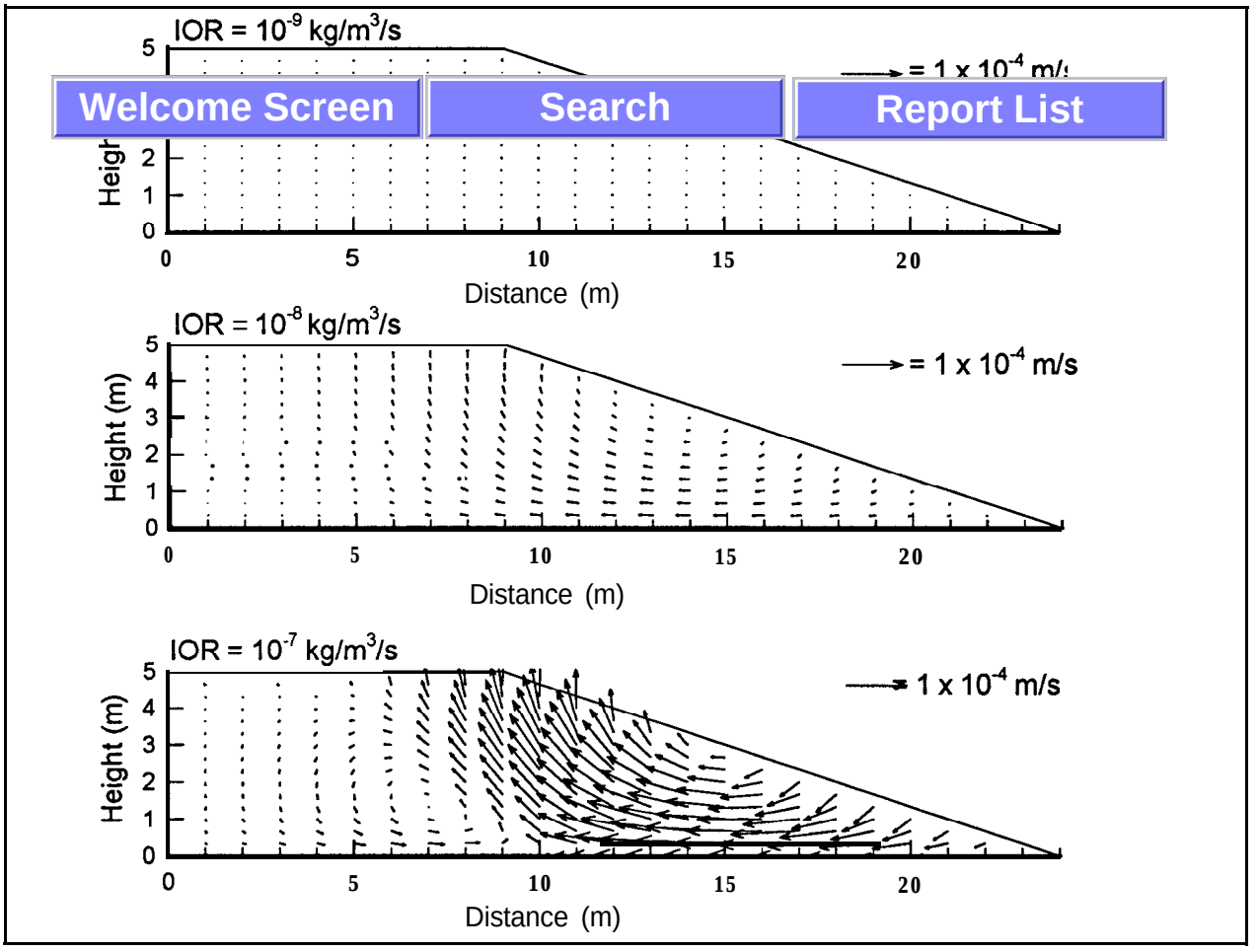

Figure IV - 16: **FIDHELM Results - Pile 7/12: Air flow velocity, K=1.0x10^{-8} m^2, Time = 1 year.**

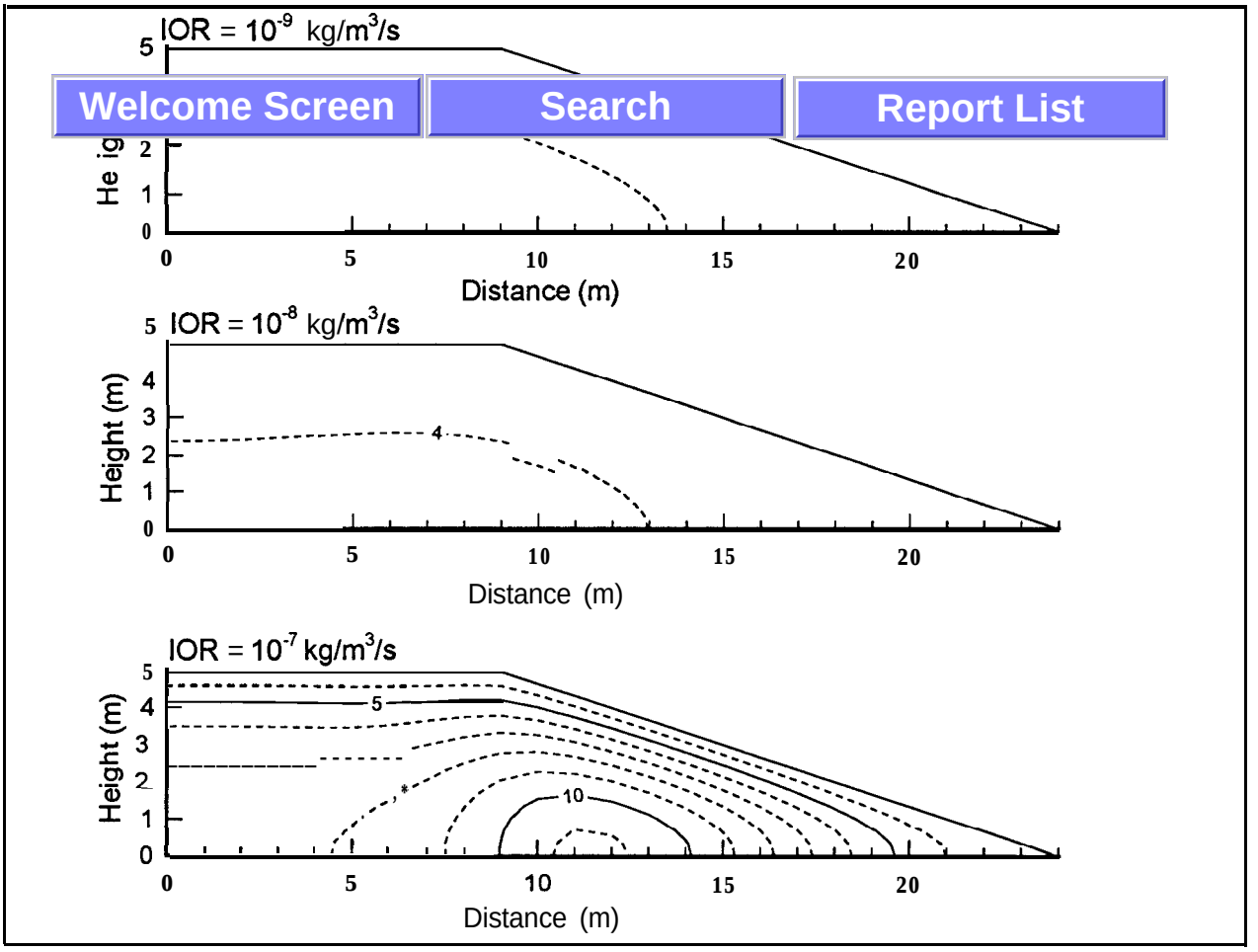

Figure IV - 17: **FIDHELM Results - Pile 7/12: Temperature iso - values (A =1°C), K=1.0x10^{-8} m^2, Time = 1 year.**

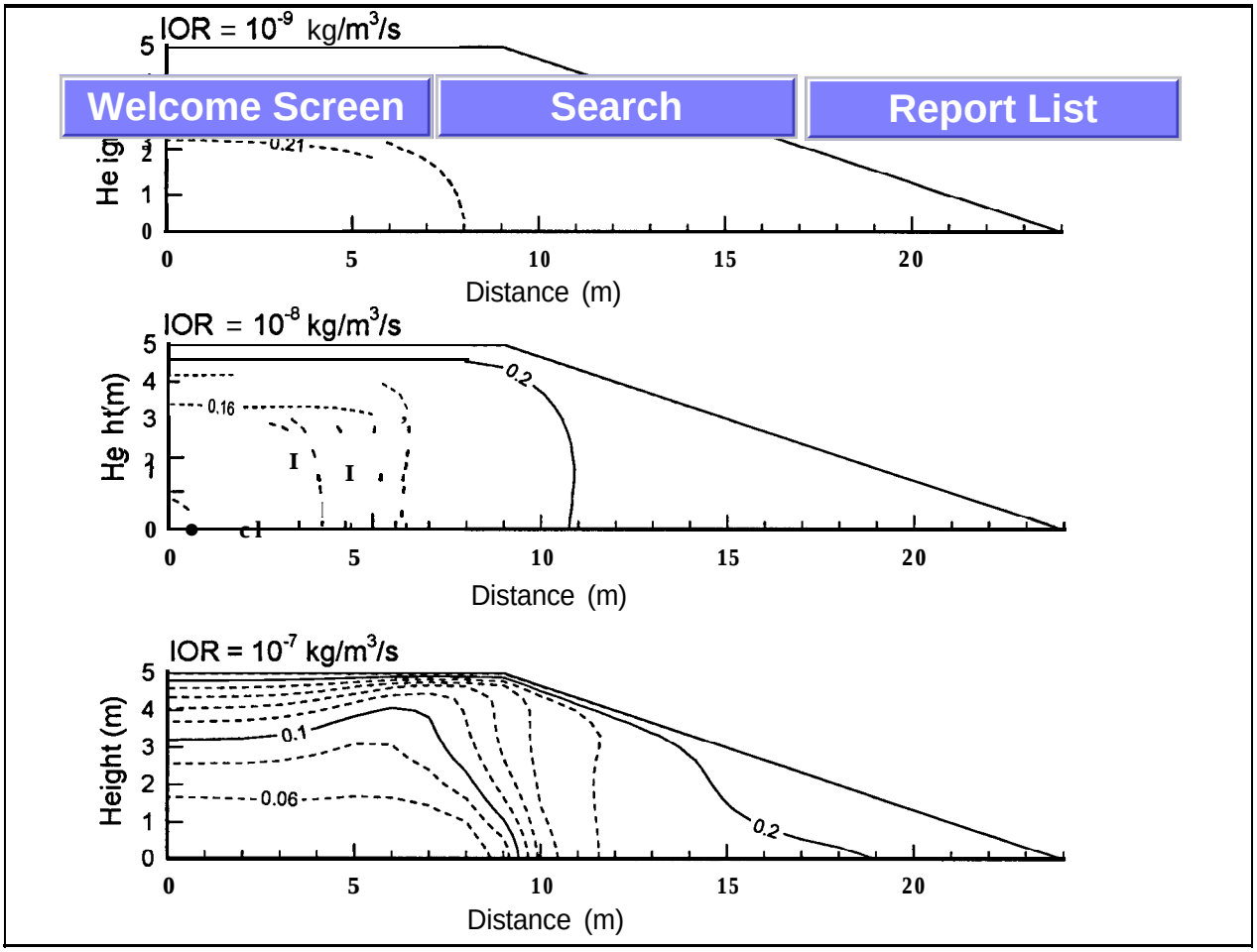

Figure IV - 18: **FIDHELM Results - Pile 7/12: Gaseous oxygen mass fraction iso-values (Δ=0.02), K=1.0x10^{-8}m^2, Time = 1 year.**

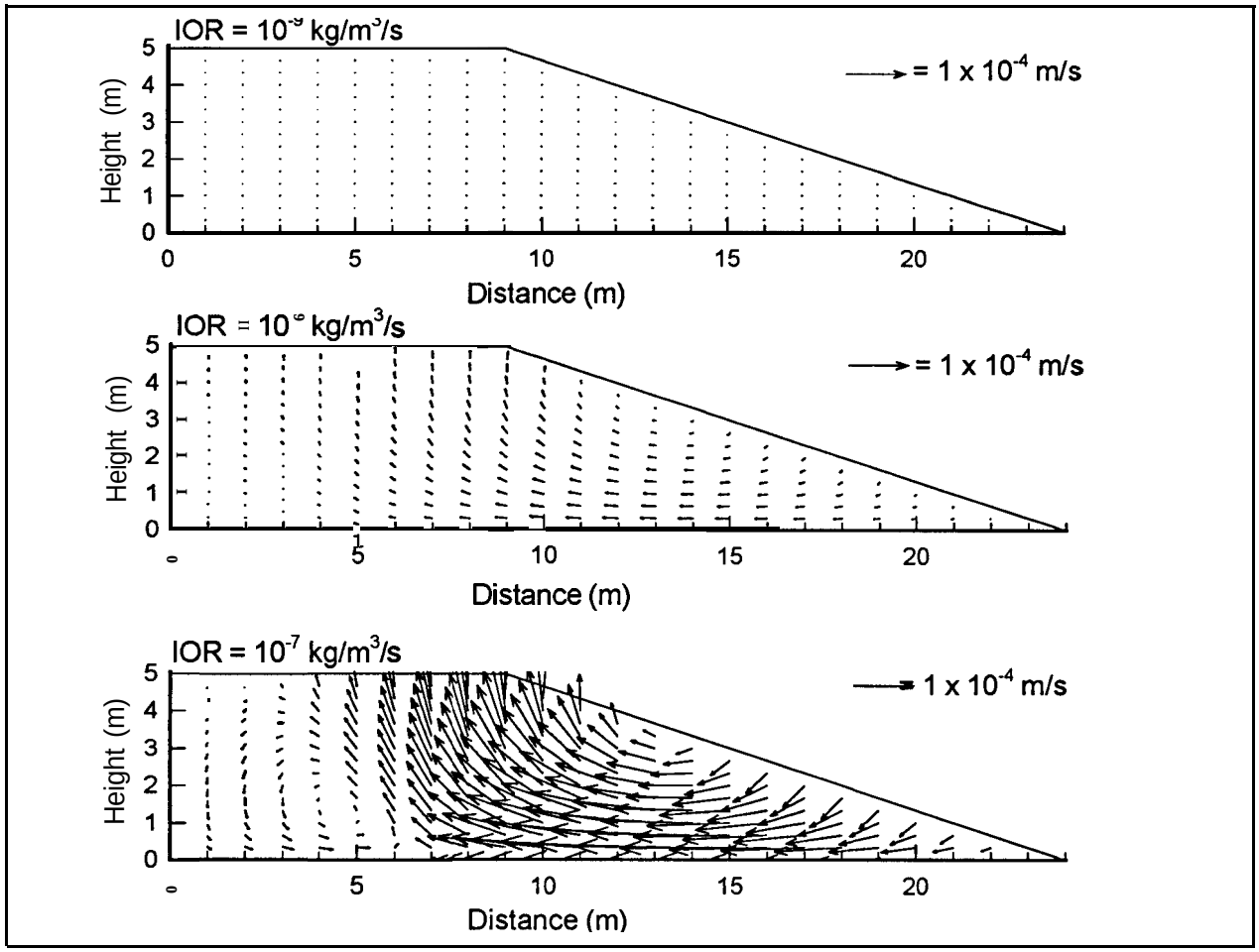

Figure IV - 19: **FIDHELM Results - Pile 7/12: Air flow velocity, K=1.0x10^{-8} m^2, Time = 10 years.**

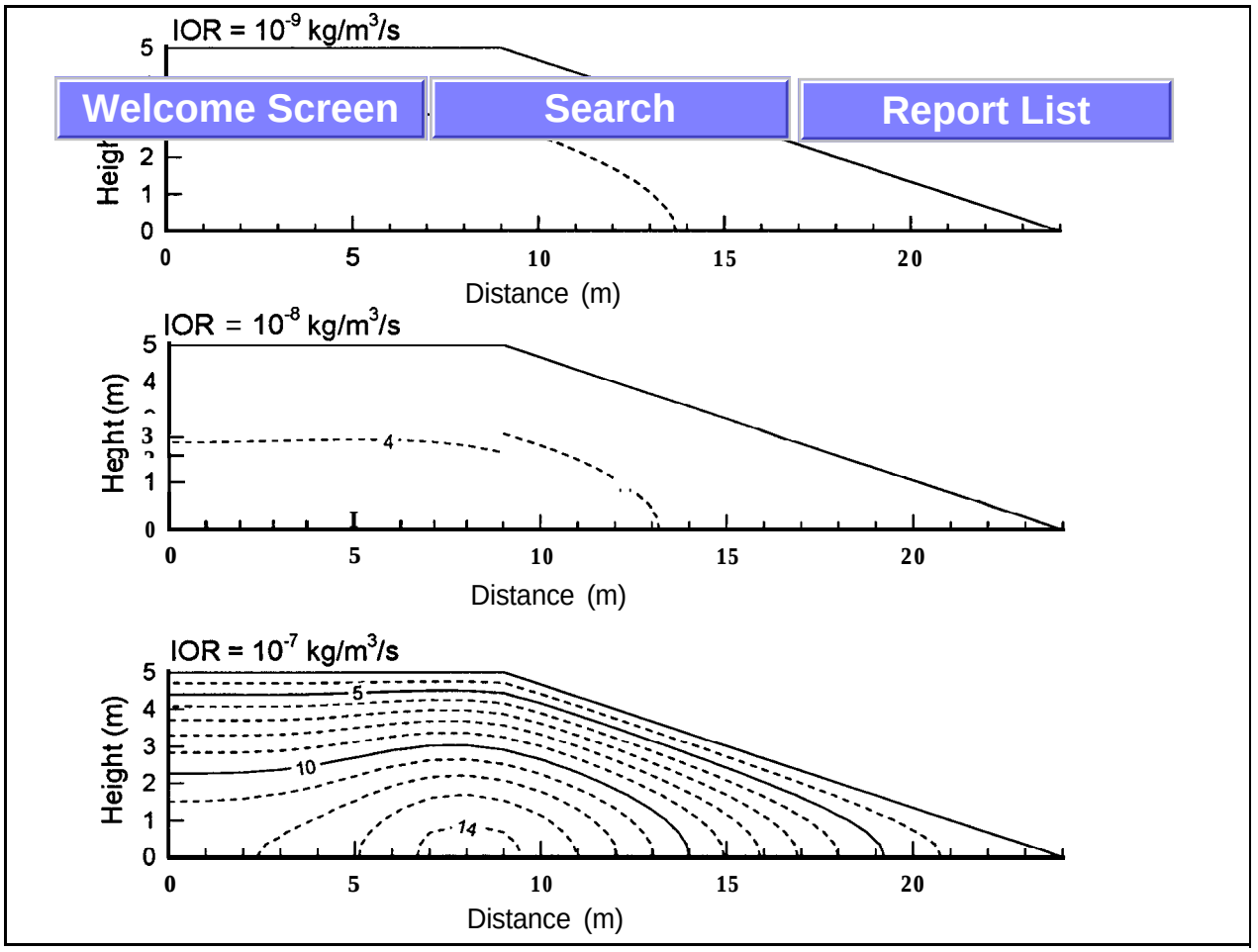

Figure IV - 20: **FIDHELM Results - Pile 7/12: Temperature iso - values (A =1°C), K=1.0x10^{-8} m^2, Time = 10 years.**

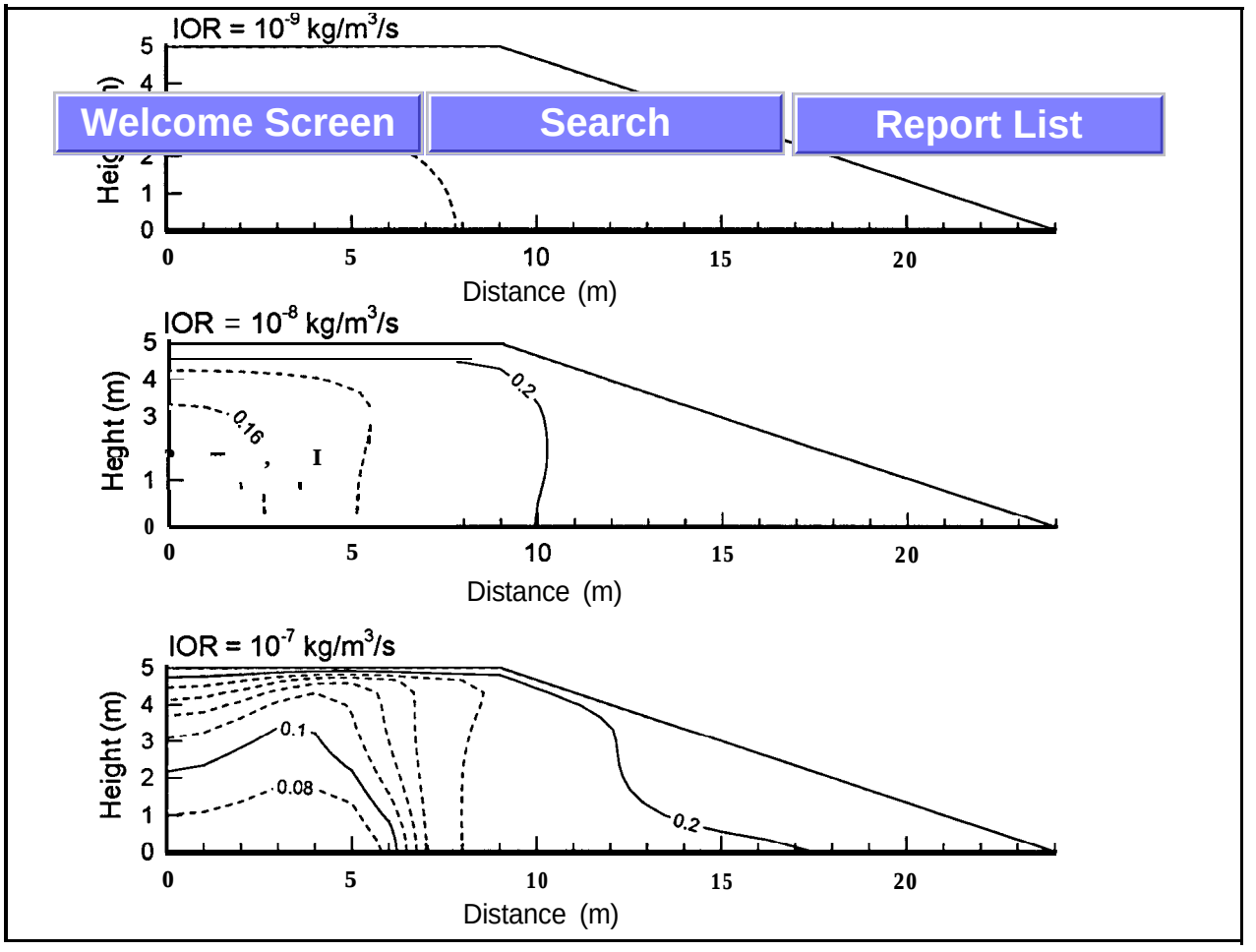

Figure IV - 21: **FIDHELM Results - Pile 7/12: Gaseous oxygen mass fraction iso-values (Δ=0.02), K=1.0x10^{-8}m^2, Time = 10 years.**

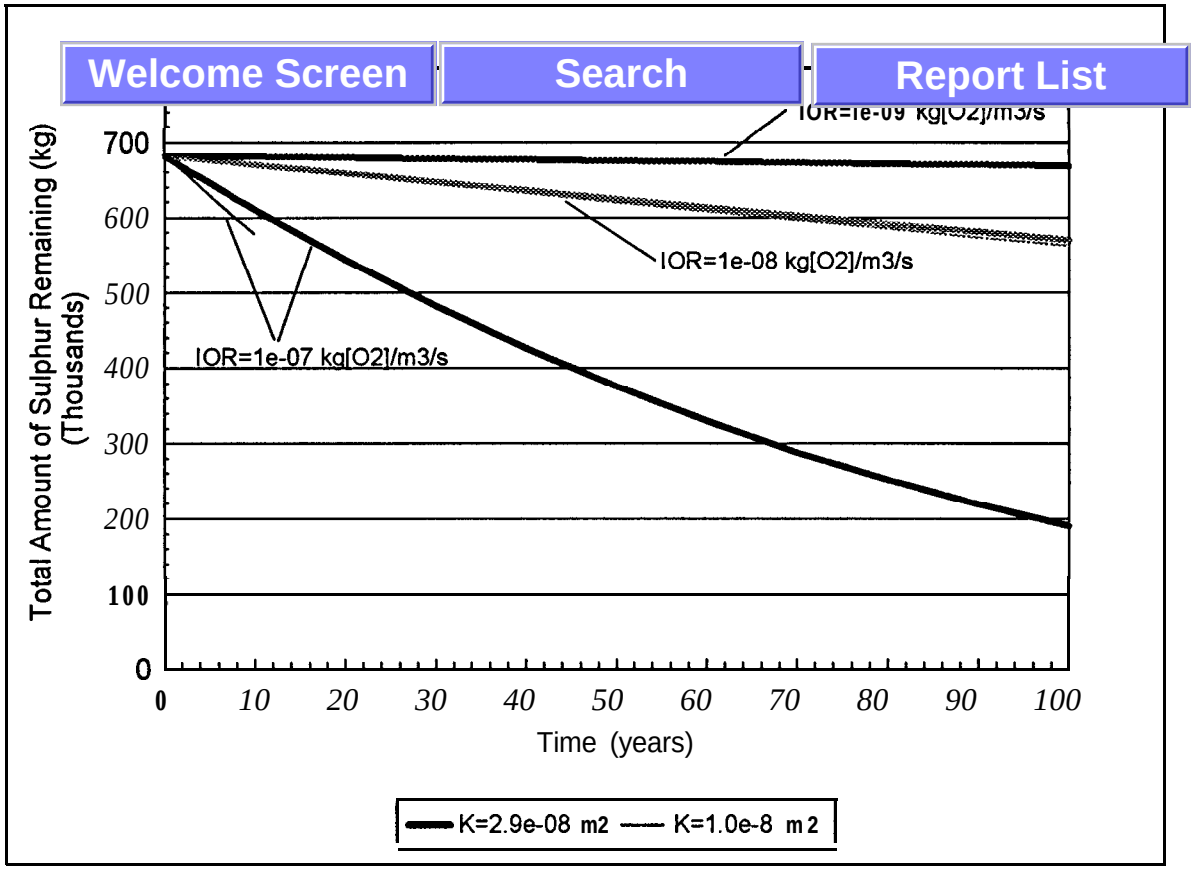

Figure IV - 22: **FIDHELM Results - Pile 7/12: Total amount of sulphur remaining from solid phase versus time.**

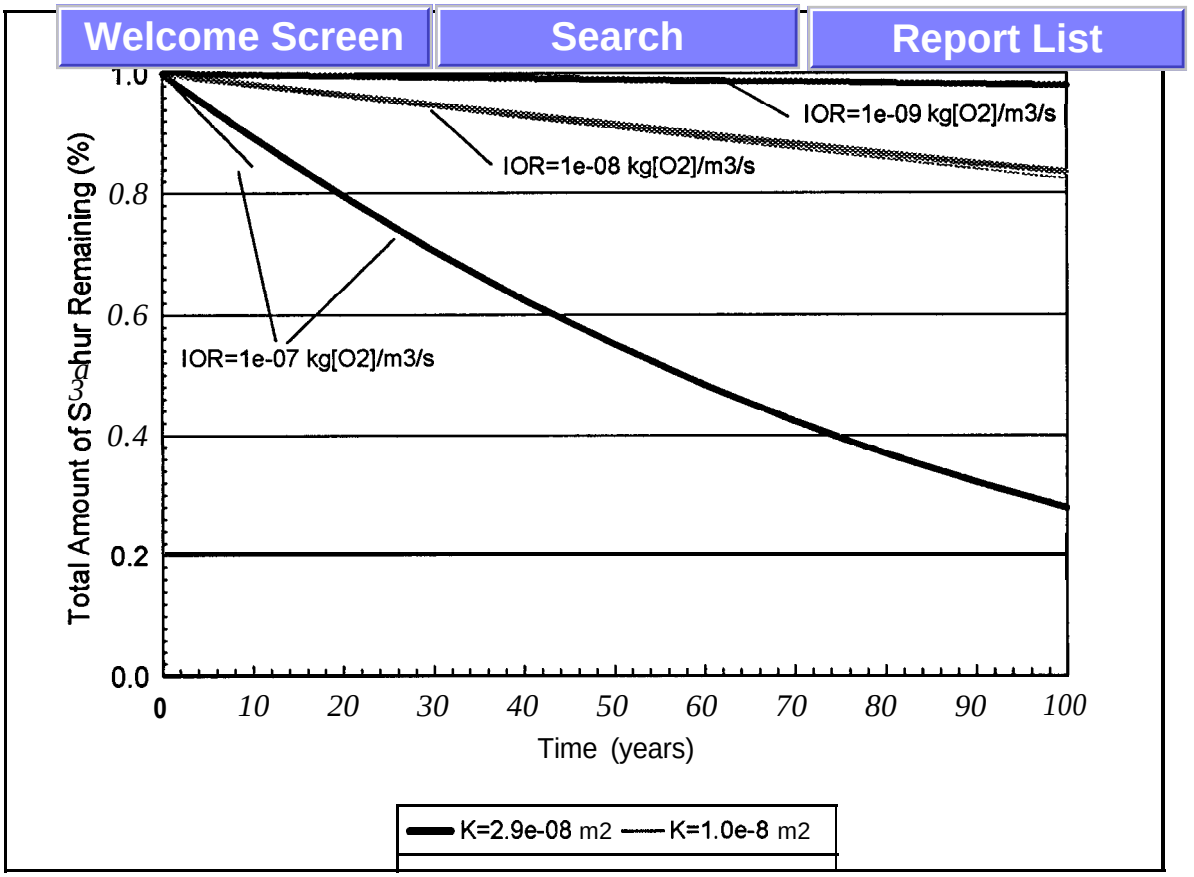

Figure IV - 23: **FIDHELM Results - Pile 7/12: Normalized total amount of sulphur remaining from solid phase versus time.**

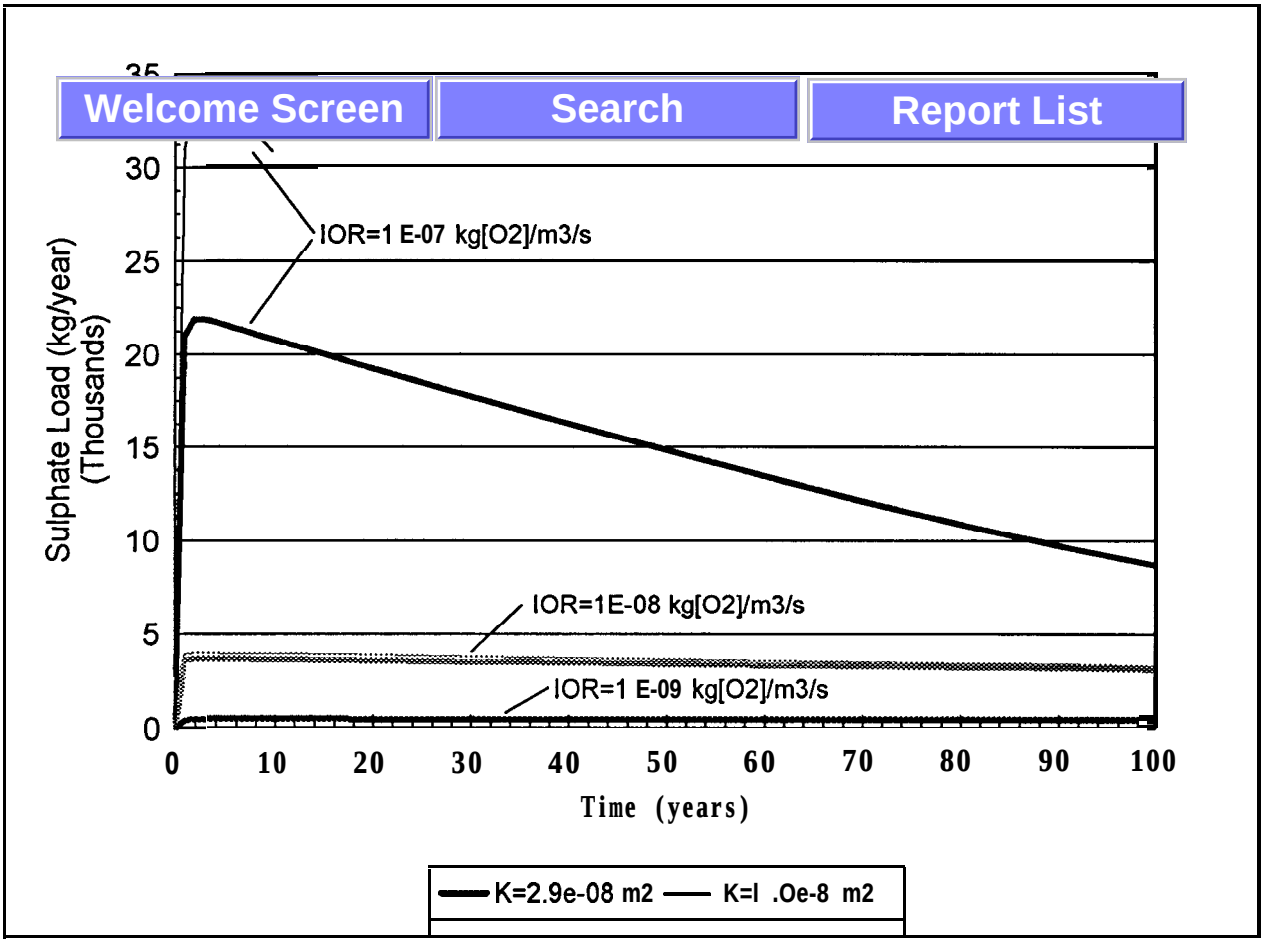

Figure IV - 24: **FIDHELM Results - Pile 7/12: Sulphate load from aqueous phase versus time.**

FIDHELM RESULTS

PILE 18B

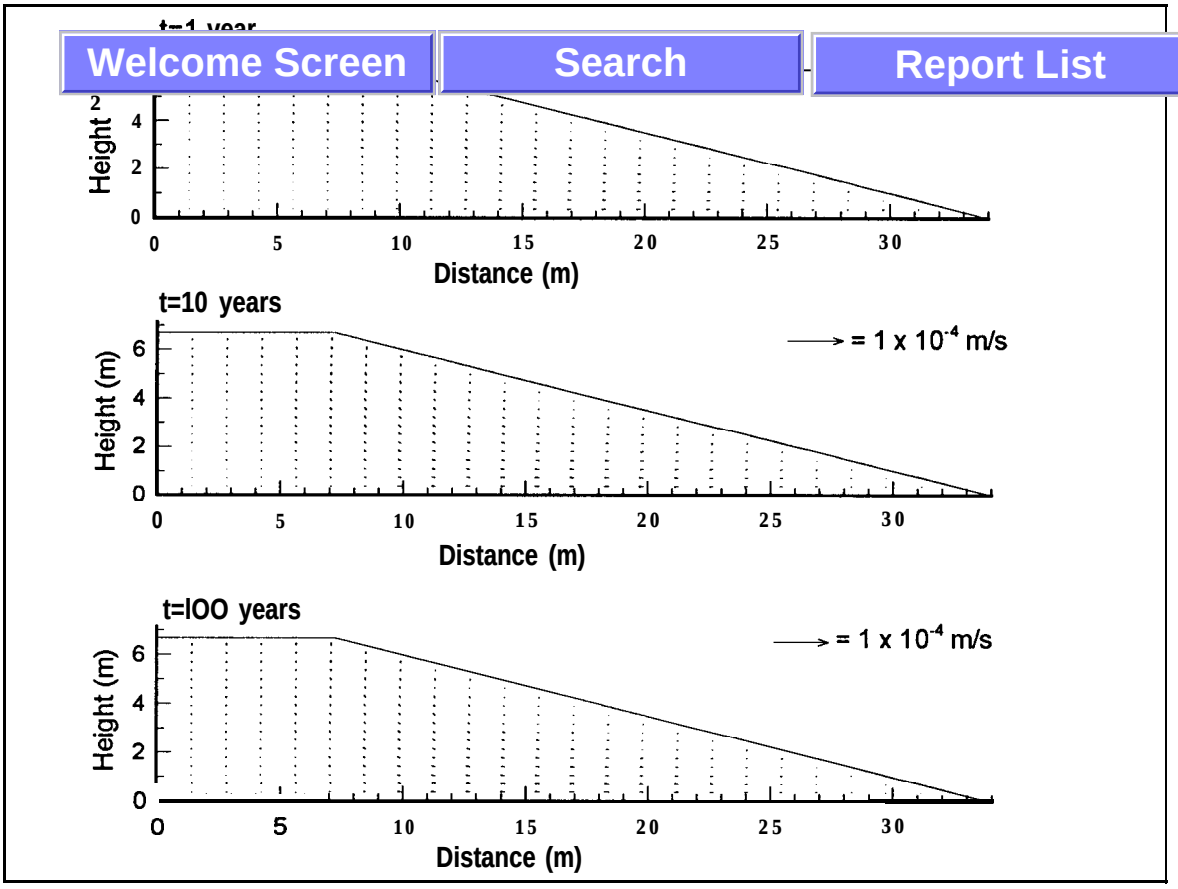

Figure IV - 25: **FIDHELM Results - Pile 18b: Air flow velocity, $K=2.9x10^{-9}$ m^2, $IOR=10^{-8}$ $kg[O_2]/m^3/s$.**

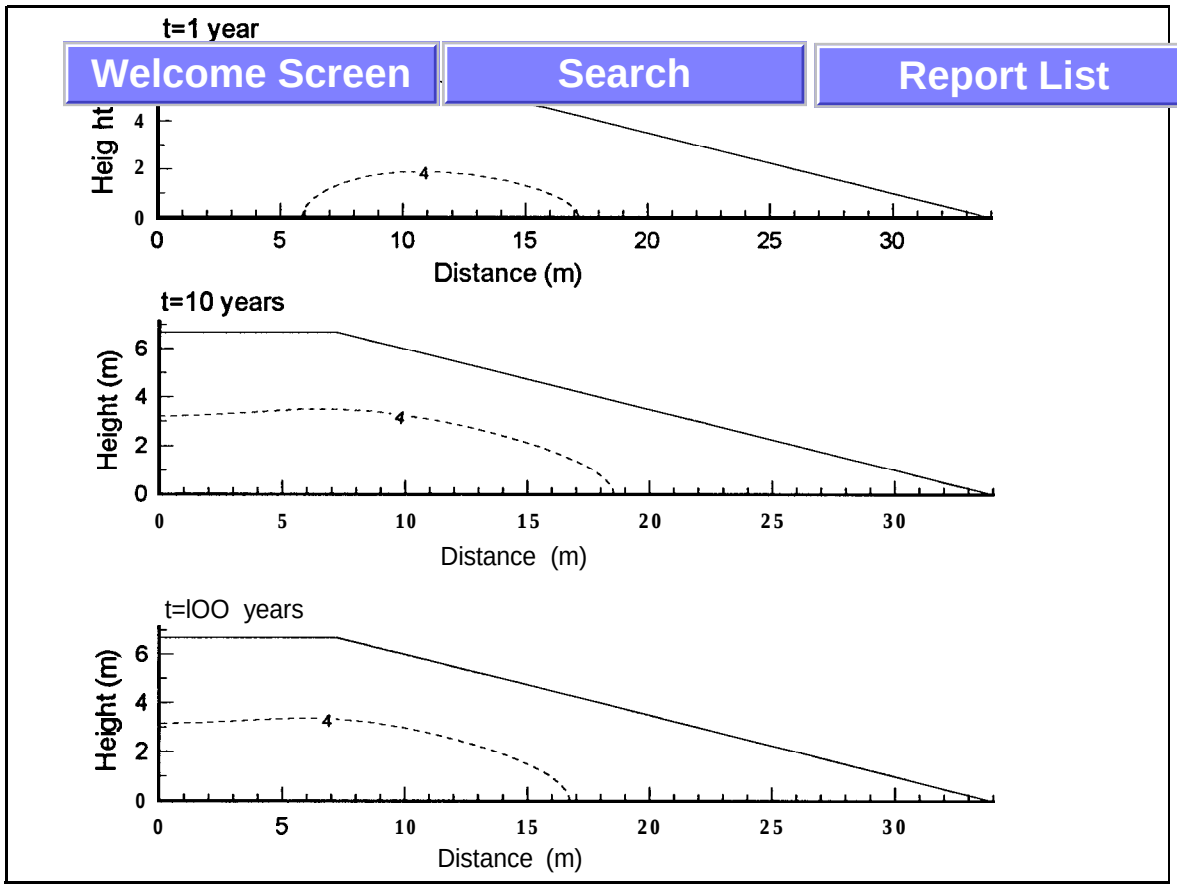

Figure IV - 26: **FIDHELM Results - Pile 18b: Temperature iso - values (A =1°C), K=2.9x10^{-9} m^2, IOR =10^{-8} kg[O_2]/m^3/s.**

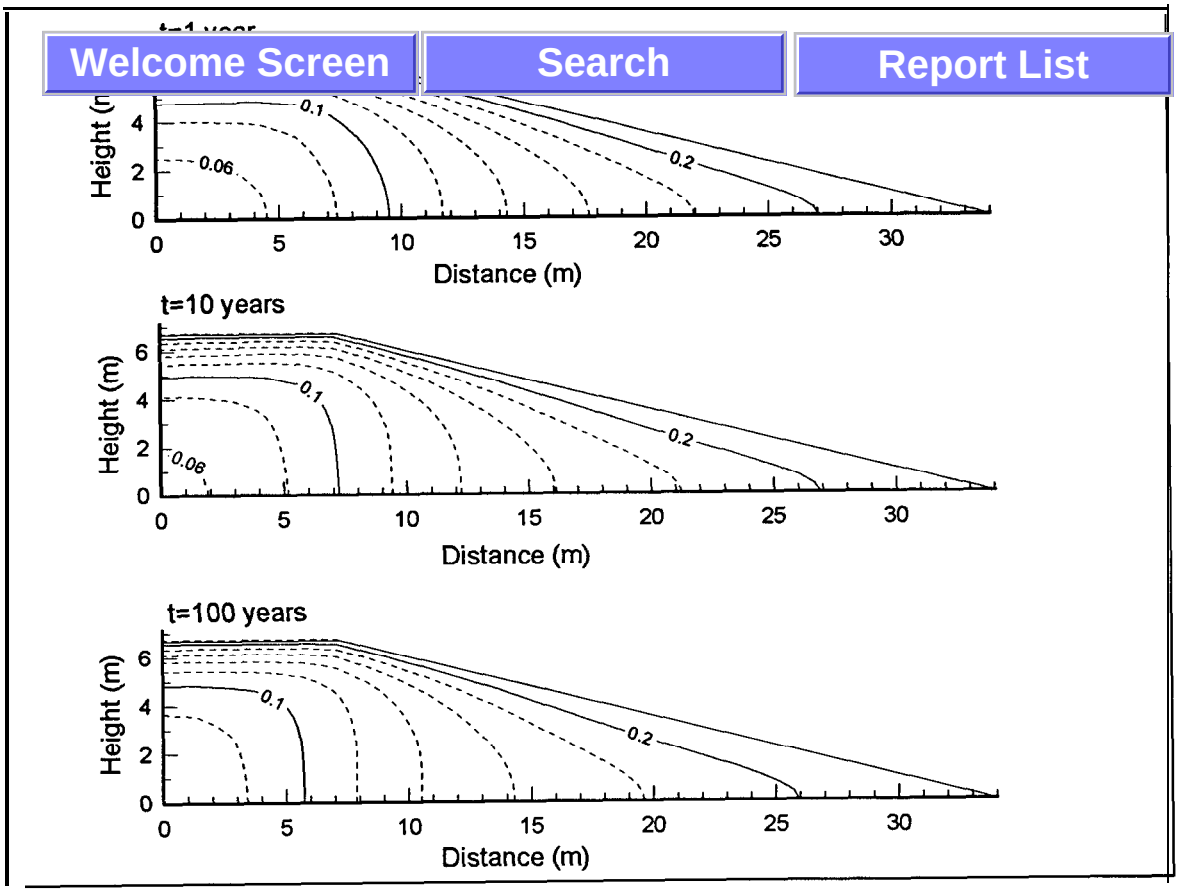

Figure IV - 27: **FIDHELM Results - Pile 18b: Gaseous oxygen mass fraction iso - values (Δ=0.02), K=2.9x10^{-9} m^2, IOR =10^{-8} kg[O_2]/m^3/s.**

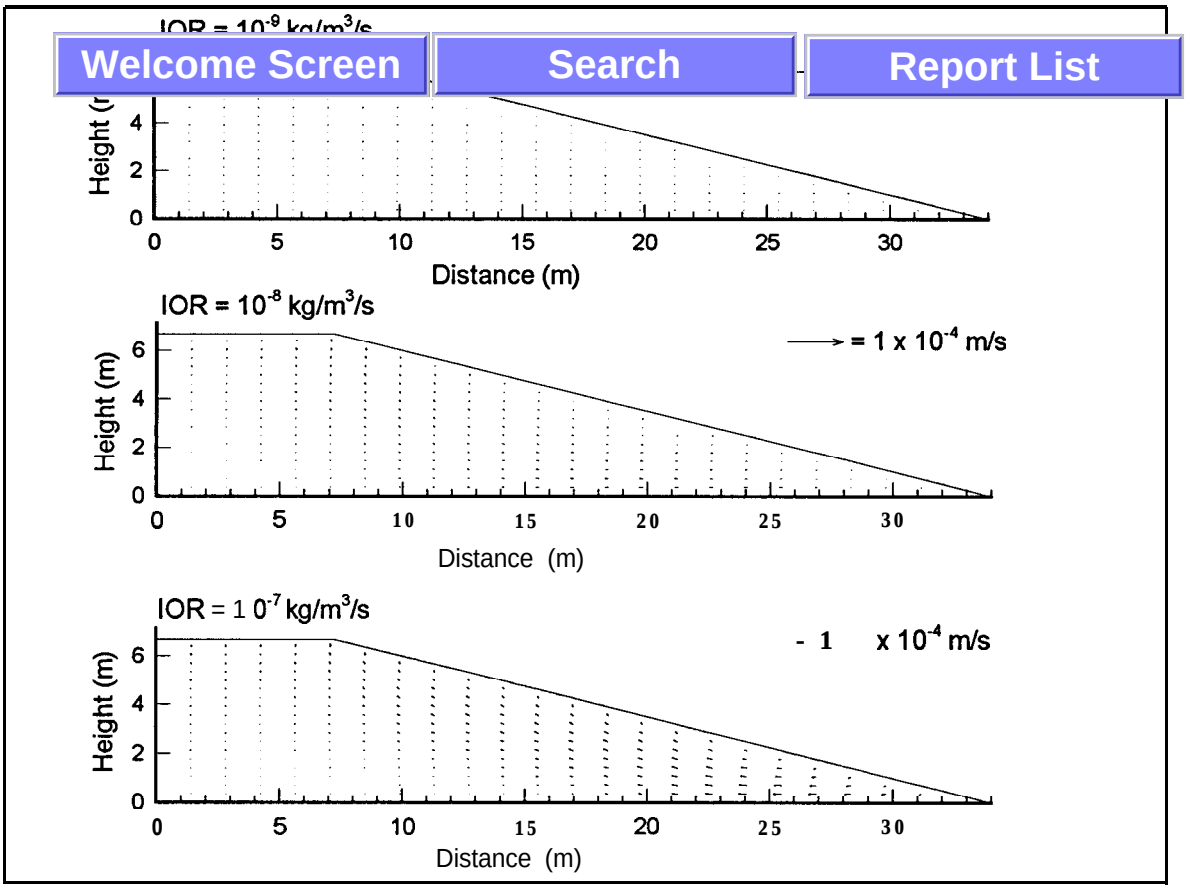

Figure IV - 28: **FIDHELM Results - Pile 18b: Air flow velocity, K=2.9x10^{-9} m^2, Time = 1 year.**

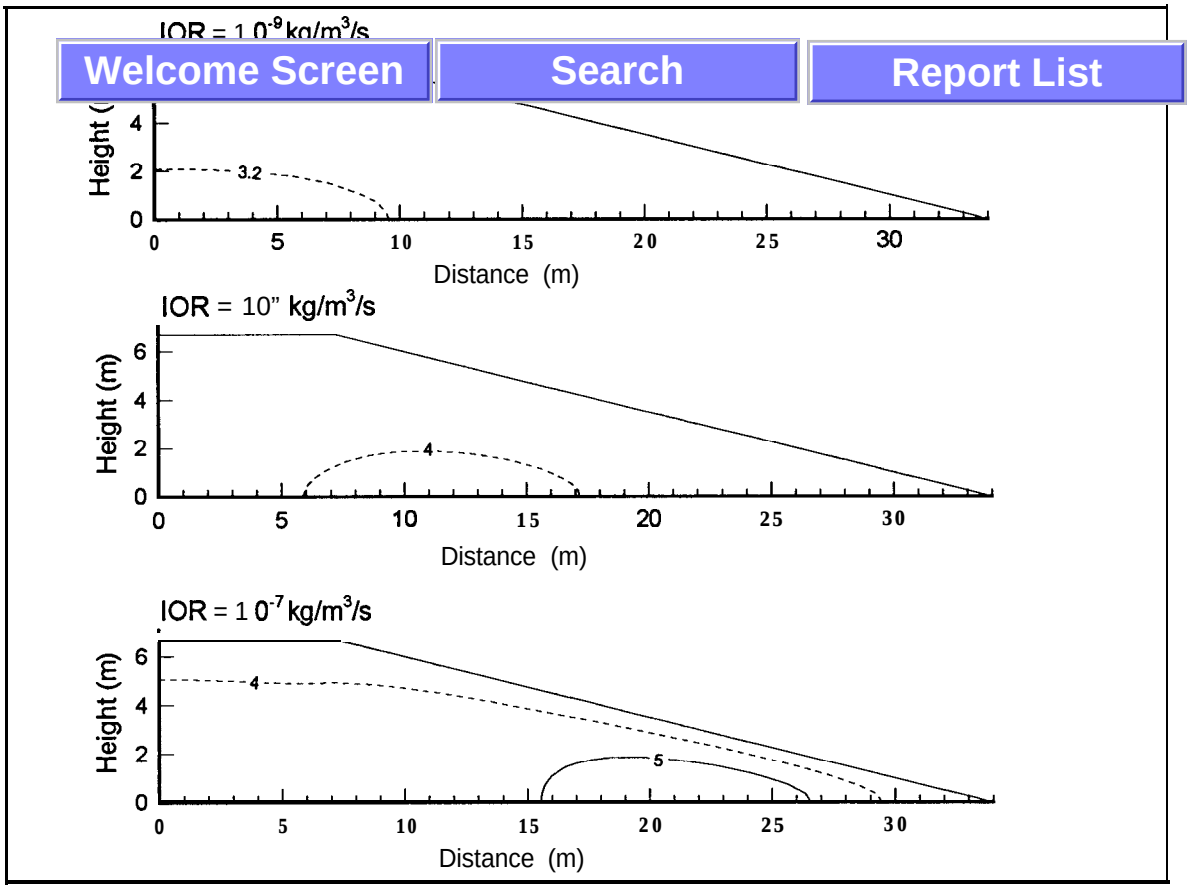

Figure IV - 29: **FIDHELM Results - Pile 18b: Temperature iso - values (A =1°C), K=2.9x10^{-9}m^2, Time = 1 year.**

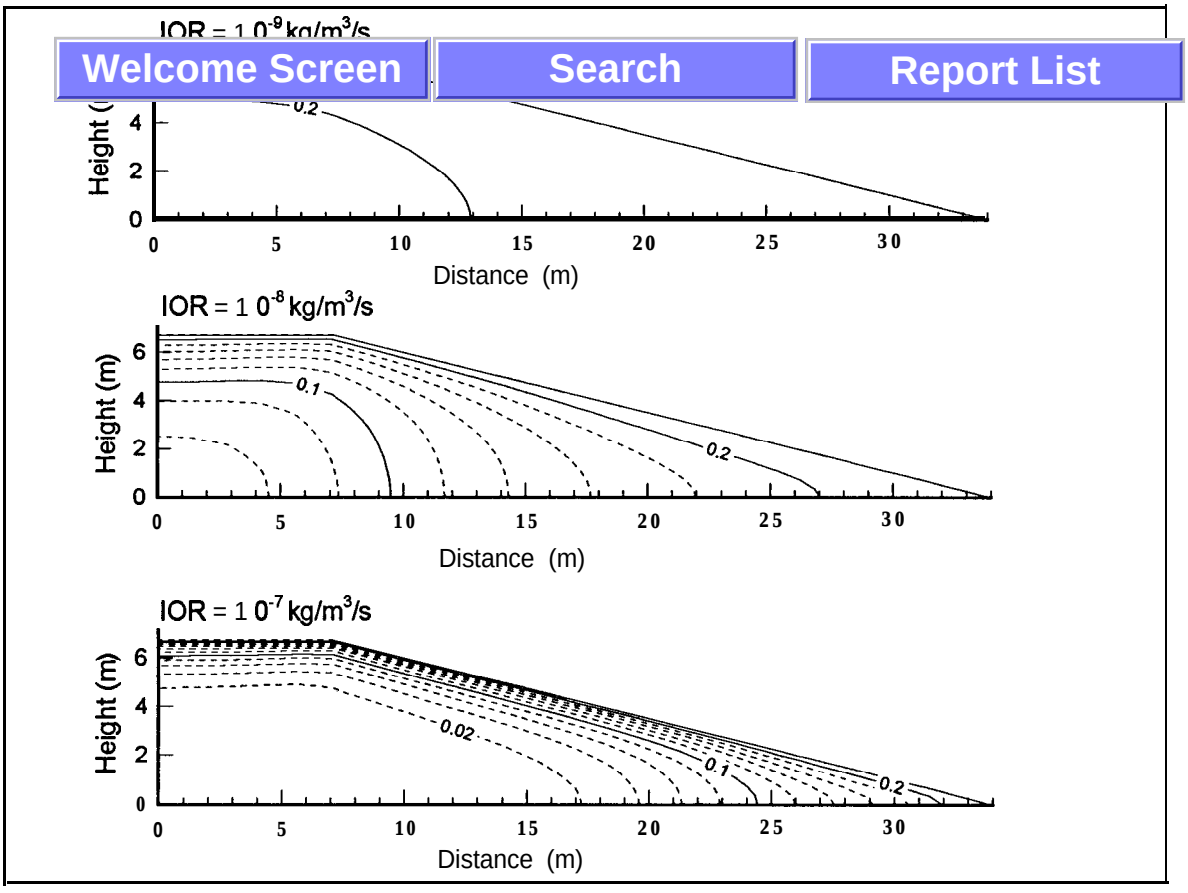

Figure IV - 30: **FIDHELM Results - Pile 18b: Gaseous oxygen mass fraction iso-values (Δ=0.02), K=2.9x10^{-9}m^2, Time = 1 year.**

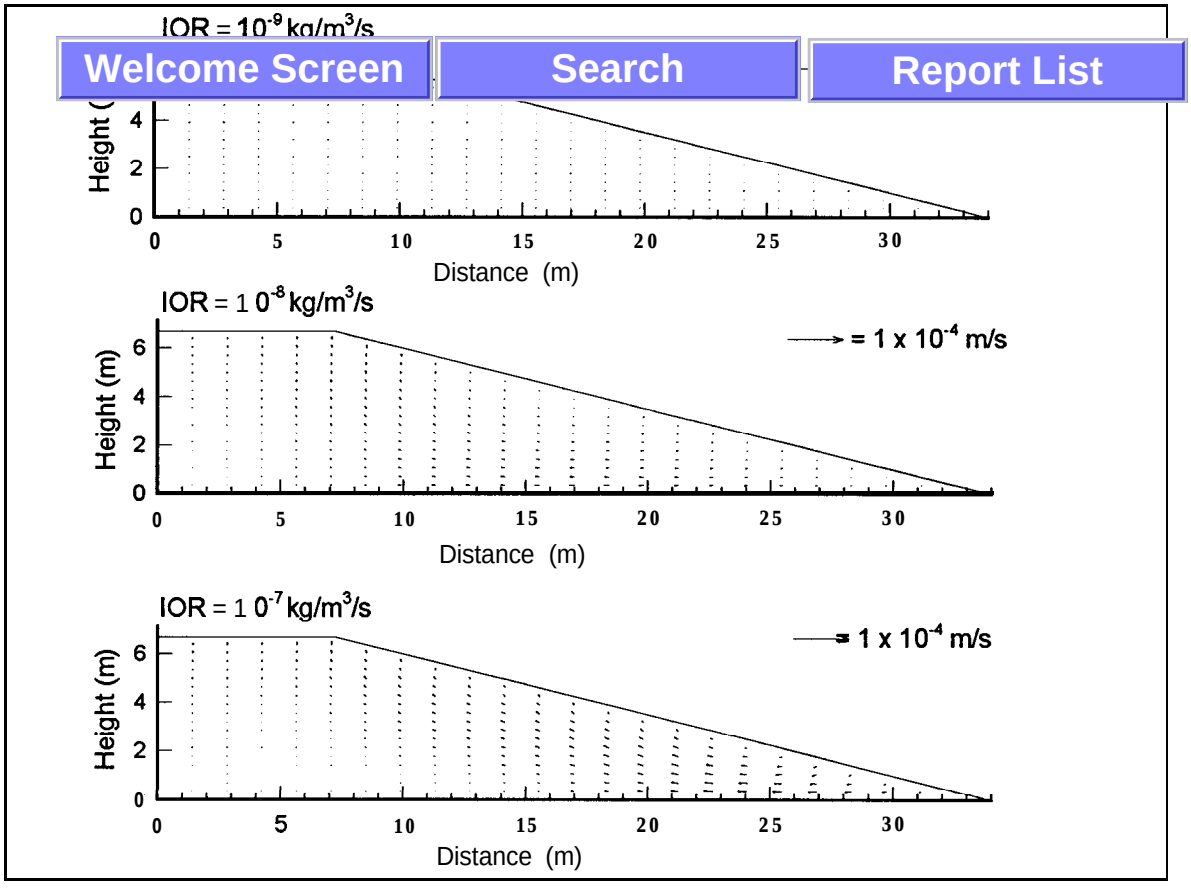

Figure IV - 31: **FIDHELM Results - Pile 18b: Air flow velocity, K=2.9x10^{-9} m^2, Time = 10 years.**

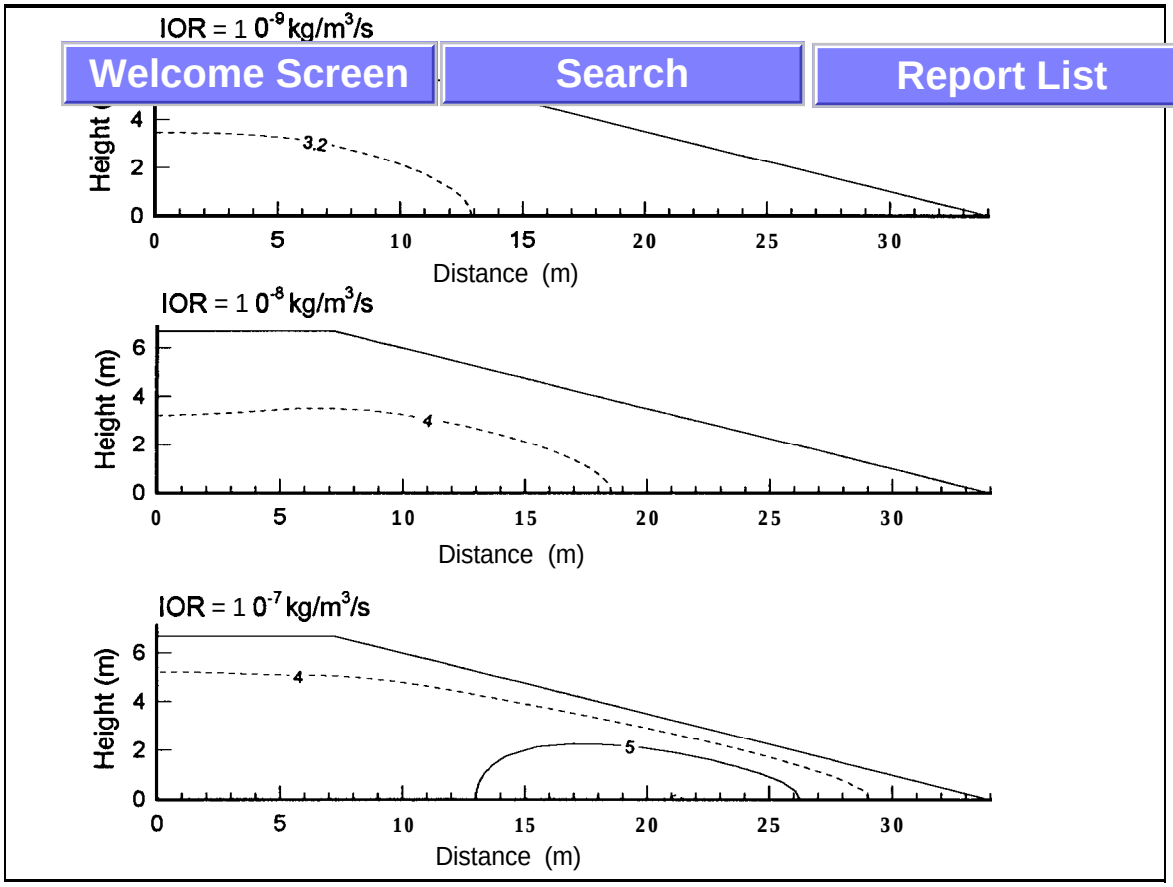

Figure IV - 32: **FIDHELM Results - Pile 18b: Temperature iso - values (A =1°C), K=2.9x10^{-9} m^2, Time = 10 years.**

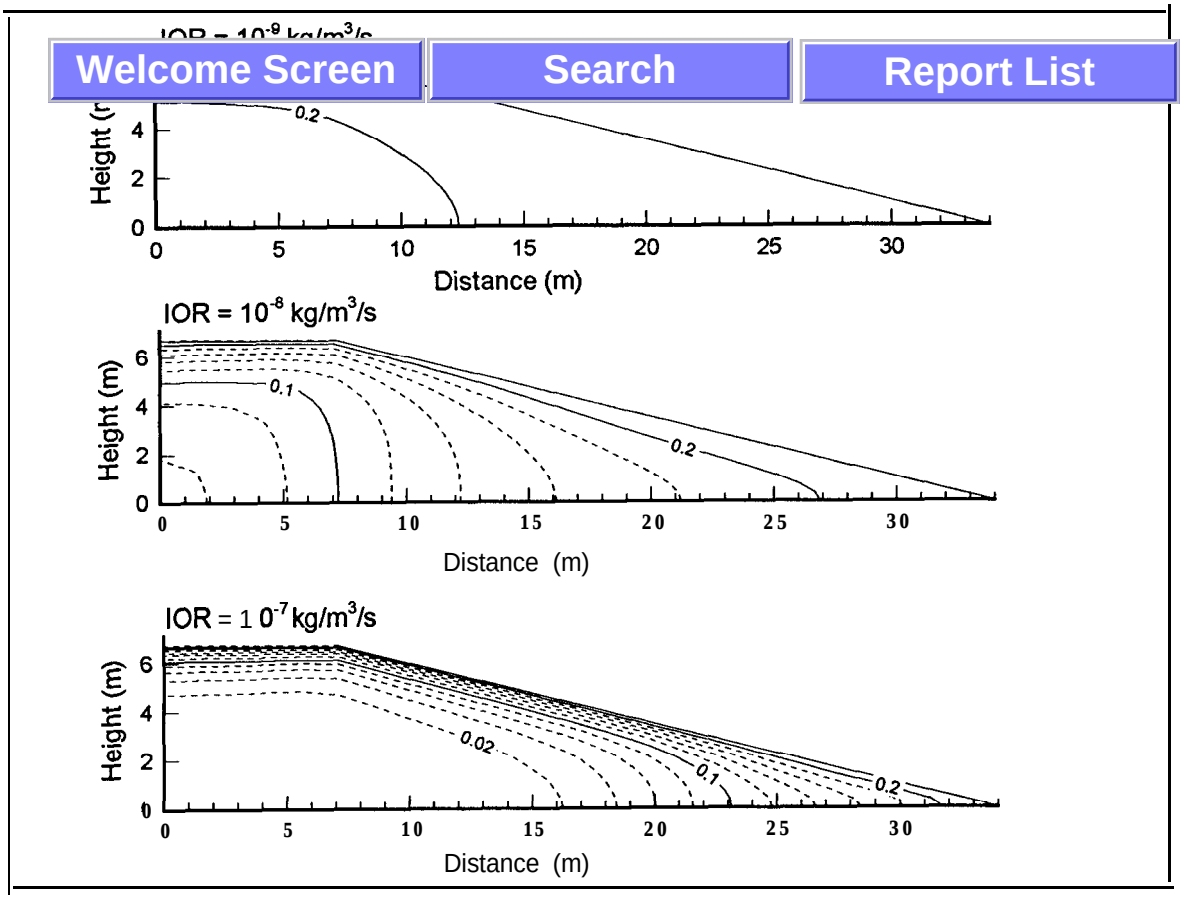

Figure IV - 33: **FIDHELM Results - Pile 18b: Gaseous oxygen mass fraction iso-values (Δ=0.02), K=2.9x10^{-9}m^2, Time = 10 years.**

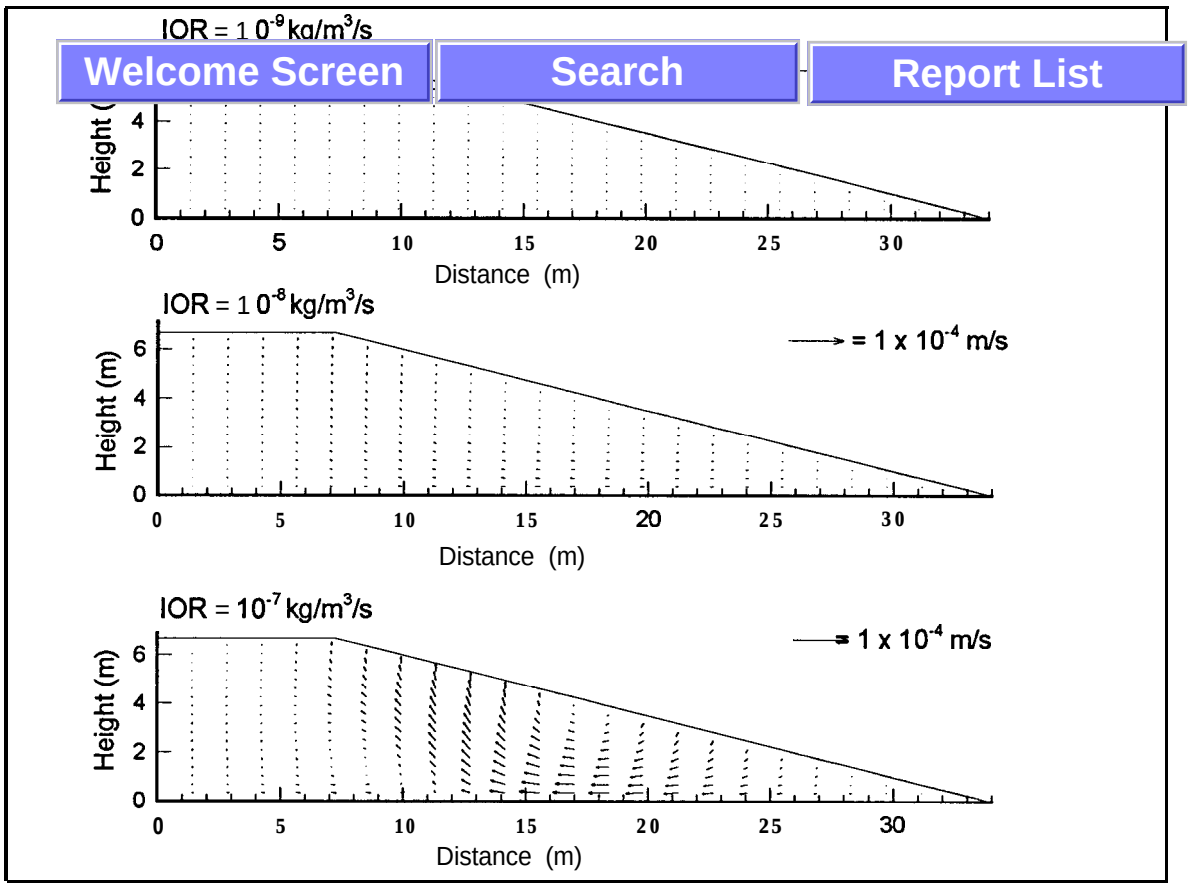

Figure IV - 34: **FIDHELM Results - Pile 18b: Air flow velocity, K=2.9x10^{-9} m^2, Time = 100 years.**

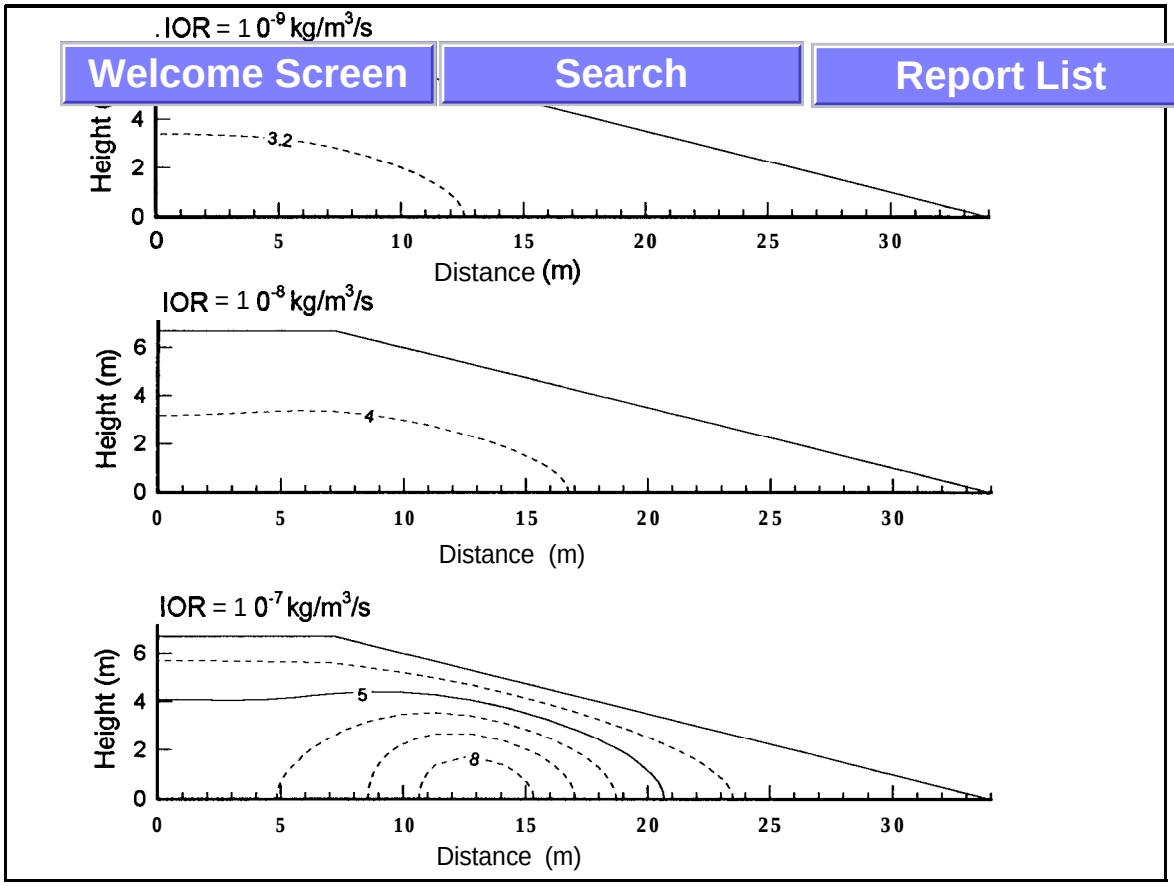

Figure IV - 35: **FIDHELM Results - Pile 18b: Temperature iso - values (A =1°C), K=2.9x10^{-9} m^2, Time = 100 years.**

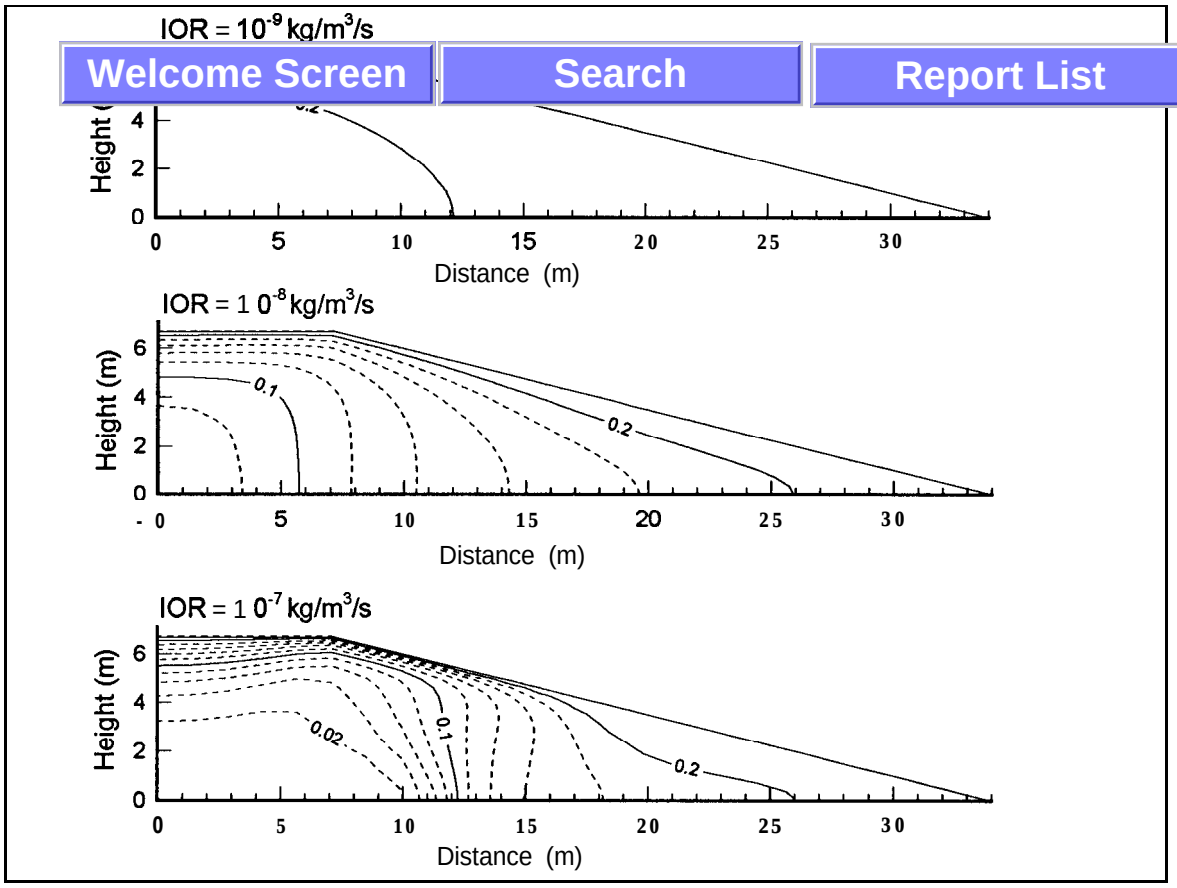

Figure IV - 36: **FIDHELM Results - Pile 18b: Gaseous oxygen mass fraction iso-values (Δ=0.02), K=2.9x10^{-9}m^2, Time = 100 years.**

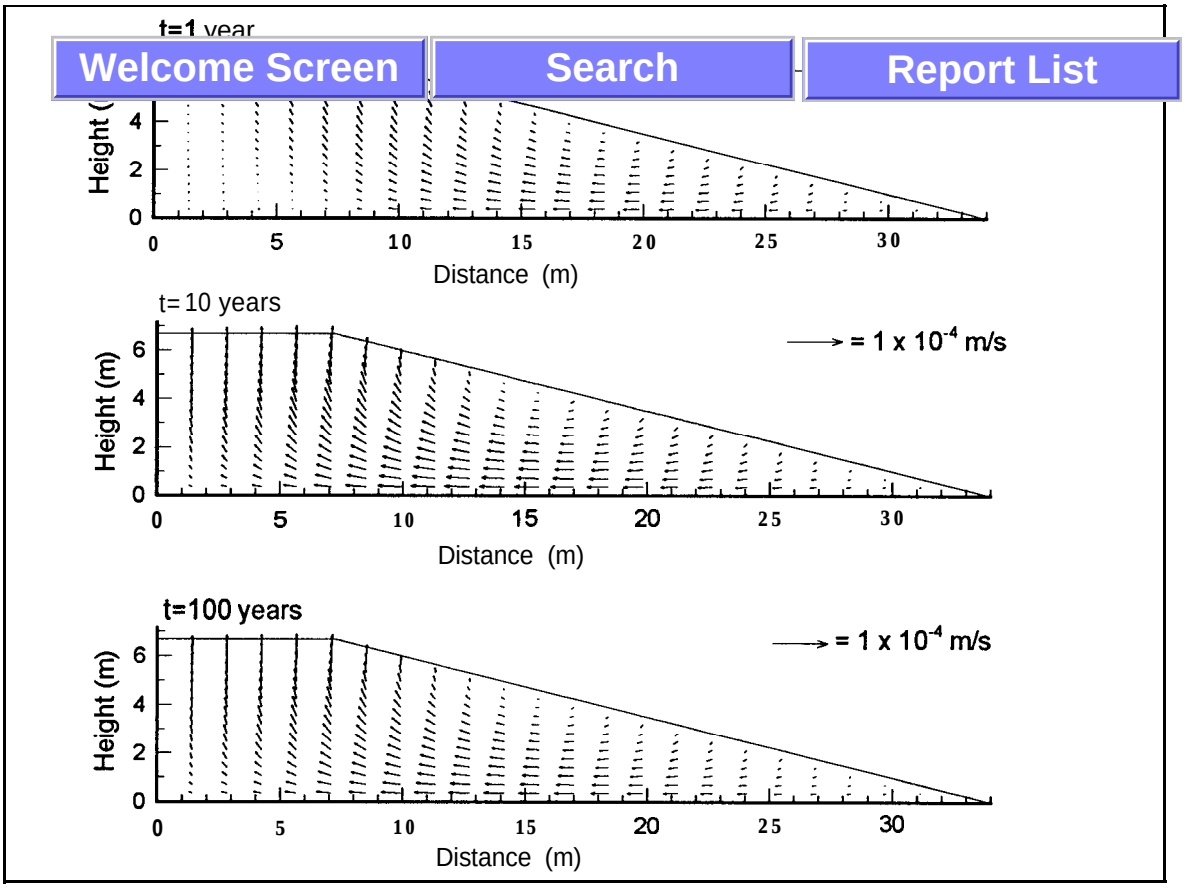

Figure IV - 37: **FIDHELM Results - Pile 18b: Air flow velocity, $K=1.0x10^{-8}\ m^2$, $IOR=10^{-8}\ kg[O_2]/m^3/s$.**

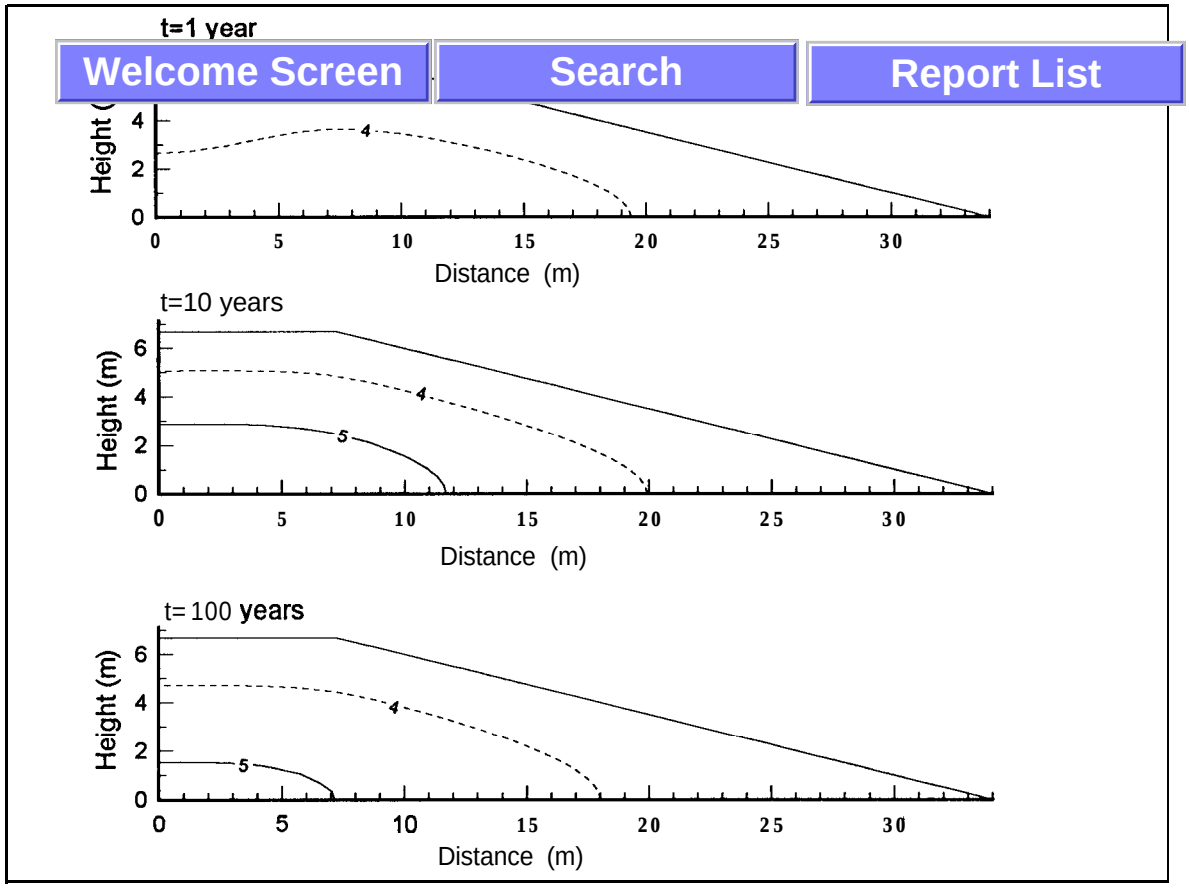

Figure IV - 38: **FIDHELM Results - Pile 18b: Temperature iso - values (A =1°C), K=1.0x10^{-8} m^2, IOR =10^{-8} kg[O_2]/m^3/s.**

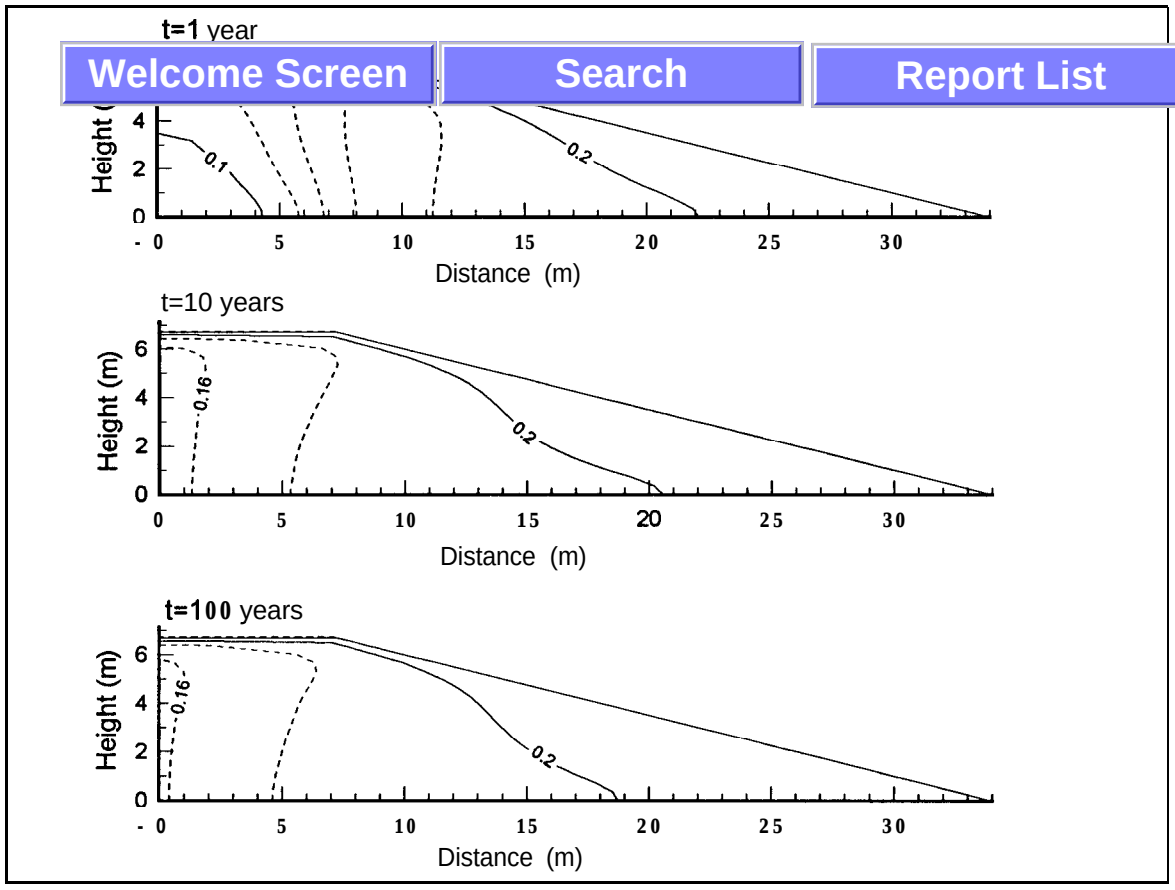

Figure IV - 39: **FIDHELM Results - Pile 18b: Gaseous oxygen mass fraction iso-values (Δ=0.02), K=1.0x10^{-8} m^2, IOR =10^{-8} kg[O_2]/m^3/s.**

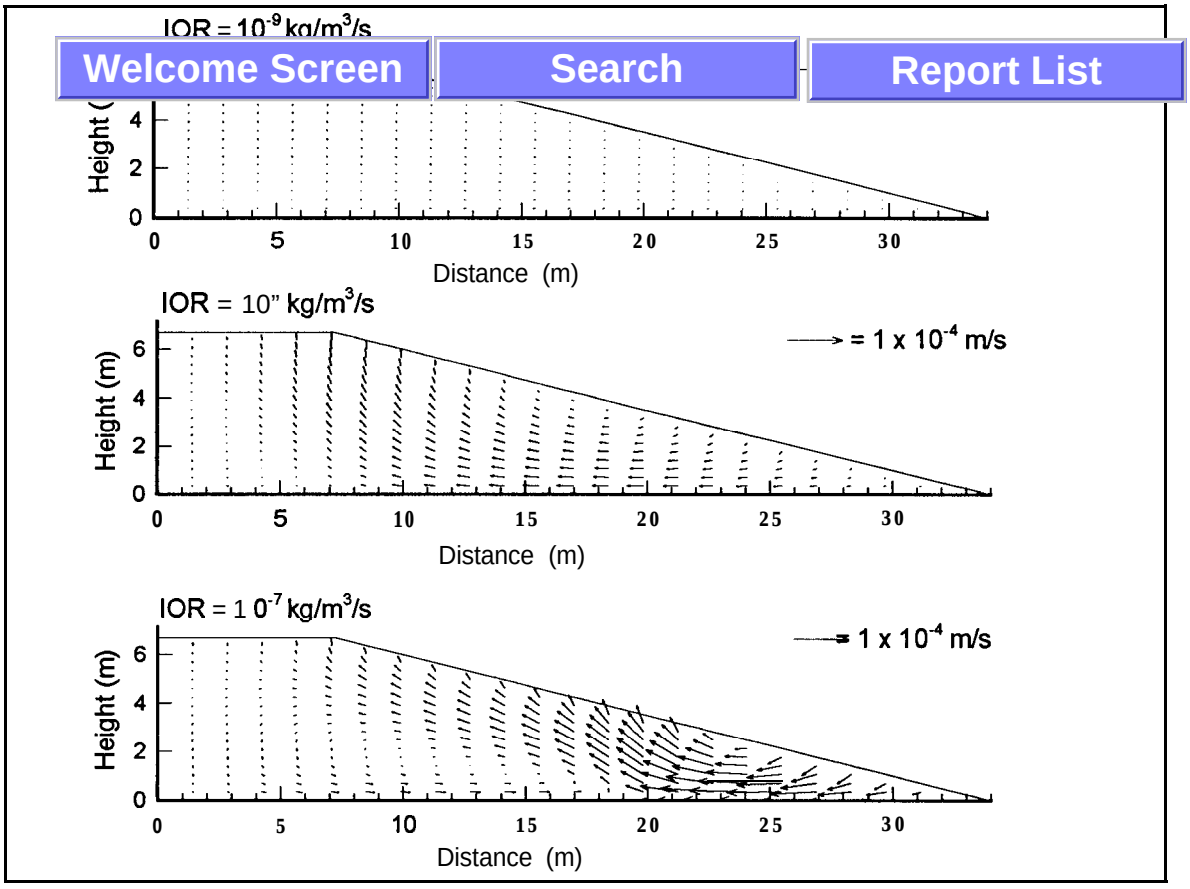

Figure IV - 40: **FIDHELM Results - Pile 18b: Air flow velocity, K=1.0x10^{-8} m^2, Time = 1 year.**

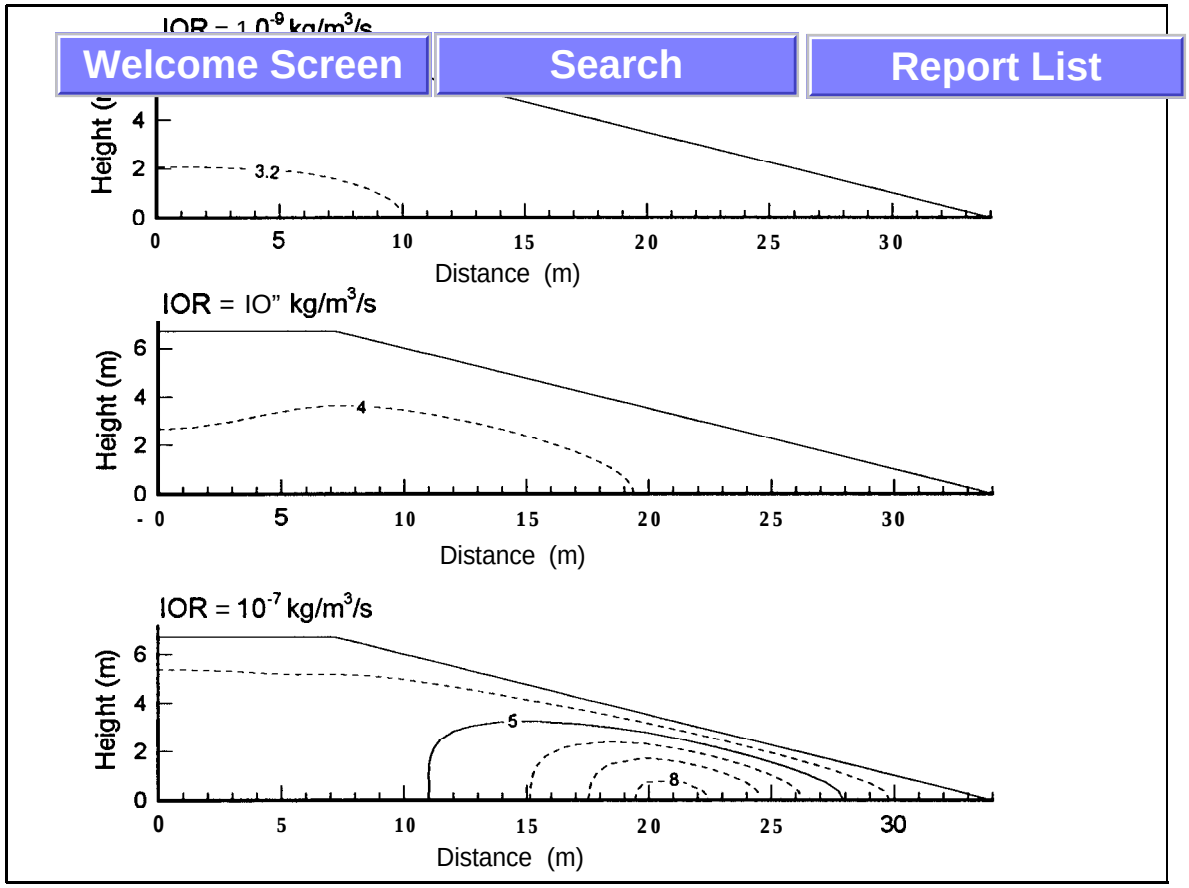

Figure IV - 41: **FIDHELM Results - Pile 18b: Temperature iso - values (A =1°C), K=1.0x10^{-8} m^2, Time = 1 year.**

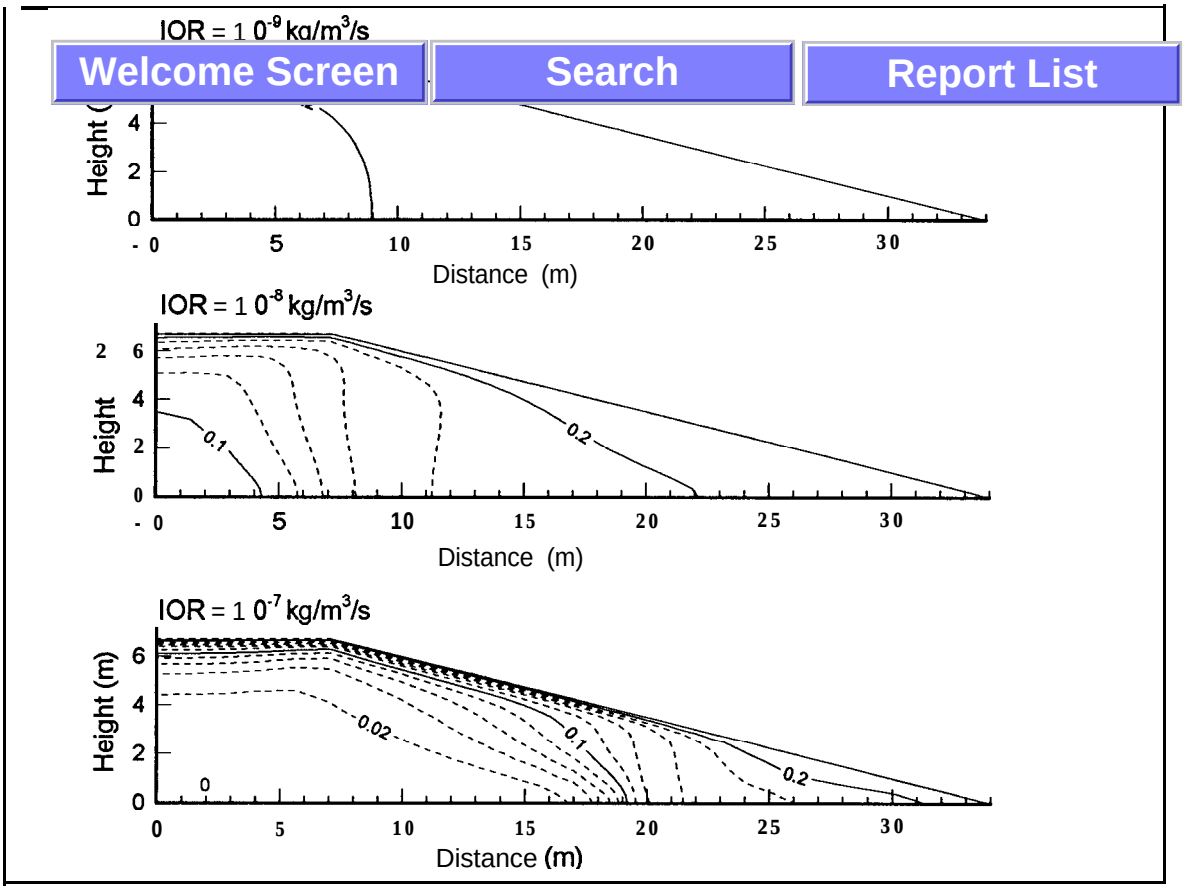

Figure IV - 42: **FIDHELM Results - Pile 18b: Gaseous oxygen mass fraction iso-values (Δ=0.02), K=1.0x10^{-8}m^2, Time = 1 year.**

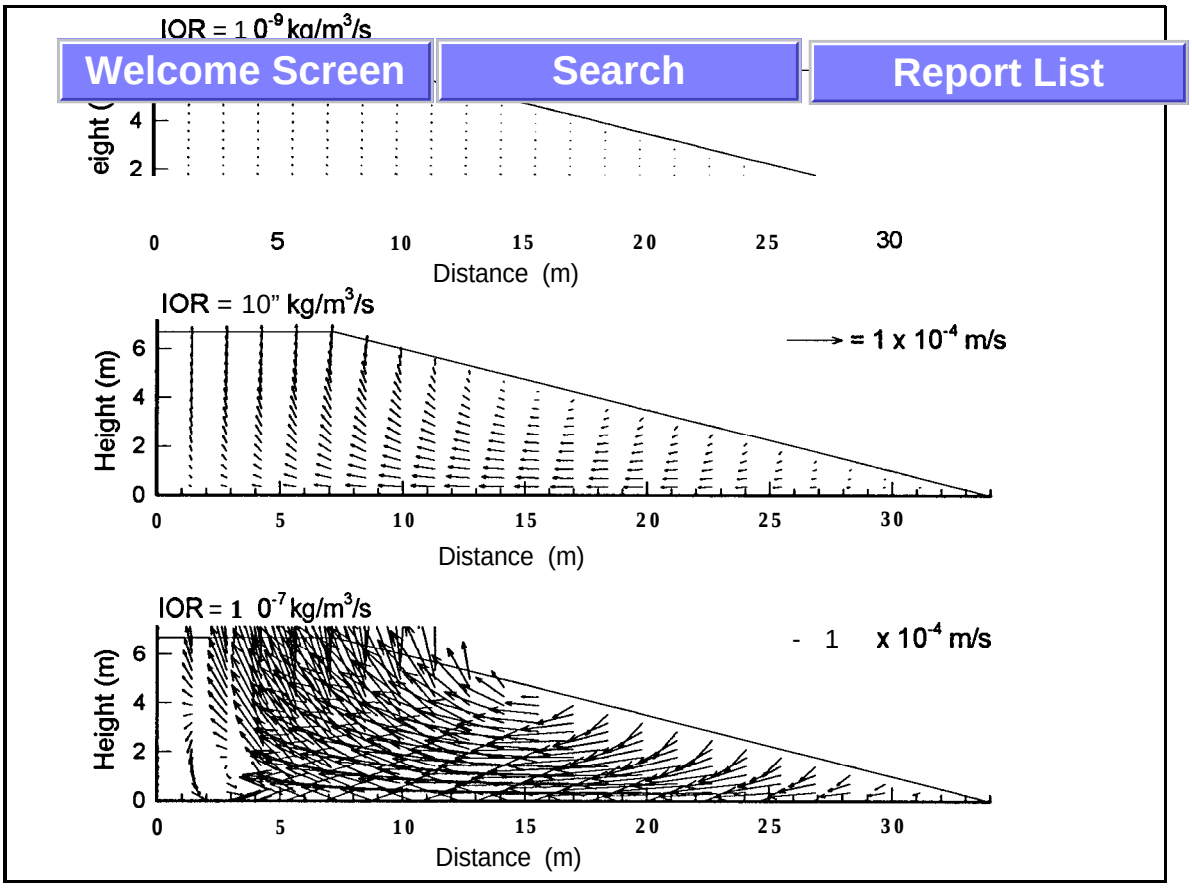

Figure IV - 43: **FIDHELM Results - Pile 18b: Air flow velocity, K=1.0x10^{-8} m^2, Time = 10 years.**

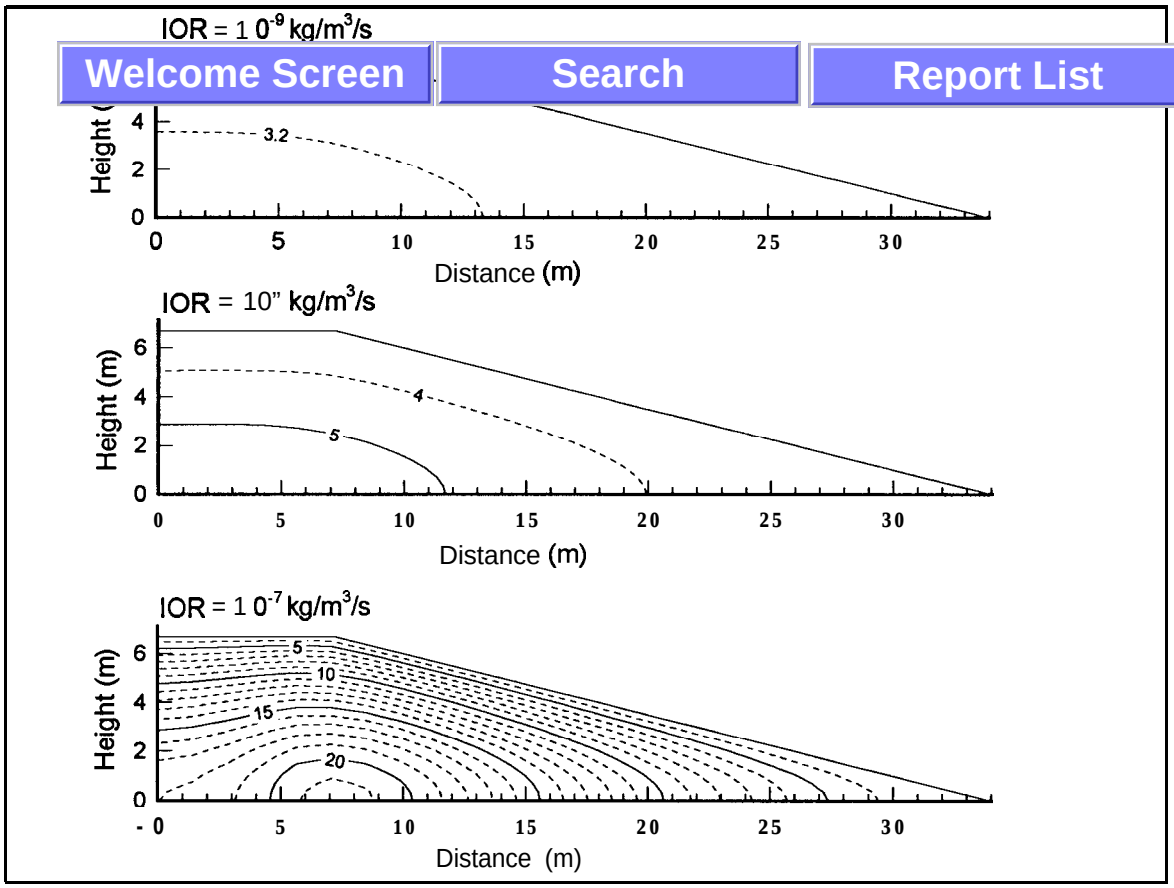

Figure IV - 44: **FIDHELM Results - Pile 18b: Temperature iso - values (A =1°C), K=1.0x10^{-8} m^2, Time = 10 years.**

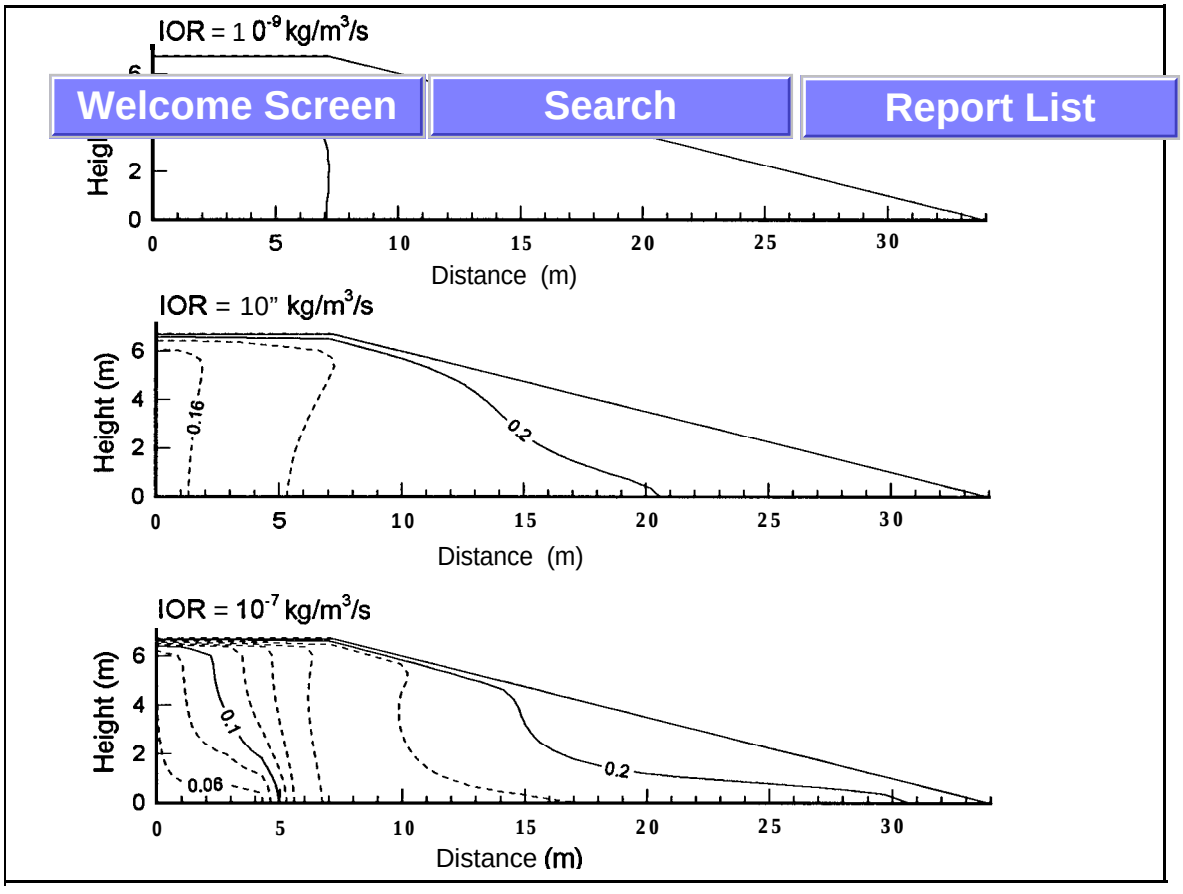

Figure IV - 45: **FIDHELM Results - Pile 18b: Gaseous oxygen mass fraction iso-values (Δ=0.02), K=1.0x10^{-8}m^2, Time = 10 years.**

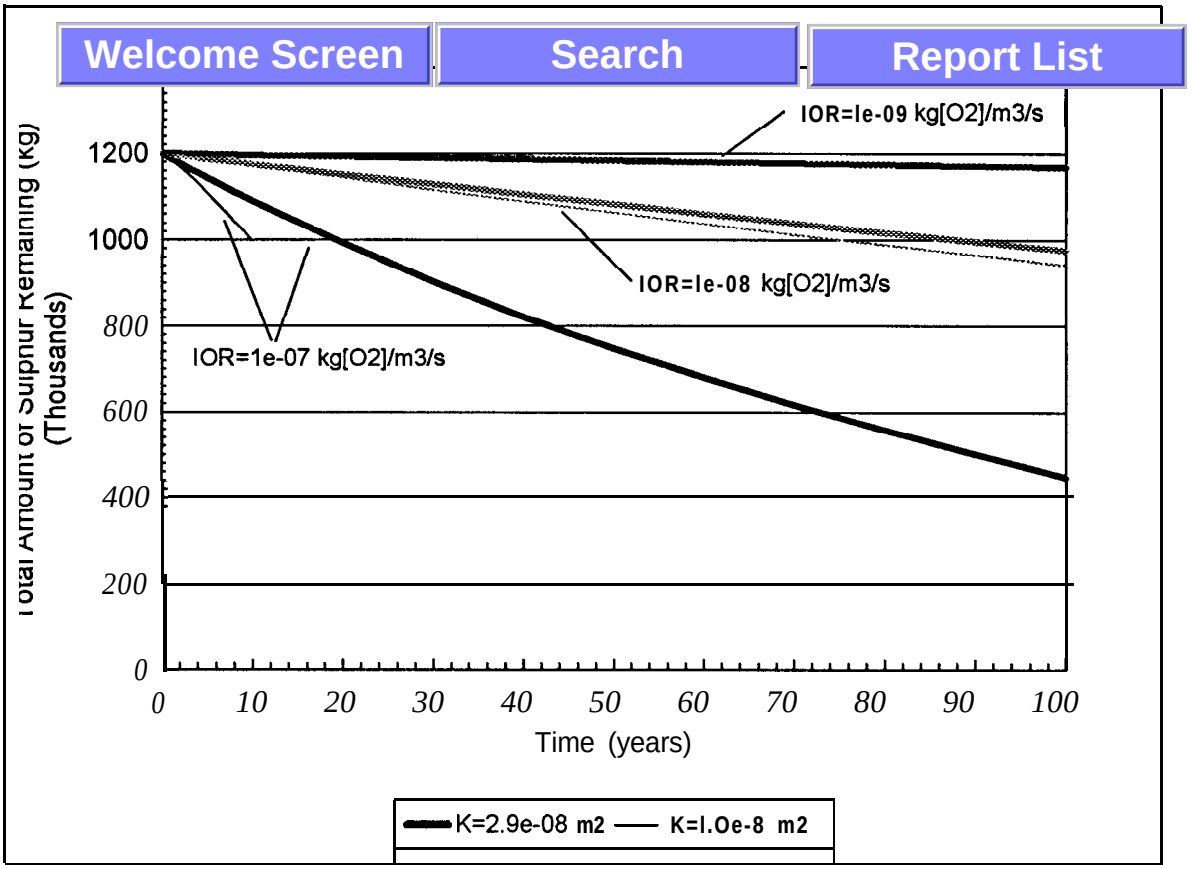

Figure IV - 46: **FIDHELM Results - Pile 18B: Total amount of sulphur remaining from solid phase versus time.**

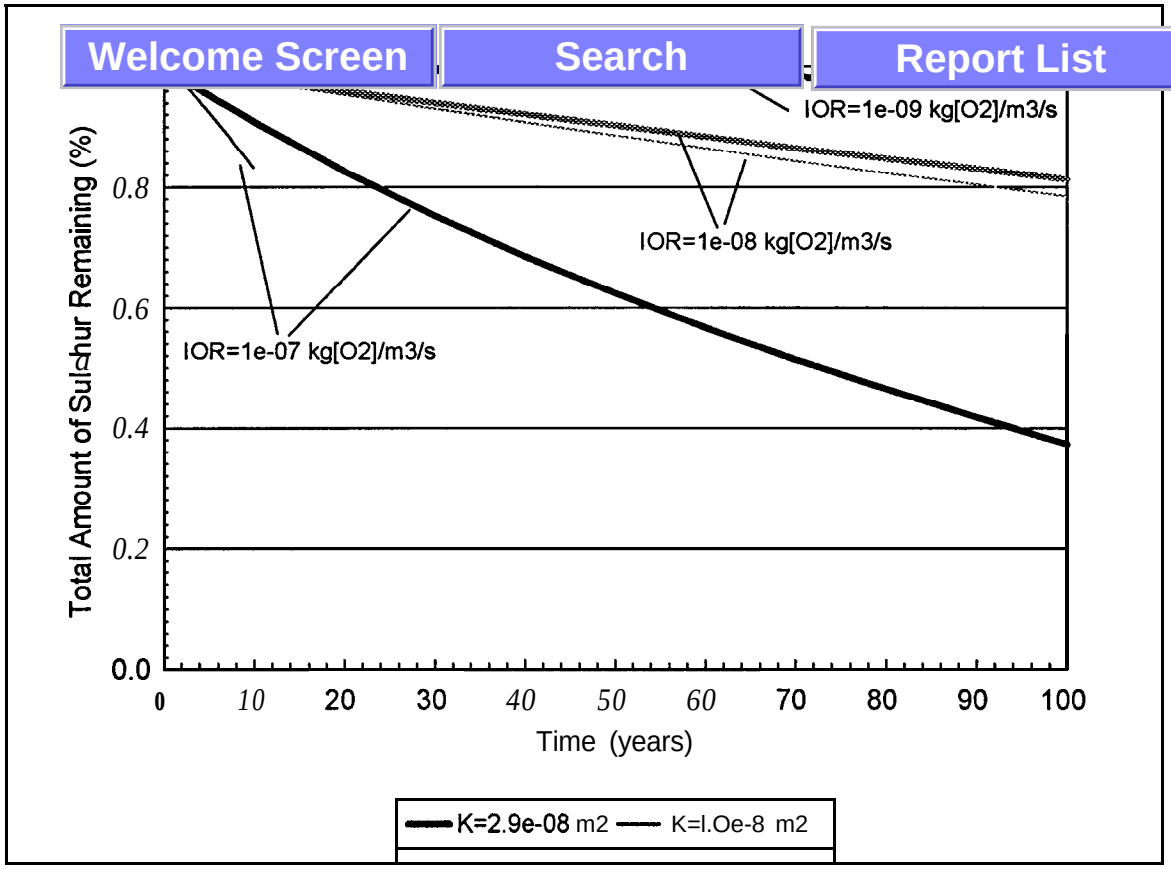

Figure IV - 47: **FIDHELM Results - Pile 18B: Normalized total amount of sulphur remaining from solid phase versus time.**

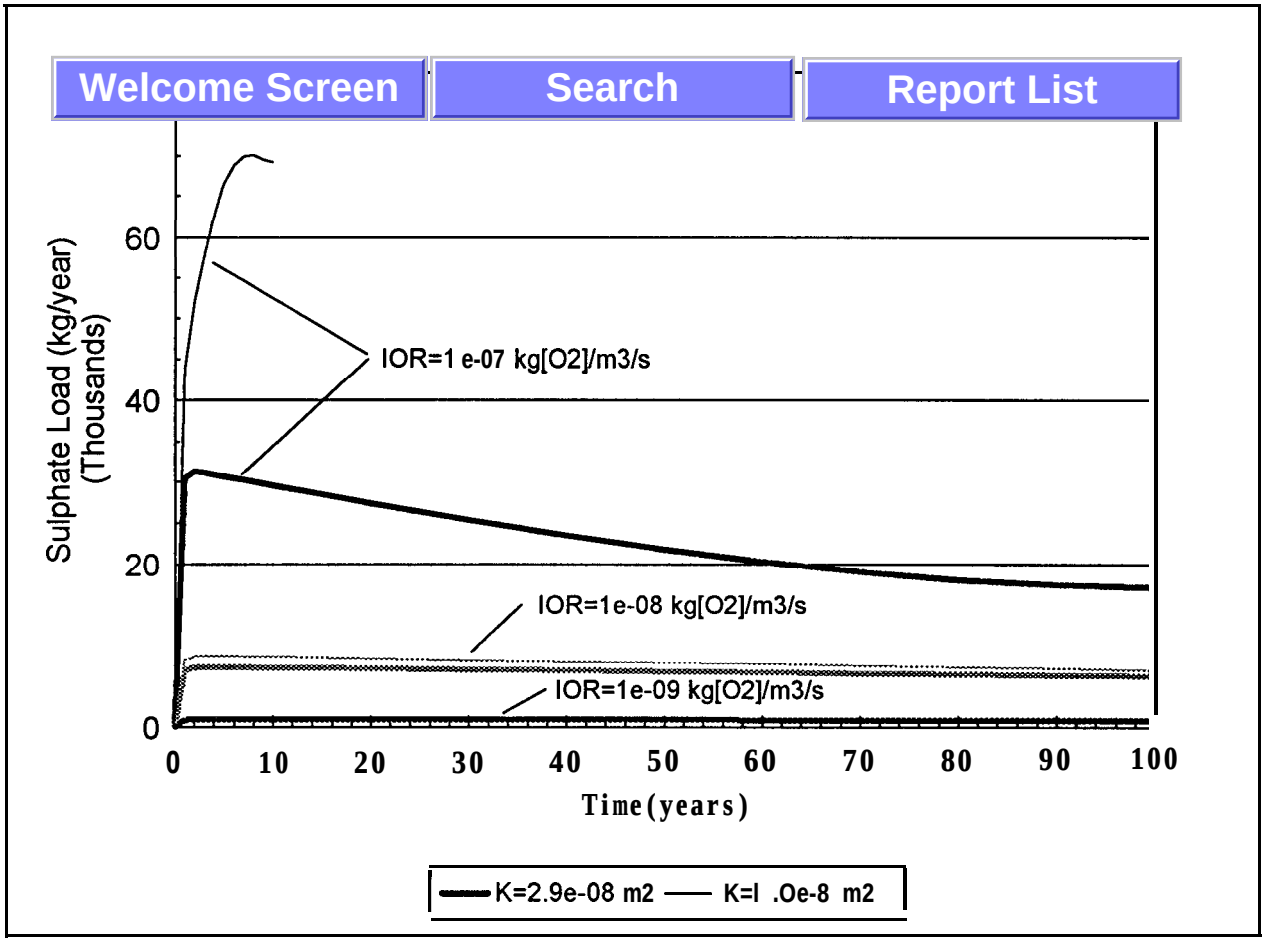

Figure IV - 48: **FIDHELM Results - Pile 18B: Sulphate load from aqueous phase versus time.**

FIDHELM RESULTS

PILE 17

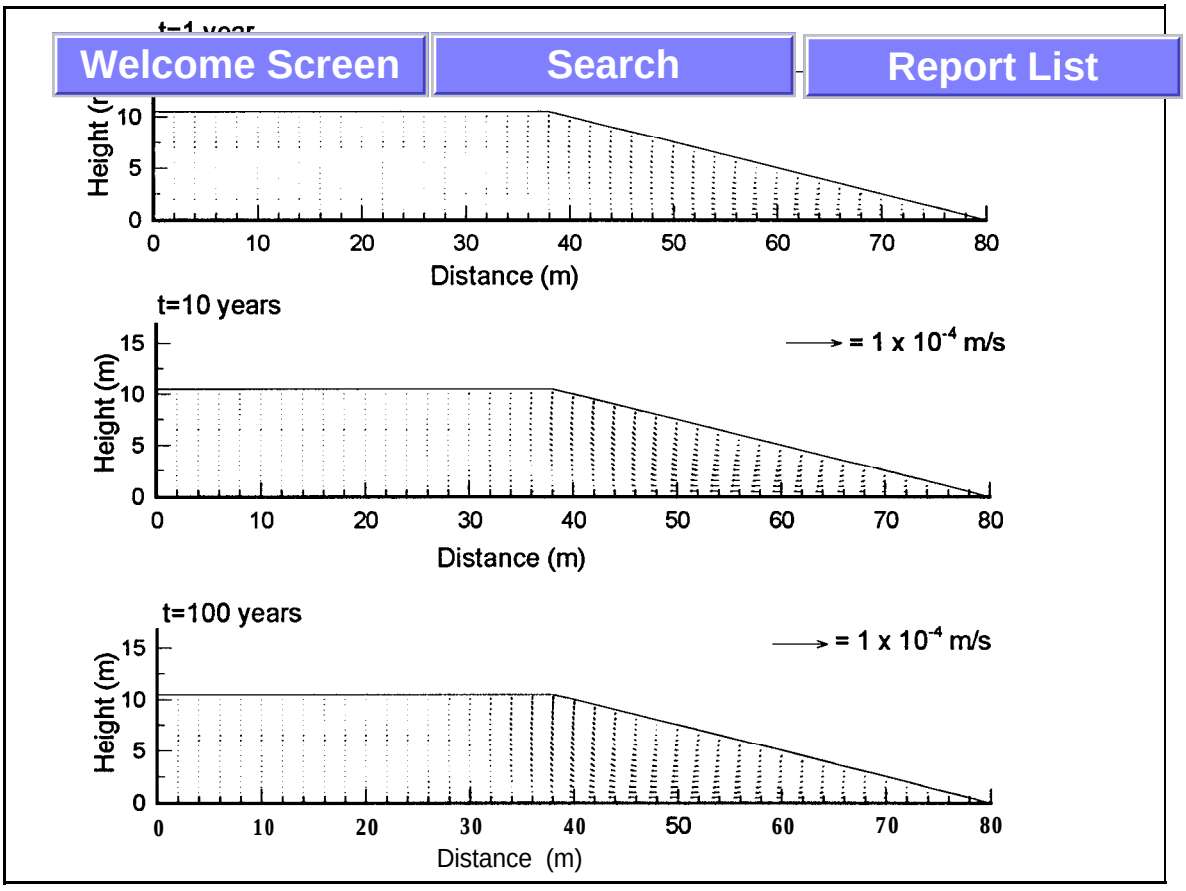

Figure IV - 49: **FIDHELM Results - Pile 17: Air flow velocity, K=2.9x10^{-9} m^2, IOR=10^{-8} kg[O_2]/m^3/s.**

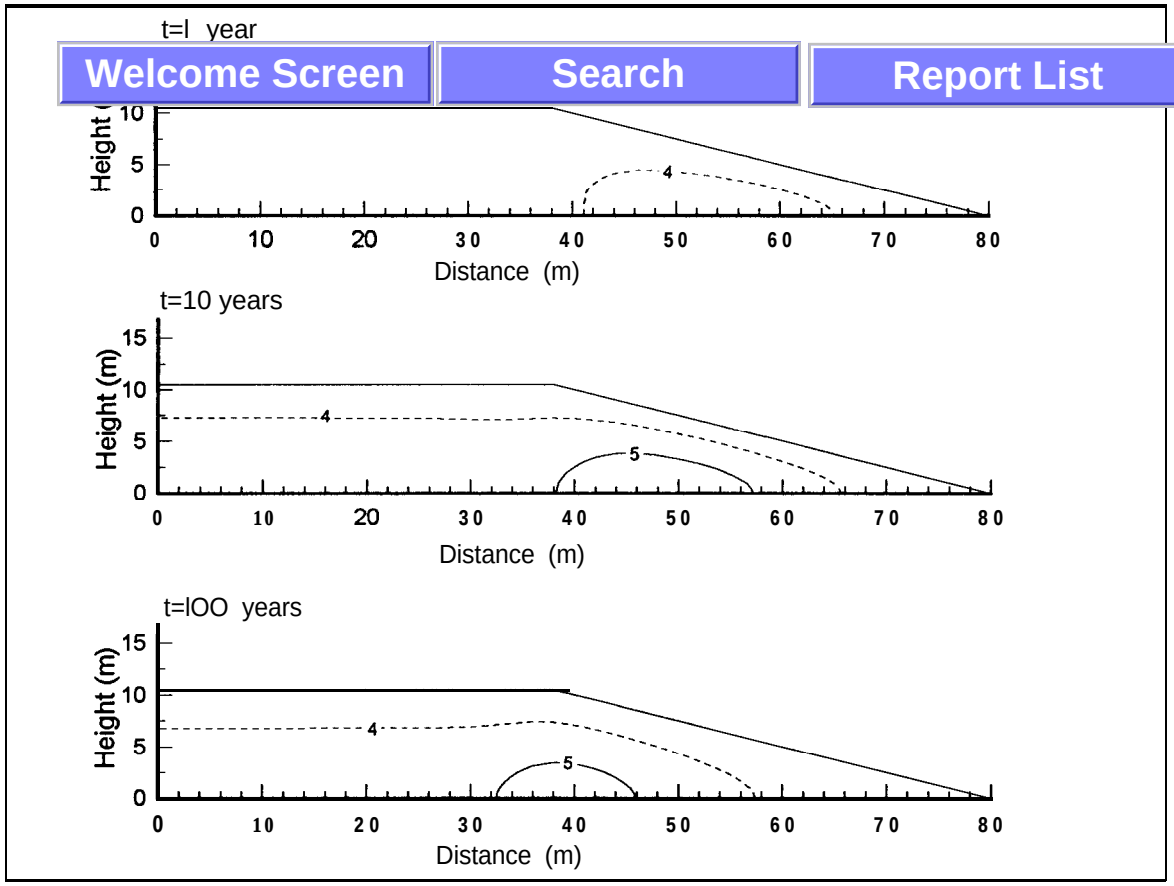

Figure IV - 50: **FIDHELM Results - Pile 17: Temperature iso - values (A =1°C), $K=2.9x10^{-9}\ m^2$, $IOR=10^{-8}\ kg[O_2]/m^3/s$.**

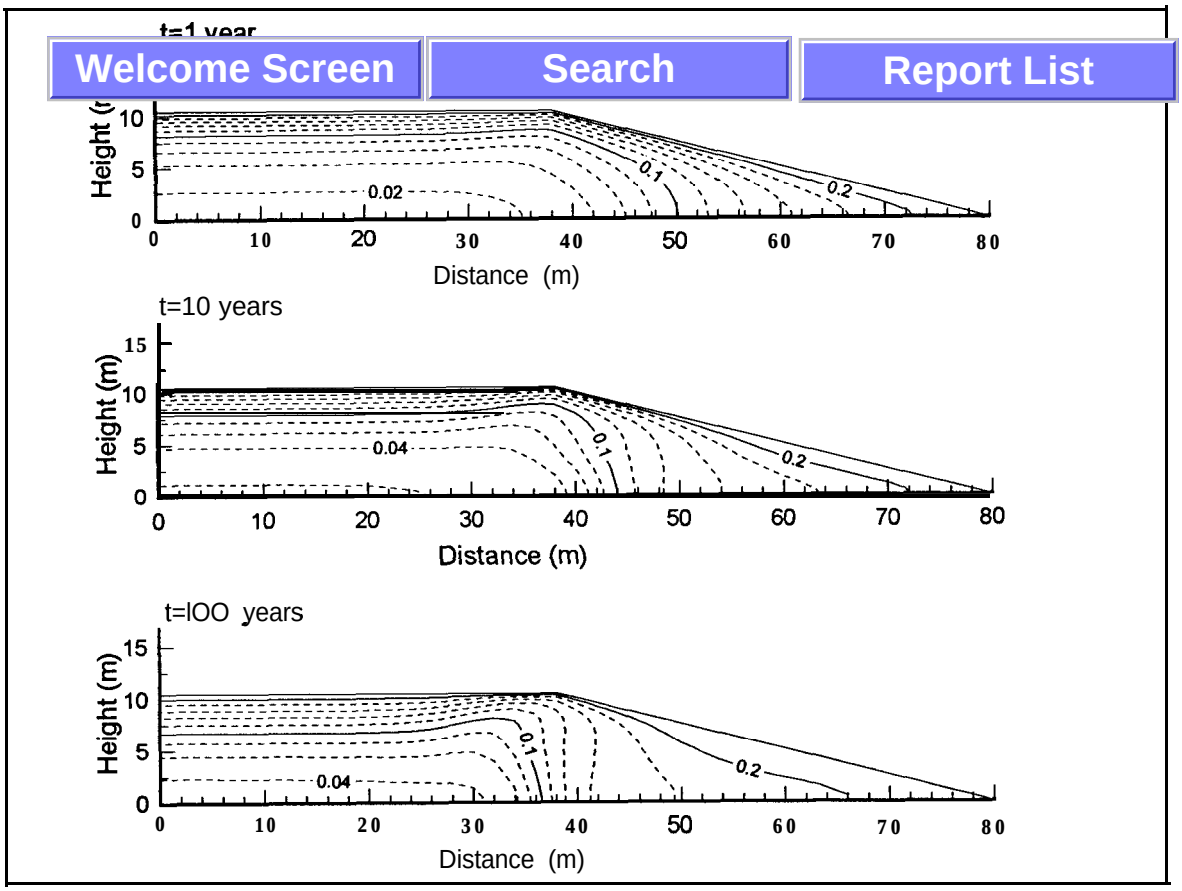

Figure IV - 51: **FIDHELM Results - Pile 17: Gaseous oxygen mass fraction iso-values (Δ=0.02), K=2.9x10^{-9} m^2, IOR =10^{-8} kg[O_2]/m^3/s.**

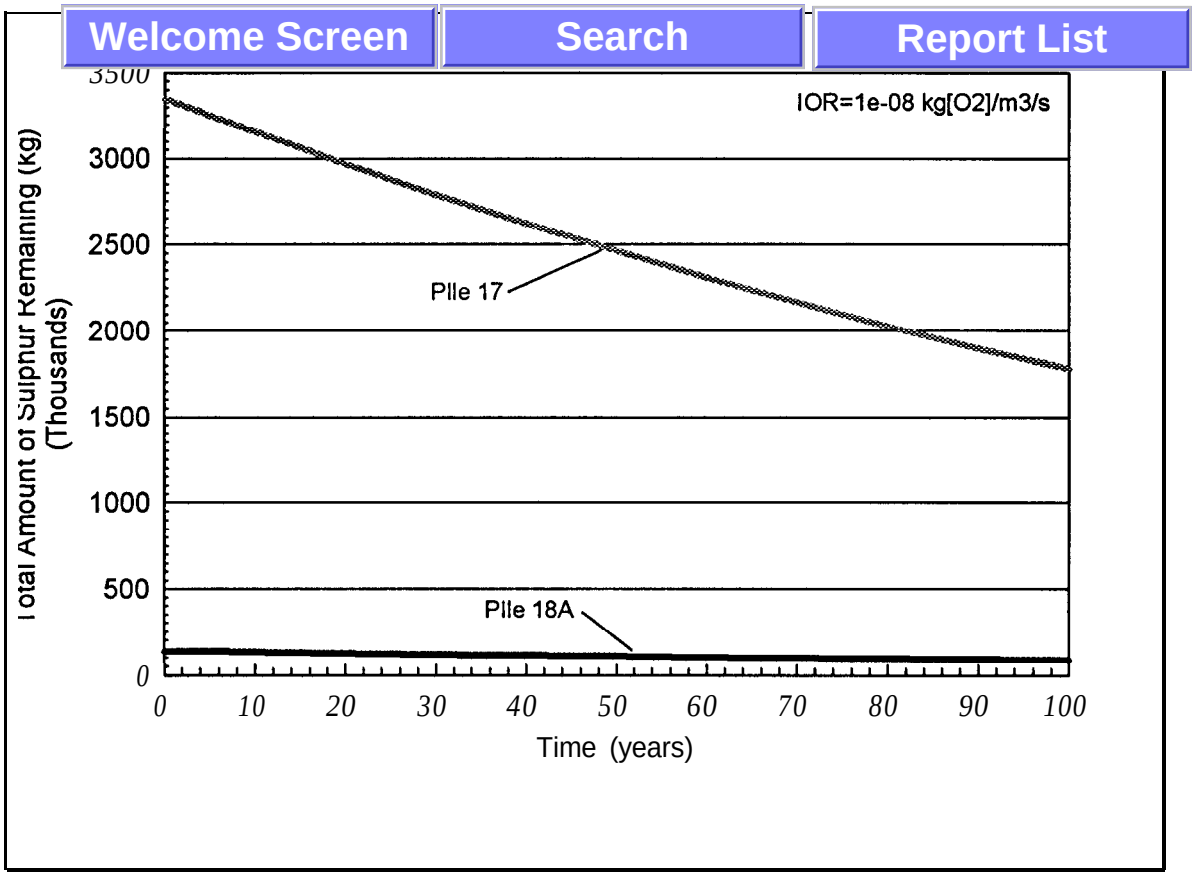

Figure IV - 52: **FIDHELM Results - Pile 18A and Pile 17: Total amount of sulphur remaining from solid phase versus time.**

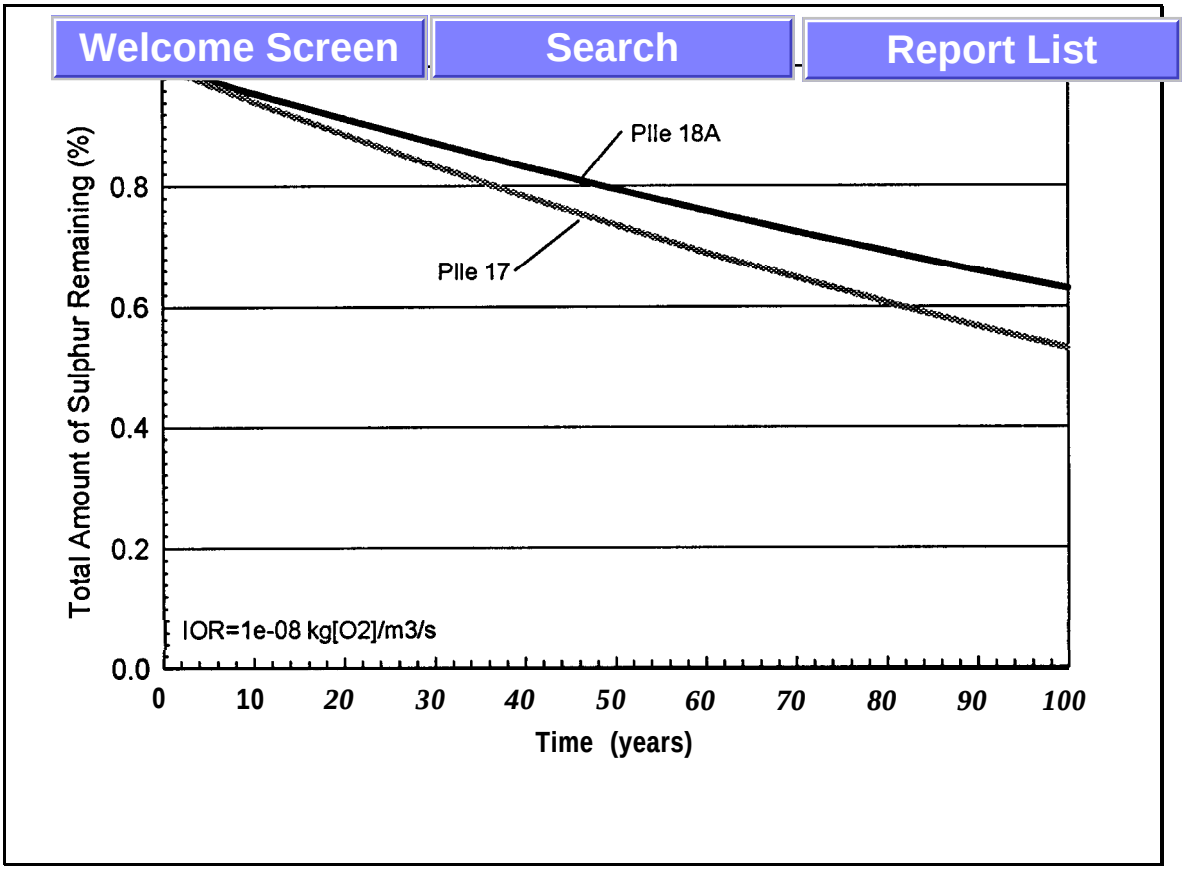

Figure IV - 53: **FIDHELM Results - Pile 18B and Pile 17: Normalized total amount of sulphur remaining from solid phase versus time.**

FIDHELM RESULTS

PILE 18A

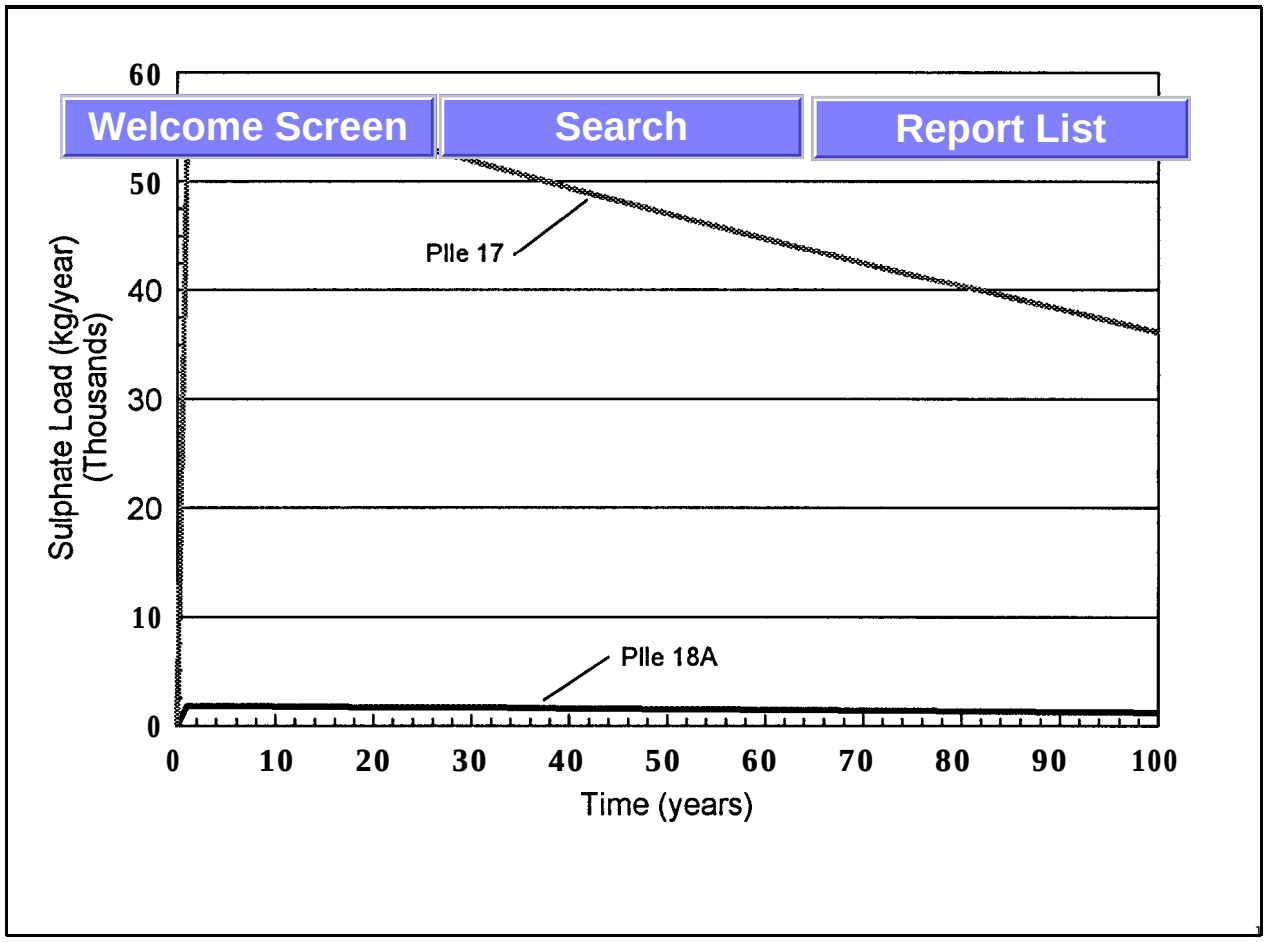

Figure IV - 54: **FIDHELM Results - Pile 18A and Pile 17: Sulphate load from aqueous phase versus time.**

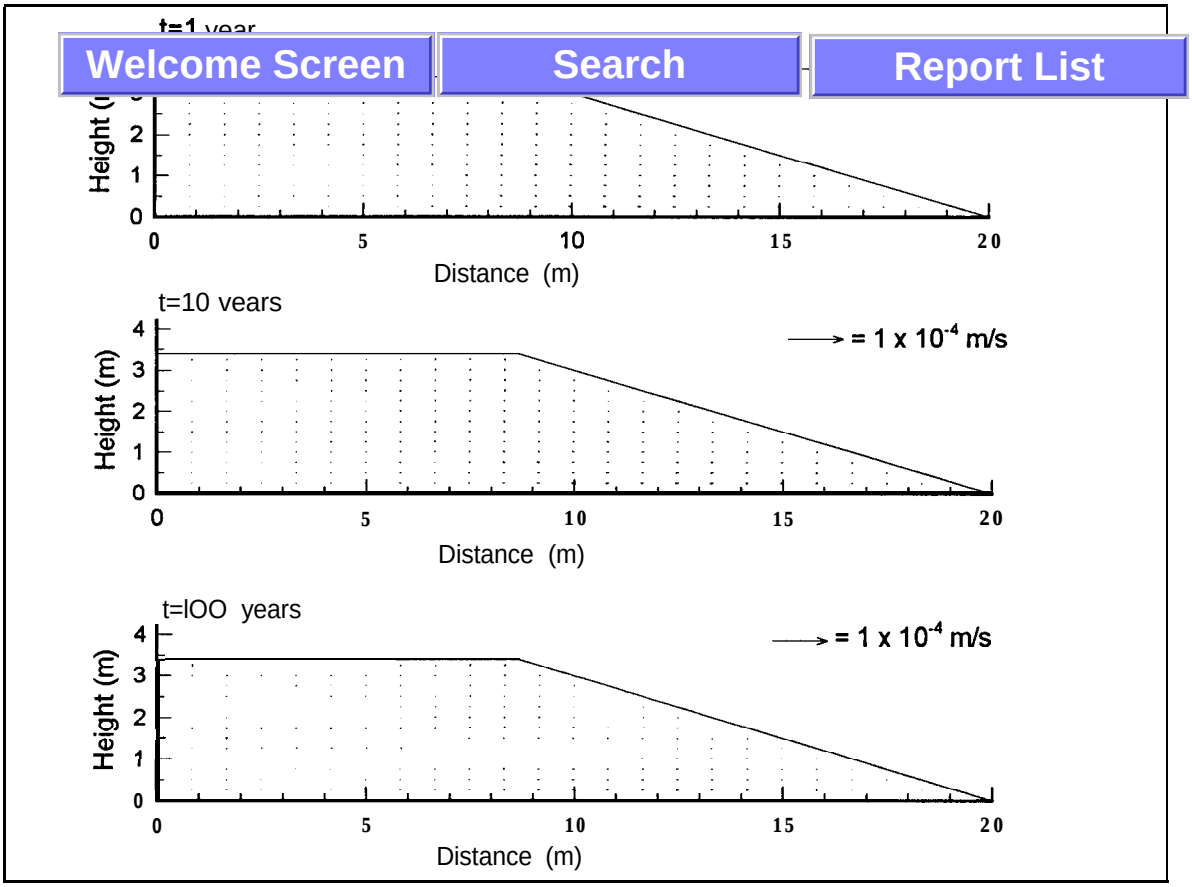

Figure IV - 55: **FIDHELM Results - Pile 18a: Air flow velocity, $K=2.9x10^{-9}$ m^2, $IOR=10^{-8}$ $kg[O_2]/m^3/s$.**

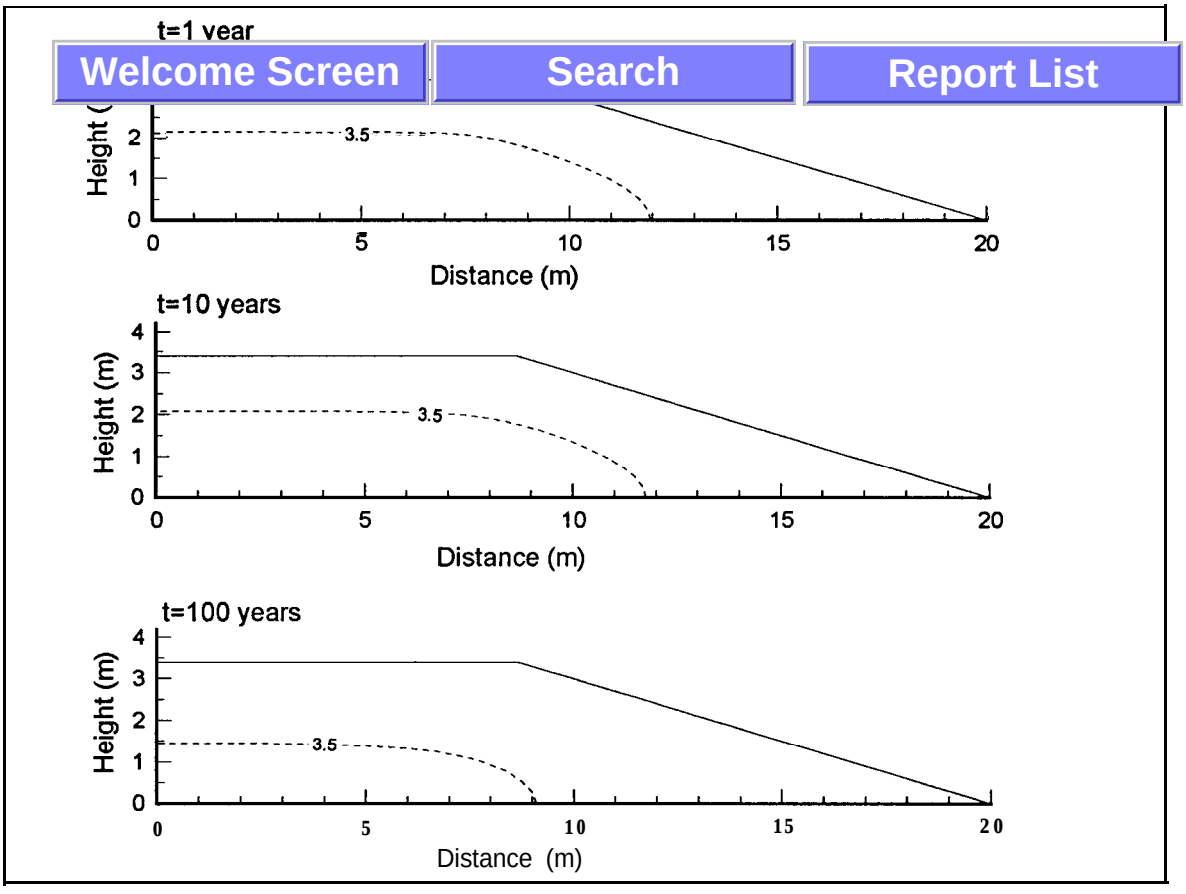

Figure IV - 56: **FIDHELM Results - Pile 18a: Temperature iso - values (Δ=1°C), K=2.9x10^{-9} m^2, IOR =10^{-8} kg[O_2]/m^3/s.**

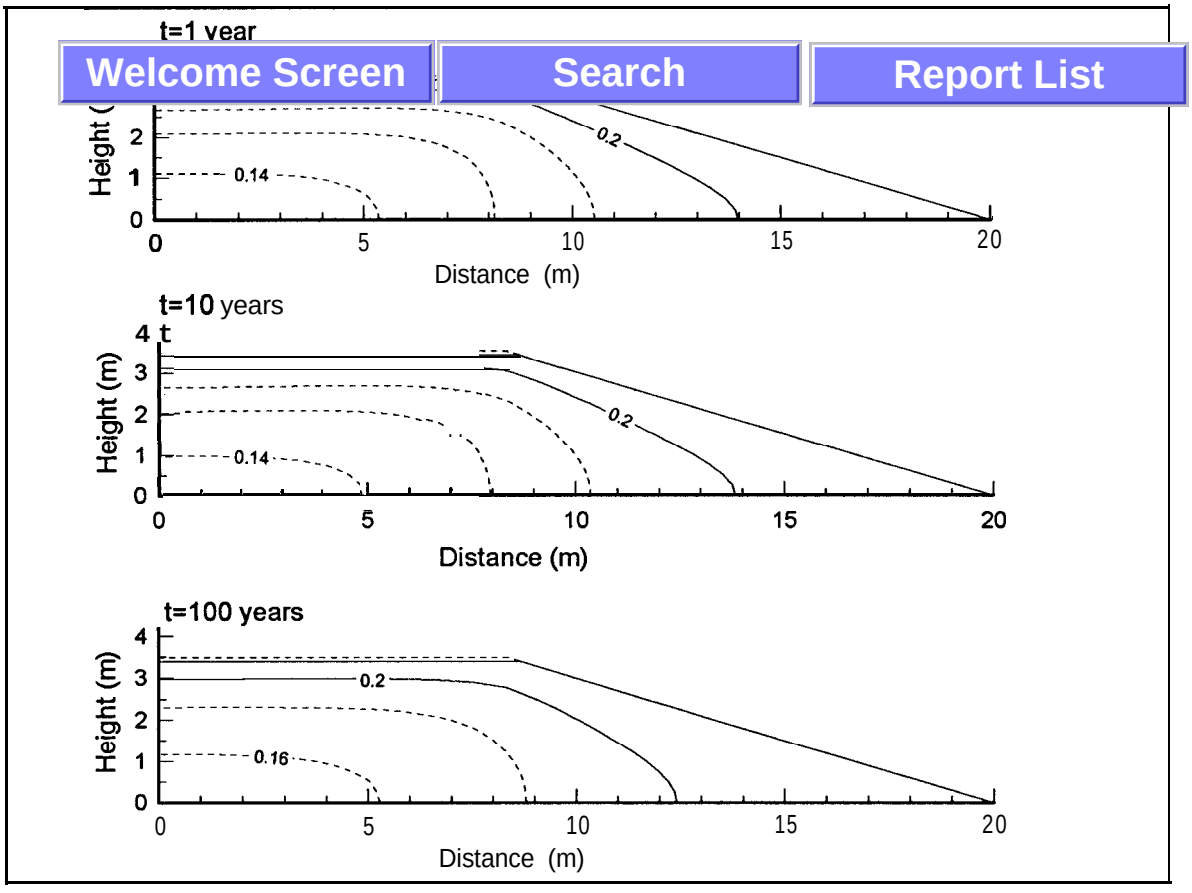

Figure IV - 57: **FIDHELM Results - Pile 18a: Gaseous oxygen mass fraction iso-values (Δ=0.02), K=2.9x10^{-9} m^2, IOR =10^{-8} kg[O_2]/m^3/s.**

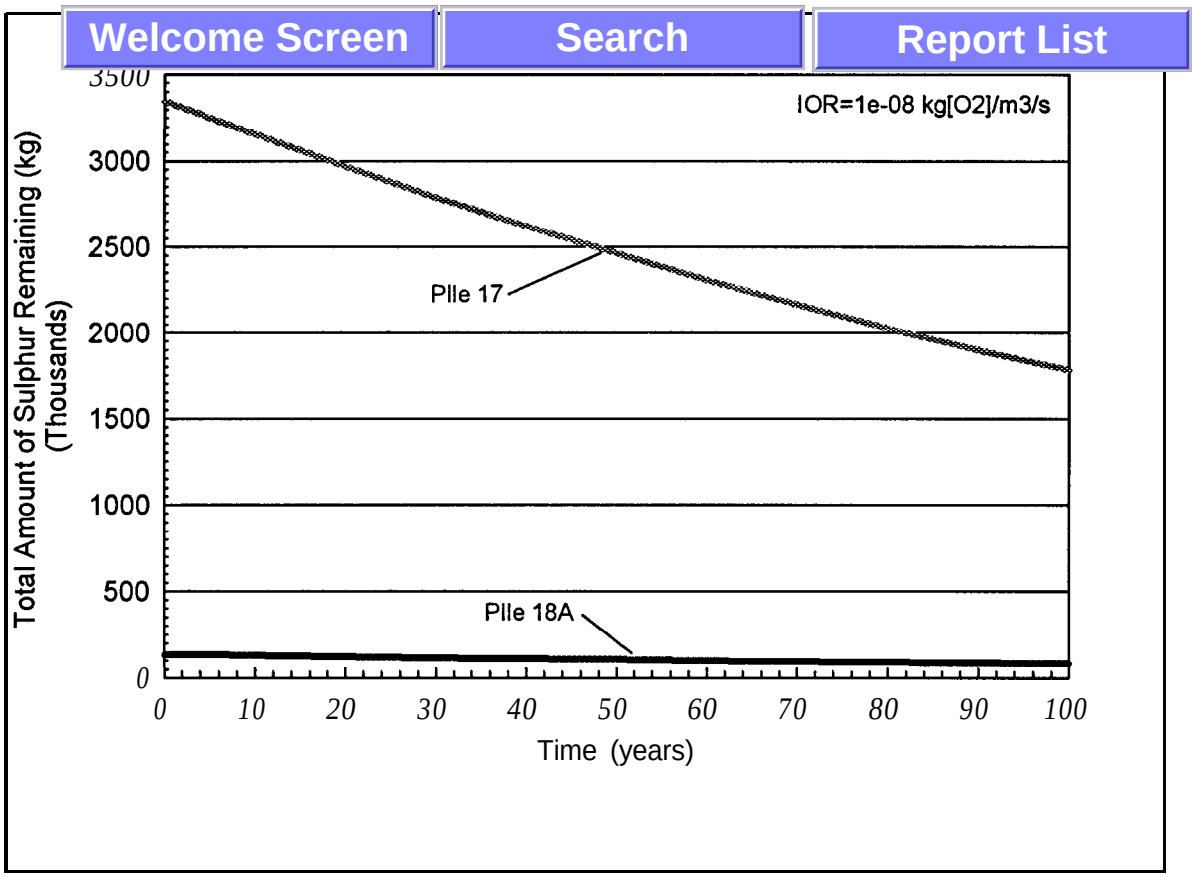

Figure IV - 58: **FIDHELM Results - Pile 18A and Pile 17: Total amount of sulphur remaining from solid phase versus time.**

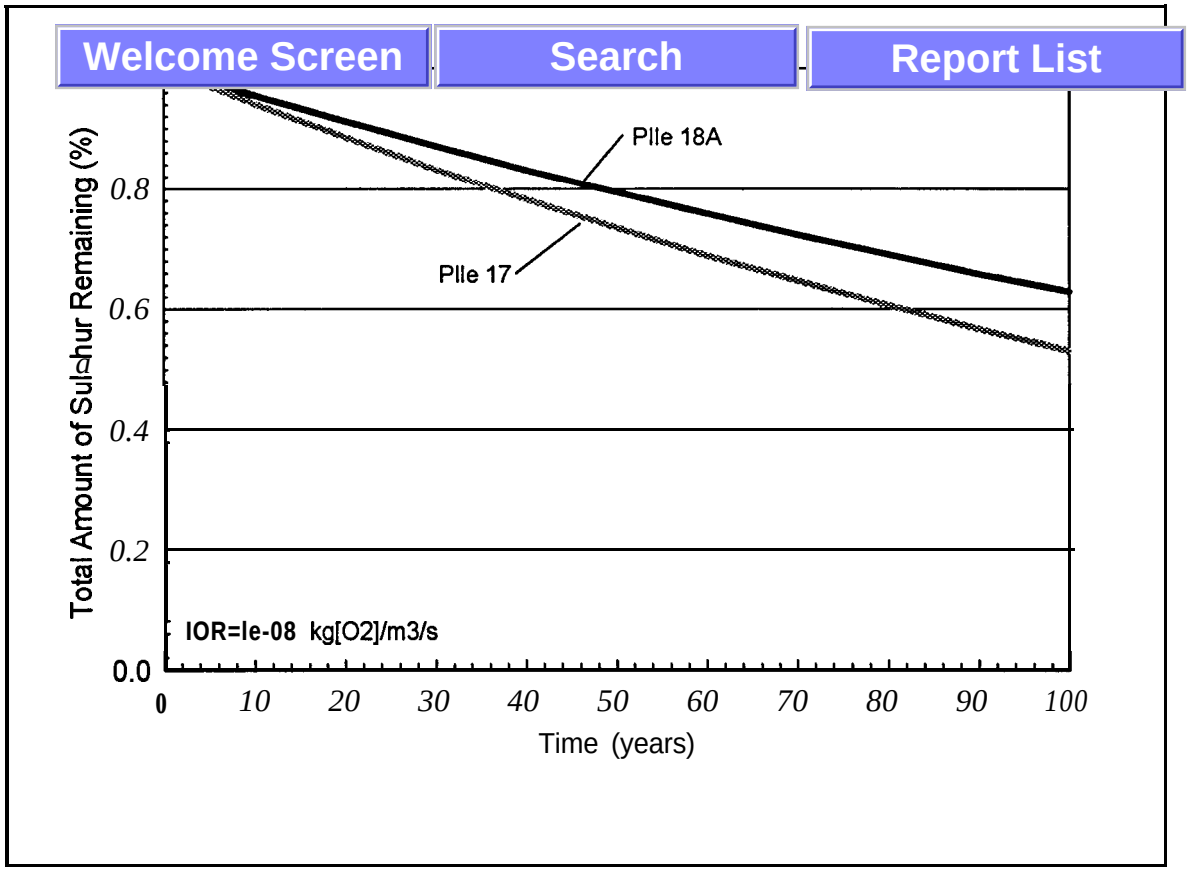

Figure IV - 59: **FIDHELM Results - Pile 18B and Pile 17: Normalized total amount of sulphur remaining from solid phase versus time.**

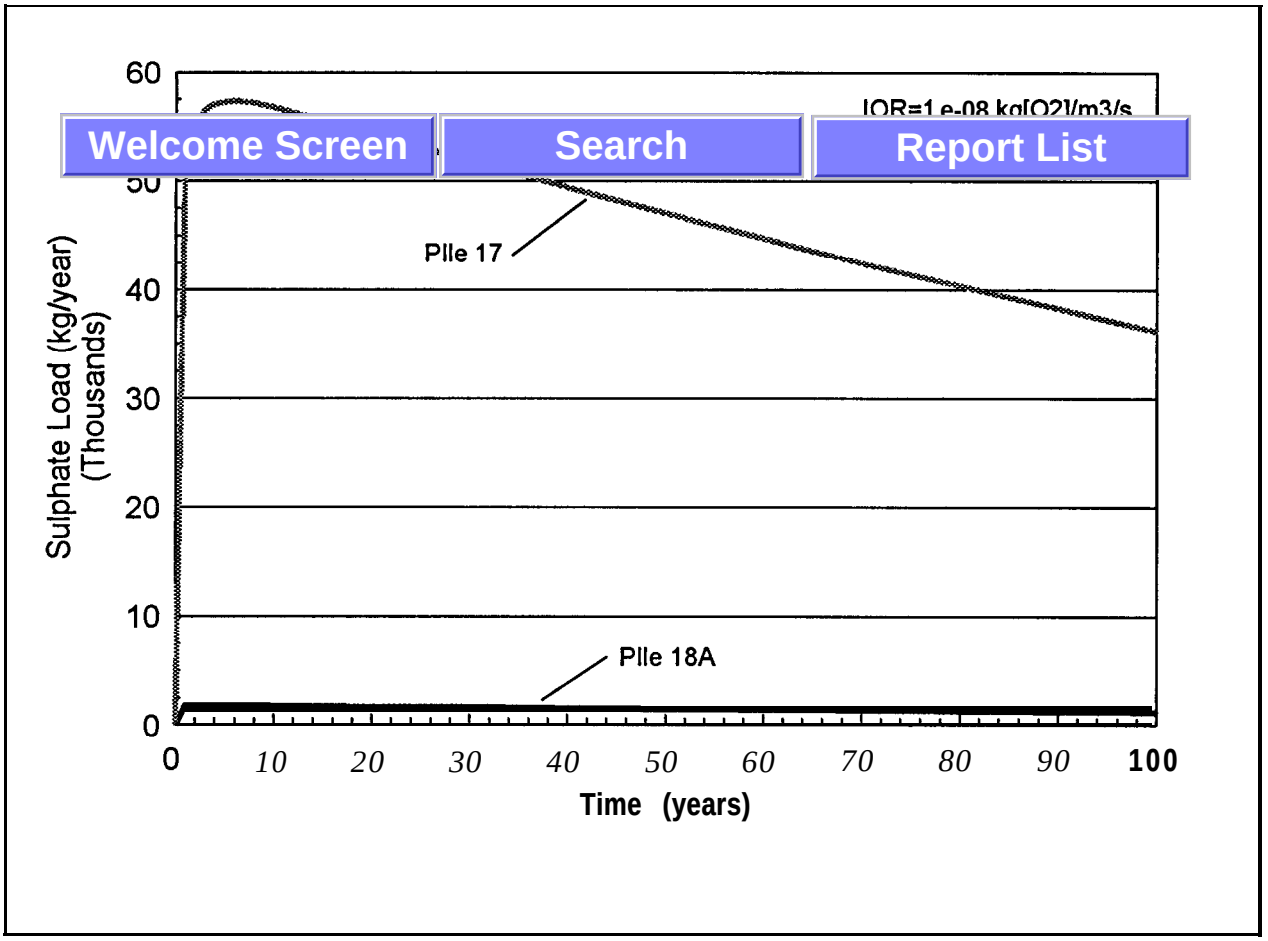

Figure IV - 60: **FIDHELM Results - Pile 18A and Pile 17: Sulphate load from aqueous phase versus time.**